frontiers | Research Topics

Perspectives in genetic and epigenetic regulatory mechanisms in dental and craniofacial biology

Edited by
Weimin Lin, Dian Jing, Yunshu Wu and Long Guo

Published in
Frontiers in Genetics
Frontiers in Pediatrics

ISSN 1664-8714
ISBN 978-2-8325-4187-6
DOI 10.3389/978-2-8325-4187-6

About Frontiers

Frontiers is more than just an open access publisher of scholarly articles: it is a pioneering approach to the world of academia, radically improving the way scholarly research is managed. The grand vision of Frontiers is a world where all people have an equal opportunity to seek, share and generate knowledge. Frontiers provides immediate and permanent online open access to all its publications, but this alone is not enough to realize our grand goals.

Frontiers journal series

The Frontiers journal series is a multi-tier and interdisciplinary set of open-access, online journals, promising a paradigm shift from the current review, selection and dissemination processes in academic publishing. All Frontiers journals are driven by researchers for researchers; therefore, they constitute a service to the scholarly community. At the same time, the *Frontiers journal series* operates on a revolutionary invention, the tiered publishing system, initially addressing specific communities of scholars, and gradually climbing up to broader public understanding, thus serving the interests of the lay society, too.

Dedication to quality

Each Frontiers article is a landmark of the highest quality, thanks to genuinely collaborative interactions between authors and review editors, who include some of the world's best academicians. Research must be certified by peers before entering a stream of knowledge that may eventually reach the public - and shape society; therefore, Frontiers only applies the most rigorous and unbiased reviews. Frontiers revolutionizes research publishing by freely delivering the most outstanding research, evaluated with no bias from both the academic and social point of view. By applying the most advanced information technologies, Frontiers is catapulting scholarly publishing into a new generation.

What are Frontiers Research Topics?

Frontiers Research Topics are very popular trademarks of the *Frontiers journals series*: they are collections of at least ten articles, all centered on a particular subject. With their unique mix of varied contributions from Original Research to Review Articles, Frontiers Research Topics unify the most influential researchers, the latest key findings and historical advances in a hot research area.

Find out more on how to host your own Frontiers Research Topic or contribute to one as an author by contacting the Frontiers editorial office: frontiersin.org/about/contact

Perspectives in genetic and epigenetic regulatory mechanisms in dental and craniofacial biology

Topic editors

Weimin Lin — Sichuan University, China

Dian Jing — Shanghai Jiao Tong University, China

Yunshu Wu — Peking University Hospital of Stomatology, China

Long Guo — Laboratory for Bone and Joint Diseases, RIKEN Center for Integrative Medical Sciences, Japan

Citation

Lin, W., Jing, D., Wu, Y., Guo, L., eds. (2024). *Perspectives in genetic and epigenetic regulatory mechanisms in dental and craniofacial biology*. Lausanne: Frontiers Media SA. doi: 10.3389/978-2-8325-4187-6

Table of contents

frontiers in Genetics

ORIGINAL RESEARCH
published: 25 March 2022
doi: 10.3389/fgene.2022.788259

Crucial Roles of microRNA-16-5p and microRNA-27b-3p in Ameloblast Differentiation Through Regulation of Genes Associated With Amelogenesis Imperfecta

Akiko Suzuki[1,2], *Hiroki Yoshioka*[1,2], *Teng Liu*[3], *Aania Gull*[1,2], *Naina Singh*[2], *Thanh Le*[1,2], *Zhongming Zhao*[3,4,5]* and *Junichi Iwata*[1,2,5]*

[1]Department of Diagnostic and Biomedical Sciences, School of Dentistry, The University of Texas Health Science Center at Houston, Houston, TX, United States, [2]Center for Craniofacial Research, The University of Texas Health Science Center at Houston, Houston, TX, United States, [3]Center for Precision Health, School of Biomedical Informatics, The University of Texas Health Science Center at Houston, Houston, TX, United States, [4]Human Genetics Center, School of Public Health, The University of Texas Health Science Center at Houston, Houston, TX, United States, [5]MD Anderson Cancer Center UTHealth Graduate School of Biomedical Sciences, Houston, TX, United States

OPEN ACCESS

Edited by:
James Kennedy Hartsfield, University of Kentucky, United States

Reviewed by:
Brad A. Amendt, The University of Iowa, United States
Anne George, University of Illinois at Chicago, United States

***Correspondence:**
Zhongming Zhao
Zhongming.Zhao@uth.tmc.edu
Junichi Iwata
Junichi.Iwata@uth.tmc.edu

Specialty section:
This article was submitted to Genetics of Common and Rare Diseases, a section of the journal Frontiers in Genetics

Received: 08 October 2021
Accepted: 11 March 2022
Published: 25 March 2022

Citation:
Suzuki A, Yoshioka H, Liu T, Gull A, Singh N, Le T, Zhao Z and Iwata J (2022) Crucial Roles of microRNA-16-5p and microRNA-27b-3p in Ameloblast Differentiation Through Regulation of Genes Associated With Amelogenesis Imperfecta. Front. Genet. 13:788259. doi: 10.3389/fgene.2022.788259

Amelogenesis imperfecta is a congenital disorder within a heterogeneous group of conditions characterized by enamel hypoplasia. Patients suffer from early tooth loss, social embarrassment, eating difficulties, and pain due to an abnormally thin, soft, fragile, and discolored enamel with poor aesthetics and functionality. The etiology of amelogenesis imperfecta is complicated by genetic interactions. To identify mouse amelogenesis imperfecta-related genes (mAIGenes) and their respective phenotypes, we conducted a systematic literature review and database search and found and curated 70 mAIGenes across all of the databases. Our pathway enrichment analysis indicated that these genes were enriched in tooth development-associated pathways, forming four distinct groups. To explore how these genes are regulated and affect the phenotype, we predicted microRNA (miRNA)-gene interaction pairs using our bioinformatics pipeline. Our miRNA regulatory network analysis pinpointed that miR-16-5p, miR-27b-3p, and miR-23a/b-3p were hub miRNAs. The function of these hub miRNAs was evaluated through ameloblast differentiation assays with/without the candidate miRNA mimics using cultured mouse ameloblast cells. Our results revealed that overexpression of miR-16-5p and miR-27b-3p, but not miR-23a/b-3p, significantly inhibited ameloblast differentiation through regulation of mAIGenes. Thus, our study shows that miR-16-5p and miR-27b-3p are candidate pathogenic miRNAs for amelogenesis imperfecta.

Keywords: enamel, amelogenesis imperfecta, tooth defects, pathogenic gene, microRNA, ameloblast differentiation

INTRODUCTION

Enamel is composed of inorganic and organic matter and water. The inorganic component, called hydroxyapatite, mainly comprises calcium, phosphate, magnesium, potassium, fluoride, and sodium, whereas the organic component includes enamel matrix proteins and enzymes. FAM20C is a Golgi-localized serine/threonine-protein kinase that is activated by FAM20A

(Cui et al., 2015; Ohyama et al., 2016) and phosphorylates enamel matrix proteins, including Amelogenin (AMELX), Amelotin (AMTN), and Enamelin (ENAM), for mineralization (Ishikawa et al., 2012; Tagliabracci et al., 2012; Wang et al., 2013; Cui et al., 2015). The phosphorylated enamel matrixes provide a platform for further mineralization, during which they are cleaved and degraded by MMP20 and KLK4, and then removed from the hydroxyapatite crystals (Hu et al., 2007; Hu and Simmer, 2007). A failure in the degradation of the enamel matrixes leads to retention of enamel matrix residues between the hydroxyapatite crystals, abnormal crystal formation, and immature enamel formation (Simmer and Hu, 2002; Kwak et al., 2016; Yamazaki et al., 2019). Recent studies suggest that WDR72 may be important for the resorption of the enamel matrixes (especially for AMELX) from the extracellular matrix (ECM) through endocytosis of ameloblasts (Katsura et al., 2014; Wang et al., 2015).

Amelogenesis imperfecta (a.k.a. enamel hypoplasia) is a congenital disorder that affects the tooth surface and is characterized by abnormal enamel formation (Gadhia et al., 2012; Williams and Letra, 2018). The frequency of the condition varies among different populations worldwide, e.g., 1:700 in Sweden (Backman and Holm, 1986), 43:10,000 in Turkey (Altug-Atac and Erdem, 2007), and 1:14,000 in the United States (Crawford et al., 2007). The disorder may manifest by itself through a mutation in genes encoding enamel proteins or may accompany other morphological defects in tooth development (Aldred et al., 2003; Stephanopoulos et al., 2005; Smith et al., 2017). The affected enamel displays a wide range of severity of abnormalities, ranging from pits and grooves on the tooth's surface to a complete loss of enamel, which results in easily brittle and worn teeth. These patients suffer from poor esthetic appearance due to tooth discoloration, abnormal tooth shape, open bite, and premature tooth loss, in addition to tooth pain, eating difficulties, and frequent and full-mouth dental maintenance and treatment (Hashem et al., 2013).

Based on the distinct phenotype and mode of inheritance, amelogenesis imperfecta can be divided into four major categories: hypoplastic enamel, hypomaturation enamel, hypocalcified enamel, and hypomature-hypoplastic enamel with taurodontism (Aldred and Crawford, 1995; Aldred et al., 2003). In hypoplastic enamel (type I), the enamel is thinner than usual but can retain its typical hardness and translucency. Due to the enamel matrix's malfunction, the mature enamel layer often presents pits and grooves; other consequences of the thin enamel include lack of occlusion owing to small or absent cusps in the posterior molars. A distinct difference in density between dentin and the enamel layers can be seen in radiographs (Witkop, 1988; Wright, 2006). In the case of hypomaturation enamel (type II), the enamel is softer than normal due to a failure in protein removal during the maturation stage of amelogenesis. These enamel proteins that remain in the matrixes compromise the enamel matrix structure and crystal growth. While enamel thickness appears normal, its hardness is lower, resulting in pits on the surface and rapid wear. In radiographs, the enamel layer appears similar to dentin due to reduced density (Witkop, 1988; Wright, 2006). In hypocalcified enamel (type III), the enamel is softer, rougher, and more prone to rapid wear than in type II cases due to abnormal mineralization (Witkop, 1988; Urzua et al., 2011). While the enamel appears to be of normal thickness, the abnormal mineralization leads to extremely brittle teeth without a smooth and translucent appearance. The dentin in these cases is more radiopaque than the enamel (Witkop, 1988; Wright, 2006). Lastly, in the hypomature/hypoplastic enamel with taurodontism (type IV), patients have thin, pitted enamel with enlarged pulp chambers in the molars (Witkop, 1988; Wright, 2006).

Clinically, patients often present a mixed phenotype. Treatment for amelogenesis imperfecta consists in the prevention of gradual occlusal wear, in which case early detection is beneficial. Full-mouth prosthetics can preserve the remaining enamel, prevent further tooth loss, and reduce pain caused by dentin exposure (Strauch and Hahnel, 2018).

While various genetic mutations have been reported in amelogenesis imperfecta, the regulatory network remains unknown. MicroRNAs (miRNAs), typically 21–22 nucleotide long, negatively regulate gene expression at the post-transcriptional stage and usually have multiple target genes and control their expression at the regulatory network level (Guo et al., 2010; Li et al., 2020). Recent studies suggest that miRNAs play crucial roles in tooth development (Fan et al., 2015; Farmer and Mcmanus, 2017; Jin et al., 2017); therefore, this study aimed to identify the regulatory network of genes and miRNAs associated with amelogenesis imperfecta. A better understanding of the mechanism of amelogenesis imperfecta can potentially lead to the development of novel preventive and therapeutic interventions.

MATERIALS AND METHODS

Eligibility Criteria for the Systematic Review

This systematic review followed the publishing guidelines and checklist established by PRISMA (Preferred Reporting Items for Systematic Review and Meta-Analysis). Articles were included and excluded based on the following eligibility criteria: 1) Inclusion criteria: described genes causing or potentially associated with amelogenesis imperfecta and enamel hypoplasia in species other than humans; published as original articles (not as review articles, editorials, dissertations, conference proceedings, or comments); and published in the English language; 2) Exclusion criteria: gene mutations were not described in the original articles; enamel defects resulting from exposure to environmental risk factors; cell-based experiments, molecular and biochemical analyses, structural and component analyses, and evolutional researches; and the articles failed to fit in any of the above criteria but did not include amelogenesis imperfecta candidate genes or related information.

Information Sources and Search

The search for articles was conducted through three central literature databases: Medline (Ovid), PubMed (National Library of Medicine), and Embase (Ovid). In addition, relevant articles were searched in Scopus (Elsevier) to retrieve any studies

missed in the database searches. Concepts included in the search to identify studies were *amelogenesis imperfecta* and *genetics* (gene mutation). No specific species was included in the keywords since our review included all species. A combination of Medical Subject Headings (MeSH) terms and titles, abstracts, and keywords was developed to obtain the initial Medline search string, and then adapted to the searches of the other databases. The Mouse Genome Informatics (MGI) database was searched using keywords "amelogenesis imperfecta," "enamel hypoplasia," "tooth enamel," "tooth mineralization," and "enamel mineralization" in order to provide a means of comparison and validation for the systematic review and identify genes that were potentially missed in the database searches.

Study Selection and Data Collection

The citations searched were stored in Rayyan (https://rayyan.qcri.org/welcome), an online application for systematic reviews that stores the citations/results, automatically processes the removal of duplicates obtained through various database searches, and tracks the decisions made during the systematic review. The primary Excel workbook designed for the systematic review (http://libguides.sph.uth.tmc.edu/excel_SR_workbook) was also used for tracking search strategies and results. A Cohen's kappa test was conducted by two screeners to check the reliability of study selection during title and abstract screening. After achieving a >90% score for the Cohen's Kappa test, all the titles and abstracts found through the database search were full-text reviewed by the two screeners independently. All the screening results were recorded in the Primary Excel workbook, and a codebook for data collection from eligible articles was developed as previously described (Sangani et al., 2015).

Bioinformatics Analysis

The Database for Annotation, Visualization, and Integrated Discovery (DAVID) (http://david.abcc.ncifcrf.gov/) was used for the gene set enrichment analysis. Gene Ontology (GO), including its Biological Process (BP), Molecular Function (MF), and Cellular Component (CC), and the Kyoto Encyclopedia of Genes and Genomes (KEGG) pathways were used as reference gene sets (Sun H. et al., 2019). The top five most significant pathways or GO terms were selected for further analysis. k-means was used to cluster the gene functional enrichment results and the square error to extract the closest clusters. The highly-expressed mouse tooth miRNAs were retrieved from the publications (Cao et al., 2010). The miRNA-mAIGene regulations were integrated using the data from four databases: TargetScan (version 7.1) (Agarwal et al., 2015), miRanda (August 2010 Release) (John et al., 2004), miRTarBase (Release 7.0) (Huang et al., 2020), and PITA (version 6) (Kertesz et al., 2007). Considering the possibility of false results and multiple targets for each miRNA in these databases, the intersection of miRanda and PITA was merged with the intersection of TargetScan and miRTarBase to obtain reliable miRNA-mAIGene pairs. This conservative approach was demonstrated to effectively reduce the prediction of false-positive miRNA-mAIGene pairs (Jiang et al., 2016; Bonnet et al., 2020). Each gene set (GO term or KEGG pathway) containing at least two genes was used in the core miRNA family-based regulatory network. A Fisher's exact test was applied to assess the enrichment significance of the miRNAs. All networks were visualized using Cytoscape (Shannon et al., 2003).

Cell Culture

The mHAT9d mouse dental epithelial cell line originated from the apical bud of the incisors was a gift from Dr. Hidemitsu Harada (Iwate Medical University, Iwate, Japan). mHAT9d cells were cultured in Dulbecco's Modified Eagle Medium: Nutrient Mixture F-12 (DMEM/F12; Thermo Fisher Scientific) supplemented with B-27 (Thermo Fisher Scientific), 25 ng/ml basic FGF (233-FB; R&D Systems), 20 ng/ml EGF (2028-EG; R&D Systems), and penicillin/streptomycin (Otsu et al., 2016). The LS8 cell line (Chen et al., 1992) was provided by Dr. Malcolm Snead (University of Southern California). Cells were plated at a density of 60,000 cells onto a 12-well cell culture plate and maintained until 80% confluence. The cells were treated with mimic for a negative control, miR-16-5p, miR-23a-3p, miR-23b-3p, miR-27b-3p, or miR-214-3p (mirVana miRNA mimic, Thermo Fischer Scientific) using Lipofectamine RNAiMAX transfection reagent (Thermo Fisher Scientific), according to the manufacturer's protocol (24 pmol of mimic and 3 μL of transfection reagent in 1 ml of medium per well). After 24 h of treatment, the cells at 100% confluence were cultured with differentiation medium [including 15 μg/ml retinoic acid (R2625, Sigma Aldrich) and 0.1 μM dexamethasone (D4902, Sigma Aldrich)] in order to induce ameloblast differentiation.

Bromodeoxyuridine (BrdU) Incorporation Assay

mHAT9d cells were plated onto ibiTreat 8-well μ-slides (ibidi GmbH, Munich district, Germany) at a density of 10,000/chamber and cultured until 80% confluence. Cells were then treated with a mimic for miR-16-5p, miR-27b-3p, or control using Lipofectamine RNAiMAX transfection reagent (4.8 pmol of mimic with 0.48 μL of transfection reagent in 200 μL of proliferation medium). After 24 h of transfection, the cells were cultured under differentiation medium for 48 h. In addition, cells were treated with 100 μg/ml BrdU (Sigma Aldrich) for 1 h at day 2 of differentiation (n = 6 per group) and visualized with a rat monoclonal antibody against BrdU (ab6326; Abcam, 1:1,000), as previously described (Yoshioka et al., 2021a). BrdU-positive cells were quantified using images from six independent experiments.

RNA Extraction and Quantitative Reverse Transcription-Polymerase Chain Reaction

Total RNAs were isolated from cells treated with mimics for the target miRNAs or negative control (n = 6 per group) using the QIAshredder and RNeasy mini extraction kit or the miRNeasy mini kit (QIAGEN), as previously described (Suzuki et al., 2019; Yan et al., 2020). In addition, total RNAs were isolated from ameloblasts at each stage of differentiation (pre-secretion, secretion, and maturation) in the lower incisors of 8-week old

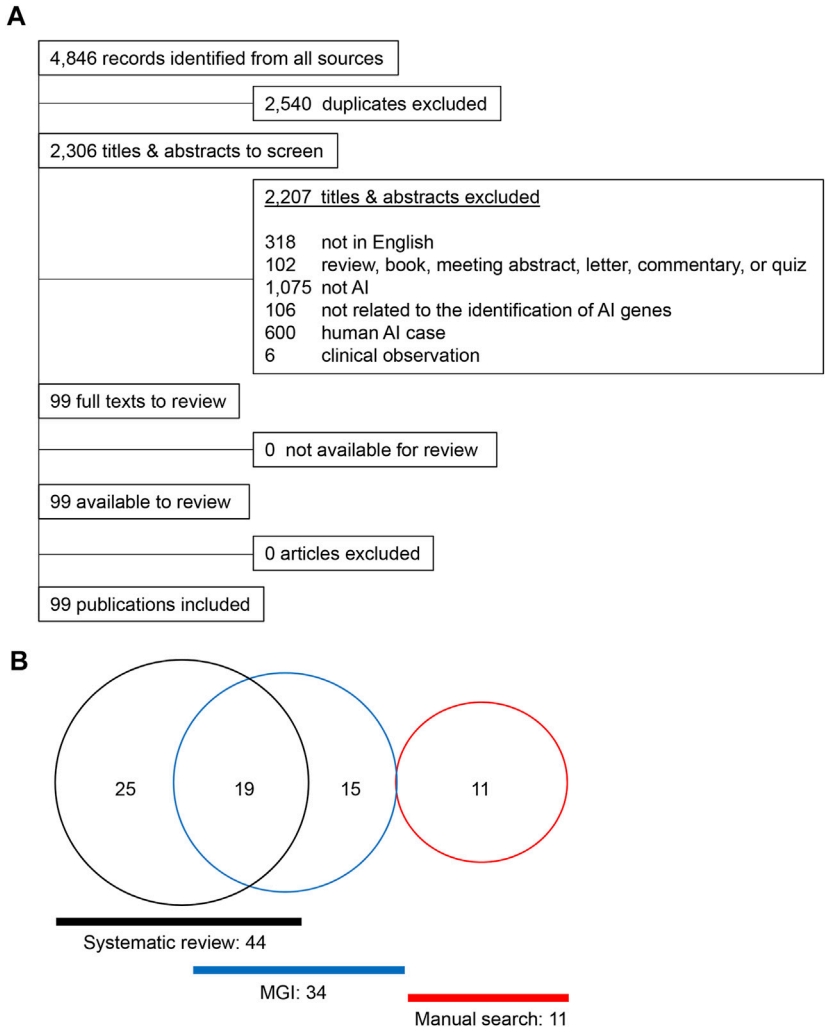

FIGURE 1 | Summary of the literature search. **(A)** PRISMA flowchart for amelogenesis imperfecta articles in different species other than humans. **(B)** Venn diagram for the amelogenesis imperfecta study.

males C57BL/6J mice (n = 3). Briefly, the lower incisors were extracted, and ameloblasts were manually dissected and separated into three parts [apical 1/3 (pre-secretion), middle 1/3 (secretion), and incisal 1/3 (maturation) between the cervical loop and bony ridge of the incisor] under a dissection microscope. cDNA was reverse-transcribed with the iScript Reverse Transcription Super Mix (BioRad) and amplified with the iTaq Universal SYBER Green Super Mix (BioRad) using a CFX96 Touch Real-Time PCR Detection System (BioRad). The expression of genes was normalized with *Gapdh*. miRNA expression during ameloblast differentiation was detected with Taqman Fast Advanced Master Mix and Taqman Advanced miR cDNA Synthesis Kit (Thermo Fisher Scientific), according to the manufacturer's instructions. The PCR primers used are listed in **Supplementary Table S1**.

Immunofluorescence Analysis

The cells were plated onto ibiTreat 8-well μ-slides (ibidi GmbH, Munich district, Germany) at a density of 10,000/chamber and maintained until 80% confluency. The cells were then treated with mimics for miR-16-5p, miR-27b-3p, or a negative control, using Lipofectamine RNAiMAX transfection reagent (4.8 pmol of mimic with 0.48 μL of transfection reagent in 200 μL of differentiation medium) (n = 4 per group). After 24 h of treatment, the medium was replaced with differentiation medium for 2 days. AMELX expression was detected with anti-AMELX rabbit polyclonal antibody (ab153915, Abcam, 1: 250), as previously described (Yoshioka et al., 2021b). Immunofluorescent images were captured with a confocal microscope (Ti-E, Nikon United States).

Immunoblotting

The cells were plated onto 12-well plates at a density of 60,000 per well, maintained until 80% confluence, and treated with either miR-16-5p, miR-27b-3p, or a negative control mimic, for 24 h (n = 3 per group). The cells were then cultured in ameloblast differentiation medium for another 48 h. The treated cells were

TABLE 1 | Single mutation mouse models with enamel defects

#	Gene Symbol	Gene Name	Location	Enamel Phenotype	Mouse Strain	PMID	Human Disease
1	*Alpl*	alkaline phosphatase, liver/bone/kidney	4 D3	hypoplastic	*Alpl*$^{-/-}$	10371245	hypophosphatasia-enamel hypoplasia
2	*Ambn*	ameloblastin	5 E1	hypoplastic hypoplastic or hypocalcified hypoplastic hypoplastic	Tg (under Amelx) *Ambn*$^{\Delta 5-6}$ *Ambn*$^{LacZ/LacZ}$ *Ambn*$^{-/-}$	12657627 15583034; 19375505 31402633 16612084	isolated AI
3	*Amelx*	amelogenin, X-linked	X F5	hypoplastic hypomineralized hypoplastic hypoplastic hypoplastic and hypomineralized hypoplastic and hypomineralized	*Amelx*$^{-/-}$ Tg (M180-ΔA, M180ΔA-FLAG) and Tg (M180-ΔB, M180ΔB-HA) Tg (M180-P70T) *Amelx* $^{p.Y64H/p.Y64H}$ Tg (M194) Tg (CTRNC)	11406633; 18390542; 18701811; 22243229 16707492; 11243888; 12619931 17384027 20067920; 24363885 25117480 20042744	isolated AI
4	*Amtn*	amelotin	5 E1	hypomaturation and hypomineralized	*Amtn*$^{-/-}$	25715379	isolated AI
5	*Arhgap6*	Rho GTPase activating protein 6	X F5	hypoplastic	*Arhgap6*$^{-/-}$	16007484	isolated AI
6	*Ascl5* (a.k.a. *AmeloD*)	achaete-scute family bHLH transcription factor 5	1 E4	hypoplastic	*Asc5*$^{-/-}$	30504223	
7	*Bcl11b*	B cell leukemia/lymphoma 11B	12 F1	hypomineralized	*Bcl11b*$^{S826G/-}$	23727454	
8	*Bmp2*	bone morphogenetic protein 2	2 F2	hypomineralized	*Osx-Cre;Bmp2*$^{F/F}$	21597270; 25545831	
9	*Cftr*	cystic fibrosis transmembrane conductance regulator	6 A2	hypomineralized	*Cftr*$^{-/-}$	9206347; 8708137; 12161463	cystic fibrosis—AI
10	*Cldn3*	claudin 3	5 G2	hypomineralized	*Cldn3*$^{-/-}$	28596736	
11	*Cldn16*	claudin 16	16 B2	hypoplastic and hypomineralized	*Cldn16*$^{-/-}$	2642691	familial hypercalciuria and hypomagnesemia with nephrocalcinosis (FHHNC)—AI
12	*Cnnm4*	cyclin M4	1 B	hypomineralized	*Cnnm4*$^{-/-}$	24339795	Jalili syndrome—AI
13	*Col17a1*	collagen, type XVII alpha 1	19 D1	hypomaturation and hypomineralized	*Col17a1*$^{-/-}$	19036806	Junctional epidermolysis bullosa—AI
14	*Csf1* (a.k.a. *Mcsf*)	colony-stimulating factor 1 (macrophage)	3 F2	hypoplastic hypoplastic	OP/OP OP/OP; Tg (csCSF-1)	17126805 17126805	
15	*Ctnnb1*	catenin beta 1	9 F4	hypomineralized	*Amelx-Cre;Ctnnb1* $^{\Delta ex3F/F}$	30066216	
16	*Dlx3*	distal-less homeobox 3	11 D	hypomineralized	*K14-Cre;Dlx3*$^{F/F}$	27760456; 29745813	trichodentoosseous syndrome—AI
17	*Dmp1*	dentin matrix protein 1	5 E5	hypoplastic and hypomineralized	*Dmp1*$^{-/-}$	14966118; 14514755	hypophosphatemia—AI
18	*Dspp*	dentin sialophosphoprotein	5 E5	hypoplastic	Tg (under Amelx)	16014627	dentinogenesis imperfecta type II—AI

(Continued on following page)

TABLE 1 | (*Continued*) Single mutation mouse models with enamel defects

#	Gene Symbol	Gene Name	Location	Enamel Phenotype	Mouse Strain	PMID	Human Disease
19	*Eda*	ectodysplasin-A	X C3	hypoplastic (no enamel)	Tg (under K14)	12812793	hypohidrotic ectodermal dysplasias not AI
20	*Enam*	enamelin	5 E1	hypomaturation	*Enam*$^{Rgsc521/Rgsc521}$	15649948; 20598351	isolated AI
				hypoplastic	*Enam*$^{Rgsc395/Rgsc395}$ & *Enam*$^{Rgsc514/Rgsc514}$	15649948	
				hypoplastic	*Enam*$^{p.Q176X/p.Q176X}$ (ATE1)	15271968; 17652207	
				hypoplastic or no enamel	*Enam*$^{LacZ/LacZ}$	18252720; 24603688	
				no enamel or hypoplastic	*Enam*$^{p.S55I/p.S55I}$ or *Enam*$^{p.S55I/+}$	28334996	
21	*Fam20a*	family with sequence similarity 20, member A	11 E1	hypoplastic and hypomineralized	*Fam20a*$^{-/-}$	22732358	enamel-renal-gingival syndrome—AI
				hypoplastic and hypomineralized	*K14-Cre;Fam20a*$^{F/F}$	27281036	
				hypoplastic (no enamel)	*Sox2-Cre;Fam20a*$^{F/F}$	31667691	
22	*Fam20c*	family with sequence similarity 20, member C	5 G2	hypoplastic (no enamel)	*Fam20c*$^{-/-}$	22732358	Raine syndrome—AI
				hypoplastic and hypomineralized	*K14-Cre;Fam20c*$^{F/F}$	24026952	
				hypoplastic and hypomineralized	*Sox2-Cre;Fam20c*$^{F/F}$	22936805	
23	*Fam83h*	family with sequence similarity 83, member H	15 D3	hypoplastic	*Fam83h*$^{-/-}$	30714208	isolated AI
				hypoplastic	Tg (truncated protein 1–296)	31060110	
24	*Fgfr1*	fibroblast growth factor receptor 1	8 A2	hypoplastic	*K14-Cre;Fgfr1*$^{F/F}$	18296607	Pfeiffer syndrome—not AI Jackson-Weiss syndrome—not AI
25	*Foxo1*	forkhead box O1	3 C	hypomaturation	*Rx-Cre;Foxo1*$^{F/F}$ & *K14-Cre;Foxo1*$^{F/F}$	22291941	
26	*Gdnf*	glial cell line derived neurotrophic factor	15 A1	hypoplastic	*Gdnf*$^{-/-}$	11878293	Hirschsprung disease type 3—not AI
27	*Gja1* (a.k.a. *Cx43*)	gap junction protein, alpha 1	10 B4	hypoplastic	*PGK-Cre;Cx43*$^{G138R/+}$	18003637	oculodentodigital dysplasia - AI
				hypoplastic	*Gja1*$^{G60S/+}$ a.k.a. *Gja1*$^{Jrt/+}$	16155213; 20127707	
28	*Hmgn2*	high mobility group nucleosomal binding domain 2	4 D3	hypoplastic	Tg (under K14)	23975681	
29	*Hras*	Harvey rat sarcoma virus oncogene	7 F5	hypomineralized	*Caggs-Cre;Hras*$^{G12V/+}$	24057668; 19416908	Costello syndrome—enamel defect
30	*Irf6*	interferon regulatory factor 6	1 H6	hypoplastic	*Pitx2-Cre;Irf6*$^{F/F}$	27369589	van der Woude syndrome—not AI popliteal pterygium syndrome—not AI
31	*Itgb1*	integrin beta 1	8 E2	hypoplastic	*K14-Cre;Itgb1*$^{F/F}$	25830530	
32	*Itgb6*	integrin beta 6	2 C1.2	hypomineralized	*Itgb6*$^{-/-}$	23264742	isolated AI
33	*Klk4*	kallikrein-related peptidase 4 (prostase, enamel matrix, prostate)	7 B3	hypomineralized	*Klk4*$^{LacZ/LacZ}$	19578120	isolated AI
34	*Lama3*	laminin, alpha 3	18 A1	hypoplastic	*Lama3*$^{-/-}$	10366601	junctional epidermolysis bullosa—AI
35	*Lamb3*	laminin, beta 3	1 H6	unknown	*Lamb3*$^{Lacz/LacZ}$	27626380	junctional epidermolysis bullosa—AI
36	*Lamc2*	laminin gamma 3	1 G3	pitted enamel hypomineralized	Spontaneous (*Lamc2*^{jeb})	20336083	cortical malformation, occipital—not AI
					Tg (*TetO-Lamc2*$^{-/-}$*;K14-rtTA;TetO-HumLAMC2*)	26956061; 23029085	

(Continued on following page)

TABLE 1 | (*Continued*) Single mutation mouse models with enamel defects

#	Gene Symbol	Gene Name	Location	Enamel Phenotype	Mouse Strain	PMID	Human Disease
37	*Ltbp3*	latent transforming growth factor-beta binding protein 3	19 A	hypoplastic	*Ltbp3*$^{-/-}$	25669657; 28084688	dental anomalies and short stature (DASS)—AI
38	*Map3k7* (a.k.a. *Tak1*)	mitogen-activated protein kinase kinase 7	4 A5	hypomineralized	*CaMap3k7* (under Amelx)	29024853	cardiospondylocarpofacial syndrome—not AI frontometaphyseal dysplasia 2—not AI
39	*Med1*	mediator complex subunit 1	11 D	hypomineralized	*K14-Cre;Med1*$^{F/F}$	24949995; 28673966	
40	*Mmp20*	matrix metallopeptidase 20 (enamelysin)	9 A1	hypoplastic hypomineralized	*Mmp20*$^{-/-}$ Tg (under Amelx)	12393861; 15557396; 24466234 24466234; 29481294	isolated AI
41	*Msx2*	msh homeobox 2	13 B1	hypoplastic	*Msx2*$^{LacZ/LacZ}$	20934968; 17878071	isolated AI enlarged parietal foramina 1—not AI craniosynostosis type 2 - not AI
42	*Nectin1*	nectin cell adhesion molecule 1	9 A5	hypomineralized	*Nectin1*$^{-/-}$	18703497; 21038445	cleft lip and palate/ectodermal dysplasia 1—not AI
43	*Nectin3*	nectin cell adhesion molecule 3	16 B5	unknown	*Nectin3*$^{-/-}$	21038445	
44	*Pax9*	paired box 9	12 C1	hypoplastic	*Pax9*$^{neo/neo}$	16236760	tooth agenesis, selective, 3—not AI
45	*Plau* (a.k.a. *uPA*)	plasminogen activator, urokinase	14 A3	unknown-chalky white	Tg (under K5)	9927592; 15161662	
46	*Pitx2*	paired-like homeodomain transcription factor 2	3 G3	unknown	*Pitx2*$^{-/-}$	27626380	Axenfeld-Rieger syndrome—not AI iridogoniodysgenesis syndrome - not AI Peters anomaly—not AI
47	*Postn*	periostin, osteoblast-specific factor	3 C	unknown-chalky white unknown-chalky white but thick enamel	*Postn*$^{LacZ/LacZ}$ *Postn*$^{-/-}$	16314533 16497272	
48	*Rac1*	Rac family small GTPase 1	5 G2	hypoplastic and hypomineralized	*K14-Cre;Rac1*$^{F/F}$	22243243	mental retardation, autosomal dominant, 48—not AI
49	*Relt*	RELT tumor necrosis factor receptor	7 E2	hypomineralized	*Relt*$^{p.P390*/p.P390*}$	30506946	isolated AI
50	*Rhoa*	ras homolog family member A	9 F1-F2	hypoplastic	Tg (dominant-negative, under Amelx)	21576911; 23841780	
51	*Runx1*	runt-related transcription factor 1	16 C4	hypoplastic	*K14-Cre;Runx1*$^{F/F}$	30026553	Braddock-Carey syndrome (BCS)—AI
52	*Runx2*	runt-related transcription factor 2	17 B3	hypomineralized	*K14-Cre;Runx2*$^{F/F}$	29941908	metaphyseal dysplasia with maxillary hypoplasia and brachydactyly—AI cleidocranial dysplasia—not AI
53	*Slc4a4*	solute carrier family 4 (anion exchanger), member 4	5 E1	hypoplastic and hypomineralized	*Slc4a4*$^{-/-}$	20529845; 25012520	proximal renal tubular acidosis—AI
54	*Slc10a7*	solute carrier family 10 (sodium/bile acid cotransporter family), member 7	8 C1	hypoplastic hypomaturation and hypomineralized	*Slc10a7*$^{-/-}$ *Slc10a7*$^{-/-}$	30082715 30082715	skeletal dysplasia—AI
55	*Slc12a2*	solute carrier family 12, member 2	18 D3	hypomineralized	*Slc12a2*$^{-/-}$	29209227	

(Continued on following page)

TABLE 1 | (*Continued*) Single mutation mouse models with enamel defects

#	Gene Symbol	Gene Name	Location	Enamel Phenotype	Mouse Strain	PMID	Human Disease
56	*Slc13a5*	solute carrier family 13 (sodium-dependent citrate transporter), member 5	11 B4	hypoplastic	*Slc13a5*$^{-/-}$	28406943	Kohlschütter-Tönz syndrome (KTS)—AI early infantile epileptic encephalopathy 25 (EIEE25)-tooth hypoplasia and hypodontia—not AI
57	*Slc24a4*	solute carrier family 24 (sodium/potassium/ calcium exchanger), member 4	12 E	hypomineralized	*Slc24a4*$^{-/-}$	23375655	isolated AI
58	*Smad3*	SMAD family member 3	9 C	hypomineralized	*Smad3*$^{-/-}$	12763048	Loeys-Dietz syndrome—not AI
59	*Sp3*	trans-acting transcription factor 3	2 C3	hypoplastic (no enamel)	*Sp3*$^{-/-}$	10675334	
60	*Sp6*	trans-acting transcription factor 6	11 D	hypoplastic	*Sp6*$^{-/-}$	30504223; 18156176; 18297738	
61	*Sp7* (a.k.a. *Osx*)	trans-acting transcription factor 7 (osterix)	15 F3	unknown (die at birth)	*Sp7*$^{-/-}$	29405385	osteogenesis imperfecta type XII - not AI
62	*Stim1*	stromal interaction molecule 1	7 E2-E3	hypomineralized hypoplastic and hypomineralized	*K14-Cre;Stim1*$^{F/F}$ *Amelx-Cre;Stim1*$^{F/F}$	28732182 31329049	AI tubular aggregate myopathy—not AI Stormorken syndrome—not AI
63	*Tbx1*	T-box 1	16 A3	hypoplastic (no enamel)	*Tbx1*$^{-/-}$	19233155	22q-11.2 deletion syndrome (DiGeorge syndrome)—AI
64	*Tcirg1* (a.k.a. *ATP6a3*)	T cell, immune regulator 1, ATPase, H+ transporting, lysosomal V0 protein A3	19 A	hypomineralized	spontaneous	23174213	autosomal recessive osteopetrosis—not AI
65	*Tgfb1*	transforming growth factor, beta 1	7 A3	hypoplastic hypomineralized hypomineralized	Tg (under Dspp) *Tgfb1* $^{Tgfb3/Tgfb3}$ *K14-Cre;Tgb1*$^{F/F}$	16674659; 11116156 24056369 30243146	Camurati-Engelmann disease—not AI
66	*Tgfbr2*	transforming growth factor, beta receptor II	9 F3	hypoplastic and hypomineralized	*Amelx-Cre;Tgfbr2*$^{F/F}$	24278477	Loeys-Dietz syndrome—not AI familial thoracic aortic aneurysm and dissection - not AI
67	*Tmbim6*	transmembrane BAX inhibitor motif containing 6	15 F1	hypomineralized	*Tmbim6*$^{-/-}$	30963569	
68	*Wdr72*	WD repeat domain 72	9 D	hypomaturation and hypomineralized	*Wdr72*$^{LacZ/LacZ}$	25008349; 26247047	isolated AI

AI: amelogenesis imperfecta; OP: osteopetrotic; Tg: transgenic.

lysed with RIPA buffer (Thermo Fisher Scientific) containing a protease inhibitor cocktail (Roche) and centrifuged at 21,130 × *g* for 20 min at 4°C. The protein concentration of the supernatants was measured with the BCA protein kit (Pierce). Protein samples (30 μg) were applied to Mini-PROTEAN TGX Gels (Bio-Rad) and transferred to a polyvinylidene difluoride (PVDF) membrane. Anti-AMELX rabbit polyclonal antibody (ab153915, Abcam, 1:1,000), anti-KLK4 rabbit polyclonal antibody (PA5-109888, Thermo Fisher Scientific, 1:750), anti-MMP20 rabbit polyclonal antibody (55467-1-AP, Proteintech, 1: 750), and anti-GAPDH mouse monoclonal antibody (MAB374, Millipore, 1:6,000) were used for immunoblotting. Peroxidase-conjugated anti-rabbit IgG (7074, Cell Signaling Technology, 1: 100,000) and anti-mouse IgG (7076, Cell Signaling Technology, 1: 100,000) were used as secondary antibodies. All immunoblotting experiments were performed three times to validate the results.

Rescue Experiment

Cells were plated on 12-well cell culture plates at a density of 60,000 cells per well, or on ibiTreat 8-well μ-slides (ibidi GmbH, Munich district, Germany), at a density of 10,000 cells per well and maintained until 80% confluence. The cells were treated with mimics for a negative control, miR-16-5p, or miR-27b-3p (4.8 pmol for 12-well plates and 1.2 pmol for ibiTreat 8-well μ-slides) with a combination of overexpression vectors [100 ng (12-well plates) or 25 ng (ibiTreat 8-well μ-slides)] using Lipofectamine 3000 transfection reagent (Thermo Fisher Scientific), according

TABLE 2 | Compound mutant mouse models with enamel defects.

#	Gene Symbol	Gene Name	Location	Enamel Phenotype	Mouse Strain	PMID
1	*Ambn* and *Enam*	ameloblastin and enamelin	5 E1 and 5 E1	hypoplastic	*Ambn*$^{+/-}$;*Enam*$^{+/-}$	31478359
2	*Bmp2* and *Bmp4*	bone morphogenetic protein 2 & bone morphogenetic protein 4	2 F2 and 14 C4	hypomineralized	*K14-Cre;Bmp2*$^{F/F}$; *Bmp4*$^{F/F}$	27146352
3	*Klk4* and *Mmp20*	kallikrein related-peptidase 4 and matrix metallopeptidase 20	7 B3 and 9 A1	hypoplastic and hypomineralized	*Klk4*$^{-/-}$;*Mmp20*$^{-/-}$	27066511
4	*Stim1* and *Stim2*	stromal interaction molecule 1 and stromal interaction molecule 2	7 E2-E3 and 5 C1	hypomineralized	*K14-Cre;Stim1*$^{F/F}$; *Stim2*$^{F/F}$	28732182

TABLE 3 | Classification of enamel defects.

Phenotype	Gene Symbols
hypoplastic/no enamel/chalky-white	*Alpl*, *Ambn*, *Amelx*, *Arhgap6*, *Ascl5*, *Cldn16*, *Csf1*, *Dmp1*, *Dspp*, *Eda*, *Enam*, *Fam20a*, *Fam20c*, *Fam83h*, *Fgfr1*, *Gdnf*, *Gja1*, *Hmgn2*, *Itgb1*, *Irf6*, *Lama3*, *Ltbp3*, *Mmp20*, *Msx2*, *Pax9*, *Plau*, *Postn*, *Rac1*, *Rhoa*, *Runx1*, *Slc4a4*, *Slc13a5*, *Sp3*, *Sp6*, *Stim1*, *Tbx1*, *Tgfb1*, *Tgfbr2*, *Ambn* and *Enam*, *Klk4* & *Mmp20*
hypomaturation	*Amtn*, *Col17a1*, *Enam*, *Foxo1*, *Slc10a7*, *Wdr72*
hypomineralized/hypocalcified	*Amelx*, *Amtn*, *Bcl11b*, *Bmp2*, *Cftr*, *Cldn3*, *Cldn16*, *Cnnm4*, *Col17a1*, *Ctnnb1*, *Dlx3*, *Dmp1*, *Fam20a*, *Fam20c*, *Hras*, *Itgb6*, *Klk4*, *Lamc2*, *Map3k7*, *Med1*, *Mmp20*, *Nectin1*, *Rac1*, *Relt*, *Runx2*, *Smad3*, *Slc4a4*, *Slc10a7*, *Slc12a2*, *Slc24a4*, *Stim1*, *Tcirg1*, *Tgfb1*, *Tgfbr2*, *Tmbim6*, *Wdr72*, *Bmp2* & *Bmp4*, *Klk4* & *Mmp20*, *Stim1* & *Stim2*
unknown	*Lamb3*, *Nectin3*, *Pitx2*, *Sp7*

TABLE 4 | Functional category of amelogenesis imperfecta-related genes.

Category Name	Gene Symbols
Extracellular matrix	*Ambn*, *Amelx*, *Amtn*, *Col17a1*, *Csf1*, *Dmp1*, *Dspp*, *Enam*, *Lama3, Lamb3*, *Lamc2*, *Postn*
Enzyme	*Alpl*, *Fam20a*, *Fam20c*, *Hras*, *Klk4*, *Map3k7*, *Mmp20*, *Plau*, *Rac1*, *Rhoa*, *Tcirg1*
Receptor	*Fgfr1*, *Itgb1*, *Itgb6*, *Relt*, *Tgfbr2*
Receptor binding molecule	*Ltbp3*
Ion exchanger or transporter	*Cftr*, *Cnnm4*, *Slc4a4*, *Slc10a7*, *Slc12a2*, *Slc13a5*, *Slc24a4*
Calcium sensor or regulator	*Stim1*, *Stim2*, *Tmbim6*
Cell-cell or cell-ECM adhesion molecule	*Cldn3*, *Cldn16*, *Ctnnb1*, *Gja1*, *Nectin1*, *Nectin3*
Growth factor	*Bmp2*, *Bmp4*, *Gdnf*, *Tgfb1*
Transcriptional factor	*Ascl5*, *Bcl11b*, *Ctnnb1*, *Dlx3*, *Foxo1*, *Irf6*, *Msx2*, *Pax9*, *Pitx2*, *Runx1*, *Runx2*, *Sp3*, *Sp6*, *Sp7*, *Tbx1*
Transcriptional regulator	*Hmgn2*, *Med1*
Signal mediator	*Smad3*
Unknown	*Fam83h*, *Wrd72*

to the manufacturer's protocol, which was followed by treatment with *Eda* (Antibodies-online Inc., ABIN3291185), *Relt* (Antibodies-online Inc., ABIN4054001), or *Smad3* (Antibodies-online Inc., ABIN3809504) for the miR-16-5p mimic, or *Bmp2* (Antibodies-online Inc., ABIN4045152), *Pax9* (Antibodies-online Inc., ABIN4216431), or *Slc24a4* (Addgene, 75208) for the miR-27b-3p mimic (n = 6 per group). After 24 h of transfection, the medium was switched to differentiation medium for 2 days.

Statistical Analysis

Statistical comparisons between two groups were performed with a two-tailed Student's *t*-test. Multiple comparisons were conducted with one-way analysis of variance with the Tukey–Kramer *post hoc* test. A *p*-value of less than 0.05 was considered as statistically significant. For all groups, data were represented as mean ± SD.

RESULTS

Literature and Database Search

A total of 4,846 articles were extracted from a database compilation of multiple sources through a search conducted using Rayyan (Ouzzani et al., 2016). After resolving duplicates with RefWorks, 2,306 articles were selected for further screening. A total of 2,207 articles were excluded because there was no underlying genetic mechanism dictating the gene findings or the articles did not mention any relevant study or research conducted

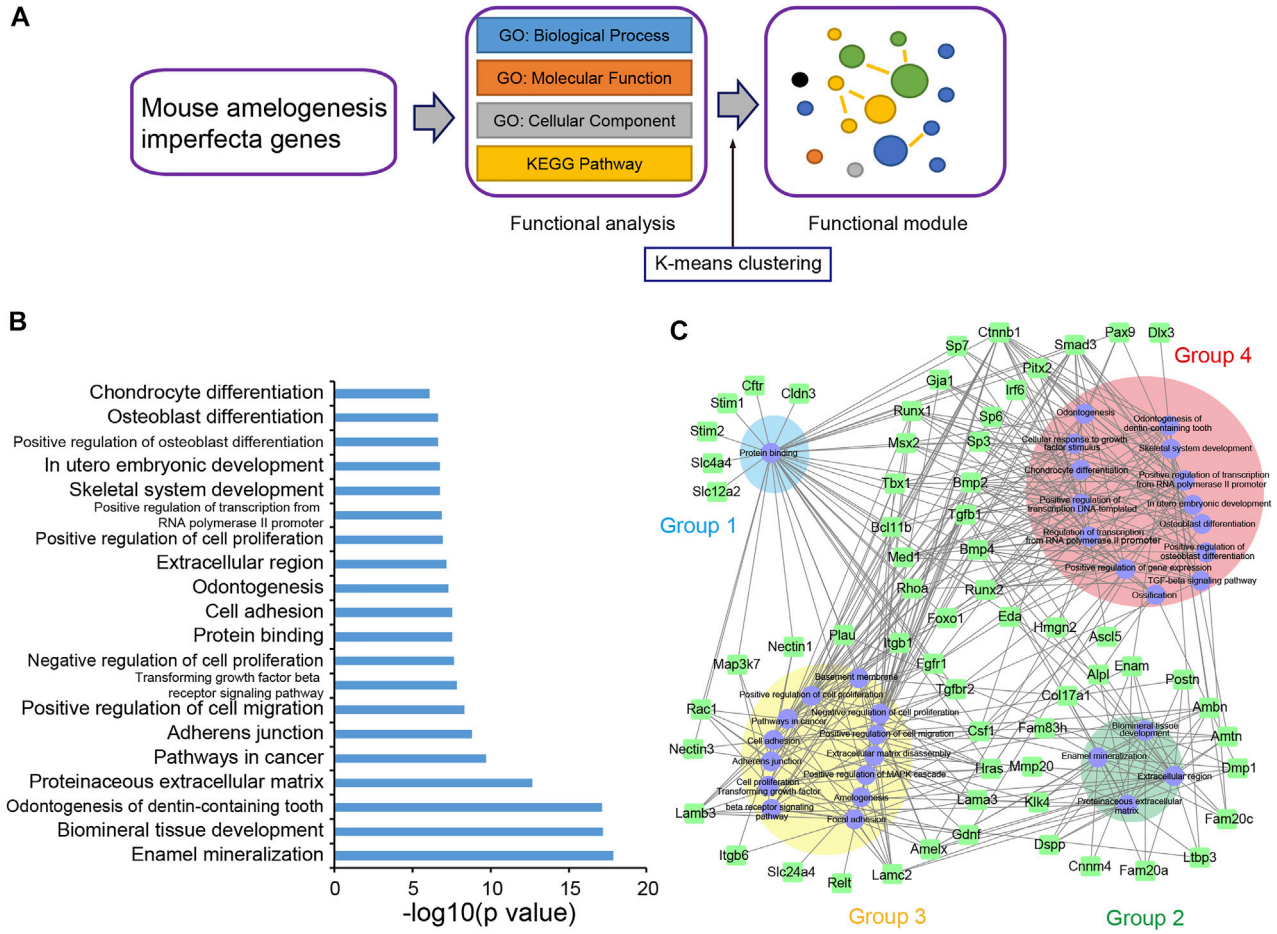

FIGURE 2 | Functional enrichment analysis of mouse amelogenesis imperfecta-related genes (mAIGenes). **(A)** Flowchart of the functional enrichment analysis. Significant Gene Ontology (GO) terms and KEGG pathways were determined by a false discovery rate (FDR) < 0.01. The significant gene sets were then clustered into functional modules using a k-means clustering algorithm. **(B)** Top 20 GO terms or KEGG pathways. Gene sets related to tooth development and cell proliferation were among the top enriched sets. **(C)** The gene set network showed four groups, which were ordered by the number of gene sets (the smallest number of gene sets was in Group 1). These gene sets were related to protein banding, enamel mineralization, cancer, and bone development, respectively.

in humans. A total of 99 articles were further reviewed and qualified through a full-text review (**Figure 1A**), referring to 89 studies in mice, seven in rats, two in dogs, and one in cattle. A total of 44 genes [42 genes in mice with single gene mutations and two additional genes (*Bmp4* and *Stim2*) in compound mutant models] were identified in mice as genes associated with amelogenesis imperfecta through the systematic review (**Supplementary Table S2**). A search of the Mouse Genome Informatics (MGI) database identified a total of 59 mouse lines after the removal of duplicates. Upon validation of the enamel phenotype through review of the extracted articles, we identified 35 genes primarily associated with amelogenesis imperfecta (**Supplementary Table S3**). Among these 35 genes, 15 were uniquely found in the MGI search, and 19 were common in the systematic review and MGI search. Through a manual literature search, we identified additional 11 genes associated with amelogenesis imperfecta (**Supplementary Table S4**). As a result, a total of 70 genes were identified and curated [68 genes in single-gene mutant mice (**Table 1**) and two additional genes (after exclusion of overlapping genes in **Table 1**) in compound mutant mice (**Table 2**)] as genes associated with amelogenesis imperfecta (a.k.a. enamel hypoplasia) in mice (**Figure 1B**), hereafter referred as mouse amelogenesis imperfecta-related genes (mAIGenes). In addition, we found that three genes in rats, three genes in dogs, and one gene in cattle were reported in amelogenesis imperfecta (**Supplementary Table S5**). Among the 70 genes, mutations in 33 genes were reported in humans with amelogenesis imperfecta in isolated or syndromic cases.

These mAIGenes were further categorized into three classes of amelogenesis imperfecta based on gross anatomical observation, histological analysis, microCT, and component analyses, which all are established in human cases: hypoplastic/enamel hypoplasia/no enamel (40 genes), hypomaturation (6 genes), hypomineralized/hypocalcified (39 genes), and unknown detailed classification (4 genes) (**Table 3**). Some genes exhibited a combined phenotype, as seen in humans. It should be noted that different mutational strategies for deletion, overexpression, or knock-in of the same gene sometimes

TABLE 5 | Top functional enrichment clusters.

Pathway	Cluster #
positive regulation of cell migration	1
transforming growth factor-beta receptor signaling pathway	1
growth factor activity	1
transforming growth factor-beta receptor binding	1
TGF-beta signaling pathway	1
apical junction complex	2
cell adhesion molecule binding	2
adherens junction	2
colorectal cancer	2
basement membrane	3
laminin-5 complex	3
pathways in cancer	3
focal adhesion	3
enamel mineralization	4
biomineral tissue development	4
odontogenesis of dentin-containing tooth	4
structural constituent of tooth enamel	4
proteinaceous extracellular matrix	5
extracellular region	5
protein binding	6

resulted in different tooth phenotypes. This suggests that subtle changes in the expression or deletion of non-coding genomic sequences may affect the expression and function of genes that are crucial for enamel formation.

Among the mAIGenes, 12 genes (*Ambn*, *Amelx*, *Amtn*, *Col17a1*, *Csf1*, *Dmp1*, *Dspp*, *Enam*, *Lama3*, *Lamb3*, *Lamc2*, and *Postn*) were grouped in the extracellular matrix (ECM) pathway, 11 genes (*Alpl*, *Fam20a*, *Fam20c*, *Hras*, *Klk4*, *Map3k7*, *Mmp20*, *Plau*, *Rac1*, *Rhoa*, and *Tcirg1*) in the enzyme pathway, and seven genes (*Cftr*, *Cnnm4*, *Slc4a4*, *Slc10a7*, *Slc12a2*, *Slc13a5*, and *Slc24a4*) in the ion exchanger/transporter pathway. Moreover, three genes (*Stim1*, *Stim2*, and *Tmbim6*) were related to a calcium ion sensor or regulator, and six genes (*Cldn3*, *Cldn16*, *Ctnnb1*, *Gja1*, *Nectin1*, and *Nectin3*) were involved in cell-cell or cell-ECM adhesions. Since ameloblasts secrete enamel proteins, mutations in genes related to ECM and enamel proteins support their causal roles in amelogenesis imperfecta. In addition, a substantial number of genes were involved in growth factor signaling cascades: four were growth factors (*Bmp2*, *Bmp4*, *Gdnf*, and *Tgfb1*), five receptors (*Fgfr1*, *Itgb1*, *Itgb6*, *Relt*, and *Tgfbr2*), 15 transcription factors (*Ascl5*, *Bcl11b*, *Ctnnb1*, *Dlx3*, *Foxo1*, *Irf6*, *Msx2*, *Pax9*, *Pitx2*, *Runx1*, *Runx2*, *Sp3*, *Sp6*, *Sp7*, and *Tbx1*), two transcriptional regulators (*Hmgn2* and *Med1*), and one a signal mediator (*Smad3*). Since these factors are involved in various developmental processes, the mutations would be related to syndromic cases with various developmental defects beyond amelogenesis imperfecta (**Table 4**).

Functional Enrichment Analysis of mAIGenes

To further explore the functional features of mAIGenes, we performed a functional enrichment analysis and functional module cluster analysis (**Figure 2A**). Using a false discovery rate (FDR) < 0.01, we obtained 32 gene sets that were significantly enriched in mAIGenes, including four pathways from Kyoto Encyclopedia of Genes and Genomes (KEGG) annotations, 24 Gene Ontology (GO) Biological Process (BP) terms, three GO Cellular Component (CC) terms, and one GO Molecular Function (MF) term (**Table 5**). Among the top 20 most significant gene sets, genes associated with tooth development (e.g., enamel mineralization, biomineral tissue development, and odontogenesis of dentin-containing tooth) were among the most significantly enriched (**Figure 2B**). To investigate how these functional terms and pathways are interrelated, we used the k-means algorithm to cluster them (**Supplementary Figure S1A**). This analysis revealed four groups (**Table 5**), including the 32 gene sets mentioned above and 63 mAIGenes in the module network (**Figure 2C**). The groups were ordered by number of gene set, with the smaller number being named first. Group 1 had one gene set— "Protein binding" —, which included *Stim1*, *Stim2*, *Slc4a4*, *Slc12a2*, etc. (**Figure 2C**), whereas Group 2 was related to biomineral development and ECM. These two pathways are closely related, since most of the biomineral development process occurs in extracellular fluids (**Figure 2C**). *Enam*, *Ambn*, *Amtn*, and *Amelx* were commonly involved in biomineralization during tooth enamel development and located at the ECM (**Figure 2C**). Cell proliferation and cancer-related gene sets were clustered in Group 3, including "Cell proliferation", "Pathways in cancer", "Cell adhesion", and "Positive regulation of cell migration" (**Figure 2C**). Group 4 highly reflected the tooth and bone development, as it contained "Odontogenesis of biomineral tissue development", "Odontogenesis of dentin-containing tooth", "Ossification", "Osteoblast differentiation", and "Skeletal system development" (**Figure 2C**). *Bmp2*, *Bmp4*, and *Runx2* connected most of the gene sets in Group 4 (**Supplementary Figure S1B**), and these genes have been reported to play critical roles in bone development.

miRNA-mAIGene Regulatory Network and Identification of Critical miRNAs

For the miRNA-mAIGene regulatory network analysis, we performed miRNA-mAIGene enrichment analysis and miRNA regulatory network analysis (**Figure 3A**). We identified 35 Highly Expressed MiRNAs (HEMs) in mouse incisors and 32 HEMs in molars with a frequency >1%; 26 mouse tooth HEMs were then curated by taking the intersection of the incisor and molar HEMs (**Supplementary Table S6**) [26]. A total of 21 of these HEMs did not have a confident -3p or -5p; therefore, we considered that these had both -3p and -5p and identified 47 HEMs, all with a certain -3p or -5p. Based on these 47 HEMs, we predicted that 32 HEMs might target the 42 mAIGenes by using our pipeline and the four miRNA-target gene databases: TargetScan, miRanda, miRTarBase, and PITA. By performing the miRNA-mAIGene regulatory relationship enrichment analysis with a cutoff adjusted p-value < 0.05, we identified 27 notable miRNAs, 41 genes, and 161 miRNA-mAIGene pairs. A total of 17 miRNAs or miRNA groups, 41 genes, and 103 miRNA-mAIGene pairs were extracted after merging the miRNAs or miRNA groups that shared the same targets (such as miR-23a/b-3p and miR-125a/b-5p) (**Table 6**). Three miRNAs (miR-16-5p, miR-27b-3p, and miR-

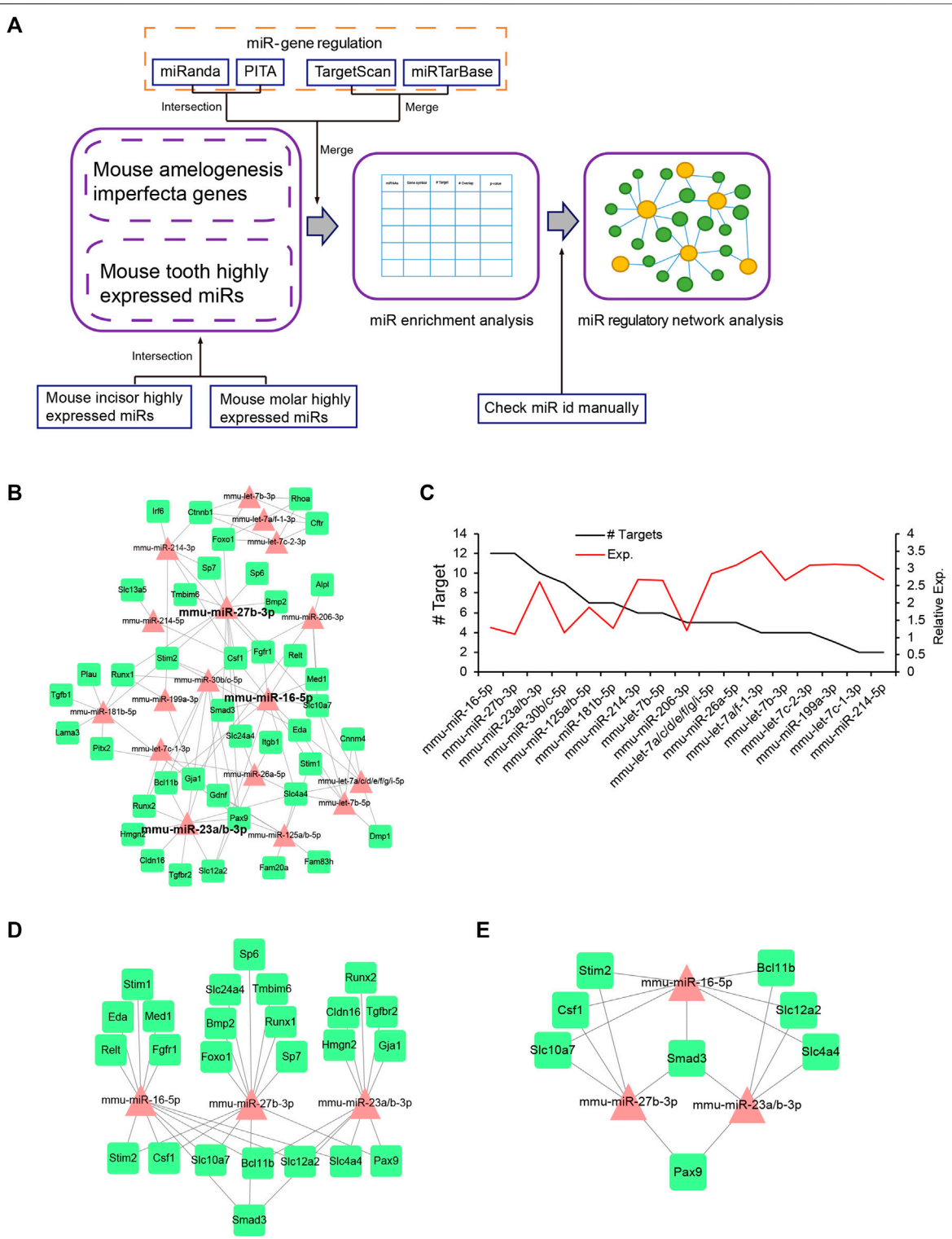

FIGURE 3 | miRNA-mAlGene regulatory network and features. **(A)** Flowchart of the miRNA regulatory network analysis. The miRNA-mAlGene pairs were first identified using four miR-target databases with adjusted *p*-value < 0.05. Next, the miRNA regulatory network analysis was performed. **(B)** The miRNA regulatory network, which included 17 miRNAs, 41 mAlGenes, and 103 miRNA-mAlGene pairs. Three miRNAs (i.e., miR-16-5p, miR-27b-3p, and miR-23a/b-3p) were the hub miRNAs in the network. **(C)** Degree distribution of the miRNAs in the miRNA-mAlGene regulatory network in B, with miR-16-5p, miR-27b-3p, and miR-23a/b-3p having the highest degrees. **(D)** The sub-network of miR-16-5p, miR-27b-3p, and miR-23a/b-3p. **(E)** The sub-network of genes regulating more than two miRNAs in **Figure 3D**.

TABLE 6 | MicroRNA (miRNA) enrichment analysis of mouse genes related to amelogenesis imperfecta.

miR ID	Target Genes	# Targets	Adjusted *p*-value	FDR
miR-16-5p	*Bcl11b*, *Csf1*, *Eda*, *Fgfr1*, *Med1*, *Relt*, *Slc4a4*, *Slc10a7*, *Slc12a2*, *Smad3*, *Stim1*, *Stim2*	12	3.94×10^{-7}	1.63×10^{-3}
miR-27b-3p	*Bmp2*, *Csf1*, *Foxo1*, *Pax9*, *Runx1*, *Slc10a7*, *Slc24a4*, *Smad3*, *Sp6*, *Sp7*, *Stim2*, *Tmbim6*	12	4.12×10^{-7}	1.69×10^{-3}
miR-23a/b-3p	*Bcl11b*, *Cldn16*, *Gja1*, *Hmgn2*, *Pax9*, *Runx2*, *Slc4a4*, *Slc12a2*, *Smad3*, *Tgfbr2*	10	8.51×10^{-6}	2.01×10^{-3}
miR-214-3p	*Csf1*, *Ctnnb1*, *Fgfr1*, *Irf6*, *Sp7*, *Stim2*	6	9.38×10^{-5}	1.43×10^{-3}
miR-30b/c-5p	*Bcl11b*, *Csf1*, *Eda*, *Gdnf*, *Gja1*, *Pax9*, *Runx1*, *Runx2*, *Stim2*	9	3.82×10^{-4}	4.49×10^{-3}
miR-125a/b-5p	*Fam20a*, *Fam83h*, *Gdnf*, *Gja1*, *Pax9*, *Slc4a4*, *Stim1*	7	7.57×10^{-4}	7.86×10^{-3}
let-7a/f-1-3p	*Cftr*, *Ctnnb1*, *Foxo1*, *Rhoa*	4	9.98×10^{-4}	9.85×10^{-3}
let-7b-3p	*Cftr*, *Ctnnb1*, *Foxo1*, *Rhoa*	4	9.98×10^{-4}	9.85×10^{-3}
let-7c-2-3p	*Cftr*, *Ctnnb1*, *Foxo1*, *Rhoa*	4	9.98×10^{-4}	9.85×10^{-3}
miR-181b-5p	*Lama3*, *Pax9*, *Plau*, *Pitx2*, *Runx1*, *Stim2*, *Tgfb1*	7	3.03×10^{-3}	2.45×10^{-2}
miR-206-3p	*Alpl*, *Csf1*, *Gja1*, *Med1*, *Slc10a7*	5	8.07×10^{-3}	5.53×10^{-2}
let-7c-1-3p	*Gdnf*, *Runx2*	2	1.29×10^{-2}	8.20×10^{-2}
let-7b-5p	*Cnnm4*, *Dmp1*, *Eda*, *Slc4a4*, *Slc10a7*, *Stim1*	6	1.77×10^{-2}	1.07×10^{-1}
miR-199a-3p	*Gja1*, *Runx1*, *Stim2*	3	3.40×10^{-2}	1.89×10^{-1}
let-7a/c/d/e/f/g/i-5p	*Cnnm4*, *Dmp1*, *Eda*, *Slc4a4*, *Slc10a7*	5	3.43×10^{-2}	1.90×10^{-1}
miR-214-5p	*Csf1*, *Slc13a5*	2	3.92×10^{-2}	2.14×10^{-1}
miR-26a-5p	*Itgb1*, *Pitx2*, *Slc4a4*, *Slc12a2*, *Slc24a4*	5	4.91×10^{-2}	2.62×10^{-1}

Adjusted p*-value < 0.05 was used as the cutoff threshold. FDR: false discovery rate. miRNAs sharing the same target genes and with the same adjusted* p*-value were merged (e.g., miR-23a/b-3p).*

23a/b-3p) were considered to be hubs in the miRNA regulatory network (**Figure 3B**) because they had the highest degrees (**Figure 3C**, **Supplementary Table S7**), which are defined as the number of partners that immediately interact with a node of interest in the network (Sun et al., 2012), and the lowest adjusted *p*-values (**Table 6**). The sub-network of miR-16-5p, miR-27b-3p, and miR-23a/b-3p showed that Smad3 was regulated by all the three hub miRNAs. *Stim2*, *Csf1*, *Slc10a7*, *Bcl11b*, *Slc12a2*, *Slc12a2*, *Slc4a4*, and *Pax9* were regulated by two of these three hub miRNAs or miRNA group, whereas the other genes were regulated by one miRNA or miRNA group (**Figures 3D,E**). As above, miR-16-5p, miR-27b-5p, and miR-23a/b-3p were considered to be promising miRNA candidates for amelogenesis imperfecta in mice.

Experimental Validation

To evaluate the function of the miRNAs predicted by the bioinformatic analyses, we conducted ameloblast differentiation assays using mHAT9d cells, a mouse dental epithelial cell line. Although the mouse ameloblast-like cells LS8 (Chen et al., 1992) have been widely used for ameloblast studies, they are limited in their ability to differentiate. We analyzed both LS8 and mHAT9d cells under differentiation conditions and found that mHAT9d cells reacted better to the induction of differentiation (**Figure 4A**). For instance, the expression of the ameloblast differentiation maker genes was induced more strongly in mHAT9d cells compared to LS8 cells (**Supplementary Figures S2, S3**). Therefore, mHAT9d cells were used in this study. We found that expression of ameloblast differentiation marker genes (i.e., *Ambn*, *Amelx*, *Enam*, *Klk4,* and *Mmp20*) was induced with ameloblast differentiation medium (**Figure 4B**, **Supplementary Figure S3**). In addition, we tested whether other genes associated with amelogenesis imperfecta were induced. Among the 27 genes regulated by miR-16-5p, miR-23a-3p, miR-23b-3p, miR-27b-3p, and miR-214-3p, we found 14 genes that were upregulated under differentiation conditions (**Supplementary Figure S4**). miR-16-5p and miR-27b-3p were induced at relatively high expression levels in mHAT9d cells, and their expression did not change under differentiation conditions (**Supplementary Figure S5A**). In addition, we found that miR-16-5p and miR-27b-3p were expressed at the pre-secretion, secretion, and maturation stages of ameloblast differentiation in mouse lower incisors (**Supplementary Figure S5B**). Overexpression of either miR-16-5p or miR-27b-3p significantly anti-correlated with downregulation of expression of *Amelx* and *Enam,* but not *Ambn*, *Klk4*, and *Mmp20*, in mHAT9d cells (**Figure 4B**). We confirmed that the expression levels of AMELX, but not KLK4 and MMP20, were decreased by overexpression of miR-16-5p and miR-27b-3p with immunoblotting (**Figure 4C**). The expression of AMELX was further confirmed by immunocytochemical analysis (**Figure 4D**). By contrast, mimics for miR-23a-3p, miR-23b-3p, and miR-214-3p did not affect the gene expression of the ameloblast differentiation makers (**Figure 4B**). These results indicate that miR-16-5p and miR-27b-3p may play a critical role in ameloblast differentiation through the regulation of genes that are crucial for ameloblast differentiation.

Next, to identify the miRNA-mAIGene regulatory mechanism(s), we conducted quantitative RT-PCR (qRT-PCR) analyses for the predicted target genes for each miRNA (*Bcl11b*, *Csf1*, *Eda*, *Fgfr1*, *Med1*, *Relt*, *Slc4a4*, *Slc10a7*, *Slc12a2*, *Smad3*, *Stim1*, and *Stim2* for miR-16-5p; *Bmp2*, *Csf1*, *Foxo1*, *Pax9*, *Runx1*, *Slc10a7*, *Slc24a4*, *Smad3*, *Sp6, Sp7*, *Stim2*, and *Tmbim6* for miR-27b-3p) in mHAT9d cells. The expression of *Eda*, *Relt*, *Slc4a4*, and *Smad3* was significantly downregulated in mHAT9d cells treated with miR-16-5p mimic (**Figure 5A**, **Supplementary Figure S6**). Similarly, the expression of *Bmp2*, *Pax9*, and *Slc24a4* was significantly downregulated in mHAT9d cells treated with miR-27b-3p mimic (**Figure 5B**, **Supplementary Figure S6**). Furthermore, we confirmed that treatment of inhibitor for either miR-16-5p or miR-27b-3p had no effect on expression of *Amelx* and *Enam*, while the expression of the target genes of

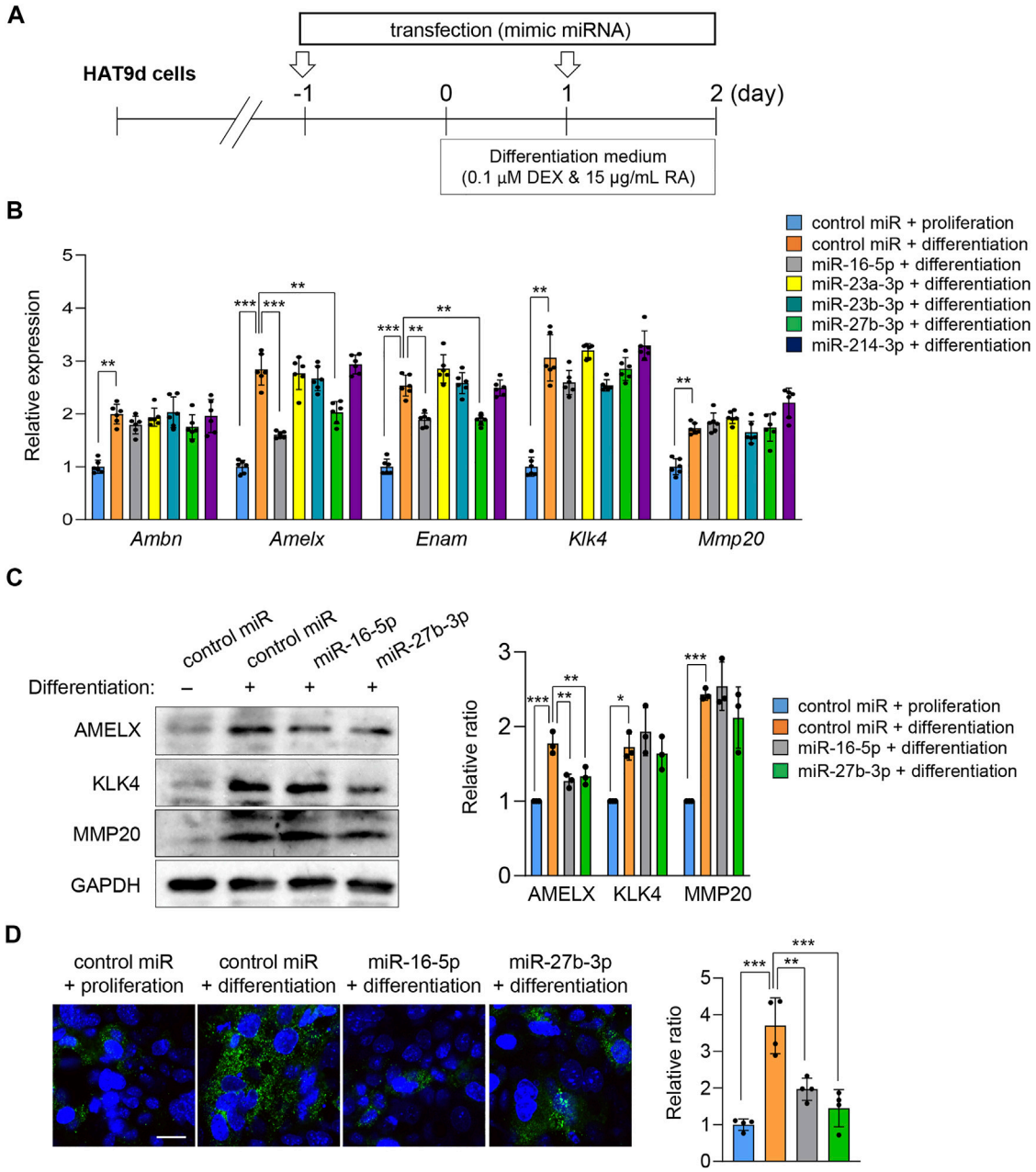

FIGURE 4 | Effects of overexpression of candidate miRNAs asssociated with amelogenesis imperfecta on ameloblast differentiation. **(A)** Schematic of the experiment. **(B)** Gene expression of the indicated genes after treatment with the mimic for the indicated miRNA in mHAT9d cells ($n = 6$). $^{**}p < 0.01$; $^{***}p < 0.001$. **(C)** Immunoblotting for AMELX, KLK4, MMP20, and GAPDH (internal control) in mHAT9d cells under the indicated conditions. Graph shows the quantification of the immunoblotting. $n = 3$ per group. $^{*}p < 0.05$; $^{**}p < 0.01$; $^{***}p < 0.001$. **(D)** ICC for AMELX in mHAT9d cells under the indicated conditions. Scale bar, 50 μm. Graph shows the quantification of images from four independent experiments. $^{**}p < 0.01$; $^{***}p < 0.001$.

each miRNA was upregulated (**Supplementary Figure S7**). Indeed, the predicted target genes contained miRNA recognition sites for their correlated miRNAs on the 3′-UTR (**Supplementary Figure S8**). By contrast, there was no potential recognition site for miR-16-5p on *Amelx* and *Enam* and for miR-27b-3p on *Amelx*, while there was a potential recognition site for miR-27b-3p on *Enam*, and treatment with either mimic or inhibitor for miR-16-5p and miR-27b-3p failed to alter the expression of *Amelx* and *Enam*, suggesting that these genes are indirectly regulated by miR-16-5p and miR-27b-3p in mHAT9d cells.

Finally, to examine the functional relevance of genes that were significantly downregulated under treatment with either miR-16-5p or miR-27b-3p mimic, we conducted rescue experiments by

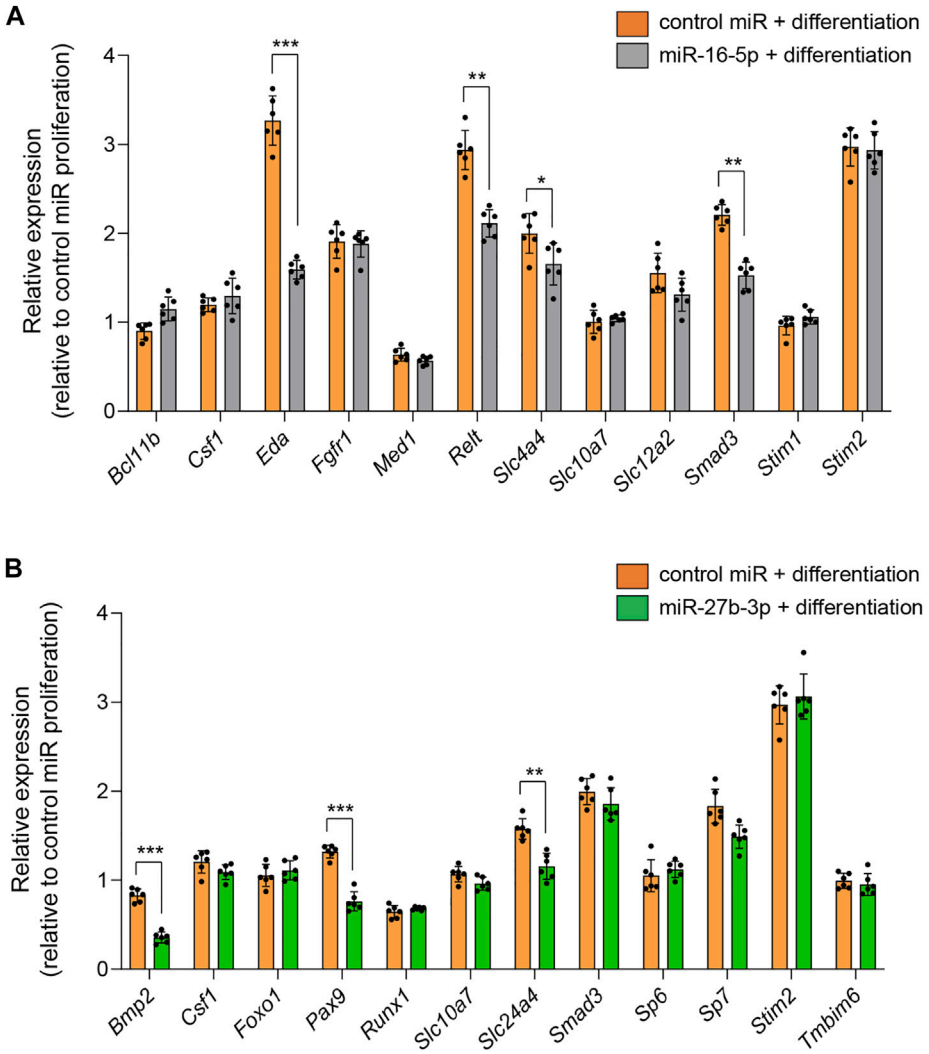

FIGURE 5 | Effects of overexpression of miR-16-5p and miR-27b-3p on expression of target genes. **(A)** Quantitative RT-PCR analyses for target genes after treatment with control and miR-16-5p mimic under differentiation conditions ($n = 6$). $^{*}p < 0.05$; $^{**}p < 0.01$; $^{***}p < 0.001$. **(B)** Quantitative RT-PCR analyses for target genes after treatment with control and miR-27b-3p mimic under differentiation conditions ($n = 6$). $^{**}p < 0.01$; $^{***}p < 0.001$.

overexpressing the target genes (**Figure 6A**). We found that overexpression of *Eda, Relt,* and *Smad3* under conditions of overexpression of miR-16-5p partially restored mRNA and protein expression of *Amelx* and *Enam* (**Figures 6B,C**). Similarly, overexpression of *Bmp2*, *Pax9*, and *Slc24a4* partially restored mRNA and protein expression of *Amelx* and *Enam* when miR-27b-3p was overexpressed (**Figures 6B,C**). Taken together, our results show that overexpression of miR-16-5p and miR-27b-3p inhibits ameloblast differentiation through the regulation of *mAIGenes*.

DISCUSSION

This study aimed to identify regulatory networks for the genes and miRNAs involved in amelogenesis imperfecta in mouse models. Through a literature and MGI searches, we identified 70 genes associated with ameloblast imperfecta and predicted 27 miRNAs to be involved in the development of amelogenesis imperfecta in mice. We found that overexpression of miR-16-5p and miR-27b-3p in mHAT9d cells suppresses *Amelx* and *Enam* under ameloblast differentiation conditions, respectively.

In this study, we found that overexpression of miR-16-5p inhibited expression of *Eda*, *Relt*, *Slc4a4*, and *Smad3*. miR-16-5p has been detected in osteosarcoma, osteoarthritis, and bone fracture healing. Its overexpression induces suppression of *SMAD3*, resulting in inhibition of cell proliferation, migration, and invasion in osteosarcoma cells (Gu et al., 2020), and in downregulation of *COL2A1* and *Aggrecan* and upregulation of *ADAMTS* in chondrocytes, which may be involved in the

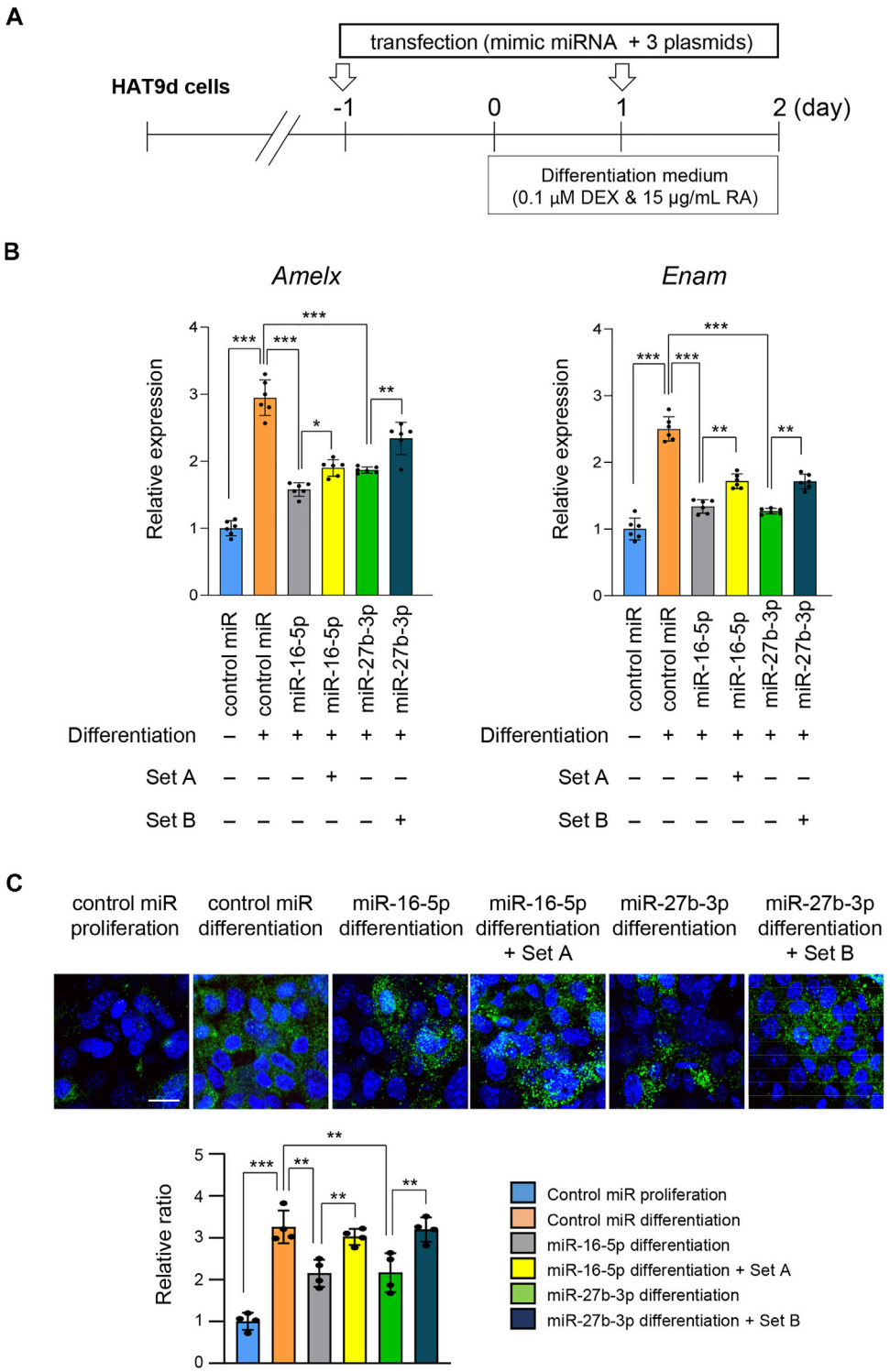

FIGURE 6 | Overexpression of target genes following overexpression of miR-16-5p and miR-27b-3p. **(A)** Schematic of the experiment. **(B)** Gene expression of Amelx and Enam following overexpression of Eda, Relt, and Smad3 under overexpression of control and miR-16-5p mimic, or of Bmp2, Pax9, and Slc24a4 under overexpression of control and miR-27b-3p mimic, in mHAT9d cells ($n = 6$). *$p < 0.05$; **$p < 0.01$; ***$p < 0.001$. **(C)** ICC for AMELX in mHAT9d cells under the indicated conditions. Scale bar, 50 μm. Graph shows the quantification of images from four independent experiments. **$p < 0.01$; ***$p < 0.001$.

development of osteoarthritis (Li et al., 2015). In addition, overexpression of miR-16-5p suppresses *BACH2* in gingival epithelial cells and *Bcl2* and *Ccnd1* in MC3T3-E1 cells, resulting in apoptosis and G1/S cell cycle arrest (Sun Y. et al., 2019; Liu et al., 2020).

RELT, a TNF receptor superfamily, is cleaved at the extracellular domain by ADAM10, a metalloprotease that is expressed at the apical loop during the transition stage of ameloblasts (Ikeda et al., 2019). ADAM10 also cleaves type XVII collagen, a component of the basement membrane (Franzke et al., 2009). Mice deficient for either *Relt* or *Col17a1* display a hypomineralized enamel defect (Asaka et al., 2009; Kim et al., 2019). Currently, no mutations in *ADAM10* have been reported in amelogenesis imperfecta in humans and mice; therefore, the role of ADAM10 in amelogenesis imperfecta is unclear.

EDA is a TNF family transmembrane protein that binds to its receptor EDAR and initiates NF-κB signaling. Overexpression of *Eda* in mice results in hypoplastic amelogenesis imperfecta (Mustonen et al., 2003); in humans, mutations in either *EDA* or *EDAR* have been found in hypohidrotic ectodermal dysplasia and isolated tooth agenesis, but not in amelogenesis imperfecta (Shen et al., 2019; Wright et al., 2019; Yu et al., 2019; Andreoni et al., 2021).

SLC4A4, a sodium bicarbonate co-transporter (NBCe1), is involved in the regulation of bicarbonate transportation and intracellular pH homeostasis (Bernardo et al., 2006; Urzua et al., 2011). Mice deficient for *Slc4a4* exhibit hypomineralized amelogenesis imperfecta; therefore, NBCe1 is responsible for a change in extracellular pH during enamel maturation (Lacruz et al., 2010; Jalali et al., 2014).

SMAD3 transduces canonical TGF-β signals together with SMAD2 and SMAD4 in the regulation of downstream genes under developmental and pathological conditions. *Smad3* knockout mice exhibit hypomineralized amelogenesis imperfecta through downregulation of genes involved in biomineralization (e.g., *Ambn*, *Amel*, *Enam*, *Mmp20*, *Klk4*, and *Gja1*) (Yokozeki et al., 2003; Poche et al., 2012).

In addition, we found that overexpression of miR-27b-3p inhibits expression of *Bmp2*, *Pax9*, and *Slc24a4*. Previous studies suggest that overexpression of miR-27b-3p in stem cells in the bone marrow or the maxillary sinus membrane suppresses osteogenic differentiation via suppression of *KDM4B* or *Sp7*, respectively (Peng et al., 2017; Zhang et al., 2020). Moreover, miR-27b-3p is downregulated in cartilage in patients with rheumatoid arthritis compared to healthy individuals. In chondrocytes, overexpression of miR-27b-3p suppresses Caspase-3 and upregulates BCL-2, resulting in apoptosis inhibition (Zhou et al., 2019).

BMP2 is a TGF-β superfamily growth factor involved in the development and homeostasis of mineral tissues (Chen et al., 2004; Halloran et al., 2020). Mice with a deletion of *Bmp2* in osteogenic and odontogenic cells (*Osx-Cre;Bmp2*$^{F/F}$ cKO) exhibit hypomineralized amelogenesis imperfecta and incisal malocclusion through downregulation of *Enam*, *Amelx*, *Mmp20*, and *Klk4* (Feng et al., 2011; Guo et al., 2015). Moreover, mice with an odontoblast-specific deletion of *Bmp2* (*Dmp1-Cre;Bmp2* and *Wnt1-Cre;Bmp2* cKO) show dentinogenesis imperfecta without enamel formation defects (Jani et al., 2018; Malik et al., 2018).

PAX9, a transcription factor, plays a role in craniofacial and skeletal development, including the development of tooth, bone, cartilage, and muscle (Monsoro-Burq, 2015; Farley-Barnes et al., 2020). Several single nucleotide polymorphisms (SNPs) in *PAX9* are reported to be associated with tooth size and shape as well as tooth agenesis (Lee et al., 2012; Wong et al., 2018; Safari et al., 2020; Alkhatib et al., 2021). While *Pax9* null mice exhibit cleft palate and tooth developmental arrest at the bud stage (Zhou et al., 2011), hypomorphic *Pax9* mutant mice exhibit hypoplastic amelogenesis imperfecta in the lower incisors and tooth agenesis of the third molars (Kist et al., 2005).

SLC24A4, a potassium-dependent sodium/calcium exchanger (NCKX4), is expressed in ameloblasts at the maturation stage and plays an important role in calcium ion transport by exchanging intracellular Ca^{2+} and K^{+} with extracellular Na^{2+} for Ca^{2+} supply into the developing enamel crystals (Hu et al., 2012; Bronckers et al., 2015). A deficiency of *Slc24a4* causes hypomineralized amelogenesis imperfecta in mice (Parry et al., 2013), and mutations in *SLC24A4* are associated with isolated amelogenesis imperfecta (either hypomineralized or hypomaturation types) in humans (Parry et al., 2013; Seymen et al., 2014; Herzog et al., 2015; Khan et al., 2020).

Our results from the rescue experiments suggest that miR-16-5p and miR-27b-3p are involved in amelogenesis imperfecta through dysregulation of mAIGenes. In summary, our systematic search for mAIGenes provides an overview of the genes involved in this condition. Our bioinformatics pipeline identified three potential miRNAs that may actively interact with mAIGenes, and two of these miRNAs were experimentally validated in mouse cell lines. These results will expand our knowledge of the genetics of amelogenesis imperfecta in animal models, which can be translated into human studies and help develop clinical approaches for diagnosis and treatment. We will need to further evaluate the functional significance of these miRNA-gene regulatory networks *in vivo*. Both the negative and positive feedback loops between the miRNAs and target genes should also be further evaluated in various cell lines and *in vivo* since miRNAs may regulate the expression of multiple genes and multiple miRNAs may regulate the expression of a single gene. In addition, transcription factors may be involved in these miRNA-gene regulatory networks; for example, a direct regulation between miRNA and mAIGenes may be bypassed through other transcription factors.

DATA AVAILABILITY STATEMENT

The original contributions presented in the study are included in the article/**Supplementary Material**, further inquiries can be directed to the corresponding authors.

AUTHOR CONTRIBUTIONS

Conceived and designed the experiments: AS, HY, and JI. Performed the systematic review: AS, AG, and NS. Performed MGI screenings: AS and TL. Performed bioinformatics analyses: TL and ZZ. Performed the experiments: HY. Prepared the manuscript: AS, HY, TL, ZZ, and JI. All authors read and approved the final manuscript.

FUNDING

This study was partially supported by grants from the NIH National Institute of Dental and Craniofacial Research (R03DE026208, R01DE026767, R03DE026509, and R03DE028340 to JI; R01LM012806, R01DE030122, R03DE027393, and R03DE028103 to ZZ) and a faculty fund from UTHealth School of Dentistry to JI. The funders had no role in study design, data collection and analysis, decision to publish, or manuscript preparation.

ACKNOWLEDGMENTS

We thank Hidemitsu Harada (Iwate Medical University, Iwate, Japan) for the mHAT9d cells and Malcolm Snead (University of Southern California) for the LS8 cells. We thank Amy Taylor (Texas Medical Center Library) for her valuable assistance with the systematic review.

SUPPLEMENTARY MATERIAL

The Supplementary Material for this article can be found online at: https://www.frontiersin.org/articles/10.3389/fgene.2022.788259/full#supplementary-material

REFERENCES

Agarwal, V., Bell, G. W., Nam, J. W., and Bartel, D. P. (2015). Predicting Effective microRNA Target Sites in Mammalian mRNAs. *Elife* 4. doi:10.7554/eLife.05005

Aldred, M. J., and Crawford, P. J. (1995). Amelogenesis Imperfecta-Ttowards a New Classification. *Oral Dis.* 1, 2–5. doi:10.1111/j.1601-0825.1995.tb00148.x

Aldred, M., Savarirayan, R., and Crawford, P. (2003). Amelogenesis Imperfecta: a Classification and Catalogue for the 21st century. *Oral Dis.* 9, 19–23. doi:10.1034/j.1601-0825.2003.00843.x

Alkhatib, R., Obeidat, B., Al-Eitan, L., Abdo, N., Obeidat, F., and Aman, H. (2021). Family-based Association Study of Genetic Analysis of Paired Box Gene 9 Polymorphisms in the Peg-Shaped Teeth in the Jordanian Arab Population. *Arch. Oral Biol.* 121, 104966. doi:10.1016/j.archoralbio.2020.104966

Altug-Atac, A. T., and Erdem, D. (2007). Prevalence and Distribution of Dental Anomalies in Orthodontic Patients. *Am. J. Orthod. Dentofacial Orthopedics* 131, 510–514. doi:10.1016/j.ajodo.2005.06.027

Andreoni, F., Sgattoni, C., Bencardino, D., Simonetti, O., Forabosco, A., and Magnani, M. (2021). Missense Mutations in EDA and EDAR Genes Cause Dominant Syndromic Tooth Agenesis. *Mol. Genet. Genomic Med.* 9, e1555. doi:10.1002/mgg3.1555

Asaka, T., Akiyama, M., Domon, T., Nishie, W., Natsuga, K., Fujita, Y., et al. (2009). Type XVII Collagen Is a Key Player in Tooth Enamel Formation. *Am. J. Pathol.* 174, 91–100. doi:10.2353/ajpath.2009.080573

Backman, B., and Holm, A.-K. (1986). Amelogenesis Imperfecta: Prevalence and Incidence in a Northern Swedish County. *Commun. Dent Oral Epidemiol.* 14, 43–47. doi:10.1111/j.1600-0528.1986.tb01493.x

Bernardo, A. A., Bernardo, C. M., Espiritu, D. J., and Arruda, J. A. L. (2006). The Sodium Bicarbonate Cotransporter: Structure, Function, and Regulation. *Semin. Nephrol.* 26, 352–360. doi:10.1016/j.semnephrol.2006.07.008

Bonnet, A. L., Sceosole, K., Vanderzwalm, A., Silve, C., Collignon, A. M., and Gaucher, C. (2020). "Isolated" Amelogenesis Imperfecta Associated with DLX3 Mutation: A Clinical Case. *Case Rep. Genet.* 2020, 8217919. doi:10.1155/2020/8217919

Bronckers, A. L. J. J., Lyaruu, D., Jalali, R., Medina, J. F., Zandieh-Doulabi, B., and Denbesten, P. K. (2015). Ameloblast Modulation and Transport of Cl−, Na+, and K+ during Amelogenesis. *J. Dent Res.* 94, 1740–1747. doi:10.1177/0022034515606900

Cao, H., Wang, J., Li, X., Florez, S., Huang, Z., Venugopalan, S. R., et al. (2010). MicroRNAs Play a Critical Role in Tooth Development. *J. Dent Res.* 89, 779–784. doi:10.1177/0022034510369304

Chen, D., Zhao, M., and Mundy, G. R. (2004). Bone Morphogenetic Proteins. *Growth Factors* 22, 233–241. doi:10.1080/08977190412331279890

Chen, L. S., Couwenhoven, R. I., Hsu, D., Luo, W., and Snead, M. L. (1992). Maintenance of Amelogenin Gene Expression by Transformed Epithelial Cells of Mouse Enamel Organ. *Arch. Oral Biol.* 37, 771–778. doi:10.1016/0003-9969(92)90110-t

Crawford, P. J., Aldred, M., and Bloch-Zupan, A. (2007). Amelogenesis Imperfecta. *Orphanet J. Rare Dis.* 2, 17. doi:10.1186/1750-1172-2-17

Cui, J., Xiao, J., Tagliabracci, V. S., Wen, J., Rahdar, M., and Dixon, J. E. (2015). A Secretory Kinase Complex Regulates Extracellular Protein Phosphorylation. *Elife* 4, e06120. doi:10.7554/eLife.06120

Fan, Y., Zhou, Y., Zhou, X., Xu, X., Pi, C., Xu, R., et al. (2015). Epigenetic Control of Gene Function in Enamel Development. *Cscr* 10, 405–411. doi:10.2174/1574888x10666150305104730

Farley-Barnes, K. I., Deniz, E., Overton, M. M., Khokha, M. K., and Baserga, S. J. (2020). Paired Box 9 (PAX9), the RNA Polymerase II Transcription Factor, Regulates Human Ribosome Biogenesis and Craniofacial Development. *Plos Genet.* 16, e1008967. doi:10.1371/journal.pgen.1008967

Farmer, D. J. T., and Mcmanus, M. T. (2017). MicroRNAs in Ectodermal Appendages. *Curr. Opin. Genet. Develop.* 43, 61–66. doi:10.1016/j.gde.2016.12.006

Feng, J., Yang, G., Yuan, G., Gluhak-Heinrich, J., Yang, W., Wang, L., et al. (2011). Abnormalities in the Enamel in Bmp2-Deficient Mice. *Cells Tissues Organs* 194, 216–221. doi:10.1159/000324644

Franzke, C.-W., Bruckner-Tuderman, L., and Blobel, C. P. (2009). Shedding of Collagen XVII/BP180 in Skin Depends on Both ADAM10 and ADAM9. *J. Biol. Chem.* 284, 23386–23396. doi:10.1074/jbc.m109.034090

Gadhia, K., Mcdonald, S., Arkutu, N., and Malik, K. (2012). Amelogenesis Imperfecta: an Introduction. *Br. Dent J.* 212, 377–379. doi:10.1038/sj.bdj.2012.314

Gu, Z., Li, Z., Xu, R., Zhu, X., Hu, R., Xue, Y., et al. (2020). miR-16-5p Suppresses Progression and Invasion of Osteosarcoma via Targeting at Smad3. *Front. Pharmacol.* 11, 1324. doi:10.3389/fphar.2020.01324

Guo, A.-Y., Sun, J., Jia, P., and Zhao, Z. (2010). A Novel microRNA and Transcription Factor Mediated Regulatory Network in Schizophrenia. *BMC Syst. Biol.* 4, 10. doi:10.1186/1752-0509-4-10

Guo, F., Feng, J., Wang, F., Li, W., Gao, Q., Chen, Z., et al. (2015). Bmp2 Deletion Causes an Amelogenesis Imperfecta Phenotype via Regulating Enamel Gene Expression. *J. Cel. Physiol.* 230, 1871–1882. doi:10.1002/jcp.24915

Halloran, D., Durbano, H. W., and Nohe, A. (2020). Bone Morphogenetic Protein-2 in Development and Bone Homeostasis. *J. Dev. Biol.* 8. doi:10.3390/jdb8030019

Hashem, A., Kelly, A., O'Connell, B., and O'sullivan, M. (2013). Impact of Moderate and Severe Hypodontia and Amelogenesis Imperfecta on Quality of Life and Self-Esteem of Adult Patients. *J. Dentistry* 41, 689–694. doi:10.1016/j.jdent.2013.06.004

Herzog, C. R., Reid, B. M., Seymen, F., Koruyucu, M., Tuna, E. B., Simmer, J. P., et al. (2015). Hypomaturation Amelogenesis Imperfecta Caused by a Novel

SLC24A4 Mutation. *Oral Surg. Oral Med. Oral Pathol. Oral Radiol.* 119, e77–e81. doi:10.1016/j.oooo.2014.09.003

Hu, J.-C., and Simmer, J. (2007). Developmental Biology and Genetics of Dental Malformations. *Orthod. Craniofac. Res.* 10, 45–52. doi:10.1111/j.1601-6343.2007.00384.x

Hu, J. C.-C., Chun, Y.-H. P., Al Hazzazzi, T., and Simmer, J. P. (2007). Enamel Formation and Amelogenesis Imperfecta. *Cells Tissues Organs* 186, 78–85. doi:10.1159/000102683

Hu, P., Lacruz, R. S., Smith, C. E., Smith, S. M., Kurtz, I., and Paine, M. L. (2012). Expression of the Sodium/calcium/potassium Exchanger, NCKX4, in Ameloblasts. *Cells Tissues Organs* 196, 501–509. doi:10.1159/000337493

Huang, H. Y., Lin, Y. C., Li, J., Huang, K. Y., Shrestha, S., Hong, H. C., et al. (2020). miRTarBase 2020: Updates to the Experimentally Validated microRNA-Target Interaction Database. *Nucleic Acids Res.* 48, D148–D154. doi:10.1093/nar/gkz896

Ikeda, A., Shahid, S., Blumberg, B. R., Suzuki, M., and Bartlett, J. D. (2019). ADAM10 Is Expressed by Ameloblasts, Cleaves the RELT TNF Receptor Extracellular Domain and Facilitates Enamel Development. *Sci. Rep.* 9, 14086. doi:10.1038/s41598-019-50277-y

Ishikawa, H. O., Xu, A., Ogura, E., Manning, G., and Irvine, K. D. (2012). The Raine Syndrome Protein FAM20C Is a Golgi Kinase that Phosphorylates Bio-Mineralization Proteins. *PLoS One* 7, e42988. doi:10.1371/journal.pone.0042988

Jalali, R., Guo, J., Zandieh-Doulabi, B., Bervoets, T. J. M., Paine, M. L., Boron, W. F., et al. (2014). NBCe1 (SLC4A4) a Potential pH Regulator in Enamel Organ Cells during Enamel Development in the Mouse. *Cell Tissue Res* 358, 433–442. doi:10.1007/s00441-014-1935-4

Jani, P., Liu, C., Zhang, H., Younes, K., Benson, M. D., and Qin, C. (2018). The Role of Bone Morphogenetic Proteins 2 and 4 in Mouse Dentinogenesis. *Arch. Oral Biol.* 90, 33–39. doi:10.1016/j.archoralbio.2018.02.004

Jiang, W., Mitra, R., Lin, C.-C., Wang, Q., Cheng, F., and Zhao, Z. (2016). Systematic Dissection of Dysregulated Transcription Factor-miRNA Feed-Forward Loops across Tumor Types. *Brief Bioinform* 17, 996–1008. doi:10.1093/bib/bbv107

Jin, Y., Wang, C., Cheng, S., Zhao, Z., and Li, J. (2017). MicroRNA Control of Tooth Formation and Eruption. *Arch. Oral Biol.* 73, 302–310. doi:10.1016/j.archoralbio.2016.08.026

John, B., Enright, A. J., Aravin, A., Tuschl, T., Sander, C., and Marks, D. S. (2004). Human MicroRNA Targets. *Plos Biol.* 2, e363. doi:10.1371/journal.pbio.0020363

Katsura, K. A., Horst, J. A., Chandra, D., Le, T. Q., Nakano, Y., Zhang, Y., et al. (2014). WDR72 Models of Structure and Function: a Stage-specific Regulator of Enamel Mineralization. *Matrix Biol.* 38, 48–58. doi:10.1016/j.matbio.2014.06.005

Kertesz, M., Iovino, N., Unnerstall, U., Gaul, U., and Segal, E. (2007). The Role of Site Accessibility in microRNA Target Recognition. *Nat. Genet.* 39, 1278–1284. doi:10.1038/ng2135

Khan, S. A., Khan, M. A., Muhammad, N., Bashir, H., Khan, N., Muhammad, N., et al. (2020). A Novel Nonsense Variant in SLC24A4 Causing a Rare Form of Amelogenesis Imperfecta in a Pakistani Family. *BMC Med. Genet.* 21, 97. doi:10.1186/s12881-020-01038-6

Kim, J. W., Zhang, H., Seymen, F., Koruyucu, M., Hu, Y., Kang, J., et al. (2019). Mutations in RELT Cause Autosomal Recessive Amelogenesis Imperfecta. *Clin. Genet.* 95, 375–383. doi:10.1111/cge.13487

Kist, R., Watson, M., Wang, X., Cairns, P., Miles, C., Reid, D. J., et al. (2005). Reduction of Pax9 Gene Dosage in an Allelic Series of Mouse Mutants Causes Hypodontia and Oligodontia. *Hum. Mol. Genet.* 14, 3605–3617. doi:10.1093/hmg/ddi388

Kwak, S. Y., Yamakoshi, Y., Simmer, J. P., and Margolis, H. C. (2016). MMP20 Proteolysis of Native Amelogenin Regulates Mineralization *In Vitro*. *J. Dent Res.* 95, 1511–1517. doi:10.1177/0022034516662814

Lacruz, R. S., Nanci, A., White, S. N., Wen, X., Wang, H., Zalzal, S. F., et al. (2010). The Sodium Bicarbonate Cotransporter (NBCe1) Is Essential for normal Development of Mouse Dentition. *J. Biol. Chem.* 285, 24432–24438. doi:10.1074/jbc.m110.115188

Lee, W.-C., Yamaguchi, T., Watanabe, C., Kawaguchi, A., Takeda, M., Kim, Y.-I., et al. (2012). Association of Common PAX9 Variants with Permanent Tooth Size Variation in Non-syndromic East Asian Populations. *J. Hum. Genet.* 57, 654–659. doi:10.1038/jhg.2012.90

Li, A., Jia, P., Mallik, S., Fei, R., Yoshioka, H., Suzuki, A., et al. (2020). Critical microRNAs and Regulatory Motifs in Cleft Palate Identified by a Conserved miRNA-TF-Gene Network Approach in Humans and Mice. *Brief Bioinform* 21, 1465–1478. doi:10.1093/bib/bbz082

Li, L., Jia, J., Liu, X., Yang, S., Ye, S., Yang, W., et al. (2015). MicroRNA-16-5p Controls Development of Osteoarthritis by Targeting SMAD3 in Chondrocytes. *Cpd* 21, 5160–5167. doi:10.2174/1381612821666150909094712

Liu, X., Su, K., Kuang, S., Fu, M., and Zhang, Z. (2020). miR-16-5p and miR-145-5p Trigger Apoptosis in Human Gingival Epithelial Cells by Down-Regulating BACH2. *Int. J. Clin. Exp. Pathol.* 13, 901–911.

Malik, Z., Alexiou, M., Hallgrimsson, B., Economides, A. N., Luder, H. U., and Graf, D. (2018). Bone Morphogenetic Protein 2 Coordinates Early Tooth Mineralization. *J. Dent Res.* 97, 835–843. doi:10.1177/0022034518758044

Monsoro-Burq, A. H. (2015). PAX Transcription Factors in Neural Crest Development. *Semin. Cel Develop. Biol.* 44, 87–96. doi:10.1016/j.semcdb.2015.09.015

Mustonen, T., Pispa, J., Mikkola, M. L., Pummila, M., Kangas, A. T., Pakkasjärvi, L., et al. (2003). Stimulation of Ectodermal Organ Development by Ectodysplasin-A1. *Develop. Biol.* 259, 123–136. doi:10.1016/s0012-1606(03)00157-x

Ohyama, Y., Lin, J.-H., Govitvattana, N., Lin, I.-P., Venkitapathi, S., Alamoudi, A., et al. (2016). FAM20A Binds to and Regulates FAM20C Localization. *Sci. Rep.* 6, 27784. doi:10.1038/srep27784

Otsu, K., Ida-Yonemochi, H., Fujiwara, N., and Harada, H. (2016). The Semaphorin 4D-RhoA-Akt Signal Cascade Regulates Enamel Matrix Secretion in Coordination with Cell Polarization during Ameloblast Differentiation. *J. Bone Miner Res.* 31, 1943–1954. doi:10.1002/jbmr.2876

Ouzzani, M., Hammady, H., Fedorowicz, Z., and Elmagarmid, A. (2016). Rayyan-a Web and mobile App for Systematic Reviews. *Syst. Rev.* 5, 210. doi:10.1186/s13643-016-0384-4

Parry, D. A., Poulter, J. A., Logan, C. V., Brookes, S. J., Jafri, H., Ferguson, C. H., et al. (2013). Identification of Mutations in SLC24A4, Encoding a Potassium-dependent Sodium/calcium Exchanger, as a Cause of Amelogenesis Imperfecta. *Am. J. Hum. Genet.* 92, 307–312. doi:10.1016/j.ajhg.2013.01.003

Peng, W., Zhu, S., Li, X., Weng, J., and Chen, S. (2017). miR-27b-3p Suppressed Osteogenic Differentiation of Maxillary Sinus Membrane Stem Cells by Targeting Sp7. *Implant Dent* 26, 492–499. doi:10.1097/id.0000000000000637

Poché, R. A., Sharma, R., Garcia, M. D., Wada, A. M., Nolte, M. J., Udan, R. S., et al. (2012). Transcription Factor FoxO1 Is Essential for Enamel Biomineralization. *PLoS One* 7, e30357. doi:10.1371/journal.pone.0030357

Safari, S., Ebadifar, A., Najmabadi, H., Kamali, K., and Abedini, S. S. (2020). Screening PAX9, MSX1 and WNT10A Mutations in 4 Iranian Families with Non-syndromic Tooth Agenesis. *Avicenna J. Med. Biotechnol.* 12, 236–240.

Sangani, D., Suzuki, A., Vonville, H., Hixson, J. E., and Iwata, J. (2015). Gene Mutations Associated with Temporomandibular Joint Disorders: A Systematic Review. *OAlib* 2. doi:10.4236/oalib.1101583

Seymen, F., Lee, K.-E., Tran Le, C. G., Yildirim, M., Gencay, K., Lee, Z. H., et al. (2014). Exonal Deletion of SLC24A4 Causes Hypomaturation Amelogenesis Imperfecta. *J. Dent Res.* 93, 366–370. doi:10.1177/0022034514523786

Shannon, P., Markiel, A., Ozier, O., Baliga, N. S., Wang, J. T., Ramage, D., et al. (2003). Cytoscape: A Software Environment for Integrated Models of Biomolecular Interaction Networks. *Genome Res.* 13, 2498–2504. doi:10.1101/gr.1239303

Shen, L., Liu, C., Gao, M., Li, H., Zhang, Y., Tian, Q., et al. (2019). Novel Mutation of EDA Causes New Asymmetrical X-linked Hypohidrotic Ectodermal Dysplasia Phenotypes in a Female. *J. Dermatol.* 46, 731–733. doi:10.1111/1346-8138.14978

Simmer, J., and Hu, J. (2002). Expression, Structure, and Function of Enamel Proteinases. *Connect. Tissue Res.* 43, 441–449. doi:10.1080/713713530

Smith, C. E. L., Poulter, J. A., Antanaviciute, A., Kirkham, J., Brookes, S. J., Inglehearn, C. F., et al. (2017). Amelogenesis Imperfecta; Genes, Proteins, and Pathways. *Front. Physiol.* 8, 435. doi:10.3389/fphys.2017.00435

Stephanopoulos, G., Garefalaki, M.-E., and Lyroudia, K. (2005). Genes and Related Proteins Involved in Amelogenesis Imperfecta. *J. Dent Res.* 84, 1117–1126. doi:10.1177/154405910508401206

Strauch, S., and Hahnel, S. (2018). Restorative Treatment in Patients with Amelogenesis Imperfecta: A Review. *J. Prosthodont.* 27, 618–623. doi:10.1111/jopr.12736

Sun, H., Kim, P., Jia, P., Park, A. K., Liang, H., and Zhao, Z. (2019a). Distinct Telomere Length and Molecular Signatures in Seminoma and Non-seminoma of Testicular Germ Cell Tumor. *Brief Bioinform* 20, 1502–1512. doi:10.1093/bib/bby020

Sun, J., Gong, X., Purow, B., and Zhao, Z. (2012). Uncovering MicroRNA and Transcription Factor Mediated Regulatory Networks in Glioblastoma. *Plos Comput. Biol.* 8, e1002488. doi:10.1371/journal.pcbi.1002488

Sun, Y., Xiong, Y., Yan, C., Chen, L., Chen, D., Mi, B., et al. (2019b). Downregulation of microRNA-16-5p Accelerates Fracture Healing by Promoting Proliferation and Inhibiting Apoptosis of Osteoblasts in Patients with Traumatic Brain Injury. *Am. J. Transl Res.* 11, 4746–4760.

Suzuki, A., Yoshioka, H., Summakia, D., Desai, N. G., Jun, G., Jia, P., et al. (2019). MicroRNA-124-3p Suppresses Mouse Lip Mesenchymal Cell Proliferation through the Regulation of Genes Associated with Cleft Lip in the Mouse. *BMC Genomics* 20, 852. doi:10.1186/s12864-019-6238-4

Tagliabracci, V. S., Engel, J. L., Wen, J., Wiley, S. E., Worby, C. A., Kinch, L. N., et al. (2012). Secreted Kinase Phosphorylates Extracellular Proteins that Regulate Biomineralization. *Science* 336, 1150–1153. doi:10.1126/science.1217817

Urzúa, B., Ortega-Pinto, A., Morales-Bozo, I., Rojas-Alcayaga, G., and Cifuentes, V. (2011). Defining a New Candidate Gene for Amelogenesis Imperfecta: from Molecular Genetics to Biochemistry. *Biochem. Genet.* 49, 104–121. doi:10.1007/s10528-010-9392-6

Wang, S. K., Hu, Y., Yang, J., Smith, C. E., Nunez, S. M., Richardson, A. S., et al. (2015). Critical Roles for WDR 72 in Calcium Transport and Matrix Protein Removal during Enamel Maturation. *Mol. Genet. Genomic Med.* 3, 302–319. doi:10.1002/mgg3.143

Wang, X., Jung, J., Liu, Y., Yuan, B., Lu, Y., Feng, J. Q., et al. (2013). The Specific Role of FAM20C in Amelogenesis. *J. Dent Res.* 92, 995–999. doi:10.1177/0022034513504588

Williams, M. A., and Letra, A. (2018). The Changing Landscape in the Genetic Etiology of Human Tooth Agenesis, *Genes (Basel)* 9, 255. doi:10.3390/genes9050255

Witkop, C. J., Jr. (1988). Amelogenesis Imperfecta, Dentinogenesis Imperfecta and Dentin Dysplasia Revisited: Problems in Classification. *J. Oral Pathol. Med.* 17, 547–553. doi:10.1111/j.1600-0714.1988.tb01332.x

Wong, S.-W., Han, D., Zhang, H., Liu, Y., Zhang, X., Miao, M. Z., et al. (2018). Nine Novel PAX9 Mutations and a Distinct Tooth Agenesis Genotype-Phenotype. *J. Dent Res.* 97, 155–162. doi:10.1177/0022034517729322

Wright, J. T., Fete, M., Schneider, H., Zinser, M., Koster, M. I., Clarke, A. J., et al. (2019). Ectodermal Dysplasias: Classification and Organization by Phenotype, Genotype and Molecular Pathway. *Am. J. Med. Genet.* 179, 442–447. doi:10.1002/ajmg.a.61045

Wright, J. T. (2006). The Molecular Etiologies and Associated Phenotypes of Amelogenesis Imperfecta. *Am. J. Med. Genet.* 140A, 2547–2555. doi:10.1002/ajmg.a.31358

Yamazaki, H., Tran, B., Beniash, E., Kwak, S. Y., and Margolis, H. C. (2019). Proteolysis by MMP20 Prevents Aberrant Mineralization in Secretory Enamel. *J. Dent Res.* 98, 468–475. doi:10.1177/0022034518823537

Yan, F., Jia, P., Yoshioka, H., Suzuki, A., Iwata, J., and Zhao, Z. (2020). A Developmental Stage-specific Network Approach for Studying Dynamic Co-regulation of Transcription Factors and microRNAs during Craniofacial Development. *Development* 147.

Yokozeki, M., Afanador, E., Nishi, M., Kaneko, K., Shimokawa, H., Yokote, K., et al. (2003). Smad3 Is Required for Enamel Biomineralization. *Biochem. Biophysical Res. Commun.* 305, 684–690. doi:10.1016/s0006-291x(03)00806-4

Yoshioka, H., Mikami, Y., Ramakrishnan, S. S., Suzuki, A., and Iwata, J. (2021a). MicroRNA-124-3p Plays a Crucial Role in Cleft Palate Induced by Retinoic Acid. *Front. Cel Dev. Biol.* 9, 621045. doi:10.3389/fcell.2021.621045

Yoshioka, H., Wang, Y. Y., Suzuki, A., Shayegh, M., Gajera, M. V., Zhao, Z., et al. (2021b). Overexpression of miR-1306-5p, miR-3195, and miR-3914 Inhibits Ameloblast Differentiation through Suppression of Genes Associated with Human Amelogenesis Imperfecta. *Int. J. Mol. Sci.* 22. doi:10.3390/ijms22042202

Yu, M., Wong, S. W., Han, D., and Cai, T. (2019). Genetic Analysis: Wnt and Other Pathways in Nonsyndromic Tooth Agenesis. *Oral Dis.* 25, 646–651. doi:10.1111/odi.12931

Zhang, G., Zhou, Y., Su, M., Yang, X., and Zeng, B. (2020). Inhibition of microRNA -27b-3p Relieves Osteoarthritis Pain via Regulation of KDM4B -dependent DLX5. *Biofactors* 46, 788–802. doi:10.1002/biof.1670

Zhou, J., Gao, Y., Zhang, Z., Zhang, Y., Maltby, K. M., Liu, Z., et al. (2011). Osr2 Acts Downstream of Pax9 and Interacts with Both Msx1 and Pax9 to Pattern the Tooth Developmental Field. *Develop. Biol.* 353, 344–353. doi:10.1016/j.ydbio.2011.03.012

Zhou, Y., Li, S., Chen, P., Yang, B., Yang, J., Liu, R., et al. (2019). MicroRNA-27b-3p Inhibits Apoptosis of Chondrocyte in Rheumatoid Arthritis by Targeting HIPK2. *Artif. Cell Nanomedicine, Biotechnol.* 47, 1766–1771. doi:10.1080/21691401.2019.1607362

Conflict of Interest: The authors declare that the research was conducted in the absence of any commercial or financial relationships that could be construed as a potential conflict of interest.

Publisher's Note: All claims expressed in this article are solely those of the authors and do not necessarily represent those of their affiliated organizations, or those of the publisher, the editors and the reviewers. Any product that may be evaluated in this article, or claim that may be made by its manufacturer, is not guaranteed or endorsed by the publisher.

frontiers in Genetics

CASE REPORT
published: 25 March 2022
doi: 10.3389/fgene.2022.829613

Case Report: Prenatal Diagnosis of a Novel Variant c.251dupT (p.N87Kfs*6) in *BCOR* Resulting in Oculofaciocardiodental Syndrome Using Whole-Exome Sequencing

Jianlong Zhuang[1], Chunnuan Chen[2], Yu'e Chen[3], Shuhong Zeng[1], Yuying Jiang[1], Yuanbai Wang[1], Xinying Chen[1], Yingjun Xie[4,5] and Gaoxiong Wang[6]**

[1]Prenatal Diagnosis Center, Quanzhou Women's and Children's Hospital, Quanzhou, China, [2]Department of Neurology, The Second Affiliated Hospital of Fujian Medical University, Quanzhou, China, [3]Ultrasonography, Quanzhou Women's and Children's Hospital, Quanzhou, China, [4]Department of Obstetrics and Gynecology, Key Laboratory for Major Obstetric Diseases of Guangdong Province, The Third Affiliated Hospital of Guangzhou Medical University, Guangzhou, China, [5]Key Laboratory of Reproduction and Genetics of Guangdong Higher Education Institutes, The Third Affiliated Hospital of Guangzhou Medical University, Guangzhou, China, [6]Quanzhou Women's and Children's Hospital, Quanzhou, China

OPEN ACCESS

Edited by:
Sadeq Vallian,
University of Isfahan, Iran

Reviewed by:
Aideen McInerney-Leo,
The University of Queensland, Australia
Valentina Massa,
University of Milan, Italy

***Correspondence:**
Gaoxiong Wang
wanggaoxiong2013@163.com
Yingjun Xie
xieyjun@mail2.sysu.edu.cn

Specialty section:
This article was submitted to Genetics of Common and Rare Diseases, a section of the journal Frontiers in Genetics

Received: 06 December 2021
Accepted: 22 February 2022
Published: 25 March 2022

Citation:
Zhuang J, Chen C, Chen Y, Zeng S, Jiang Y, Wang Y, Chen X, Xie Y and Wang G (2022) Case Report: Prenatal Diagnosis of a Novel Variant c.251dupT (p.N87Kfs*6) in BCOR Resulting in Oculofaciocardiodental Syndrome Using Whole-Exome Sequencing. Front. Genet. 13:829613. doi: 10.3389/fgene.2022.829613

Background: Oculofaciocardiodental (OFCD) syndrome is an X-linked dominant syndrome caused by BCOR *variants*, which manifests only in females and presumed leading to male lethality. Herein, we aim to present a prenatal diagnosis for OFCD syndrome associated with a novel hemizygous variant in *BCOR* gene.

Case presentation: A 29-year-old pregnant woman from Quanzhou Fujian Province, China, with fetal ultrasound anomalies, was enrolled in this study. A normal 46, XY karyotype with no abnormalities was observed in the fetus detected on microarray. Furthermore, a whole-exome sequencing (WES) detection result demonstrated that a novel hemizygous variant of c.251dupT (p.N87Kfs*6) in the *BCOR* gene was identified in the fetus, which was a frameshift mutation and classified as a likely pathogenic variant, and may lead to OFCD syndrome according to the clinical feature of the fetus. In this case, male lethality had not occurred by the end of the second trimester, then termination of the pregnancy was conducted at a gestational age of 26 weeks. Sanger sequencing of parental samples revealed that the variant was maternally transmitted, which was consistent with the OFCD syndrome phenotypic features observed in her.

Conclusions: In the study, we first present the affected male with a novel variant in *BCOR* that leads to the OFCD syndrome. Additionally, our study broadened the spectrum of *BCOR* results in the OFCD syndrome and provided the valuable references for prenatal genetic consultation.

Keywords: oculofaciocardiodental, chromosomal microarray analysis, whole-exome sequencing, BCOR, frameshift mutation, hemizygous variant

INTRODUCTION

With the continuous application and development of high-throughput sequencing technology, whole-exome sequencing (WES) based on next-generation sequencing technology has been increasingly used in scientific research and clinical diagnosis. The human exome contains about 180,000 exons, accounting for only 1% of the whole human genome; however, around 85% of the variants related to diseases exist in the exon region (Choi et al., 2009; Ng et al., 2010). Recent studies have shown that variants in a single gene would exhibit fetal ultrasound abnormalities *in utero*, with normal karyotype and chromosomal microarray analysis results. An additional pathogenic mutation detection rate of 6.2%–80.0% was observed by prenatal WES detection over chromosomal microarray analysis (CMA) detection (Best et al., 2018; Lord et al., 2019; Petrovski et al., 2019). Therefore, it is of great value using WES technology to investigate pathogenic mutations of fetal ultrasonic structural abnormalities at a single-gene level.

Pathogenic variants in the BCL-6 corepressor (*BCOR*, OMIM: 300485) on chromosome Xp11.4 will result in two distinct syndromes including oculofaciocardiodental syndrome (OFCD, OMIM: 300166) and Lenz microphthalmia syndrome (OMIM: 309800) (Ng et al., 2004). OFCD syndrome is a rare X-linked dominant genetic disorder, which typically affects females and is presumed to lead to male lethality caused by a variety of *BCOR* null mutations including deletional, nonsense, splicing, truncating, and frameshift mutations (Wilkie et al., 1993; Ragge et al., 2019). It is characterized by congenital cataract, dental anomalies, skeletal abnormalities, cardiac septal defect, cleft palate, etc. (Ng et al., 2004; Hilton et al., 2009). In contrast, Lenz microphthalmia syndrome is an X-linked recessive inheritance pattern, which showed normal clinical phenotype in females, and only affected males with microphthalmia, intellectual disability, skeletal and urogenital malformations, and other anomalies. While a previous study conducted by Horn et al. (Horn et al., 2005) indicated that the *BOCR* gene may not be the major gene in the Lenz microphthalmia syndrome, to date, only one specific missense mutation of c.254C > T (p.P85L) in *BCOR* has been reported to associate with the Lenz microphthalmia syndrome (Temtamy et al., 2000; Ersin et al., 2003).

To date, only a previous report, which referred to a prenatal diagnosis analysis of the Lenz microphthalmia syndrome associated with the typical mutation of c.254C > T, was conducted in 2013 (Suzumori et al., 2013). No report of prenatal diagnosis analysis of X-linked dominant OFCD syndrome relevant to the *BCOR* gene was observed. In this study, we report the first case of prenatal diagnosis for the OFCD syndrome in an affected male with a novel frameshift mutation in the *BCOR* gene.

CASE PRESENTATION

A 29-year-old gravida 2, para 1 pregnant woman from Quanzhou Fujian Province, China, referred to the Prenatal Diagnosis Center of Quanzhou Women's and Children's Hospital at the gestational age of 16 + 2 weeks. Her husband was 31 years old, and the couple denied any family history of inheritance disease and consanguinity. At her first pregnancy, a female infant was delivered at the gestational age of 39 + 6 weeks in 2019. At present, she is 2.5 years old with a normal phenotype. At this pregnancy, the second trimester Down's screening was performed, and moderate risk of trisomy 21 (1/552) was observed. The subsequent noninvasive prenatal testing test results elicited a low risk of T21, T18, and T13. However, ultrasonic examination conducted at 17 + 6 weeks of gestation suggested the possibility of fetal duodenal obstruction and a variety of soft index abnormalities, including an enhanced echo of fetal renal parenchyma and punctate hyperechoic of the left ventricle.

After genetic counseling and informed consent, amniocentesis was performed at 20 weeks. Karyotype analysis combined with CMA was used to detect fetal chromosomal abnormalities and copy number variants, while no obvious abnormalities were found. At the gestational age of 24 weeks, a three-dimensional color Doppler ultrasound was performed and indicated several fetal structure anomalies including fetal right nasal fissure, duodenal obstruction, cleft palate, ventricular septal defect, and toe syndactyly (**Figure 1**).

The remaining amniotic fluid was used for DNA extraction and further WES detection. The WES detection result delineated a novel hemizygous variant of c.251dupT (p.N87Kfs*6) in exon 4 of the *BCOR* gene, which was identified in the male fetus (**Figure 2**). It was a frameshift mutation and classified as a likely pathogenic variant according to the ACMG guidelines (Richards et al., 2015), with no frequency that has been reported in databases including gnomAD, 1000 genomes, dbSNP, Clinvar, ExAC, as well as PubMed databases. According to the variant type and fetal clinical phenotypes, the frameshift mutation in the *BCOR* gene may lead to OFCD syndrome. Male lethality was not observed by the end of the second trimester, then termination of pregnancy was conducted at the gestational age of 26 weeks. Segregation analysis indicated that the variant in the *BCOR* gene was inherited from his mother who exhibited a phenotype associated with OFCD syndrome including long, thin face, flat nasal bridge, broad nasal tip, high palate, microphthalmia, dental anomalies (teeth are crowded and irregularly arranged), and ventricular septal defect, but with normal mental and physical development and without congenital cataract. Moreover, the novel variant in the *BCOR* gene was absent in the proband's sister who exhibits a normal clinical phenotype.

DISCUSSION AND CONCLUSION

Variants of the *BCOR* gene will result in two distinct syndromes including the OFCD syndrome and Lenz microphthalmia syndrome. A prenatal diagnosis analysis for the Lenz microphthalmia syndrome associated with typically missense mutation of c.254C > T was also identified (Suzumori et al., 2013). To date, no information is available on prenatal diagnosis

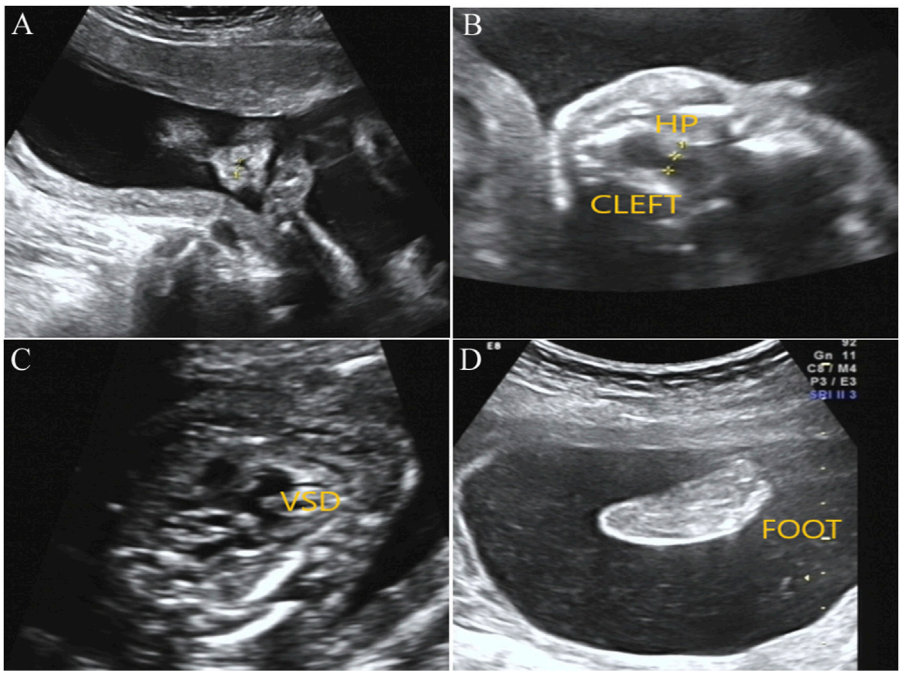

FIGURE1 | Prenatal ultrasound examination results in the fetus with *BOCR* variant. **(A)** Ultrasound detection results showed right alar fissure in the fetus. **(B)** Fetal ultrasound results indicated continuous interruption of cleft palate. HP, hard palate. **(C)** Fetal ultrasound results elicited fetal ventricular septal defect (VSD). **(D)** Toe syndactyly was also observed in the fetus by ultrasound examination.

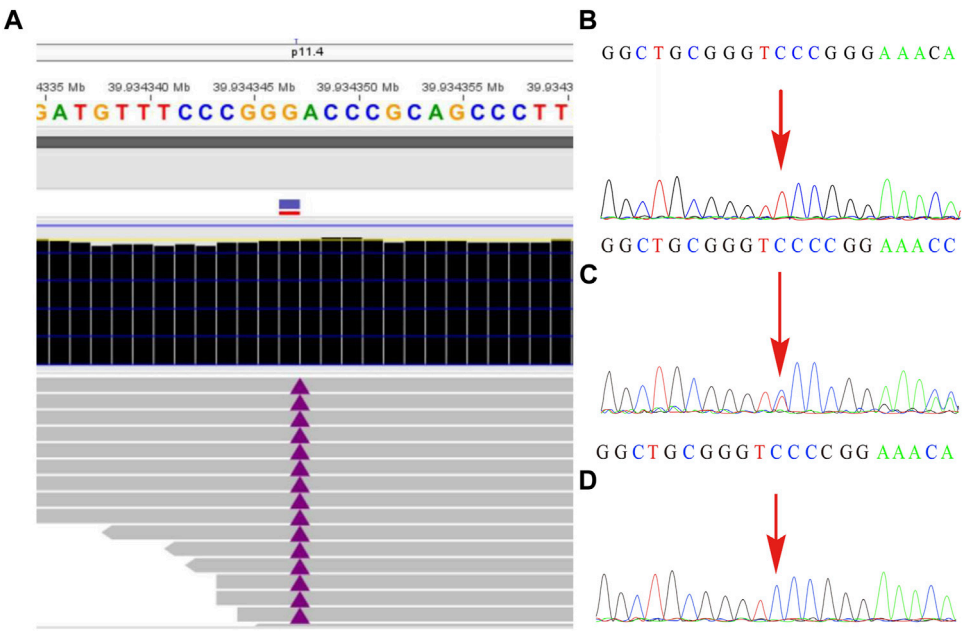

FIGURE2 | The variant in the *BCOR* gene was detected by whole-exome sequencing and further verified by Sanger sequencing. **(A)** A frameshift mutation c.251dupT (p.N87Kfs*6) of the *BCOR* gene in the fetus was detected by WES technology. **(B)** shows the hemizygosity of the variant in the affected fetus, while **(C)** demonstrated that the mother was heterozygous and **(D)** showed that the frameshift variant was not present in his father.

analysis of the OFCD syndrome that associates with the *BCOR* gene variants. Here, the first case of prenatal diagnosis for the OFCD syndrome with a novel frameshift mutation c.251dupT (p.N87Kfs*6) in exon 4 of the *BCOR* gene was identified. Moreover, this was also the first case of a male fetus who carried the *BCOR* mutation that resulted in OFCD syndrome to the best of our knowledge. It is worth noting that for the affected male fetus, the mother was still undergoing pregnancy at 26 weeks of gestation.

OFCD syndrome is typically caused by *BCOR* variants that lead to premature termination codons, including frameshift mutations in the form of small deletions or duplications, or microdeletions in the *BCOR* gene. The Lenz microphthalmia syndrome is usually caused by missense mutations, which only lead to changes in amino acids. In the present study, we report a novel frameshift variant of c.251dupT (p.N87Kfs*6) in exon 4 of the *BCOR* gene in a male fetus, and ultrasound examination results showed that the fetus had several fetal structure anomalies including fetal right nasal fissure, duodenal obstruction, cleft palate, ventricular septal defect, and toe syndactyly. This hemizygous variant has never been reported and has no frequency in the database, which was classified as a likely pathogenic variant according to the ACMG guidelines (PVS1 + PM2). Additionally, the fetus' mother harbored the same variant and exhibited a phenotype associated with the OFCD syndrome including facial deformity, microphthalmia, dental anomalies, and ventricular septal defect. According to the inheritance pattern and the clinical phenotypes in the fetus and his mother, we believe that the novel frameshift mutation in *BCOR* would lead to the OFCD syndrome.

Phenotypic variability was also present in the OFCD syndrome and shows different clinical symptoms in the same family (Lozić et al., 2012). A previous study conducted by Davoody et al. elicited a heterozygous frameshift variant of c.2858_2859delAA (p.K593SfsX7) in exon 4 of the *BCOR* gene was identified in a female patient with characteristic facial features, while no indication of atrial septal defect or ventricular septal defect existed (Davoody et al., 2012). Additionally, a novel mutation c.265G > A on exon 4 was identified in a Japanese female and diagnosed as OFCD syndrome that exhibits clinical phenotypes including congenital cataract, ventricular septal defect, dental deformity, and without cleft palate (Kato et al., 2018). The largest study (Hilton et al., 2009) reported 34 female patients in 20 families with variants of the *BCOR* gene exhibiting the OFCD syndrome. All of the patients had congenital cataract, and microphthalmia and/or microcornea that were observed in 28 cases. In contrast, the study conducted by Michelle et al. (Hamline et al., 2020) showed that 55% (23/42) of OFCD animals had lens opacification (indicative of cataracts), and 35% (8/23) were affected bilaterally, which showed clinical diversity of ocular deformity. In the present case, the mother did not have a cataract feature and cleft palate, while a high palate was observed. Moreover, *BCOR* hemizygosity mouse model showed early male embryo lethality by E9.5 (Cox et al., 2010; Hamline et al., 2020). Interestingly, in our study, the mother of the affected male fetus was still undergoing pregnancy at 26 weeks of gestation. Moreover, more work needs to be done to determine whether the male embryo with the presented variant in the *BCOR* gene will lead to lethality in the third trimester.

In conclusion, a prenatal diagnosis was first conducted eliciting a novel frameshift mutation c.251dupT (p.N87Kfs*6) in exon 4 of the *BCOR* gene and resulted in the OFCD syndrome. Moreover, the affected male fetus of the OFCD syndrome was first reported, and the pregnancy was still ongoing at the end of the second trimester. Our study provides valuable data for prenatal genetic consultation of OFCD syndrome and further strengthened the application value of WES in prenatal diagnosis.

DATA AVAILABILITY STATEMENT

The raw data supporting the conclusion of this article will be made available by the authors, without undue reservation.

ETHICS STATEMENT

The studies involving human participants were reviewed and approved by the Ethics Committee, and approval was obtained from the Institutional Ethics Committee of Quanzhou Women's and Children's Hospital for the commencement of the study (2020, No. 31). The patients/participants provided their written informed consent to participate in this study. Written informed consent was obtained from the individual(s) for the publication of any potentially identifiable images or data included in this article.

AUTHOR CONTRIBUTIONS

JZ designed and wrote the article. YC, XC, SZ, and YW performed the karyotype analysis, ultrasound detection, and analyzed the data. CC, YJ, GW, and YX revised and polished the paper. All authors approved the final article.

FUNDING

This research was supported by the Fujian Provincial Health Commission Youth Science and Technology Project (2020QNB045) and Quanzhou City Science and Technology Project (2020C026R).

ACKNOWLEDGMENTS

We wish to express our appreciation to the Fujian Provincial Health Commission and Quanzhou City Science and Technology Bureau for funding this work. We also express our appreciation to the patient and his family members who participated in this study.

REFERENCES

Best, S., Wou, K., Vora, N., Van der Veyver, I. B., Wapner, R., and Chitty, L. S. (2018). Promises, Pitfalls and Practicalities of Prenatal Whole Exome Sequencing. *Prenat Diagn.* 38 (1), 10–19. doi:10.1002/pd.5102

Choi, M., Scholl, U. I., Ji, W., Liu, T., Tikhonova, I. R., Zumbo, P., et al. (2009). Genetic Diagnosis by Whole Exome Capture and Massively Parallel DNA Sequencing. *Pnas* 106 (45), 19096–19101. doi:10.1073/pnas.0910672106

Cox, B. J., Vollmer, M., Tamplin, O., Lu, M., Biechele, S., Gertsenstein, M., et al. (2010). Phenotypic Annotation of the Mouse X Chromosome. *Genome Res.* 20 (8), 1154–1164. doi:10.1101/gr.105106.110

Davoody, A., Chen, I. P., Nanda, R., Uribe, F., and Reichenberger, E. J. (2012). Oculofaciocardiodental Syndrome: a Rare Case and Review of the Literature. *Cleft Palate Craniofac. J.* 49 (5), e55–60. doi:10.1597/10-256

Ersin, N. K., Tugsel, Z., Gökce, B., Ozpinar, B., and Eronat, N. (2003). Lenz Microphthalmia Syndrome with Dental Anomalies: a Case Report. *J. Dent Child. (Chic)* 70 (3), 262–265.

Hamline, M. Y., Corcoran, C. M., Wamstad, J. A., Miletich, I., Feng, J., Lohr, J. L., et al. (2020). OFCD Syndrome and Extraembryonic Defects Are Revealed by Conditional Mutation of the Polycomb-Group Repressive Complex 1.1 (PRC1.1) Gene BCOR. *Dev. Biol.* 468 (1-2), 110–132. doi:10.1016/j.ydbio.2020.06.013

Hilton, E., Johnston, J., Whalen, S., Okamoto, N., Hatsukawa, Y., Nishio, J., et al. (2009). BCOR Analysis in Patients with OFCD and Lenz Microphthalmia Syndromes, Mental Retardation with Ocular Anomalies, and Cardiac Laterality Defects. *Eur. J. Hum. Genet.* 17 (10), 1325–1335. doi:10.1038/ejhg.2009.52

Horn, D., Chyrek, M., Kleier, S., Lüttgen, S., Bolz, H., Hinkel, G.-K., et al. (2005). Novel Mutations in BCOR in Three Patients with Oculo-Facio-Cardio-Dental Syndrome, but None in Lenz Microphthalmia Syndrome. *Eur. J. Hum. Genet.* 13 (5), 563–569. doi:10.1038/sj.ejhg.5201391

Kato, J., Kushima, K., and Kushima, F. (2018). New Radiological Findings and Radiculomegaly in Oculofaciocardiodental Syndrome with a Novel BCOR Mutation. *Medicine (Baltimore)* 97 (49), e13444. doi:10.1097/md.0000000000013444

Lord, J., McMullan, D. J., Eberhardt, R. Y., Rinck, G., Hamilton, S. J., Quinlan-Jones, E., et al. (2019). Prenatal Exome Sequencing Analysis in Fetal Structural Anomalies Detected by Ultrasonography (PAGE): a Cohort Study. *Lancet* 393 (10173), 747–757. doi:10.1016/S0140-6736(18)31940-8

Lozić, B., Ljubković, J., Pandurić, D. G., Saltvig, I., Kutsche, K., Krželj, V., et al. (2012). Oculo-facio-cardio-dental Syndrome in Three Succeeding Generations: Genotypic Data and Phenotypic Features. *Braz. J. Med. Biol. Res.* 45 (12), 1315–1319. doi:10.1590/s0100-879x2012007500150

Ng, D., Thakker, N., Corcoran, C. M., Donnai, D., Perveen, R., Schneider, A., et al. (2004). Oculofaciocardiodental and Lenz Microphthalmia Syndromes Result from Distinct Classes of Mutations in BCOR. *Nat. Genet.* 36 (4), 411–416. doi:10.1038/ng1321

Ng, S. B., Buckingham, K. J., Lee, C., Bigham, A. W., Tabor, H. K., Dent, K. M., et al. (2010). Exome Sequencing Identifies the Cause of a Mendelian Disorder. *Nat. Genet.* 42 (1), 30–35. doi:10.1038/ng.499

Petrovski, S., Aggarwal, V., Giordano, J. L., Stosic, M., Wou, K., Bier, L., et al. (2019). Whole-exome Sequencing in the Evaluation of Fetal Structural Anomalies: a Prospective Cohort Study. *The Lancet* 393 (10173), 758–767. doi:10.1016/s0140-6736(18)32042-7

Ragge, N., Isidor, B., Bitoun, P., Odent, S., Giurgea, I., Cogné, B., et al. (2019). Expanding the Phenotype of the X-Linked BCOR Microphthalmia Syndromes. *Hum. Genet.* 138 (8-9), 1051–1069. doi:10.1007/s00439-018-1896-x

Richards, S., Aziz, N., Bale, S., Bick, D., Das, S., Gastier-Foster, J., et al. (2015). Standards and Guidelines for the Interpretation of Sequence Variants: a Joint Consensus Recommendation of the American College of Medical Genetics and Genomics and the Association for Molecular Pathology. *Genet. Med.* 17 (5), 405–424. doi:10.1038/gim.2015.30

Suzumori, N., Kaname, T., Muramatsu, Y., Yanagi, K., Kumagai, K., Mizuno, S., et al. (2013). Prenatal Diagnosis of X-Linked Recessive Lenz Microphthalmia Syndrome. *J. Obstet. Gynaecol. Res.* 39 (11), 1545–1547. doi:10.1111/jog.12081

Temtamy, S. A., Ismail, S. I., and Meguid, N. A. (2000). Lenz Microphthalmia Syndrome: Three Additional Cases with Rare Associated Anomalies. *Genet. Couns.* 11 (2), 147–152.

Wilkie, A. O. M., Taylor, D., Scambler, P. J., and Baraitser, M. (1993). Congenital Cataract, Microphthalmia and Septal Heart Defect in Two Generations. *Clin. Dysmorphol.* 2 (2), 114–119. doi:10.1097/00019605-199304000-00003

Conflict of Interest: The authors declare that the research was conducted in the absence of any commercial or financial relationships that could be construed as a potential conflict of interest.

frontiers | Frontiers in Genetics

SYSTEMATIC REVIEW
published: 09 June 2022
doi: 10.3389/fgene.2022.875490

Oral Phenotype of Singleton–Merten Syndrome: A Systematic Review Illustrated With a Case Report

Margot Charlotte Riou[1,2,3], *Muriel de La Dure-Molla*[2,3,4], *Stéphane Kerner*[2,3], *Sophie Rondeau*[5], *Adrien Legendre*[6], *Valerie Cormier-Daire*[4] *and Benjamin P. J. Fournier*[1,2,3]*

[1]Centre de Recherche des Cordeliers, UMRS 1138, Molecular Oral Pathophysiology, Université de Paris, INSERM, Sorbonne Université, Paris, France, [2]Dental Department, Reference Center for Oral and Dental Rare Diseases, AP-HP, Rothschild Hospital (ORARES), Paris, France, [3]Dental Faculty, Université de Paris, Paris, France, [4]INSERM U1163 Institut Imagine, Paris, France, [5]Department of Genetics, Necker Enfants Malades Hospital, Paris Descartes-Sorbonne Paris Cité University, Paris, France, [6]Laboratoire de Biologie Médicale Multisites Seqoia—FMG2025, Paris, France

OPEN ACCESS

Edited by:
Francesca Diomede,
University of Studies G. d'Annunzio Chieti and Pescara, Italy

Reviewed by:
Mary MacDougall,
University of British Columbia, Canada
Gillian Inara Rice,
The University of Manchester, United Kingdom

***Correspondence:**
Benjamin P. J. Fournier
benjamin.fournier2@aphp.fr

Specialty section:
This article was submitted to Genetics of Common and Rare Diseases, a section of the journal Frontiers in Genetics

Received: 14 February 2022
Accepted: 27 April 2022
Published: 09 June 2022

Citation:
Riou MC, de La Dure-Molla M, Kerner S, Rondeau S, Legendre A, Cormier-Daire V and Fournier BPJ (2022) Oral Phenotype of Singleton–Merten Syndrome: A Systematic Review Illustrated With a Case Report. Front. Genet. 13:875490. doi: 10.3389/fgene.2022.875490

Background: Singleton–Merten syndrome type 1 (SGMRT1) is a rare autosomal dominant disorder caused by *IFIH1* variations with blood vessel calcifications, teeth anomalies, and bone defects.

Aim: We aimed to summarize the oral findings in SGMRT1 through a systematic review of the literature and to describe the phenotype of a 10-year-old patient with SGMRT1 diagnosis.

Results: A total of 20 patients were described in the literature, in nine articles. Eight *IFIH1* mutations were described in 11 families. Delayed eruption, short roots, and premature loss of permanent teeth were the most described features (100%). Impacted teeth (89%) and carious lesions (67%) were also described. Our patient, a 10-year-old male with Singleton–Merten syndrome, presented numerous carious lesions, severe teeth malposition, especially in the anterior arch, and an oral hygiene deficiency with a 100% plaque index. The panoramic X-ray did not show any dental agenesis but revealed very short roots and a decrease in the jaw alveolar bone height. The whole-genome sequencing analysis revealed a heterozygous *de novo* variant in *IFIH1* (NM_022168.4) c.2465G > A (p.Arg822Gln).

Conclusion: Confused descriptions of oral features occurred in the literature between congenital findings and "acquired" pathology, especially carious lesions. The dental phenotype of these patients encompasses eruption anomalies (delayed eruption and impacted teeth) and lack of root edification, leading to premature loss of permanent teeth, and it may contribute to the diagnosis. An early diagnosis is essential to prevent teeth loss and to improve the quality of life of these patients.

Systematic Review Registration: [https://www.crd.york.ac.uk/prospero/], identifier [CRD42022300025].

Keywords: Singleton–Merten syndrome, rare diseases, oral physiopathology, genetics, type 1 interferonopathy

INTRODUCTION

Singleton–Merten syndrome type 1 (SGMRT1, OMIM: 182250) is a rare autosomal dominant disorder associated with severe calcification of the ascending aorta and valves; acro-osteolysis widened medullary cavities of the distal limbs, scoliosis, and tooth anomalies (Singleton and Merten, 1973). The clinical characteristics of SMS showed a large variability of expressions. Psoriasis, muscular weakness, and glaucoma represent less frequently observed symptoms (Feigenbaum et al., 2013). Since its first description in 1973, few cases have been reported because of its low prevalence (1 < 1,000,000). A first missense heterozygous variant in the interferon-induced helicase C domain-containing protein 1 (*IFIH1*) gene was identified in three families (Rutsch et al., 2015). Since then, seven other pathogenic variants have been identified in patients with SGMRT1 (Bursztejn et al., 2015; de Carvalho et al., 2017; Takeichi et al., 2018; Vengoechea and DiMonda, 2020; Xiao et al., 2021; Hasegawa et al., 2022).

IFIH1 encodes MDA5 protein, a member of the RIG-1-like receptor (RLR) family, which functions as a cytoplasmic pattern-recognition receptor recognizing viral double-stranded RNA (dsRNA) and secreted bacterial nucleic acids. Moreover, variants in the *DDX58* gene that encodes an RNA helicase were identified in individuals with similar phenotypes without dental anomalies (Jang et al., 2015). On the other hand, variants in the *IFIH1* gene were also causative of the Aicardi-Goutieres syndrome (AGS-7; OMIM 615846), an autosomal dominant inflammatory disorder characterized by severe neurologic impairment such as progressive encephalopathy, spastic paraplegia, and calcification of basal ganglia (Crow et al., 2015). The recent studies have also reported overlapping of the clinical findings of both syndromes (Bursztejn et al., 2015; Xiao et al., 2021; Hasegawa et al., 2022). Consequently, clinical diagnosis may be challenging.

Dental findings in SGMRT1 are described by OMIM as "delayed primary tooth exfoliation and permanent tooth eruption, truncated tooth root formation, early-onset periodontal disease, and severe root and alveolar bone resorption associated with dysregulated mineralization, leading to tooth loss" (SGMRT1, OMIM: 182250). Other authors describe "root dysplasia" (Takeichi et al., 2018), "primary dentition as hollow shells" (Vengoechea and DiMonda, 2020) or "severe dysplasia of root cementum and dentin" (Pettersson et al., 2017). Other features such as root defects seem unclear, and the frequency of their occurrence is not known. Moreover, craniofacial defects are reported but without precise description or prevalence.

We examined a patient with SGMRT1 and observed oral and craniofacial features. We, therefore, wondered whether the

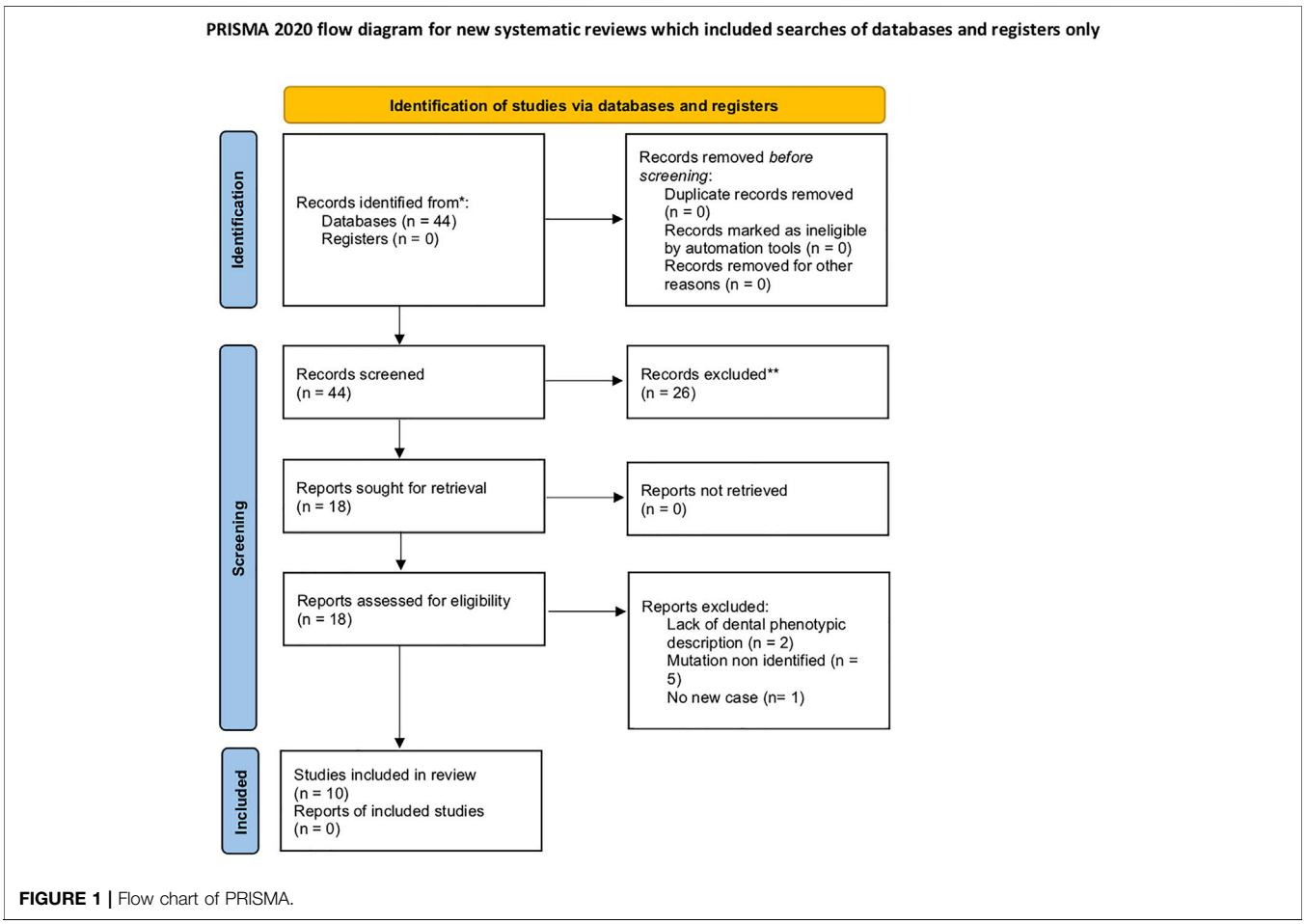

FIGURE 1 | Flow chart of PRISMA.

TABLE 1 | Mutation description.

Gene	Gene	Protein	Domain	Patient number (N; %)	Family number (N; %)	Article
IFIH1	c.986T > C	p.Leu329Pro	Hel1 domain*	1 (5%)	1 (8%)	(Vengoechea and DiMonda, 2020)
IFIH1	c.992C > G	p.Thr331Arg	Hel1 domain	2 (10%)	1 (8%)	(de Carvalho et al., 2017)
IFIH1	c.992C > T	p.Thr331Ile	Hel1 domain	3 (15%)	1 (8%)	(de Carvalho et al., 2017)
IFIH1	c.1465G > A	p.Ala489Thr	Hel1 domain	1 (5%)	1 (8%)	(Bursztejn et al., 2015)
IFIH1	c.1465G > T	p.Ala489Ser	Hel1 domain	1 (5%)	1 (8%)	(Xiao et al., 2021)
IFIH1	c.2390A > T	p.Asp797Val	Hel2 domain	1 (5%)	1 (8%)	(Hasegawa et al., 2022)
IFIH1	c.2465G > A	p.Arg822Gln	Hel2 domain*	9 (45%)	4 (33%)	(Feigenbaum et al., 2013; Rutsch et al., 2015; Pettersson et al., 2017)
IFIH1	c.2561T > A	p.Met854Lys	Hel2-CTD connection	1 (5%)	1 (8%)	(Takeichi et al., 2018)
IFIH1	NR	NR	NR	1 (5%)	1 (8%)	(Ghadiam and Mungee, 2017)
Total				20 (100%)	12 (100%)	

**The mutation associated domain was not notified in the article—NR: non-reported—all percentages have been rounded to the closet unit.*

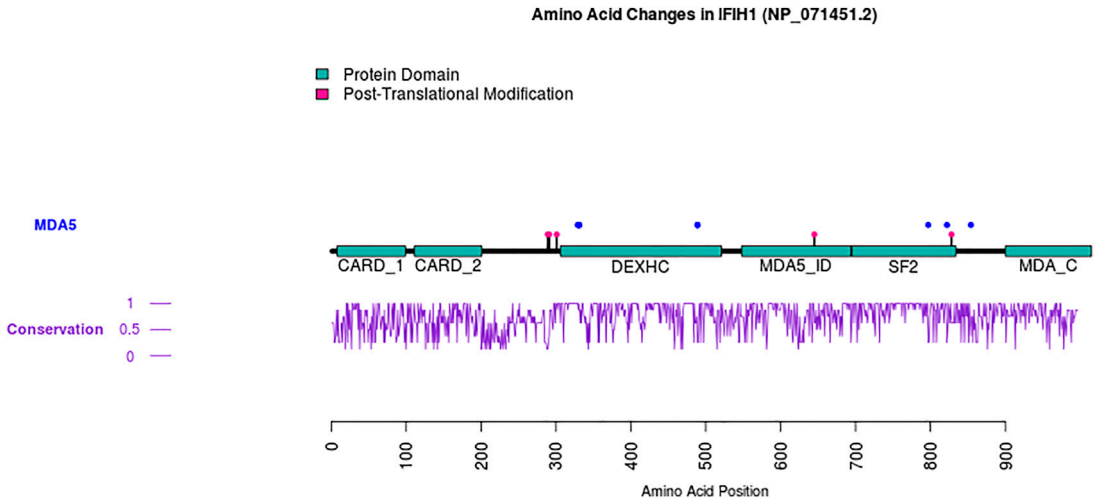

FIGURE 2 | Visualization of the SMGRT1 mutations in MDA5. Plots of all disease-causing mutations in MDA5 associated to SGMRT1. The conservation score is between 0 and 1, with 0 indicating no other sequences matching the reference (*Homo sapiens* NP_071451.2) at the position, and 1 indicating all sequences matching the reference at that position. CARD1: caspase activation and recruitment domain found in MDA5, first repeat; CARD2: caspase activation and recruitment domain found in MDA5, second repeat; DEXHC: DEXH-box helicase domain of RLR-2; MDA5_ID: insert domain of MDA5; SF2: C-terminal helicase domain of the endoribonuclease dicer; MDA_C: C-terminal domain of melanoma differentiation-associated protein 5. The hotspot is represented in orange.

observed clinical manifestations were constant in previously reported cases. The purpose of this work was to summarize the oral signs associated with the SGMRT1 through a systematic review of the literature. We illustrated and compared it with a description of a clinical case. A more precise description of the clinical manifestations may allow an easier clinical diagnosis.

REVIEW OF THE LITERATURE

Methods

We conducted a systematic review of the literature using the PubMed database up until September 2021. To ensure its reproducibility, PRISMA guidelines were followed (Page et al., 2021), and the PRISMA flowchart was filled. The search term was "Singleton–Merten". We aimed to precisely determine the oral clinical features of SGMRT1 patients with reported *IFIH1* variants. This review was registered with n°CRD42022300025.

Inclusion and Exclusion Criteria

The inclusion criteria were as follows: articles in English or French and the phenotype in a human patient with an *IFIH1* mutation. The exclusion criteria were as follows: another language than English or French, animals or *in vitro* studies, narrative reviews, and lack of patient's phenotype description, and Singleton–Merten patients with a variant in *DDX58*, or for whom the genetic cause has not been defined.

TABLE 2 | Patients' dental descriptions.

Patient		Delayed eruption	Carious lesions	Short roots	Premature loss of teeth	Impacted tooth	Dental agenesis	Low height of alveolar bone	Mutation	Article	Evidence grade
Age	Gender										
9	M	Yes	No	Yes	Yes	-	Yes	Yes	c. 2390A > T	(Hasegawa et al., 2022)	4
41	M	-	-	Yes	Yes	No	-	No	c.1465G > A	(Bursztejn et al., 2015)	4
30	M	-	-	-	Yes	-	-	Yes	c.1465G > T	(Xiao et al., 2021)	4
28	F	Yes	No	Yes	Yes	Yes	No	Yes	c.2465G > A	(Pettersson et al., 2017)	4
-	F	Yes	-	Yes	Yes	Yes	-	-			
5	F	-	-	Yes	Yes	Yes	-	-		(Feigenbaum et al., 2013;	4
25	M	-	-	-	Yes	Yes	-	-		Rutsch et al., 2015)	
4	M	Yes	Yes	Yes	Yes	-	No	Yes			
3	F	Yes	Yes	Yes	Yes	Yes	No	Yes			
3	M	Yes	-	Yes	Yes	Yes	No	-			
Child	M	-	-	-	Yes	-	-	-			
3	F	Yes	Yes	Yes	Yes	-	Yes	-			
7	F	Yes	-	Yes	-	Yes	-	Yes	c.2561T > A	(Takeichi et al., 2018)	4
30	F	-	-	-	-	Yes	-	-	c.986T > C	(Vengoechea and DiMonda, 2020)	4
9	F	Yes	-	Yes	Yes	-	-	-	c.992C > G	(de Carvalho et al., 2017)	4
47	M	Yes	-	Yes	Yes	-	-	-			
18	F	Yes	-	-	-	-	-	-	c.992C > T		
45	F	-	-	-	Yes	-	-	-			
27	F	-	-	-	Yes	-	-	-			
30	M	Yes	-	-	-	-	-	-	-	(Ghadiam and Mungee, 2017)	4

Article Selection

The articles were evaluated for eligibility by title/abstract and then full-text screening using the Rayyan website (Ouzzani et al., 2016). Two reviewers assessed the articles separately. The recorded data were as follows: title/journal/date of publication of the article; authors; the number of patients, and their age/gender; mutation description and; description of dental phenotype with delayed eruption/carious lesions/short roots/premature loss of teeth/dental agenesis/low height of alveolar bone. We had chosen to group the different root manifestations/pathology/anomaly (resorption and lack of edification) under the term "short roots".

Visualization of Mutations

Using the Reference sequence of the *IFIH1* gene (NM_022168.4) and the associated protein sequence of melanoma differentiation-associated protein 5 (MDA5) (NP_071451.2), the domains in which the various mutations were located were determined using the Plot Protein website (Turner, 2013). For the conservation analysis, a multiple sequence alignment was generated using the following orthologs of human IFIH1: house mouse (NP_082111.2), zebrafish (NP_001295492.1), Norway rat (NP_001102669.1), pig (NP_001093664.1), tropical clawed frog (NP_031749133.1), chimpanzee (NP_˚16805442.2), and coelacanth (NP_014348983.1).

SEM Observation

A first permanent maxillary molar and a second primary mandibular molar were observed using SEM. The teeth were collected following the relevant guidelines related to research involving the patients' samples in France (ethical approval n˚19.11.04.64248, ORCELL). The samples were dehydrated using an ethanol gradient, before being thinly coated with gold using a Q15OR ES system (Quorum Technologies Ltd., East Sussex, UK). Then, it was observed using a SEM (TM3030 Tabletop Microscope, Hitachi) under few magnifications (from x1,5 k to x3,0 k) with a composite view.

RESULTS

Article Selection

A total of 44 articles were retrieved from the PubMed database. After full-text screening, 11 articles were included and analyzed (**Figure 1**), of which six were case reports and five were case series; two articles described the same patients: clinical description for the first one and mutation description for the second one. A total of 22 patients were described, 11 girls and 11 boys.

Mutation Description

Eight *IFIH1* mutations were described (**Table 1**) in 11 families. One hotspot mutation seems to be evident (c.2465G > A) with nine patients through four families. To visualize the positions of protein domains and their amino acid boundaries' positions, we used the RefSeq IFIH1, found on NCBI protein, NP_071451.2, containing 1025 amino acid residues (**Figure 2**). Five mutations were in helicase domain 1 (Hel1), two in helicase domain 2 (Hel2), and the last one in the pincer domain, which connects Hel2 and the C-terminal domain (CTD). In one article (Ghadiam

TABLE 3 | Oral and dental phenotypes of Singleton–Merten patients.

	Yes (%)	No (%)	NR (%)	% Among patients with oral examination (% yes)
Delayed eruption	12 (60%)	0 (0%)	8 (40%)	100
Carious lesions	3 (15%)	2 (10%)	15 (75%)	60
Short roots	11 (55%)	0 (0%)	9 (45%)	100
Premature loss of permanent teeth	16 (80%)	0 (0%)	4 (20%)	100
Impacted teeth	8 (40%)	1 (5%)	11 (55%)	89
Dental agenesis	2 (10%)	4 (20%)	14 (70%)	33
Low height of alveolar bone	6 (30%)	1 (5%)	13 (65%)	86

N: number of concerned patients; NR: non-reported.

and Mungee, 2017), an *IFIH1* mutation was reported but was neither described nor detailed.

Phenotype Description

The dental findings descriptions are summarized in **Table 2**. When signs were not reported, we specified ("not reported").

The most frequent dental findings were as follows: short roots, delayed eruption, and premature loss of permanent teeth (present in 100% of screened patients). The patients showed in addition impacted permanent teeth (89%), a decreased height of alveolar bone (86%), and carious lesions (67%). Two patients were described with dental agenesis (**Table 3**). However, oral data were absent in almost 50% of patients, and the most constant sign examined or reported was "premature loss of permanent teeth".

The patient described by Takeichi et al. (2018) showed a different oral phenotype/manifestation. On the X-rays, we observed that none of the primary and permanent teeth were erupted, while all the dental germs were visible in the jawbones.

CASE-REPORT

A 10-year-old child was referred to the Reference Centre of Oral and Dental Rare Diseases at Rothschild Hospital (AP-HP). Written informed consent was obtained from the patient and his legal guardian mother for the publication of any potentially identifiable images or data included in this article. The patient experienced pain due to numerous carious lesions, associated with dental and jawbone anomalies visible on the panoramic radiograph (**Figure 3**). He was the third child of a sibship of four healthy children from a non-consanguineous union. He had recently arrived in France, for medical reasons. According to his mother, he walked until he was 1 year old and then progressively developed walking difficulties and muscle weakness requiring a wheelchair at 10 years of age. He presented cutaneous xerosis and ophthalmologic glaucoma. No intellectual disability was noticed.

We observed dysmorphic facial features: fine and space hair, cranial malformation as trigonocephaly with a triangular face, discrete hypertelorism, long arched eyebrow, and low set-ears. He had clubfeet, joint retractions, and scoliosis. The weight and height were below—2SD. Intra-oral examination revealed multiple caries, severe teeth malposition, especially in the anterior arch, and oral hygiene deficiency with a 100% plaque index (**Figure 3**). On X-ray examination, we did not find any dental agenesis. All the germs of the permanent teeth were visible, including the third permanent molars. The examination revealed the presence of thin roots in primary teeth and undeveloped roots in permanent teeth. The roots were shortened beyond the first root third despite the closure of the dental apices. Almost all primary teeth and permanent molars presented extensive-stage caries with abscesses (ICDAS codes 5 and 6, RC 6). The teeth morphology showed a bulbous-shaped crown, with normal pulp chamber volume. Teeth were mobile (mobility II-III). We observed a moderate to severe gingival inflammation: bright surface inflammation, erythema, edema and/or hypertrophy of gingiva, and some spontaneous bleedings. We did not observe deep pockets or recessions. The panoramic X-ray revealed a reduction in the alveolar bone height. The whole-genome sequencing analysis revealed a heterozygous *de novo* variant in the *IFIH1 gene* (NM_022168.4) c.2465G > A (p.Arg822Gln).

SEM analysis showed that neither enamel nor dentin defects were associated with SGMRT1, and normal cementum was present. Indeed, we observed normal enamel prisms, dentin tubules, and a visible cementum layer.

DISCUSSION

The oral phenotype of Singleton–Merten syndrome was confusing in the literature. The most frequent anomaly concerns root, dental eruption, and premature tooth loss. In this systematic review, 100% of the case reports described "short roots" and "premature loss of permanent teeth." The short root is a quantitative tooth anomaly easily recognizable on X-rays. Regarding the X-rays available within articles, the short roots were mostly concerned with permanent dentition (primary teeth show long and fine roots). The shortness of the roots may result from congenital root deficiency during root formation or in the radicular resorption process. Root resorption is defined as a progressive loss of dentin and cementum through the continued action of osteoclastic cells (Fuss et al., 2003). In this literature review, the authors described indifferently "short roots" (Pettersson et al., 2017), "loss of root tooth structure," and "aggressive resorptive process" (Feigenbaum et al., 2013). We analyzed the available X-rays to clarify these findings. We did not

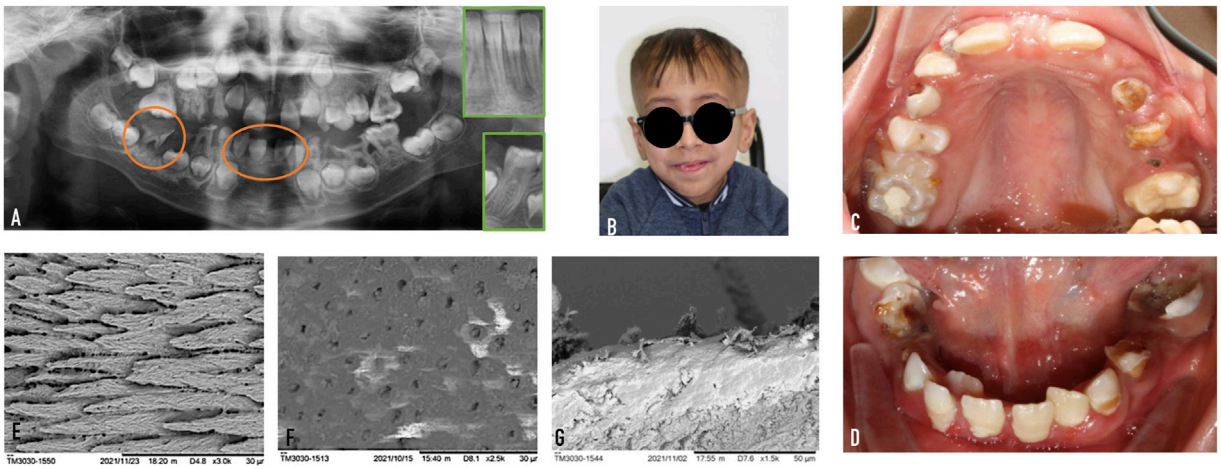

FIGURE 3 | Case report. **(A)** Orthopantomogram X-ray of our 10-year-old Singleton-Merten patient. In orange, a first permanent molar (tooth n°46) and central permanent mandibular incisors (teeth n° 31–41) with short roots were highlighted. To compare, a healthy patient's teeth are shown in a green insert. **(B)** Photography of the patient. **(C,D)** Intra-oral photographies of the maxillary and the mandibular arch. **(E)** First molar enamel. **(F)** Second temporary molar dentin. **(G)** First molar cement.

find any radiographic signs of resorption, such as an enlargement of the root canal, an asymmetric bowl-shaped radiolucency, or an asymmetric loss of root, as described in classical root resorption (Patel and Saberi, 2018). Conversely, we observed closed root apices. We suggested that the root defects observed in SGMRT1 patients are an impairment in root elongation more than in a resorption phenomenon. This lack of root development seems to be the cause of the premature loss of permanent teeth, as described by the majority of the authors (Feigenbaum et al., 2013; Bursztejn et al., 2015; Rutsch et al., 2015; de Carvalho et al., 2017; Pettersson et al., 2017; Xiao et al., 2021; Hasegawa et al., 2022) and as observed in the patient. Teeth root anomalies are also observed in radicular dentin dysplasia and Fraser syndrome. We can discriminate the SGMRT1 patients from radicular dentin dysplasia because of the lack of pulp obliteration and from Fraser syndrome because of the lack of short roots in primary teeth (de La Dure-Molla et al., 2015; Luder, 2015).

When reported, "delayed eruption" was observed in 100% of the patients, and "impacted teeth," in 89%. Delayed eruption and impacted teeth can be difficult to discriminate. A normal eruption occurred over a period of 2 years, and a delayed eruption is defined by a tooth eruption more than 2 SD beyond the mean eruption age (de La Dure-Molla et al., 2019). The eruption must be tracked over time to determine if teeth are impacted or had just a delayed eruption. In this review, the patients were often too young, and this finding must be reevaluated in adults. So we cannot conclude if the tooth eruption has been delayed or failed. In our patient, no impacted tooth was noticed. However, three patients had no tooth eruption (Singleton and Merten, 1973; Takeichi et al., 2018). For the patients described by Singleton and Merten, no genetic analysis was performed; for the second report, the patient was diagnosed with SMS and AGS-7. We concluded that the pathology of an eruption occurring in SMS must be confirmed by a refined analysis comparing the dental age and civil age.

Furthermore, a great diversity of features appeared in the various case reports, such as deficiency of alveolar bone and carious lesions. Several SGMRT1 patients presented a deficiency of alveolar bone growth. Osteopenia is often reported in SGMRT1 patients' limbs, which might be also found in jawbones. The alveolar bone growth is directly linked to root development and teeth eruption. The absence of root elongation and the premature loss of the teeth may therefore lead to this defective bone.

Our patient was in mixed dentition. The remaining primary teeth had thin roots with normal length, and all erupted permanent teeth had short roots and mobility. Clinical examination and SEM observation did not reveal any dental tissue (enamel, dentin, and cementum) anomalies. A radiological exam was necessary to identify the root anomalies. Here, we reported a heterozygous *de novo* variant in *IFIH1* c.2465G > A (p.Arg822Gln). This variant has been previously described in Singleton–Merten syndrome in nine patients through four families (Feigenbaum et al., 2013; Rutsch et al., 2015; Pettersson et al., 2017). It is the most prevalent reported hotspot. Until now, all reported variants are missense with a gain-of-function effect and an enhanced expression of type I interferon-stimulated genes (Rice et al., 2020).

The role of *IFIH1* is still poorly understood, and a systematic description of dental signs in patients with an *IFIH1* mutation should help improve the understanding of its function in odontogenesis. IFIH1 gain-of-function is associated with dysregulation of mineralization genes in pulp cells (Lu et al., 2014). However, its role in odontogenesis, root edification, periodontium development, and homeostasis is yet to be explored. *IFIH1* plays a role in response to viral infection and then participates in nuclear factor kappa-B (NFkB) and interferon regulatory factors (IRF) activation. Amazingly, the SGMRT1 patients do not present any reported higher risks of viral infections. The only infectious feature reported in SGMRT1

patients was dental caries. It is an infectious disease linked to bacteria (Chardin et al., 2006). Finally, confused descriptions on oral features occurred in the literature between congenital findings and "acquired" pathology in the SGMT1 patients. Indeed, caries can be explained by oral hygiene deficiency and painful or mobile teeth. It may also be attributed to the muscular weakness or glaucoma exhibited by some SGMRT1 patients.

CONCLUSION

The dental anomalies observed in SGMRT1 seem to affect mainly permanent teeth with variable expressivity. Two main features appeared constant: tooth permanent short roots with closed apex inducing premature loss and tooth eruption defects (delayed or potentially impacted teeth). The pathological exfoliation of the permanent teeth could be considered a pathognomonic and could help in diagnosis. A more systematic description of the dental phenotype with well-defined diagnosis criteria is necessary to better understand the dental phenotype in these patients. Also, an oral evaluation and a follow-up by a dental surgeon are recommended. A fundamental research is needed to understand the dental root formation and tooth eruption and the *IFIH1* impact on these processes.

DATA AVAILABILITY STATEMENT

The original contributions presented in the study are included in the article/supplementary material; further inquiries can be directed to the corresponding author.

AUTHOR CONTRIBUTIONS

BF developed the framework for the review. BF, MD-M, and MR formulated the search strategy used to identify publications. MR and BF performed the primary screening in Rayyan, with MD-M resolving any conflicts on study inclusion. Data extraction and analysis were conducted by MR and BF. BF, MR, MD-M, VC-D, and SK performed writing and primary editing. MR, MD-M and BF took care of the patient. All authors contributed to the manuscript and approved the submitted version.

FUNDING

This research was made possible through access to the data generated by the France Genomic Medicine Plan 2025. This research was supported by the INSERM/APHP Interface grant (BPJF).

REFERENCES

Bursztejn, A.-C., Briggs, T. A., del Toro Duany, Y., Anderson, B. H., O'Sullivan, J., Williams, S. G., et al. (2015). Unusual Cutaneous Features Associated with a Heterozygous Gain-Of-Function Mutation inIFIH1: Overlap between Aicardi-Goutières and Singleton-Merten Syndromes. *Br. J. Dermatol* 173 (6), 1505–1513. doi:10.1111/bjd.14073

Chardin, H., Barsotti, O., and Bonnaure-Mallet, M. (2006). *Microbiologie en odonto-stomatologie*. Paris, France: Maloine, x+329.

Crow, Y. J., Chase, D. S., Lowenstein Schmidt, J., Szynkiewicz, M., Forte, G. M., Gornall, H. L., et al. (2015). Characterization of Human Disease Phenotypes Associated with Mutations in TREX1, RNASEH2A, RNASEH2B, RNASEH2C, SAMHD1, ADAR, and IFIH1. *Am. J. Med. Genet. A* 167A (2), 296–312. doi:10.1002/ajmg.a.36887

de Carvalho, L. M., Ngoumou, G., Park, J. W., Ehmke, N., Deigendesch, N., Kitabayashi, N., et al. (2017). Musculoskeletal Disease in MDA5-Related Type I Interferonopathy: A Mendelian Mimic of Jaccoud's Arthropathy. *Arthritis & Rheumatology* 69 (10), 2081–2091. doi:10.1002/art.40179

de La Dure-Molla, M., Fournier, B. P., Manzanares, M. C., Acevedo, A. C., Hennekam, R. C., Friedlander, L., et al. (2019). Elements of Morphology: Standard Terminology for the Teeth and Classifying Genetic Dental Disorders. *Am. J. Med. Genet. A* 179 (10), 1913–1981. doi:10.1002/ajmg.a.61316

de La Dure-Molla, M., Philippe Fournier, B., and Berdal, A. (2015). Isolated Dentinogenesis Imperfecta and Dentin Dysplasia: Revision of the Classification. *Eur. J. Hum. Genet.* 23 (4), 445–451. doi:10.1038/ejhg.2014.159

Feigenbaum, A., Müller, C., Yale, C., Kleinheinz, J., Jezewski, P., Kehl, H. G., et al. (2013). Singleton-Merten Syndrome: an Autosomal Dominant Disorder with Variable Expression. *Am. J. Med. Genet.* 161 (2), 360–370. doi:10.1002/ajmg.a.35732

Fuss, Z., Tsesis, I., and Lin, S. (2003). Root Resorption - Diagnosis, Classification and Treatment Choices Based on Stimulation Factors. *Dent. Traumatol. Off. Publ. Int. Assoc. Dent. Traumatol. août* 19 (4), 175–182. doi:10.1034/j.1600-9657.2003.00192.x

Ghadiam, H., and Mungee, S. (2017). Singleton Merten Syndrome: A Rare Cause of Early Onset Aortic Stenosis. *Case Rep. Cardiol.* 2017, 8197954. doi:10.1155/2017/8197954

Hasegawa, K., Tanaka, H., Futagawa, N., Miyahara, H., Higuchi, Y., and Tsukahara, H. (2022). A Novel Pathogenic Variant P. Asp797Val in IFIH1 in a Japanese Boy with Overlapping Singleton-Merten Syndrome and Aicardi-Goutières Syndrome. *Am. J Med Genet. Pt A* 188 (1), 249–252. doi:10.1002/ajmg.a.62478

Jang, M.-A., Kim, E. K., Now, H., Nguyen, N. T. H., Kim, W.-J., Yoo, J.-Y., et al. (2015). Mutations in DDX58, Which Encodes RIG-I, Cause Atypical Singleton-Merten Syndrome. *Am. J. Hum. Genet.* 96 (2), 266–274. doi:10.1016/j.ajhg.2014.11.019

Lu, C., Mamaeva, O. A., Cui, C., Amm, H., Rutsch, F., and MacDougall, M. (2014). Establishment of Singleton-Merten Syndrome Pulp Cells: Evidence of Mineralization Dysregulation. *Connect. Tissue Res.* 55 Suppl 1 (Suppl. 1), 57–61. doi:10.3109/03008207.2014.923880

Luder, H. U. (2015). Malformations of the Tooth Root in Humans. *Front. Physiol.* 6, 307. doi:10.3389/fphys.2015.00307

Ouzzani, M., Hammady, H., Fedorowicz, Z., and Elmagarmid, A. (2016). Rayyan-a Web and Mobile App for Systematic Reviews. *Syst. Rev.* 5 (1), 210. doi:10.1186/s13643-016-0384-4

Page, M. J., McKenzie, J. E., Bossuyt, P. M., Boutron, I., Hoffmann, T. C., Mulrow, C. D., et al. (2021). The PRISMA 2020 Statement: an Updated Guideline for Reporting Systematic Reviews. *Syst. Rev.* 10 (1), 89. doi:10.1186/s13643-021-01626-4

Patel, S., and Saberi, N. (2018). The Ins and Outs of Root Resorption. *Br. Dent. J.* 224 (9), 691–699. doi:10.1038/sj.bdj.2018.352

Pettersson, M., Bergendal, B., Norderyd, J., Nilsson, D., Anderlid, B. M., Nordgren, A., et al. (2017). Further Evidence for Specific IFIH1 Mutation as a Cause of Singleton-Merten Syndrome with Phenotypic Heterogeneity. *Am. J. Med. Genet.* 173 (5), 1396–1399. doi:10.1002/ajmg.a.38214

Rice, G. I., Park, S., Gavazzi, F., Adang, L. A., Ayuk, L. A., Van Eyck, L., et al. (2020). Genetic and Phenotypic Spectrum Associated with IFIH1 Gain-of-function. *Hum. Mutat.* 41 (4), 837–849. doi:10.1002/humu.23975

Rutsch, F., MacDougall, M., Lu, C., Buers, I., Mamaeva, O., Nitschke, Y., et al. (2015). A Specific IFIH1 Gain-Of-Function Mutation Causes Singleton-Merten Syndrome. *Am. J. Hum. Genet.* 96 (2), 275–282. doi:10.1016/j.ajhg.2014.12.014

Singleton, E. B., and Merten, D. F. (1973). An Unusual Syndrome of Widened Medullary Cavities of the Metacarpals and Phalanges, Aortic Calcification

and Abnormal Dentition. *Pediatr. Radiol.* 1 (1), 2–7. doi:10.1007/bf00972817

Takeichi, T., Katayama, C., Tanaka, T., Okuno, Y., Murakami, N., Kono, M., et al. (2018). A Novel IFIH1 Mutation in the Pincer Domain Underlies the Clinical Features of Both Aicardi-Goutières and Singleton-Merten Syndromes in a Single Patient. *Br. J. Dermatol* 178 (2), e111. doi:10.1111/bjd.15869

Turner, T. (2013). Plot Protein: Visualization of Mutations. *J. Clin. Bioinforma.* 3 (1), 14. doi:10.1186/2043-9113-3-14

Vengoechea, J., and DiMonda, J. (2020). A Case of Singleton-Merten Syndrome without Cardiac Involvement Harboring a Novel IFIH1 Variant. *Am. J. Med. Genet.* 182 (6), 1535–1536. doi:10.1002/ajmg.a.61556

Xiao, W., Feng, J., Long, H., Xiao, B., and Luo, Z. H. (2021). Case Report: Aicardi-Goutières Syndrome and Singleton-Merten Syndrome Caused by a Gain-Of-Function Mutation in IFIH1. *Front. Genet.* 12, 660953. doi:10.3389/fgene.2021.660953

Conflict of Interest: The authors declare that the research was conducted in the absence of any commercial or financial relationships that could be construed as a potential conflict of interest.

Publisher's Note: All claims expressed in this article are solely those of the authors and do not necessarily represent those of their affiliated organizations, or those of the publisher, the editors, and the reviewers. Any product that may be evaluated in this article, or claim that may be made by its manufacturer, is not guaranteed or endorsed by the publisher.

frontiers | Frontiers in Genetics

TYPE Original Research
PUBLISHED 17 August 2022
DOI 10.3389/fgene.2022.947126

OPEN ACCESS

EDITED BY
Babak Behnam,
National Sanitation Foundation International, United States

REVIEWED BY
Lucimara Neves,
University of São Paulo, Brazil
Yongchu Pan,
Nanjing Medical University, China

*CORRESPONDENCE
Zhong-Lin Jia,
zhonglinjia@sina.com

SPECIALTY SECTION
This article was submitted to Genetics of Common and Rare Diseases, a section of the journal Frontiers in Genetics

RECEIVED 18 May 2022
ACCEPTED 08 July 2022
PUBLISHED 17 August 2022

CITATION
Li M-J, Shi J-Y, Zhang B-H, Chen Q-M, Shi B and Jia Z-L (2022), Targeted re-sequencing on 1p22 among non-syndromic orofacial clefts from Han Chinese population.
Front. Genet. 13:947126.
doi: 10.3389/fgene.2022.947126

Targeted re-sequencing on 1p22 among non-syndromic orofacial clefts from Han Chinese population

Mu-Jia Li[1,2], Jia-Yu Shi[3], Bi-He Zhang[1,2], Qian-Ming Chen[1], Bing Shi[1,2] and Zhong-Lin Jia[1,2]*

[1]State Key Laboratory of Oral Diseases and National Clinical Research Center for Oral Diseases, West China Hospital of Stomatology, Sichuan University, Chengdu, China, [2]Department of Cleft Lip and Palate, West China Hospital of Stomatology, Sichuan University, Chengdu, China, [3]Division of Growth and Development and Section of Orthodontics, School of Dentistry, University of California, Los Angeles, Los Angeles, CA, United States

Rs560426 at 1p22 was proved to be associated with NSCL/P (non-syndromic cleft lip with or without the palate) in several populations, including Han Chinese population. Here, we conducted a deep sequencing around rs560426 to locate more susceptibility variants in this region. In total, 2,293 NSCL/P cases and 3,235 normal controls were recruited. After sequencing, association analysis was performed. Western blot, RT-qPCR, HE, immunofluorescence staining, and RNA sequencing were conducted for functional analyses of the selected variants. Association analysis indicated that rs77179923 was the only SNP associated with NSCLP specifically (p = 4.70E-04, OR = 1.84), and rs12071152 was uniquely associated with LCLO (p = 4.00E-04, OR = 1.30, 95%CI: 1.12–1.51). Moreover, *de novo* harmful rare variant NM_004815.3, NP_004806.3; c.1652G>C, p.R551T in *ARHGAP29* resulted in a decreased expression level of *ARHGAP29*, which in turn affected NSCL/P-related biological processes; however, no overt cleft palate (CP) phenotype was observed. In conclusion, rs12071152 was a new susceptible variant, which is specifically associated with LCLO among the Han Chinese population. Allele A of it could increase the risk of having a cleft baby. Rs77179923 and rare variant NM_004815.3, NP_004806.3; c.1652G>C, p.R551T at 1p22 were both associated with NSCLP among the Han Chinese population. However, this missense variation contributes to no overt CP phenotype due to dosage insufficiency or compensation from other genes.

KEYWORDS

1p22, targeted re-sequencing, association analysis, LCLO, RNA sequencing

Introduction

Non-syndromic cleft lip with or without the palate (NSCL/P), one of the most common orofacial clefts, has an average prevalence of 1/1,000 live births worldwide, with a relatively high prevalence among Asians (Croen et al., 1998; Tolarova and Cervenka, 1998; Mossey and Modell, 2012). The affected kids usually suffer from a number of problems related to clefts, such as speech, hearing, and psychological disorders (Lewis et al., 2017). It is necessary for them to receive coordinated multidisciplinary care that lasts from the stage of infant to adulthood, which imposes a heavy financial burden on their families.

NSCL/P is a complex disorder, with genetic and environmental factors and their interplay involved (Dixon et al., 2011; Rahimov et al., 2012; Worley et al., 2018). However, genes play a dominant role (Grosen et al., 2010; Dixon et al., 2011; Rahimov et al., 2012; Baldacci et al., 2018). Thus, lots of studies have been designed to shed light on the susceptibility genes or loci for NSCL/P, among which genome-wide association studies (GWASs) have identified an unprecedented number of genetic variants associated with it, and to date, over 40 risk loci for NSCL/P have been identified (Leslie and Marazita, 2013; Lin-Shiao et al., 2019). However, those findings only account for about 20% estimated heritability of NSCL/P (Beaty et al., 2016; Lin-Shiao et al., 2019); the missing heritability is partially attributed to the strict significance threshold of GWAS, which leads to the failed detection of that single-nucleotide polymorphism (SNP) with modest effect (Manolio et al., 2009; Tam et al., 2019); in addition, those risk loci identified by GWAS are usually driven by associated genetic variants due to linkage disequilibrium (Altshuler et al., 2008; Dickson et al., 2010), thus making it difficult to pinpoint the casual variants. Based on this, high-depth sequencing targeted at those risk loci is a cost-effective method to identify variants with larger effect sizes that are missed by GWAS, and this would also facilitate the discernment of casual variants (Manolio et al., 2009; Sazonovs and Barrett, 2018).

1p22, which contains rs560426, was initially identified as one of the risk loci for NSCL/P because of the statistically significant association between rs560426 and NSCL/P via GWAS (Beaty et al., 2010). Our previous study indicated that rs560426 was significantly associated with NSCL/P among the Han Chinese population, which further conferred susceptibility to 1p22. Rs560426 is located in *ABCA4* gene, which is surely excluded from the candidate susceptibility genes in 1p22 due to its expression restricted to the retina (Beaty et al., 2010). Leslie et al. (2012) identified several rare variants that were associated with NSCL/P in *ARHGAP29*, which is adjacent to *ABCA4* and expressed in the developing face. Therefore, *ARHGAP29* was highly suspected as a susceptibility gene of NSCL/P in 1p22. From then on, a surge of studies focused on 1p22, and plenty of rare variants in *ARHGAP29* were identified in multiple ethnicities (Leslie et al., 2012; Butali et al., 2014; Chandrasekharan and Ramanathan, 2014; Letra et al., 2014; Gowans et al., 2016; Savastano et al., 2017).

In this study, we aim to conduct a deep screening targeting the 1p22 locus to fully dig into susceptibility SNPs or indels through bioinformatics, statistics analysis, and functional experiments, hoping to identify more susceptibility variants at this locus for NSCL/P among the Han Chinese population.

Materials and methods

Sample collection and ethics statement

In total, 159 NSCL/P cases were included in the deep sequencing phase of our study, whereas 542 controls' WGS data with an average coverage of 39.89 was downloaded from the Novogene internal database (http://www.novogene.com/); 2,134 NSCL/P (1047 NSCLO and 1087 NSCLP) and 2,693 normal controls from West China Second University Hospital, Sichuan University, were recruited in the replication phase. Cases were collected between 2016 and 2018 from the Cleft Lip and Palate Surgery Department of West China Hospital of Stomatology, Sichuan University. All the participants were self-recognized as the Han Chinese and denied family history as well as other congenital diseases, therein, the phenotype of the patients was assessed by both physicians and geneticists. More details of samples are shown in Supplementary Table S1.

Our study abides by the STOBE (Strengthening the Reporting of Observational Studies in Epidemiology) guidelines and was approved by HEC (the Hospital Ethics Committee) of West China Hospital of Stomatology. All individuals voluntarily joined this study with informed consent (WCHSIRB-D-2016-012R1).

Targeted region deep sequencing

DNA was extracted from peripheral blood of each sample by the salting-out method. After quality control, 1.0 μg of each DNA sample was enriched by using Agilent SureSelectXT Custom kit. Then, sequencing was conducted on the Illumina Hiseq X Ten platform to get paired-end 150bp reads by Novogene (China). The sequenced region was selected around rs560426 (GRCh37/hg19, chr1:94,453,779 to 94,739,314) based on the LD structure in CHB/JPT HapMap project.

Bioinformatics analysis

After removing adapter-related reads, N-containing reads, and low-quality reads, the clean sequence data were mapped to the human genome GRCh37/hg19 by Burrows–Wheeler Aligner (BWA) software (Li and Durbin, 2009). Then, 943 single

nucleotide variants (SNPs) and 390 insertion/deletions (In/Dels) were identified by the Sequence Alignment Map (SAM tools) (Li et al., 2009) and merged by VCF (variant call format) tools (version 0.1.13) (Danecek et al., 2011). Later, variants were annotated by ANNOVAR (version 201707) (Wang et al., 2010), followed by function prediction via SIFT (Ng and Henikoff, 2003), v1.3 CADD (Kircher et al., 2014), Polyphen-2 (http://genetics.bwh.harvard.edu/pph2/) (Adzhubei et al., 2013), and MutationTaster (http://www.mutationtaster.org/) (Schwarz et al., 2010).

Statistical analysis

In the discovery phase, variants were categorized as either common or rare. Variants with MAF (minor allele frequency) ≥1% were referred to as common variants (they were Single nucleotide polymorphisms or SNPs), and case–control association analysis was performed after excluding SNPs that deviated from Hardy–Weinberg equilibrium (HWE). Three rare variants selected by three conditions were enrolled into burden analysis calculated by the R package SKAT: ① MAF <1% in the CHB population (Beijing Han Chinese population) and CHS population (Southern Han Chinese population) from 1000 Genomes Project database and Novogene internal database; ② MAF <0.001 in the Genome Aggregation Database (GnomAD); ③ at least two prediction tools suggested its harmfulness (SIFT, v1.3 CADD, Polyphen-2, and MutationTaster).

In the replication phase, SNP genotyping data were retrieved from two GWASs we have ever participated in (Sun et al., 2015; Huang et al., 2019). PLINK software (version 1.9) was used to perform the HWE test, calculate MAF, and perform a case–control association analysis for each SNP (Purcell et al., 2007). The threshold of *P*-value is 0.05/99 = 5.05E-04.

Sanger sequencing

Three novel harmful rare variants, which were not reported in a public database, such as dbSNP (https://www.ncbi.nlm.nih.gov/SNP/) (Smigielski et al., 2000), 1000 Genome (https://www.internationalgenome.org/), ExAC (http://exac.broadinstitute.org) (version 0.3.1) (Lek et al., 2016), CADD (http://cadd.gs.washington.edu/snv) (Rentzsch et al., 2018), and HGMD (http://www.hgmd.org) (Stenson et al., 2009), were further validated in carriers and their parents by Sanger sequencing, and PCR primers for genomic sequence were designed using Primer 3 (https://bioinfo.ut.ee/primer3-0.4.0/) (Supplementary Table S2). Then, for amplification, a mixture of Taq polymerase enzyme, PCR primers, water, and DNA sample was prepared. The amplified DNA products were then sequenced using the ABI 3730 Sequencer and analyzed with Sequence Scanner v1.0.

Cell culture and transient transfection

HEK-293T cell line was cultured in Dulbecco's modified Eagle medium (DMEM) with 10% fetal bovine serum (PAN Biotech, Germany) and 1% Penicillin–Streptomycin Solution (Gibco, Foster City, CA, United States).

Full-length cDNA of *ARHGAP29* (NM_004815.3) was synthesized and sub-cloned into pcDNA3.1 plasmid, to which site-directed mutagenesis was applied and thus obtained pcDNA3.1-*ARHGAP29*^{R551T} plasmid (GeneChem, China). Then, they were transfected into HEK-293T cells by using Lipofectamine 3000 (Invitrogen, Carlsbad, CA) according to the manufacturer's instructions, respectively.

Construction of the *Arhgap29*^{R553T} mutant mouse model

The homology analysis of the amino acid sequences of human and mouse ARHGAP29 revealed that the 553rd amino acid of mouse ARHGAP29 was identical to the 551st amino acid of humans. Therefore, the CRISPR/Cas9 system was used to engineer a single base substitution mutation from G to C at the 1658th nucleotide of the cDNA of the *Arhgap29* gene in the C57BL/6J mouse, resulting in a change from arginine (R) to threonine (T) at the 553rd amino acid. This part of the experiment was conducted by Gempharmtech Biotechnology Company (China), from whom we acquired F1 heterozygous *Arhgap29*$^{R553T/+}$ mice for the subsequent experiments.

Due to the limited number of F1 heterozygous *Arhgap29*$^{R553T/+}$ mice, they were crossed to C57BL/6J wild-type mice to generate a sufficient number of heterozygous mice. After genotyping the offsprings, heterozygous *Arhgap29*$^{R553T/+}$ mice were chosen to be maintained. To be specific, 1–2 mm tail tissue was cut off from each mouse, from which DNA was extracted and amplified by PCR (Forward primer: CCACCACTTCTGTGGTGTCCTTG, reverse primer: CTACCCATGTTCTGCCTGTTGAG), both of which were completed using One Step Mouse Genotyping Kit (Vazyme, China). Sanger sequencing was then performed on those PCR products to confirm the genotype of each mouse.

After that, heterozygous *Arhgap29*$^{R553T/+}$ mice were crossed overnight, females were examined for the presence of a vaginal plug the next morning, and the day when the vaginal plug was observed was designated as embryonic day 0.5 (E0.5).

RNA extraction

RNA was extracted from each group of HEK-293T cells using RNA-easy Isolation Reagent (Vazyme, China) 48 h after

TABLE 1 Replication of the association analysis in 1p22.

SNP	A1	NSCL/P		NSCLP		NSCLO	
		P	OR (95%CI)	*P*	OR (95%CI)	*P*	OR (95%CI)
rs2282229	A	0.150	0.84 (0.67–1.06)	0.640	1.08 (0.78–1.49)	0.021	0.71 (0.54–0.95)
rs11165065	A	0.350	0.91 (0.75–1.11)	0.370	1.13 (0.87–1.47)	0.057	0.79 (0.62–1.01)
rs560426	C	0.430	1.05 (0.94–1.17)	0.730	1.03 (0.88–1.20)	0.550	1.04 (0.91–1.20)
rs77179923	**T**	0.013	1.47 (1.08–2.00)	**4.70E-04**	**1.84(1.31–2.58)**	0.640	1.13 (0.68–1.89)
rs12088309	C	0.050	1.11 (1.00–1.23)	0.190	1.10 (0.95–1.28)	0.066	1.13 (0.99–1.28)
rs2297636	C	0.077	1.10 (0.99–1.22)	0.700	1.03 (0.89–1.19)	0.018	1.17 (1.03–1.33)
rs12057375	T	0.043	1.13 (1.00–1.26)	0.140	1.13 (0.96–1.32)	0.110	1.12 (0.97–1.30)
rs3789434	C	0.050	1.12 (1.00–1.26)	0.170	1.12 (0.95–1.31)	0.110	1.12 (0.98–1.30)
rs4147810	G	0.042	1.13 (1.00–1.26)	0.140	1.13 (0.96–1.32)	0.100	1.13 (0.98–1.30)
rs2297635	A	0.048	1.12 (1.00–1.26)	0.170	1.12 (0.95–1.31)	0.110	1.12 (0.97–1.30)
rs3789438	T	0.040	1.13 (1.01–1.27)	0.160	1.12 (0.96–1.31)	0.093	1.13 (0.98–1.30)
rs11165079	T	0.340	0.94 (0.82–1.07)	0.580	0.95 (0.79–1.14)	0.340	0.93 (0.79–1.09)
rs11165080	G	0.300	0.93 (0.82–1.06)	0.560	0.95 (0.79–1.14)	0.300	0.92 (0.78–1.08)
rs1931570	T	0.340	0.94 (0.82–1.07)	0.600	0.95 (0.79–1.15)	0.340	0.93 (0.79–1.09)
rs1931566	G	0.340	0.94 (0.82–1.07)	0.590	0.95 (0.79–1.14)	0.330	0.92 (0.79–1.08)
rs12071152	A	0.002	1.19 (1.06–1.33)	0.060	1.16 (0.99–1.36)	9.40E-04	1.27 (1.10–1.46)

The table shows SNPs with $p < 0.05$ in the replication phase. A1, minor allele; SNP, single nucleotide polymorphism; NSCL/P, non-syndromic cleft lip with or without the palate; NSCLP, non-syndromic cleft lip with the cleft palate; NSCLO, non-syndromic cleft lip only. OR refers to odds ratio. 95%CI refers to 95% confidence interval. *P* refers to *P*-value for this test. The bold characters indicated the significant SNPs after multiple corrections (significant threshold is 5.05E-04).

transfection. At E13.5, RNA was extracted from the secondary palate of homozygous *Arhgap29*$^{R553T/R553T}$ and wild-type mice. A total of 500 ng RNA was undertaken reverse transcription PCR to form cDNA by Takara PrimeScript kit.

RNA sequencing

Using the BGISEQ-500 platform, RNA sequencing was performed on the cDNA library of *Arhgap29*$^{R553T/R553T}$ and wild-type mice (BGI, China). In each group, two biological replications were included. Using DEseq2 and the Gene Ontology (GO) database, differential gene expression analysis and annotation for the biological process of DEGs (differential expression genes) were conducted.

Quantitative real-time qPCR

RT-qPCR was performed by using Takara TB Green Premix ExTaq. *GAPDH* was chosen as a reference gene, and primers are shown in Supplementary Table S3. Results were analyzed using the $2^{-\Delta\Delta Ct}$ method. Each of the three biological replications was accompanied by three technical replications. Statistical analysis was calculated by the unpaired two-tailed t-test in GraphPad Prism 8 software.

Western blot

Furthermore, 48 h after transfection, after discarding the culture medium and washing with PBS, 250 μl of lysate was added to each well (containing 10 dsμl of PMSF per 1000 μl of RIPA) (Beyotime, China), carefully pipetted, and placed on ice for 10 min. Then, the lysate was collected and centrifuged at 10,000g for 3 min, the supernatant was diluted with ×5 loading buffer (Beyotime, China) and boiled for 10 min.

Subsequently, protein samples were separated by electrophoresis in agarose gels and transferred onto PVDF membranes, which were then blocked by 5% milk for 1 h and incubated with rabbit anti-human Arhgap29 antibody (Novus Biologicals, United States) at 4°C overnight, followed by incubation with anti-rabbit antibody (Proteintech, China) at room temperature for 1 h. At last, proteins were visualized by ECL substrate (Epizyme, China).

Micro-CT scanning

Three homozygous *Arhgap29*$^{R553T/R553T}$ and wild-type mice were selected and their entire body bone tissues were scanned by Micro-CT. The X-ray tube voltage was set to 70 kV, and the current was 114 A. The reconstruction was performed with Mimics 21.0.

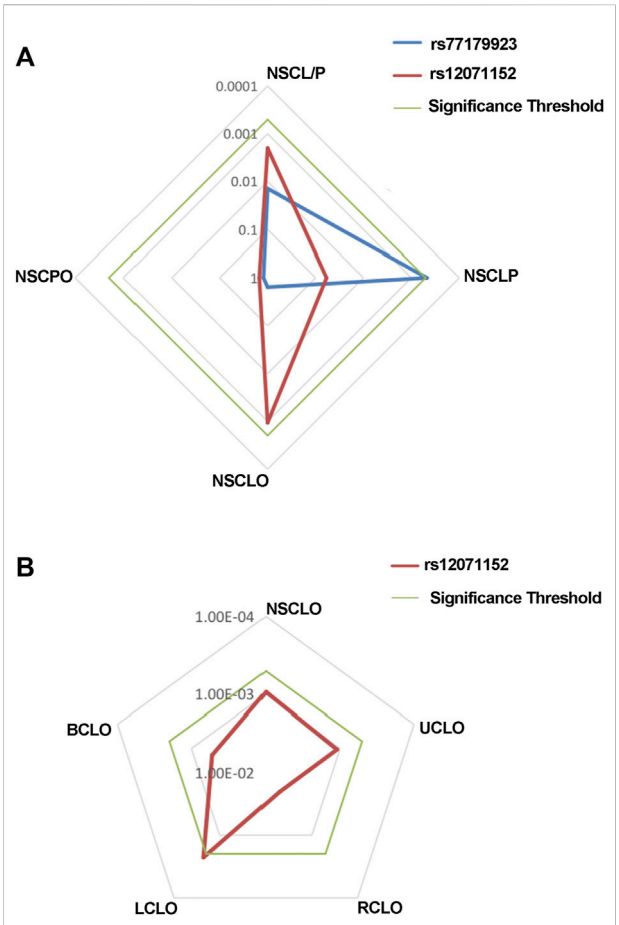

FIGURE 1
Radar chat for the replication of the association analysis. Log *P* value with base 10 were shown in the chat, while blue, red and green line indicate the result of rs77179923, rs12071152 and significance threshold respectively. Significance threshold in the replication phase is 5.05E-04, which is adjusted by multiple correction.

HE and immunofluorescence staining

Embryos from E13.5 to E15.5 were fixed overnight in 4% paraformaldehyde and then fixed in paraffin. Serial paraffin sections of 7 μm were collected and deparaffinized in xylene and rehydrated with a range of ethanol concentrations. For regular histology, hematoxylin and eosin were used to stain tissue sections. For immunofluorescence, after heat-induced antigen retrieval, samples were blocked for 1 h with 5% bovine serum albumin in phosphate-buffered saline. The rabbit anti-human Arhgap29 antibody (Novus Biologicals, United States) was incubated overnight at 4°C. Following a PBST wash, rabbit IgG Alexa 488 (Abcam, United States) was applied for 1 h at room temperature, followed by another wash. Images were captured after mounting samples with DAPI.

Results

Rs77179923 was specifically associated with NSCLP

By targeted region sequencing, we detected a total of 943 single nucleotide variations (SNVs) and 390 In/Dels. Of them, 656 SNVs were recognized as common variants and recruited into case–control association analysis, whereas 3 rare variants were enrolled in burden analysis (data did not show any significance).

In the discovery phase, 99 of the 656 SNVs in our targeted region were identified to be potential susceptibility variants of NSCL/P with a *P*-value less than 0.05 (Supplementary Figure S1 and Supplementary Table S4). Subsequently, all the 99 SNPs were replicated among 1,626 NSCL/P cases and 2,255 controls. According to the significance threshold after multiple corrections, the SNPs with a *P*-value less than 5.05E-04 are associated with the replication phase.

MAF and HWE (Supplementary Table S5) of the replicated SNPs were calculated, and those SNPs with MAF above 1% and *P*-value of HWE above 0.05 were recruited into the association analysis. Interestingly, we found that rs77179923 was specifically associated with NSCLP (p = 4.70E-04, OR = 1.84, 95%CI: 1.31–2.58), and its T allele was at risk for NSCLP, which indicated that the carries could have a higher risk to give birth a cleft baby. Rs12071152 was marginally associated with NSCLO (p = 9.40E-04, OR = 1.27, 95%CI:1.10–1.46). None of SNPs was identified to be associated with NSCL/P (Table1 and Figure 1A).

Rs12071152 was uniquely associated with LCLO

To further test if the 99 SNPs associated with sub-phenotypes of NSCLO, we divided NSCLO into BCLO (bilateral cleft lip only), UCLO (unilateral cleft lip only), RCLO (right cleft lip only), and LCLO (left cleft lip only). Intriguingly, we noticed that rs12071152 showed specific association with LCLO (p = 4.00E-04, OR = 1.30, 95%CI: 1.12–1.51); although the association between rs12071152 and NSCLO (p = 9.40E-04, OR = 1.27, 95%CI: 1.10–1.46) did not survive after multiple corrections, its association with BCLO (p = 0.002, OR = 1.28, 95%CI:1.10–1.49), RCLO (p = 0.005, OR = 1.24, 95%CI:1.07–1.45), and UCLO (p = 0.001, OR = 1.27, 95%CI:1.10–1.47) were all not reached the significance threshold of 5.05E-04 (Table 2; Figure 1B). Our data indicated that there existed genetic heterogeneity among BCLO, UCLO, RCLO, and LCLO.

TABLE 2 Replication of the association analysis in 1p22 among sub-phenotype of NSCLO.

SNP	A1	BCLO		LCLO		RCLO		UCLO	
		P	OR (95%CI)	*P*	OR (95%CI)	*P*	OR (95%CI)	*P*	OR (95%CI)
rs2282229	A	0.026	0.71 (0.52–0.96)	0.031	0.72 (0.54–0.97)	0.038	0.73 (0.54–0.98)	0.039	0.74 (0.55–0.99)
rs11165065	A	0.046	0.77 (0.59–1.00)	0.065	0.79 (0.62–1.02)	0.056	0.78 (0.60–1.01)	0.067	0.79 (0.62–1.02)
rs2297636	C	0.019	1.19 (1.03–1.37)	0.034	1.16 (1.01–1.33)	0.039	1.16 (1.01–1.33)	0.044	1.15 (1.00–1.31)
rs10782976	G	0.055	0.86 (0.74–1.00)	0.028	0.85 (0.73–0.98)	0.068	0.87 (0.75–1.01)	0.039	0.86 (0.74–0.99)
rs4147804	A	0.067	0.87 (0.74–1.01)	0.039	0.86 (0.74–0.99)	0.087	0.88 (0.75–1.02)	0.054	0.87 (0.75–1.00)
rs4147803	C	0.053	0.86 (0.74–1.00)	0.030	0.85 (0.73–0.98)	0.070	0.87 (0.75–1.01)	0.043	0.86 (0.75–1.00)
rs3761911	A	0.079	0.87 (0.75–1.02)	0.040	0.86 (0.74–0.99)	0.114	0.89 (0.76–1.03)	0.063	0.87 (0.76–1.01)
rs1931572	C	0.080	0.87 (0.75–1.02)	0.041	0.86 (0.74–0.99)	0.115	0.89 (0.76–1.03)	0.064	0.87 (0.76–1.01)
rs12407620	A	0.079	0.87 (0.75–1.02)	0.040	0.86 (0.74–0.99)	0.114	0.89 (0.76–1.03)	0.063	0.87 (0.76–1.01)
rs1931571	T	0.080	0.87 (0.75–1.02)	0.041	0.86 (0.74–0.99)	0.115	0.89 (0.76–1.03)	0.064	0.87 (0.76–1.01)
rs12730118	A	0.065	0.87 (0.74–1.01)	0.033	0.85 (0.74–0.99)	0.095	0.88 (0.76–1.02)	0.052	0.87 (0.75–1.00)
rs7550646	G	0.065	0.87 (0.74–1.01)	0.033	0.85 (0.74–0.99)	0.095	0.88 (0.76–1.02)	0.053	0.87 (0.75–1.00)
rs6698524	G	0.065	0.87 (0.74–1.01)	0.033	0.85 (0.74–0.99)	0.095	0.88 (0.76–1.02)	0.053	0.87 (0.75–1.00)
rs6701591	A	0.066	0.87 (0.74–1.01)	0.033	0.85 (0.74–0.99)	0.096	0.88 (0.76–1.02)	0.053	0.87 (0.75–1.00)
rs34497591	T	0.065	0.87 (0.74–1.01)	0.033	0.85 (0.74–0.99)	0.095	0.88 (0.76–1.02)	0.053	0.87 (0.75–1.00)
rs1931569	A	0.065	0.87 (0.74–1.01)	0.033	0.85 (0.74–0.99)	0.095	0.88 (0.76–1.02)	0.053	0.87 (0.75–1.00)
rs1931568	G	0.065	0.87 (0.74–1.01)	0.033	0.85 (0.74–0.99)	0.095	0.88 (0.76–1.02)	0.053	0.87 (0.75–1.00)
rs1931567	C	0.065	0.87 (0.74–1.01)	0.033	0.85 (0.74–0.99)	0.095	0.88 (0.76–1.02)	0.053	0.87 (0.75–1.00)
rs34781620	G	0.065	0.87 (0.74–1.01)	0.033	0.85 (0.74–0.99)	0.095	0.88 (0.76–1.02)	0.053	0.87 (0.75–1.00)
rs12071152	**A**	0.002	1.28 (1.10–1.49)	**4.00E-04**	**1.30(1.12–1.51)**	0.005	1.24 (1.07–1.45)	0.001	1.27 (1.10–1.47)
rs17398522	C	0.065	0.87 (0.74–1.01)	0.033	0.85 (0.74–0.99)	0.095	0.88 (0.76–1.02)	0.053	0.87 (0.75–1.00)
rs6686599	A	0.055	0.86 (0.74–1.00)	0.034	0.85 (0.74–0.99)	0.083	0.88 (0.75–1.02)	0.054	0.87 (0.75–1.00)
rs7546201	A	0.030	0.84 (0.72–0.98)	0.015	0.83 (0.72–0.97)	0.048	0.86 (0.74–1.00)	0.026	0.85 (0.74–0.98)
rs6541410	G	0.034	0.85 (0.73–0.99)	0.017	0.84 (0.72–0.97)	0.053	0.86 (0.74–1.00)	0.029	0.85 (0.74–0.98)
rs58544825	A	0.042	0.85 (0.73–0.99)	0.021	0.84 (0.73–0.97)	0.064	0.87 (0.75–1.01)	0.035	0.86 (0.74–0.99)
rs7512276	G	0.047	0.86 (0.73–1.00)	0.023	0.84 (0.73–0.98)	0.070	0.87 (0.75–1.01)	0.037	0.86 (0.74–0.99)
rs2483793	A	0.046	0.86 (0.73–1.00)	0.021	0.84 (0.73–0.97)	0.068	0.87 (0.75–1.01)	0.035	0.86 (0.74–0.99)
rs7551877	A	0.072	0.87 (0.74–1.01)	0.046	0.86 (0.74–1.00)	0.091	0.88 (0.75–1.02)	0.064	0.87 (0.75–1.01)

The table shows SNPs with $p < 0.05$ in the replication phase. A1, minor allele; SNP, single nucleotide polymorphism; BCLO, bilateral cleft lip only; UCLO, unilateral cleft lip only; RCLO, right cleft lip only; LCLO, left cleft lip only; OR refers to odds ratio. 95%CI refers to 95% confidence interval. P refers to *P*-value for this test. The bold characters indicated the significant SNPs after multiple corrections (significant threshold is 5.05E-04).

De novo harmful rare variant *ARHGAP29*^{R551T} was identified to be associated with NSCLP

Three harmful rare variants were identified to be novel (NM_000350.2: c.979C>T in *ABCA4* and NM_004815.3: c.1652G>C and NM_004815.3: c.559G>A in *ARHGAP29*), which have not been reported in public databases such as 1000 Genome, Esp6500, ExAC, and GnomAD.

We validated all of them by Sanger sequencing on carriers and their parents, through which NM_000350.2: c.979C>T in *ABCA4* and NM_004815.3: c.559G>A in *ARHGAP29* were shown to be inherited from the parents of carriers, whereas NM_004815.3: c.1652G>C in *ARHGAP29* was proved to be *de novo*, and it resulted in a missense mutation of 551 amino acids (p.R551T) of ARHGAP29 that is highly conserved across several species (Figure 2A). Then, NM_004815.3: c.1652G>C was further screened among 508 NSCLP cases and 438 normal controls, but it did not appear. Based on the conservation and harmfulness, we speculated that NM_004815.3: c.1652G>C in *ARHGAP29*, a *de novo* harmful rare variant, would be a risk factor for NSCLP.

ARHGAP29^{R551T} results in a decreased expression level of *ARHGAP29 in vitro*

Expression of fluorescence demonstrated that both pcDNA3.1-*ARHGAP29* and pcDNA3.1-*ARHGAP29*^{R551T} were efficiently expressed in HEK-293T cells. Western Blot revealed that the expression levels of ARHGAP29 in homozygous

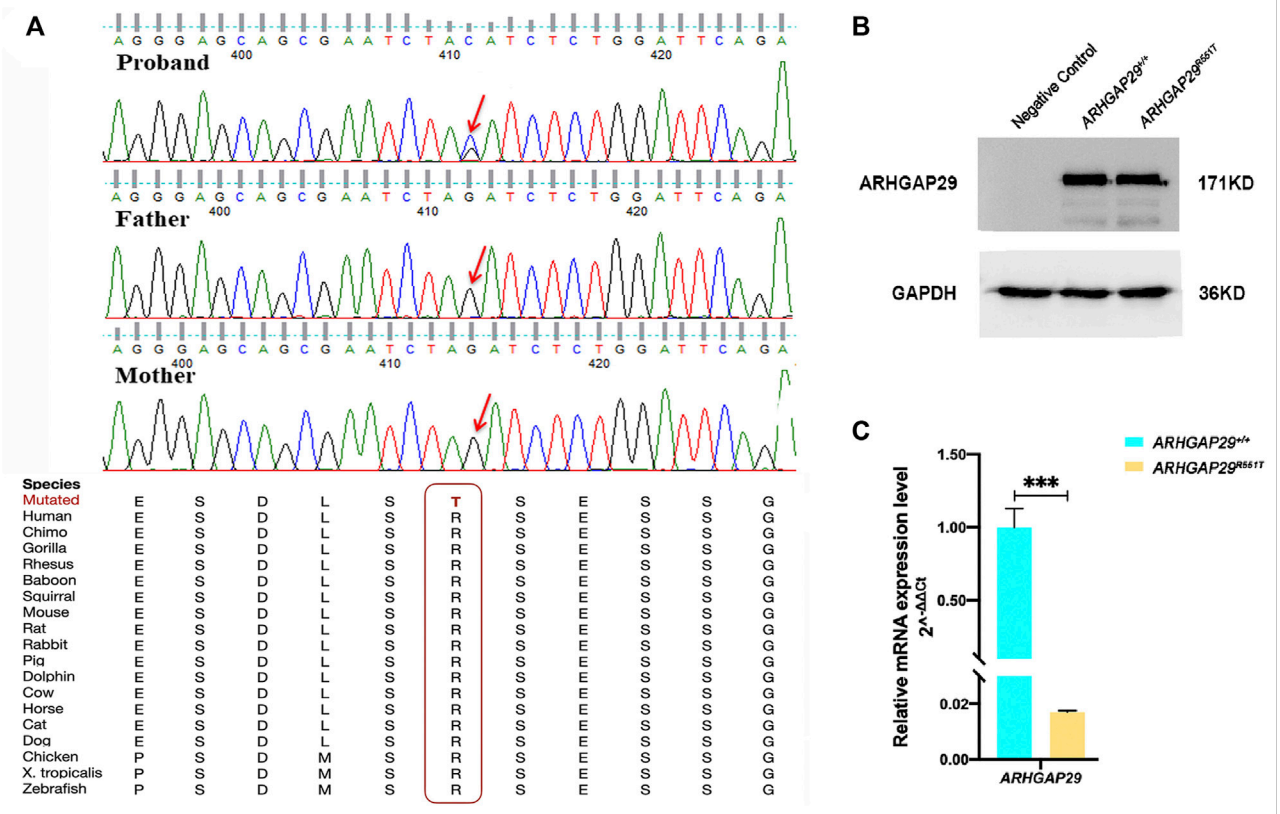

FIGURE 2
(A) Sanger sequencing results of the *de novo* harmful rare variant in *ARHGAP29*. Sequence chromatograms indicate the heterozygous variant (NM_004815.3, NP_004806.3; c.1652G>C, p.R551T). The red letter and box emphasize the cross-species conservation of the altered amino acid. **(B, C)** Western blot and RT-qPCR analysis of the *ARHGAP29* expression in HEK-293T cells 48 h after plasmid transfection. The results are presented as mean values with standard deviation (SD) normalized to *GAPDH*, and there were three biological replicates, ***$p < 0.001$.

Arhgap29$^{R553T/R553T}$ and wild-type group were comparable (Figure 2B). However, compared to the wild-type group, RT-qPCR revealed that homozygous *Arhgap29*$^{R553T/R553T}$ led to the lower mRNA expression level of *ARHGAP29* (Figure 2C).

Additionally, we examined its effect *in vivo*. At E18.5, there were no significant differences in body length, craniofacial morphology, or bone growth between *Arhgap29*$^{R553T/R553T}$ and wild-type mice embryos, and no overt cleft palate phenotype was observed (Figure 3A). From E13.5 to E15.5, HE images of coronal sections showed normal elevation and fusion of palate shelves in both *Arhgap29*$^{R553T/R553T}$ and wild-type mice embryos (Figure 3B). Furthermore, ARHGAP29 was expressed similarly in the palatal epithelium of *Arhgap29*$^{R553T/R553T}$ and wild-type mice embryos (Figure 3C).

ARHGAP29^{R551T} affects NSCL/P-related biological processes

Even though considering the decreased expression mRNA level of *ARHGAP29 in vitro*, we decided to further explore the influence of *Arhgap29*$^{R553T/R553T}$ on the transcriptome *in vivo* by RNA sequencing on the secondary palate tissue of E13.5 homozygous *Arhgap29*$^{R553T/R553T}$ and wild-type mice embryos. As predicted, the expression level of the *Arhgap29* gene transcript NM_172525.2, which is identical to the transcript, where the *de novo* harmful rare variant NM_004815.3: c.1652G>C located at the human genome, was also significantly downregulated when compared to the expression level in wild-type mice.

In addition, decreased *Arhgap29* led to significant changes in 174 genes, 121 of which were upregulated and 53 of which were downregulated (Figure 4A). The conditions for differential gene expression analysis include FPKM (wild-type)> 1, $|\log2| \geq 0.8$, and $p < 0.05$.

Gene Ontology (GO) analysis for DEGs revealed that 15 biological processes were significantly enriched in upregulated genes, of which "epithelial cell differentiation" was the most relevant term to NSCL/P. In addition, most downregulated genes were significantly enriched in biological processes related to transcription, such as "regulation of transcription, DNA-templated" and "negative regulation of transcription by RNA polymerase II" (Figure 4B).

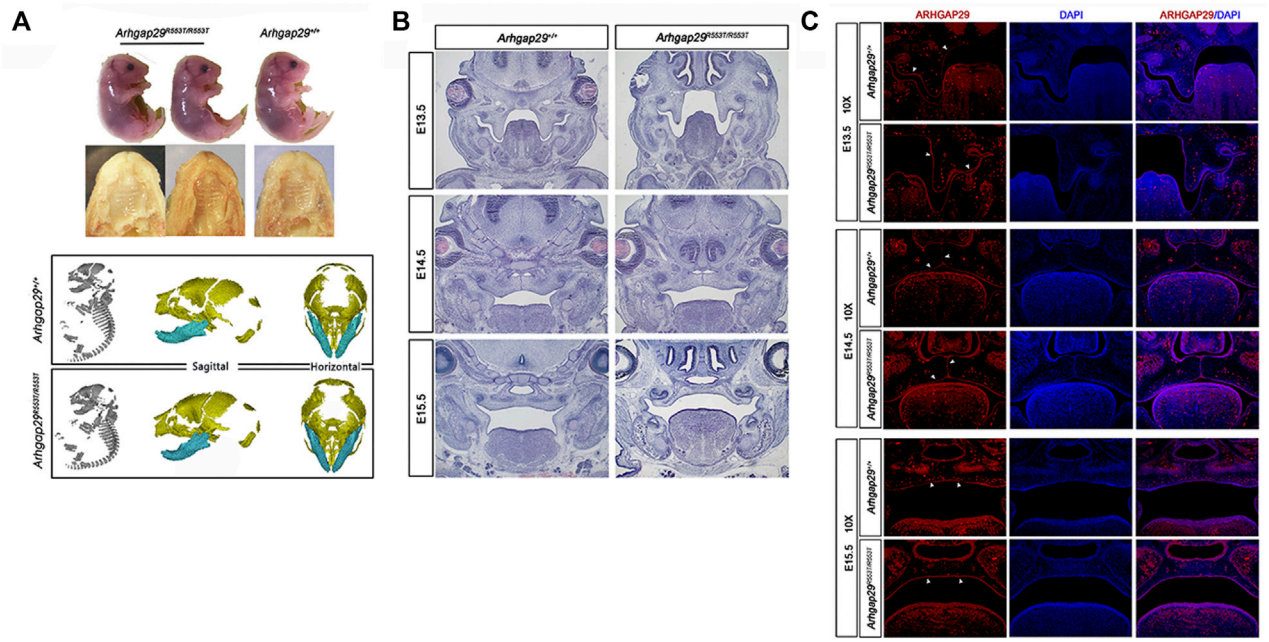

FIGURE 3
(A). Macroscopic and palatal phenotypes of E18.5 embryos; **(B,C)** HE and immunofluorescence staining of palatal coronal sections of E13.5–E15.5 embryos.

Discussion

Since GWAS indicated that 1p22 was associated with NSCL/P (Beaty et al., 2010), a large number of common and rare variants have been identified in this region (Leslie et al., 2012; Butali et al., 2014; Chandrasekharan and Ramanathan, 2014; Letra et al., 2014; Gowans et al., 2016; Savastano et al., 2017). In this study, we aim to identify additional susceptibility variants for NSCL/P in the 1p22 region among the Han Chinese population using deep sequencing.

For common variants, we performed an initial association analysis and additional replications to investigate their associations. We found that rs77179923 was specifically associated with NSCLP (p = 4.70E-04, OR = 1.84, 95%CI: 1.31–2.58) (Table 1); rs77179923 is located in the introns of *ABCA4* gene, it was once reported to be significantly associated with NSCL/P among Asian trios by Leslie et al. (2015), but subsequent research indicated that it may not be functional (Liu et al., 2017a). In addition, rs12071152 was marginally associated with NSCLO (p = 9.40E-04, OR = 1.27, 95%CI: 1.10–1.46) (Table 1), and we first identified its unique association with LCLO (p = 4.00E-04, OR = 1.30, 95%CI: 1.12–1.51) (Table 2); since it is located in the intergenic non-coding region, we used HaploReg (Version v4.1) and RegulomeDB (Version 2.0.3) to annotate rs12071152, and its A allele was observed to have altered seven motifs and showed four eQTL signals (Supplementary Tables S6, S7, and Supplementary Figure S2); these results suggested that rs12071152 is a regulatory SNP, it may function by affecting the expression of ARHGAP29 in the etiology of LCLO, whereas further validation is required.

So far, we have identified two SNPs that are specifically associated with NSCLP or LCLO. However, none were associated with the other sub-phenotypes of NSCLO, indicating genetic heterogeneity among sub-phenotypes of NSCLO. In fact, numerous studies support this viewpoint. Carlson et al. (2017) found that different regions on chromosome 13 were specifically associated with UCLO and BCLO among Asian populations; our previous study also indicated that rs1345186 in the *TP63* gene was significantly associated with RCLO rather than LCLO and BCLO among the Han Chinese population (Yin et al., 2021). Moreover, these results remind us that the risk variants are likely to be masked by other signals when the association analysis was performed between controls and cases containing several subtypes. Consequently, a more detailed classification of the phenotype will be required in future genetic research to unearth more susceptibility variants.

Rare variants, with MAF less than 0.05% (Wagner, 2013), have a higher contribution to complex traits, meaning they confer a larger effect size than common variants; a portion of the common variants that show significant association with diseases are likely to be driven by rare variant (Bodmer and Bonilla, 2008; Nelson et al., 2012; Tennessen et al., 2012; Tada et al., 2016). So far, it has been reported

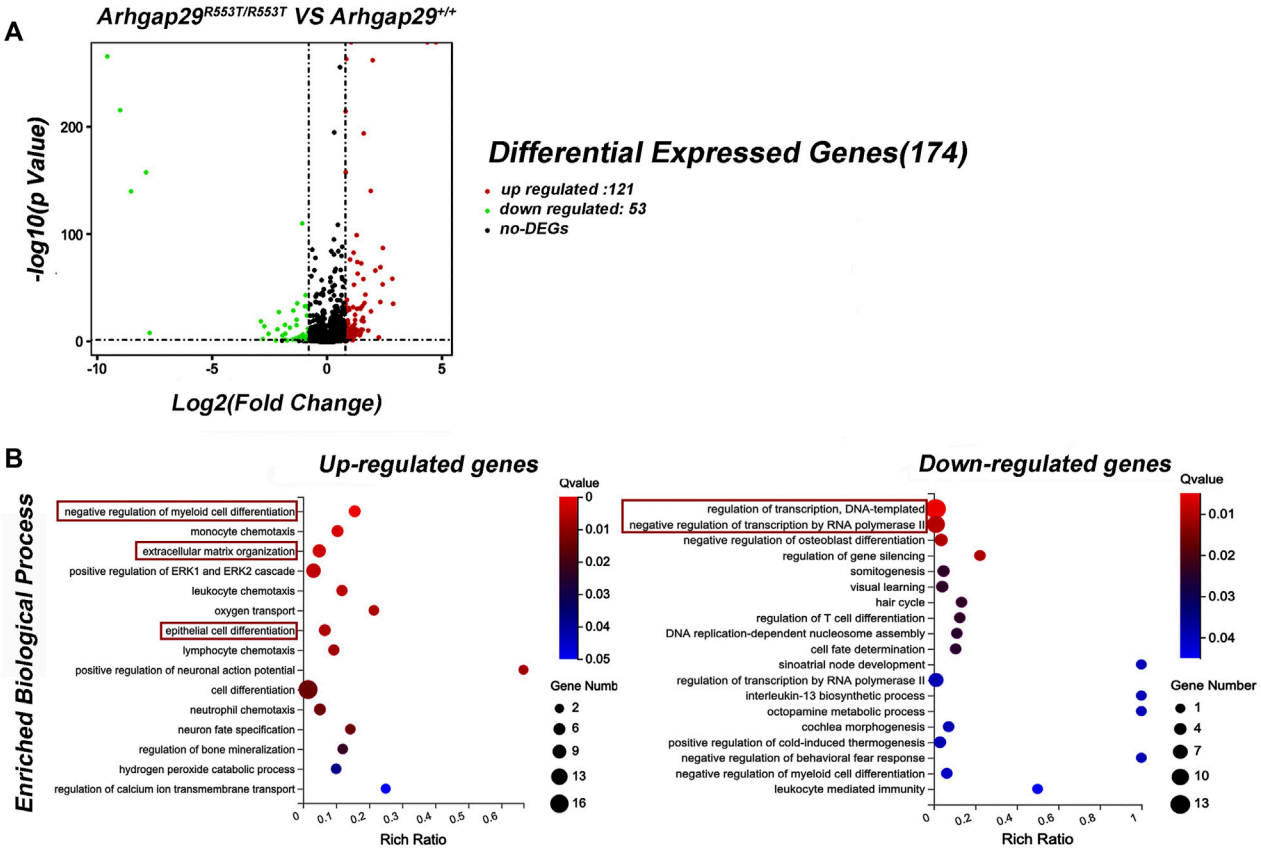

FIGURE 4
Results of RNA sequencing on *Arhgap29*$^{R553T/R553T}$ and wild-type mice. **(A)** Volcanic maps of differential expression genes. **(B)** GO analysis of DEGs. All the shown GO terms were significantly enriched with Q-value less than 0.05.

that rare variants of *ARHGAP29* play crucial roles in the etiology of NSCL/P (Chandrasekharan and Ramanathan, 2014; Liu et al., 2017b; Paul et al., 2017; Savastano et al., 2017). Liu et al. (2017b) once identified a rare variant (NM_004815.3, NP_004806.3; c.1654T>C, p.Ser552Pro) adjacent to ours in a European CPO-defected family. This mutation decreased the stability of ARHGAP29, which inhibits cell migration in immortalized human keratinocytes (iNHKs); the mutant zebrafish failed to delay epiboly, and it was thus suggested to be a loss-of-function variant (Liu et al., 2017b). In addition, Paul et al. (2017) identified a point mutation p.*K326X* at *ARHGAP29* in the NSCL/P case, and the heterozygous *Arhgap29*^{K326X} mutant mouse had abnormal adhesion prior to the formation of the palate.

Here, we identified a heterozygous missense variant NM_004815.3, NP_004806.3; c.1652G>C, p.R551T (*ARHGAP29*) that was *de novo*, highly conserved across species; it is predicted to be harmful by all *in silico* tools, and it is a pathogenic variant by the ACMG guideline (PS2, PS3, and PM2) (Richards et al., 2015). Based on this evidence and its adjacent missense mutation p.Ser552Pro functions as a loss-of-function variant (Liu et al., 2017b), we constructed a mouse model harboring *Arhgap29*^{R553T}, which is identical to *ARHGAP29*^{R551T}, to clarify its function. However, neither overt cleft palate phenotype nor abnormal palate shelves elevation or fusion was observed (Figure 3A, B). We inferred that this attributed to the insufficient dose effect of *Arhgap29*$^{R553T/R553T}$, because Western blot and immunofluorescence assay demonstrated that both *ARHGAP29*^{R551T} and *Arhgap29*^{R553T} did not affect the expression of ARHGAP29 protein (Figure 2B and Figure 3C). In addition, NSCL/P is a polygenic disease involving multiple genes; thus, the effect of *ARHGAP29*^{R551T} may be compensated by other genes or its functions in the etiology of NSCL/P by interacting with other genes in the signaling cascade of craniofacial embryology. Even though we cannot ignore the change of mRNA expression level of *ARHGAP29* result from *ARHGAP29*^{R551T}, this mouse model is valuable for identifying covariates of *Arhgap29*$^{R553T/R553T}$ at the transcriptome level, as well as discovering more NSCL/P-associated biological processes that *ARHGAP29* might participate in (Paul et al., 2017). In this study, we found that the genes affected by *Arhgap29*$^{R553T/R553T}$ were enriched in the biological processes of epithelial cell differentiation and transcriptional regulation that may be related to NSCL/P, but

whether they are truly involved in the occurrence of NSCL/P needs further in-depth research.

In conclusion, via targeted sequencing on 1p22 among the Han Chinese population, we found that rs77179923 was specifically associated with NSCLP; rs12071152 was significantly and specifically associated with LCLO. In addition, *de novo* harmful rare variants NM_004815.3, NP_004806.3; c.1652G>C, p.R551T (ARHGAP29), which decreased *ARHGAP29* expression, were identified to be a risk factor for NSCLP. We generated a mouse model harboring variant identical to the *de novo* harmful variants; although no overt phenotype was observed, several susceptibility NSCL/P-related biological processes that are affected by *Arhgap29*$^{R553T/R553T}$ were observed after RNA-sequencing of the E13.5 secondary palate; however, the mechanism requires further investigation.

Data availability statement

All the datasets generated in this article were shown in the main text and the Supplementary Material. Any questions about the data, please contact to zhonglinjia@sina.com.

Ethics statement

The studies involving human participants were reviewed and approved by the HEC (the Hospital Ethics Committee) of West China Hospital of Stomatology. Written informed consent to participate in this study was provided by the participants' legal guardian/next of kin. The animal study was reviewed and approved by HEC (the Hospital Ethics Committee) of West China Hospital of Stomatology.

Author contributions

M-JL contributed to data acquisition, analysis, and interpretation and drafted and critically revised the manuscript. J-YS and B-HZ contributed to data collection from the database and analysis. Q-MC and BS conceived and reviewed the manuscript. Z-LJ contributed to the conception, design, data acquisition, analysis, and interpretation, and critically revised the manuscript. All of them gave final approval and agreed to be accountable for all aspects of the work.

Funding

This work was supported by the National Science Funds of China (No. 82170919 and No. 81600849) and the Major frontier issues of the application foundation project of Sichuan Science and Technology Department (2020YJ0211).

Conflict of interest

The authors declare that the research was conducted in the absence of any commercial or financial relationships that could be construed as a potential conflict of interest.

Publisher's note

All claims expressed in this article are solely those of the authors and do not necessarily represent those of their affiliated organizations, or those of the publisher, the editors, and the reviewers. Any product that may be evaluated in this article, or claim that may be made by its manufacturer, is not guaranteed or endorsed by the publisher.

Supplementary material

The Supplementary Material for this article can be found online at: https://www.frontiersin.org/articles/10.3389/fgene.2022.947126/full#supplementary-material

References

Adzhubei, I., Jordan, D. M., and Sunyaev, S. R. (2013). Predicting functional effect of human missense mutations using PolyPhen-2. *Curr. Protoc. Hum. Genet.* 7, Unit7.20. doi:10.1002/0471142905.hg0720s76

Altshuler, D., Daly, M. J., and Lander, E. S. (2008). Genetic mapping in human disease. *Science* 322, 881–888. doi:10.1126/science.1156409

Baldacci, S., Gorini, F., Santoro, M., Pierini, A., Minichilli, F., and Bianchi, F. (2018). Environmental and individual exposure and the risk of congenital anomalies: a review of recent epidemiological evidence. *Epidemiol. Prev.* 42, 1–34. doi:10.19191/ep18.3-4.S1.P001.057

Beaty, T. H., Marazita, M. L., and Leslie, E. J. (2016). Genetic factors influencing risk to orofacial clefts: today's challenges and tomorrow's opportunities. *F1000Res* 5, 2800. doi:10.12688/f1000research.9503.1

Beaty, T. H., Murray, J. C., Marazita, M. L., Munger, R. G., Ruczinski, I., Hetmanski, J. B., et al. (2010). A genome-wide association study of cleft lip with and without cleft palate identifies risk variants near MAFB and ABCA4. *Nat. Genet.* 42, 525–529. doi:10.1038/ng.580

Bodmer, W., and Bonilla, C. (2008). Common and rare variants in multifactorial susceptibility to common diseases. *Nat. Genet.* 40, 695–701. doi:10.1038/ng.f.136

Butali, A., Mossey, P., Adeyemo, W., Eshete, M., Gaines, L., Braimah, R., et al. (2014). Rare functional variants in genome-wide association identified candidate genes for nonsyndromic clefts in the African population. *Am. J. Med. Genet. A* 164A, 2567–2571. doi:10.1002/ajmg.a.36691

Carlson, J. C., Taub, M. A., Feingold, E., Beaty, T. H., Murray, J. C., Marazita, M. L., et al. (2017). Identifying genetic sources of phenotypic heterogeneity in orofacial clefts by targeted sequencing. *Birth Defects Res.* 109, 1030–1038. doi:10.1002/bdr2.23605

Chandrasekharan, D., and Ramanathan, A. (2014). Identification of a novel heterozygous truncation mutation in exon 1 of ARHGAP29 in an Indian subject with nonsyndromic cleft lip with cleft palate. *Eur. J. Dent.* 8, 528–532. doi:10.4103/1305-7456.143637

Croen, L. A., Shaw, G. M., Wasserman, C. R., and Tolarova, M. M. (1998). Racial and ethnic variations in the prevalence of orofacial clefts in California, 1983-1992. *Am. J. Med. Genet.* 79, 42–47. doi:10.1002/(sici)1096-8628(19980827)79:1<42::aid-ajmg11>3.0.co;2-m

Danecek, P., Auton, A., Abecasis, G., Albers, C. A., Banks, E., DePristo, M. A., et al. (2011). The variant call format and VCFtools. *Bioinformatics* 27, 2156–2158. doi:10.1093/bioinformatics/btr330

Dickson, S. P., Wang, K., Krantz, I., Hakonarson, H., and Goldstein, D. B. (2010). Rare variants create synthetic genome-wide associations. *PLoS Biol.* 8, e1000294. doi:10.1371/journal.pbio.1000294

Dixon, M. J., Marazita, M. L., Beaty, T. H., and Murray, J. C. (2011). Cleft lip and palate: understanding genetic and environmental influences. *Nat. Rev. Genet.* 12, 167–178. doi:10.1038/nrg2933

Gowans, L. J., Adeyemo, W. L., Eshete, M., Mossey, P. A., Busch, T., Aregbesola, B., et al. (2016). Association studies and direct DNA sequencing implicate genetic susceptibility loci in the etiology of nonsyndromic orofacial clefts in sub-saharan african populations. *J. Dent. Res.* 95, 1245–1256. doi:10.1177/0022034516657003

Grosen, D., Chevrier, C., Skytthe, A., Bille, C., Mølsted, K., Sivertsen, A., et al. (2010). A cohort study of recurrence patterns among more than 54, 000 relatives of oral cleft cases in denmark: support for the multifactorial threshold model of inheritance. *J. Med. Genet.* 47, 162–168. doi:10.1136/jmg.2009.069385

Huang, L., Jia, Z., Shi, Y., Du, Q., Shi, J., Wang, Z., et al. (2019). Genetic factors define CPO and CLO subtypes of nonsyndromicorofacial cleft. *PLoS Genet.* 15, e1008357. doi:10.1371/journal.pgen.1008357

Kircher, M., Witten, D. M., Jain, P., O'Roak, B. J., Cooper, G. M., Shendure, J., et al. (2014). A general framework for estimating the relative pathogenicity of human genetic variants. *Nat. Genet.* 46, 310–315. doi:10.1038/ng.2892

Lek, M., Karczewski, K. J., Minikel, E. V., Samocha, K. E., Banks, E., Fennell, T., et al. (2016). Analysis of protein-coding genetic variation in 60, 706 humans. *Nature* 536, 285–291. doi:10.1038/nature19057

Leslie, E. J., Mansilla, M. A., Biggs, L. C., Schuette, K., Bullard, S., Cooper, M., et al. (2012). Expression and mutation analyses implicate ARHGAP29 as the etiologic gene for the cleft lip with or without cleft palate locus identified by genome-wide association on chromosome 1p22. *Birth Defects Res. A Clin. Mol. Teratol.* 94, 934–942. doi:10.1002/bdra.23076

Leslie, E. J., and Marazita, M. L. (2013). Genetics of cleft lip and cleft palate. *Am. J. Med. Genet. C Semin. Med. Genet.* 163C, 246–258. doi:10.1002/ajmg.c.31381

Leslie, E. J., Taub, M. A., Liu, H., Steinberg, K. M., Koboldt, D. C., Zhang, Q., et al. (2015). Identification of functional variants for cleft lip with or without cleft palate in or near PAX7, FGFR2, and NOG by targeted sequencing of GWAS loci. *Am. J. Hum. Genet.* 96, 397–411. doi:10.1016/j.ajhg.2015.01.004

Letra, A., Maili, L., Mulliken, J. B., Buchanan, E., Blanton, S. H., Hecht, J. T., et al. (2014). Further evidence suggesting a role for variation in ARHGAP29 variants in nonsyndromic cleft lip/palate. *Birth Defects Res. A Clin. Mol. Teratol.* 100, 679–685. doi:10.1002/bdra.23286

Lewis, C. W., Jacob, L. S., and Lehmann, C. U. (2017). The primary care pediatrician and the care of children with cleft lip and/or cleft palate. *Pediatrics* 139, e20170628. doi:10.1542/peds.2017-0628

Li, H., and Durbin, R. (2009). Fast and accurate short read alignment with burrows-wheeler transform. *Bioinformatics* 25, 1754–1760. doi:10.1093/bioinformatics/btp324

Li, H., Handsaker, B., Wysoker, A., Fennell, T., Ruan, J., Homer, N., et al. (2009). The sequence alignment/map format and SAMtools. *Bioinformatics* 25, 2078–2079. doi:10.1093/bioinformatics/btp352

Lin-Shiao, E., Lan, Y., Welzenbach, J., Alexander, K. A., Zhang, Z., Knapp, M., et al. (2019). p63 establishes epithelial enhancers at critical craniofacial development genes. *Sci. Adv.* 5, eaaw0946. doi:10.1126/sciadv.aaw0946

Liu, H., Busch, T., Eliason, S., Anand, D., Bullard, S., Gowans, L. J. J., et al. (2017b). Exome sequencing provides additional evidence for the involvement of ARHGAP29 in Mendelian orofacial clefting and extends the phenotypic spectrum to isolated cleft palate. *Birth Defects Res.* 109, 27–37. doi:10.1002/bdra.23596

Liu, H., Leslie, E. J., Carlson, J. C., Beaty, T. H., Marazita, M. L., Lidral, A. C., et al. (2017a). Identification of common non-coding variants at 1p22 that are functional for non-syndromic orofacial clefting. *Nat. Commun.* 8, 14759. doi:10.1038/ncomms14759

Manolio, T. A., Collins, F. S., Cox, N. J., Goldstein, D. B., Hindorff, L. A., Hunter, D. J., et al. (2009). Finding the missing heritability of complex diseases. *Nature* 461, 747–753. doi:10.1038/nature08494

Mossey, P. A., and Modell, B. (2012). Epidemiology of oral clefts 2012: an international perspective. *Front. Oral Biol.* 16, 1–18. doi:10.1159/000337464

Nelson, M. R., Wegmann, D., Ehm, M. G., Kessner, D., St Jean, P., Verzilli, C., et al. (2012). An abundance of rare functional variants in 202 drug target genes sequenced in 14, 002 people. *Science* 337, 100–104. doi:10.1126/science.1217876

Ng, P. C., and Henikoff, S. (2003). SIFT: Predicting amino acid changes that affect protein function. *Nucleic Acids Res.* 31, 3812–3814. doi:10.1093/nar/gkg509

Paul, B. J., Palmer, K., Sharp, J. C., Pratt, C. H., Murray, S. A., Dunnwald, M., et al. (2017). ARHGAP29 mutation is associated with abnormal oral epithelial adhesions. *J. Dent. Res.* 96, 1298–1305. doi:10.1177/0022034517726079

Purcell, S., Neale, B., Todd-Brown, K., Thomas, L., Ferreira, M. A., Bender, D., et al. (2007). PLINK: a tool set for whole-genome association and population-based linkage analyses. *Am. J. Hum. Genet.* 81, 559–575. doi:10.1086/519795

Rahimov, F., Jugessur, A., and Murray, J. C. (2012). Genetics of nonsyndromic orofacial clefts. *Cleft Palate. Craniofac. J.* 49, 73–91. doi:10.1597/10-178

Rentzsch, P., Witten, D., Cooper, G. M., Shendure, J., and Kircher, M. (2018). CADD: predicting the deleteriousness of variants throughout the human genome. *Nucleic Acids Res.* 47, D886–D894. doi:10.1093/nar/gky1016

Richards, S., Aziz, N., Bale, S., Bick, D., Das, S., Gastier-Foster, J., et al. (2015). Standards and guidelines for the interpretation of sequence variants: a joint consensus recommendation of the American college of medical genetics and genomics and the association for molecular pathology. *Genet. Med.* 17, 405–424. doi:10.1038/gim.2015.30

Savastano, C. P., Brito, L. A., Faria Á, C., Setó-Salvia, N., Peskett, E., Musso, C. M., et al. (2017). Impact of rare variants in ARHGAP29 to the etiology of oral clefts: role of loss-of-function vs missense variants. *Clin. Genet.* 91, 683–689. doi:10.1111/cge.12823

Sazonovs, A., and Barrett, J. C. (2018). Rare-variant studies to complement genome-wide association studies. *Annu. Rev. Genomics Hum. Genet.* 19, 97–112. doi:10.1146/annurev-genom-083117-021641

Schwarz, J. M., Rödelsperger, C., Schuelke, M., and Seelow, D. (2010). MutationTaster evaluates disease-causing potential of sequence alterations. *Nat. Methods* 7, 575–576. doi:10.1038/nmeth0810-575

Smigielski, E. M., Sirotkin, K., Ward, M., and Sherry, S. T. (2000). dbSNP: a database of single nucleotide polymorphisms. *Nucleic Acids Res.* 28, 352–355. doi:10.1093/nar/28.1.352

Stenson, P. D., Mort, M., Ball, E. V., Howells, K., Phillips, A. D., Thomas, N. S., et al. (2009). The human gene mutation database: 2008 update. *Genome Med.* 1, 13. doi:10.1186/gm13

Sun, Y., Huang, Y., Yin, A., Pan, Y., Wang, Y., Wang, C., et al. (2015). Genome-wide association study identifies a new susceptibility locus for cleft lip with or without a cleft palate. *Nat. Commun.* 6, 6414. doi:10.1038/ncomms7414

Tada, H., Kawashiri, M. A., Konno, T., Yamagishi, M., and Hayashi, K. (2016). Common and rare variant association study for plasma lipids and coronary artery disease. *J. Atheroscler. Thromb.* 23, 241–256. doi:10.5551/jat.31393

Tam, V., Patel, N., Turcotte, M., Bossé, Y., Paré, G., Meyre, D., et al. (2019). Benefits and limitations of genome-wide association studies. *Nat. Rev. Genet.* 20, 467–484. doi:10.1038/s41576-019-0127-1

Tennessen, J. A., Bigham, A. W., O'Connor, T. D., Fu, W., Kenny, E. E., Gravel, S., et al. (2012). Evolution and functional impact of rare coding variation from deep sequencing of human exomes. *Science* 337, 64–69. doi:10.1126/science.1219240

Tolarova, M. M., and Cervenka, J. (1998). Classification and birth prevalence of orofacial clefts. *Am. J. Med. Genet.* 75, 126–137. doi:10.1002/(sici)1096-8628(19980113)75:2<126::aid-ajmg2>3.0.co;2-r

Wagner, M. J. (2013). Rare-variant genome-wide association studies: a new frontier in genetic analysis of complex traits. *Pharmacogenomics* 14, 413–424. doi:10.2217/pgs.13.36

Wang, K., Li, M., and Hakonarson, H. (2010). ANNOVAR: functional annotation of genetic variants from high-throughput sequencing data. *Nucleic Acids Res.* 38, e164. doi:10.1093/nar/gkq603

Worley, M. L., Patel, K. G., and Kilpatrick, L. A. (2018). Cleft lip and palate. *Clin. Perinatol.* 45, 661–678. doi:10.1016/j.clp.2018.07.006

Yin, B., Shi, J. Y., Lin, Y. S., Shi, B., and Jia, Z. L. (2021). SNPs at TP63 gene was specifically associated with right-side cleft lip in Han Chinese population. *Oral Dis.* 27, 559–566. doi:10.1111/odi.13566

frontiers | Frontiers in Genetics

TYPE Brief Research Report
PUBLISHED 28 September 2022
DOI 10.3389/fgene.2022.1012025

OPEN ACCESS

EDITED BY
Augusto Rojas-Martinez,
Escuela de Medicina y Ciencias de la Salud Tec Salud, Tecnológico de Monterrey, Mexico

REVIEWED BY
Alexandre Rezende Vieira,
University of Pittsburgh, United States
Rachid Karam,
Ambry Genetics, United States

*CORRESPONDENCE
Jeremy L. Davis,
jeremy.davis@nih.gov

SPECIALTY SECTION
This article was submitted to Genetics of Common and Rare Diseases, a section of the journal Frontiers in Genetics

RECEIVED 05 August 2022
ACCEPTED 09 September 2022
PUBLISHED 28 September 2022

CITATION
Green BL, Fasaye G-A, Samaranayake SG, Duemler A, Gamble LA and Davis JL (2022), Frequent cleft lip and palate in families with pathogenic germline CDH1 variants.
Front. Genet. 13:1012025.
doi: 10.3389/fgene.2022.1012025

Frequent cleft lip and palate in families with pathogenic germline *CDH1* variants

Benjamin L. Green[1], Grace-Ann Fasaye[2], Sarah G. Samaranayake[1], Anna Duemler[2], Lauren A. Gamble[1] and Jeremy L. Davis[1]*

[1]Surgical Oncology Program, Center for Cancer Research, National Cancer Institute, National Institutes of Health, Bethesda, MD, United States, [2]Genetics Branch, Center for Cancer Research, National Cancer Institute, National Institutes of Health, Bethesda, MD, United States

Pathogenic and likely pathogenic (P/LP) germline variants in the tumor suppressor gene *CDH1* (E-cadherin) result in increased lifetime risk of diffuse-type gastric cancer and lobular breast cancer. *CDH1* variants are also associated with hereditary cleft lip and palate (CLP), the mechanism of which is not well understood. We sought to determine the prevalence of CLP in families who carry P/LP *CDH1* variants. Patients with P/LP *CDH1* variants who were enrolled in a prospective clinical trial were reviewed (NCT03030404). The cohort included 299 individuals from 153 families that had 80 unique P/LP variants in *CDH1*. The rate of CLP was 19% (29/153) in families reporting CLP in at least one family member, and 2.7% (8/299) among individuals with confirmed germline *CDH1* P/LP variants. There were 22 unique variants in *CDH1* among the 29 families that reported CLP, or a CLP rate of 27.5% per variant (22/80). 10 of the variants were not previously reported to be associated with CLP. We observed that 24% (7/29) of CLP-associated gene variants involved large-scale (≥1 exon) deletions. Among families with CLP, 69% (20/29) had a member diagnosed with gastric cancer, and 79% (23/29) had a member with breast cancer, which were similar to rates observed in non-CLP families (p >0.3 for both). Our analysis suggests that the prevalence of CLP in families with germline *CDH1* P/LP variants was high in this large cohort, and there was no genotype-phenotype pattern. Genetic testing for *CDH1* variants should be considered in families with CLP and history of either diffuse-type gastric or lobular breast cancer.

KEYWORDS

cleft lip, cleft palate, CDH1, E-cadherin, cleft lip/palate, hereditary diffuse gastric cancer syndrome

Report

E-cadherin is a glycoprotein involved in maintaining the integrity of mucosal epithelium via *trans*-homophilic binding at cell-cell junctions (Takeichi, 2014; Mendonsa et al., 2018). Germline pathogenic or likely pathogenic (P/LP) variants in the *CDH1* gene, which encodes E-cadherin, lead to the Diffuse Gastric and Lobular Breast Cancer (DGLBC, formerly hereditary diffuse gastric cancer, HDGC [MIM: 137215]) syndrome with an autosomal dominant pattern of inheritance. Lifetime disease penetrance estimates for gastric cancer and breast cancer in patients bearing a P/LP variant in *CDH1* are approximately 25–42% and 42–55%, respectively (Roberts et al., 2019; Xicola et al., 2019).

In addition to cancer phenotypes, *CDH1* variants are associated with Blepharocheilodontic syndrome (MIM: 119580) and cleft lip and palate (CLP). CLP, the most common congenital craniofacial abnormality, is a uni- or bilateral non-union of pharyngeal arch 1 structures and occurs in approximately 1 in 700 live births (Dixon et al., 2011). Most cases of CLP are idiopathic, but CLP may also present in the context of certain congenital syndromes (Venkatesh, 2009; Ghoumid et al., 2017). E-cadherin protein expression in the developing frontonasal prominence reportedly increases during weeks four–six of embryonic development (Frebourg et al., 2006), and epithelial cell adhesion is an important contributor to proper development of this structure (Cox et al., 2018). A prior study reported an association between variants in the linker regions of the E-cadherin protein and CLP, however, no mechanistic evidence has been provided to explain this phenomenon (Selvanathan et al., 2020).

TABLE 1 Family demographic and variant characteristics of CLP and non-CLP cohorts.

Characteristic, n (%)	CLP N = 29	Non-CLP N = 124
Family history of breast cancer		
Yes	23 (79)	92 (74)
No	6 (21)	32 (26)
Family history of gastric cancer		
Yes	20 (69)	92 (74)
No	9 (31)	32 (26)
Race		
White	28 (97)	111 (90)
Black	—	3 (2)
Asian	—	3 (2)
Hispanic	—	1 (1)
Multiple/Other	1 (3)	6 (5)
Variant domain		
All	2 (7)	3 (2)
Pre	—	7 (6)
Pro	2 (7)	10 (8)
Cadherin 1	7[a] (24)	18[a] (15)
Cadherin 2	—	8 (6)
Cadherin 3	1 (3)	10 (8)
Cadherin 4	6 (21)	23[b] (19)
Cadherin 5	2 (7)	16[c] (13)
Transmembrane	4 (14)	20 (16)
Cytoplasmic	5 (17)	9 (7)
Variant Type		
Deletion	8 (28)	9 (7)
Frameshift	4 (14)	33 (27)
Missense (Cryptic Splice)	1 (3)	21 (17)
Nonsense	7 (24)	40 (32)
Splice site (Canonical)	9 (31)	21 (17)

[a]Two variants are in the Pro-EC1, linker region.
[b]One variant is in the EC3-EC4 linker region.
[c]One variant is in the EC4-EC5 linker region.

To evaluate the association between *CDH1* variants and CLP, we analyzed a large single-institution cohort of 299 patients with confirmed *CDH1* P/LP variants enrolled in a prospective natural history study from 2017 through 2021. A total of 299 individual study participants were enrolled (211 female, 88 male) from 153 different families, the majority of whom identified as White (Table 1). Although the individual rate of CLP among patients with germline *CDH1* P/LP variants was 2.7% (8/299), 19% (29/153) of families identified at least one relative with CLP (Median: 1, range 1–5). Of the study participants and their relatives identified with CLP (n = 47), 15 were positive for a P/LP variant in *CDH1*, 1 was an obligate carrier, and 31 were untested but at-risk to carry the familial *CDH1* variant. Individuals with CLP were 45% (21/47) female, 19% (4/21) of whom had a personal history of breast cancer. Advanced gastric cancer was identified in 13% (6/47) of individuals with CLP. For families with CLP, 69% (20/29) reported at least one member with advanced gastric cancer, and 79% (23/29) reported breast cancer, which were similar to rates observed in non-CLP families (breast cancer $X^2 = 0.33$, $p = 0.566$; gastric cancer $X^2 = 0.33$, $p = 0.567$).

Next, we analyzed the *CDH1* genotype of the cohort (Figure 1). There were 80 unique *CDH1* P/LP variants among 153 different families. Of the 29 families that reported CLP, there were 22 unique variants in *CDH1*, 10 of which had not been associated previously with CLP (Table 2). The rate of CLP per unique *CDH1* P/LP variant was 27.5% (22/80). Truncation of E-cadherin was predicted in 55% (16/29) of families reporting CLP based on either nonsense or frameshift variants in *CDH1* (Table 2). An additional 24% (7/29) of CLP families had large deletions of ≥1 exon, including two families that were heterozygous for complete *CDH1* gene deletion. Interestingly, there were two other families in the CLP-negative cohort heterozygous for the same complete *CDH1* gene deletions that denied a known history of CLP. In contrast, there was only 1 missense cryptic splice variant in CLP-positive families (3%) compared with 21 missense mutations in the CLP-negative families (17%). The

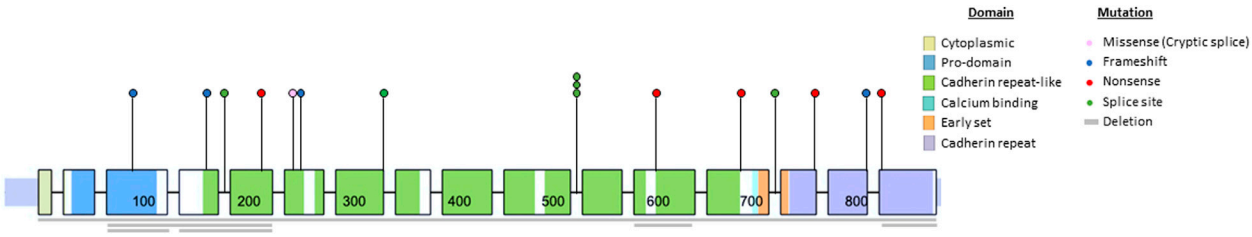

FIGURE 1
Map of variants in *CDH1* for patients reporting family history of CLP.

TABLE 2 *CDH1* variant genotype for each family with CLP.

Family	*CDH1* variant	Variant domain	Variant type	Amino acid change	Prior report in CLP
1	5′UTR_3′UTRdel	All	Deletion (Complete)	—	None
2	5′UTR_3′UTRdel	All	Deletion (Complete)	—	None
3	c.261del	Cadherin pro	Frameshift	Arg87fs	None
4	Deletion (Exon 3)	Cadherin pro	Deletion (Large)	—	None
5	Deletion (Exons 3–5)	Cadherin pro through extracellular Cadherin 1	Deletion	—	None
6	Deletion (Exons 4–5)	Cadherin pro through extracellular cadherin 1	Deletion	—	None
7	Deletion (Exon 16)	Cytoplasmic	Deletion (Large)	—	None
8	EX16_3′UTRdel	Cytoplasmic	Deletion (Large)	—	None
9	c.2430del	Cytoplasmic	Frameshift	Phe810fs	Present
10	c.2474dup	Cytoplasmic	Nonsense	p.Pro826fs	Present
11	c.2287G>T	Cytoplasmic	Nonsense	Glu763Ter	Present
12	c.480_486del	Extracellular cadherin 1	Frameshift	p.Ile161AlafsTer52	None
13	c.640del	Extracellular cadherin 1	Nonsense	Leu214Ter	None
14	c.532-1G>C	Extracellular cadherin 1	Canonical splice	—	Present
15	c.720del	Extracellular cadherin 1	Frameshift	Asn240fs	None
16	c.715G>A	Extracellular cadherin 1	Missense (Cryptic splice)	Gly239Arg	Present
17	c.1137G>A	Extracellular cadherin 3	*Canonical splice	—	Present
18	c.1565+2dupT	Extracellular cadherin 4	Canonical splice	—	Present
19	c.1565 + 1G>C	Extracellular cadherin 4	Canonical splice	—	Present
20	c.1565 + 1G>A	Extracellular cadherin 4	Canonical splice	—	Present
21	c.1565 + 1G>A	Extracellular cadherin 4	Canonical sSplice	—	Present
22	c.1565 + 1G>C	Extracellular cadherin 4	Canonical splice	—	Present
23	c.1565 + 1G>A	Extracellular cadherin 4	Canonical splice	—	Present
24	Deletion (Exon12)	Extracellular cadherin 5	Deletion (Large)	—	None
25	c.1792C>T	Extracellular cadherin 5	Nonsense	Arg598Ter	Present
26	c.2064_2065del	Transmembrane	Nonsense	p.Cys688Terfs	Present
27	c.2064_2065del	Transmembrane	Nonsense	p.Cys688Terfs	Present
28	c.2064_2065del	Transmembrane	Nonsense	p.Cys688Terfs	Present
29	c.2165-1G>C	Transmembrane	Canonical splice	—	Present

*a synonymous last nucleotide variant that abolishes the donor splice site.

missense cryptic splice variant in the CLP-positive subgroup was not located within a cadherin-repeat linker region. Surprisingly, variants located at EC-EC linker regions were found in families without a history of CLP. The most common location for a *CDH1* variant in both subgroups was in EC4. The frequency of variants of intracytoplasmic or transmembrane domains were similar in both CLP-positive and CLP-negative groups.

Here, we have reported the largest known single-institution analysis of CLP prevalence in subjects with germline *CDH1* P/LP variants. The rarity of DGLBC syndrome and *CDH1* P/LP variants presents challenges for any analysis. A prior study of *CDH1* variant data pooled from the literature and public genetic variation databases found that 13% of *CDH1* variants were associated with syndromic CLP (only DGLBC and Blepharocheilodontic syndrome) and non-syndromic CLP (Selvanathan et al., 2020). Our dataset, in contrast, allowed for CLP status to be systematically collected. We were able to determine that 27.5% of unique *CDH1* P/LP variants were associated with CLP. Additionally, 19% of families with germline *CDH1* P/LP variants reported at least one relative with CLP. These data demonstrate that CLP may be more prevalent in families with *CDH1* P/LP variants than previously described.

Identification of individuals with a *CDH1* P/LP variant provides opportunities for cancer risk reduction and early detection. Due to the high incidence of CLP in the general population, a diagnosis of isolated CLP at birth would be insufficient to recommend germline *CDH1* genetic testing. Detailed individual and family criteria for *CDH1* germline genetic testing have been developed by the International Gastric Cancer Linkage Consortium (Blair et al., 2020). Of the nine specific testing criteria, only one addresses CLP which recommends *CDH1* testing for individuals with diffuse gastric cancer at any age and a personal or family history of CLP. Based on this report, it appears quite reasonable to expand the criteria to include a recommendation for *CDH1* genetic testing in individuals with lobular breast cancer at any age with a personal or family history of CLP. Another consideration is that in families with features of hereditary cancer, there will be relatives with syndrome associated cancers who are deceased or uninterested/unable to undergo genetic testing. Therefore, we suggest that *CDH1* genetic testing criteria also include testing for unaffected individuals with a family history of CLP and diffuse gastric cancer or lobular breast cancer.

Genotype-phenotype correlations have been elusive for *CDH1*. We found no difference in the rates of CLP in families reporting a history of gastric or breast cancer. Functionally, E-cadherin can form hetero- and homodimers on the cell surface and initiates intracellular signal transduction via β-catenin signaling and cytoskeletal modulation (Mendonsa et al., 2018). A previous study suggested mechanistic associations that might explain phenotypic differences between CLP and cancer development, specifically implicating linker regions of E-cadherin enriched for CLP-associated variants (Selvanathan et al., 2020). However, we found no evidence of region-specific variants that correlated with the presence of CLP. The CLP-positive subgroup demonstrated variants throughout the entire gene, including two patients with full *CDH1* gene deletions which had not been reported previously. Interestingly, there were two additional families with full *CDH1* gene deletions that reported no CLP. In addition, the only missense mutation in the CLP + group was a known cryptic splice site, generating premature termination codon that potentially resulted in reduced abundance of *CDH1* mRNA via the nonsense-mediated decay (NMD) pathway (Kaurah et al., 2007; Karam et al., 2008). Together, these findings suggest that quantity, not quality, of functional E-cadherin may be a driver of CLP phenotype in *CDH1* P/LP carriers, and that CLP is likely a multifactorial phenotype.

Materials and methods

The study was conducted in accordance with the Declaration of Helsinki (as revised in 2013). Patients were enrolled in National Institutes of Health (NIH) protocol number 17-C-0043 (NCT ID: NCT03030404) from 2017 to 2021. The study was approved by the institutional review board of the National Institutes of Health (reference number 385481) and informed consent was taken from all patients. Patients were enrolled if they had positive genotyping for a P/LP variant in *CDH1*. Patients had genetic testing at a CLIA certified lab. Results were reviewed by a certified genetic counselor. All data were analyzed by SPSS version 25® (IBM, IL, United States). Chi-squared statistical test was used where appropriate.

Summary

Approximately 1 in 5 families with germline *CDH1* pathogenic variants identified a family member with cleft lip/palate. This rate of cleft lip/palate associated with germline *CDH1* variants should be incorporated into considerations for genetic testing in patients with a personal or family history of diffuse gastric cancer or lobular breast cancer.

Data availability statement

The original contributions presented in the study are included in the article/supplementary materials, further inquiries can be directed to the corresponding author.

Ethics statement

The studies involving human participants were reviewed and approved by Institutional Review Board of the National Institutes. Informed consent was taken from the patients involved.

Author contributions

Conceptualization: BG and JD data curation: All authors formal analysis: All authors funding acquisition: JD investigation: BG and JD methodology: All authors project administration: BG and JD resources: JD software: n/a Supervision: JD validation: All

authors visualization: BG, LG, SS writing—original draft: BG and JD writing—review and editing: All authors.

Funding

This research was supported in part by the Intramural Research Program, National Cancer Institute, National Institutes of Health.

Acknowledgments

The authors would like to acknowledge Dr. Chimene Kesserwan for providing variant classification and interpretation guidance.

Conflict of interest

The authors declare that the research was conducted in the absence of any commercial or financial relationships that could be construed as a potential conflict of interest.

Publisher's note

All claims expressed in this article are solely those of the authors and do not necessarily represent those of their affiliated organizations, or those of the publisher, the editors and the reviewers. Any product that may be evaluated in this article, or claim that may be made by its manufacturer, is not guaranteed or endorsed by the publisher.

References

Blair, V. R., McLeod, M., Carneiro, F., Coit, D. G., D'Addario, J. L., van Dieren, J. M., et al. (2020). Hereditary diffuse gastric cancer: Updated clinical practice guidelines. *Lancet. Oncol.* 21 (8), e386–e397. doi:10.1016/S1470-2045(20)30219-9

Cox, L. L., Cox, T. C., Moreno Uribe, L. M., Zhu, Y., Richter, C. T., Nidey, N., et al. (2018). Mutations in the epithelial cadherin-p120-catenin complex cause mendelian non-syndromic cleft lip with or without cleft palate. *Am. J. Hum. Genet.* 102 (6), 1143–1157. doi:10.1016/j.ajhg.2018.04.009

Dixon, M. J., Marazita, M. L., Beaty, T. H., and Murray, J. C. (2011). Cleft lip and palate: Understanding genetic and environmental influences. *Nat. Rev. Genet.* 12 (3), 167–178. doi:10.1038/nrg2933

Frebourg, T., Oliveira, C., Hochain, P., Karam, R., Manouvrier, S., Graziadio, C., et al. (2006). Cleft lip/palate and CDH1/E-cadherin mutations in families with hereditary diffuse gastric cancer. *J. Med. Genet.* 43 (2), 138–142. doi:10.1136/jmg.2005.031385

Ghoumid, J., Stichelbout, M., Jourdain, A. S., Frenois, F., Lejeune-Dumoulin, S., Alex-Cordier, M. P., et al. (2017). Blepharocheilodontic syndrome is a CDH1 pathway-related disorder due to mutations in CDH1 and CTNND1. *Genet. Med.* 19 (9), 1013–1021. doi:10.1038/gim.2017.11

Karam, R., Carvalho, J., Bruno, I., Graziadio, C., Senz, J., Huntsman, D., et al. (2008). The NMD mRNA surveillance pathway downregulates aberrant E-cadherin transcripts in gastric cancer cells and in CDH1 mutation carriers. *Oncogene* 27 (30), 4255–4260. doi:10.1038/onc.2008.62

Kaurah, P., MacMillan, A., Boyd, N., Senz, J., De Luca, A., Chun, N., et al. (2007). Founder and recurrent CDH1 mutations in families with hereditary diffuse gastric cancer. *JAMA* 297 (21), 2360–2372. doi:10.1001/jama.297.21.2360

Mendonsa, A. M., Na, T. Y., and Gumbiner, B. M. (2018). E-cadherin in contact inhibition and cancer. *Oncogene* 37 (35), 4769–4780. doi:10.1038/s41388-018-0304-2

Roberts, M. E., Ranola, J. M. O., Marshall, M. L., Susswein, L. R., Graceffo, S., Bohnert, K., et al. (2019). Comparison of CDH1 penetrance estimates in clinically ascertained families vs families ascertained for multiple gastric cancers. *JAMA Oncol.* 5, 1325–1331. doi:10.1001/jamaoncol.2019.1208

Selvanathan, A., Nixon, C. Y., Zhu, Y., Scietti, L., Forneris, F., Uribe, L. M. M., et al. (2020). CDH1 mutation distribution and type suggests genetic differences between the etiology of orofacial clefting and gastric cancer. *Genes* 11 (4), E391. doi:10.3390/genes11040391

Takeichi, M. (2014). Dynamic contacts: Rearranging adherens junctions to drive epithelial remodelling. *Nat. Rev. Mol. Cell Biol.* 15 (6), 397–410. doi:10.1038/nrm3802

Venkatesh, R. (2009). Syndromes and anomalies associated with cleft. *Indian J. Plast. Surg.* 42, S51–S55. doi:10.4103/0970-0358.57187

Xicola, R. M., Li, S., Rodriguez, N., Reinecke, P., Karam, R., Speare, V., et al. (2019). Clinical features and cancer risk in families with pathogenic CDH1 variants irrespective of clinical criteria. *J. Med. Genet.* 56 (12), 838–843. doi:10.1136/jmedgenet-2019-105991

frontiers | Frontiers in Genetics

TYPE Original Research
PUBLISHED 29 November 2022
DOI 10.3389/fgene.2022.1046989

OPEN ACCESS

EDITED BY
Weimin Lin,
Sichuan University, China

REVIEWED BY
Qi-Tong Xu,
Nanjing Medical University, China
Fangdie Ye,
Fudan University, China

*CORRESPONDENCE
Xu Tong,
500235@hospital.cqmu.edu.cn

SPECIALTY SECTION
This article was submitted to Genetics of Common and Rare Diseases, a section of the journal Frontiers in Genetics

RECEIVED 17 September 2022
ACCEPTED 14 October 2022
PUBLISHED 29 November 2022

CITATION
Shu L and Tong X (2022), Exploring the causal relationship between gastroesophageal reflux and oral lesions: A mendelian randomization study.
Front. Genet. 13:1046989.
doi: 10.3389/fgene.2022.1046989

Exploring the causal relationship between gastroesophageal reflux and oral lesions: A mendelian randomization study

Linjing Shu[1,2] and Xu Tong[1,2,3]*

[1]Stomatological Hospital of Chongqing Medical University, Chongqing, China, [2]Chongqing Key Laboratory of Oral Diseases and Biomedical Sciences, Chongqing Medical University, Chongqing, China, [3]Chongqing Municipal Key Laboratory of Oral Biomedical Engineering of Higher Education, Chongqing Medical University, Chongqing, China

Background: Clinical observations and retrospective studies have observed that patients with gastroesophageal reflux disease (GERD) have an increased probability of dental erosion, periodontitis and oral mucosal lesions and other common oral lesions. However, whether there is a genetic causal relationship between GERD and the occurrence of oral lesions has not been reported.

Methods: In this study, we extracted instrumental variables from the largest published summary statistics of the oral lesion phenotype GWAS in UK Biobank (UKBB) and GERD GWAS. Then, we performed a causal inference analysis between GERD and common oral lesions by mendelian randomization (MR) analysis with the R package "TwoSampleMR".

Results: We observed a significant causal relationship between GERD and several common oral lesion phenotypes (painful gums, loose teeth, toothache, and mouth ulcers). GERD showed a positive correlation with the occurrence of these oral lesions. After removing outlier SNPs *via* the MR-PRESSO package, our conclusions were still robust.

Conclusion: Our findings provide the first evidence for a genetic causal effect of GERD on oral lesion pathogenesis. For patients with confirmed GERD, attention should be paid to taking interventions to prevent the occurrence of oral lesions.

KEYWORDS

mendelian randomization, causal relationship, gastroesophageal reflux disease, oral disease, periodontitis, toothache, oral ulcer

Introduction

As an important part of the digestive system, the occurrence of digestive system diseases can also lead to changes in the oral environment. Gastroesophageal reflux disease (GERD) is a series of chronic symptoms and esophageal mucosal damage caused by reflux of gastric contents due to dysfunction of the lower esophageal sphincter. The prevalence of GERD in adults in Western countries ranges from 10% to 20% (Chen et al., 2014; El-Serag et al., 2014). In addition to affecting the esophagus, GERD leads to a series of extraesophageal symptoms

known as extraesophageal syndrome, including chronic cough, hoarseness, asthma, globus sensation, sleep disturbance, and oral lesions (Jung et al., 2020). Various forms of dental erosion are considered to be the most important oral manifestations of GERD, and the relationship between GERD and dental erosion and tooth loss has been widely observed. Picos et al. (2013) found that dental erosion prevalence in patients with GERD was 35% by investigating the oral health status of GERD patients. Similarly, due to the defect of tooth enamel, the incidence of dental caries in GERD patients also increased (Linnett et al., 2002). Furthermore, the colonization of the tooth surfaces by S. salivarius and Streptococcus mutans was significantly increased in children with GRED (Ersin et al., 2006). In addition, the relationship between changes in salivary flow rate and salivary buffering capacity (Hauk, 2018), changes in taste (Steele, 2016), damage to the oral mucosa, and the onset of chronic periodontitis (Song et al., 2014) have also been reported (Jajam et al., 2017). In previous studies, an increased incidence of tooth erosion, periodontitis, oral mucosal lesions, and dysgeusia was observed in patients with GERD. Although there appears to be a strong association between GERD and oral lesions, previous evidence from either cross-sectional or case-control studies, the direction of the causal relationship between oral lesions and GERD remains uncertain.

Mendelian randomization methods use genetic variation as an instrumental variable reflecting exposure factors (intermediate phenotypes). Since the alleles of genetic variation follow the Mendelian independent distribution law of random separation and combination from parents to offspring when gametes are formed, the random distribution of alleles makes the process of randomization of genetic variation in the population. The relationship between genetic variation and exposure is fixed during conception, independent of postnatal environmental exposures, confounding, and outcomes, and throughout the lifespan to rationalize causal timing (Lawlor et al., 2008). At the same time, genetic variation can be directly and accurately measured, and it can be used as an instrumental variable while avoiding the bias introduced by measurement error. Therefore, mendelian randomization takes genetic variation as an instrumental variable of the exposure factors to be studied, and it is feasible to use the relationship of "genetic variation-study outcome" to simulate the relationship of "exposure factor-study outcome" to infer disease etiology (Neeland and Kozlitina, 2017). In this study, we performed a causal inference analysis between GERD and common oral lesions by mendelian randomization analysis.

Methods

Instrumental variable selection

The GWAS summary data for gastroesophageal reflux comes from the largest published GWAS study of gastroesophageal reflux in European populations (Ong et al., 2022), which included a total sample size of 602,604, including 129,080 cases and 473,524 controls. First, this study selected SNPs that reached the genome-wide significant threshold ($p < 5 \times 10^{-8}$). At the same time, in order to avoid potential bias caused by linkage disequilibrium (LD) relationship between SNPs, we set the physical distance between SNPs >10 000 kb by setting the clump_data function in the TwoSampleMR package, and the R^2 of LD between genes <0.001, the instrumental variable is finally obtained.

GWAS summary statistics data for several common oral disease phenotypes, including loose teeth, bleeding gums, toothache, and oral ulcers were downloaded from UKBB, and β, SE, and p values were extracted for these outcome factors.

The published data used in this study were derived from analyses limited to European population data, and basic information on these subjects is presented in Table 1.

Mendelian randomization analysis

In this study, we used inverse variance weighted (IVW) as the main analysis method. And the median weighted method, weighted mode method, MR Egger method, Simple mode method and Weighted mode method were used as Supplementary Method. The IVW principle used the reciprocal of the variance of each instrumental variable as a weight for weighted calculation under the premise of ensuring that all instrumental variables were effective, and the final result was the weighted average of the effect values of all instrumental variables. The above analysis was implemented through the TwoSampleMR package.

Sensitivity analysis

First, we performed a heterogeneity test for the included instrumental SNPs using Cochran's Q test and I^2 statistic. If the test results suggested an existed heterogeneity, we further detected the outlier SNPs by MR-PRESSO package (Verbanck et al., 2018). And after removing the detected outliers SNPs, Mendelian randomization analysis was performed again and heterogeneity was checked again (Figure 1). The horizontal pleiotropy of instrumental variables was then detected by the MR-Egger method (Bowden et al., 2015). If the p-value of the intercept term of the regression equation is >0.05, it indicates that horizontal pleiotropy is not exhibited. Similarly, in order to verify the stability of the analysis results, we performed a leave-one-out analysis through the leave_one_plot ()

TABLE 1 Basic information on the GWAS applied in this study.

GWAS ID	Year	Trait	Consortium	Sample size	Number of SNPs
ebi-a-GCST90000514	2021	Gastroesophageal reflux disease	NA	6, 02, 604	23, 20, 781
ukb-b-11161	2018	Mouth/teeth dental problems: Painful gums	MRC-IEU	4, 61, 113	98, 51, 867
ukb-b-12849	2018	Mouth/teeth dental problems: Loose teeth	MRC-IEU	4, 61, 113	98, 51, 867
ukb-b-19191	2018	Mouth/teeth dental problems: Toothache	MRC-IEU	4, 61, 113	98, 51, 867
ukb-b-6458	2018	Mouth/teeth dental problems: Mouth ulcers	MRC-IEU	4, 61, 113	98, 51, 867

function in the TwoSampleMR package (Hemani et al., 2017). The funnel plot and forest plot were also generated by TwoSampleMR package. The principle of the leave-one-out method is to eliminate each SNP one by one and calculate the combined effect of the remaining SNPs, so as to determine whether the main effect of an instrumental variable leads to the causal relationship between the exposure factor and the outcome variable.

Ethical approval

The GWAS summary data used in this study were obtained from published studies that have been approved by institutional review boards in their respective studies.

Result

Causal relationship between GERD and oral lesions

After screening the GERD GWAS summary statistics, a total of 80 SNPs were selected as instrumental variables (Supplementary Table S1). After mendelian randomization analysis using the TwoSampleMR package, IVW analysis showed that GERD showed a causal relationship with almost all oral lesions, including loosen teeth (p = 3.98E-06), oral ulcer (p = 0.00779079), bleeding gum (p = 0.01627596) and toothache (p = 0.01627596). p = 0.02197819). Also, MR Egger analysis, weighted median analysis and simple mode analysis also demonstrated a causal relationship between GERD and these common oral lesions (Table 2). In addition, although the slopes

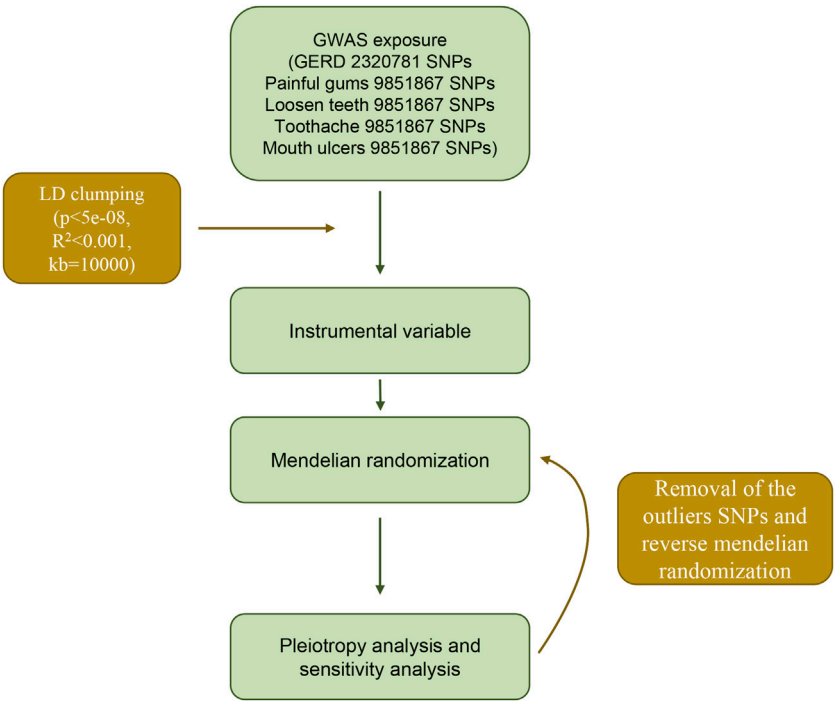

FIGURE 1
Flow chart and design of this mendelian randomization study.

TABLE 2 MR analysis results of five common methods of GERD to painful gums, loosen teeth, toothache and mouth ulcers.

ID exposure	ID outcome	Outcome	Exposure	Method	nsnp	b	se	*p* val
ebi-a-GCST90000514	ukb-b-11161	Mouth/teeth dental problems: Painful gums || id:ukb-b-11161	Gastroesophageal reflux disease || id:ebi-a-GCST90000514	MR Egger	77	0.026394347	0.007459688	0.000695244
ebi-a-GCST90000514	ukb-b-11161	Mouth/teeth dental problems: Painful gums || id:ukb-b-11161	Gastroesophageal reflux disease || id:ebi-a-GCST90000514	Weighted median	77	0.009413891	0.001913832	8.70E-07
ebi-a-GCST90000514	ukb-b-11161	Mouth/teeth dental problems: Painful gums || id:ukb-b-11161	Gastroesophageal reflux disease || id:ebi-a-GCST90000514	Inverse variance weighted	77	0.008758933	0.001328755	4.34E-11
ebi-a-GCST90000514	ukb-b-11161	Mouth/teeth dental problems: Painful gums || id:ukb-b-11161	Gastroesophageal reflux disease || id:ebi-a-GCST90000514	Simple mode	77	0.009888257	0.004979183	0.050648794
ebi-a-GCST90000514	ukb-b-11161	Mouth/teeth dental problems: Painful gums || id:ukb-b-11161	Gastroesophageal reflux disease || id:ebi-a-GCST90000514	Weighted mode	77	0.009888257	0.004699471	0.038674976
ebi-a-GCST90000514	ukb-b-12849	Mouth/teeth dental problems: Loose teeth || id:ukb-b-12849	Gastroesophageal reflux disease || id:ebi-a-GCST90000514	MR Egger	77	0.011477439	0.011342248	0.31483016
ebi-a-GCST90000514	ukb-b-12849	Mouth/teeth dental problems: Loose teeth || id:ukb-b-12849	Gastroesophageal reflux disease || id:ebi-a-GCST90000514	Weighted median	77	0.004657994	0.002465903	0.058897043
ebi-a-GCST90000514	ukb-b-12849	Mouth/teeth dental problems: Loose teeth || id:ukb-b-12849	Gastroesophageal reflux disease || id:ebi-a-GCST90000514	Inverse variance weighted	77	0.009259929	0.002007526	3.98E-06
ebi-a-GCST90000514	ukb-b-12849	Mouth/teeth dental problems: Loose teeth || id:ukb-b-12849	Gastroesophageal reflux disease || id:ebi-a-GCST90000514	Simple mode	77	0.001000642	0.006571932	0.879385406
ebi-a-GCST90000514	ukb-b-12849	Mouth/teeth dental problems: Loose teeth || id:ukb-b-12849	Gastroesophageal reflux disease || id:ebi-a-GCST90000514	Weighted mode	77	0.002186752	0.006001517	0.716596105
ebi-a-GCST90000514	ukb-b-19191	Mouth/teeth dental problems: Toothache || id:ukb-b-19191	Gastroesophageal reflux disease || id:ebi-a-GCST90000514	MR Egger	77	-0.004975838	0.00990735	0.61697218
ebi-a-GCST90000514	ukb-b-19191	Mouth/teeth dental problems: Toothache || id:ukb-b-19191	Gastroesophageal reflux disease || id:ebi-a-GCST90000514	Weighted median	77	0.00254743	0.002373421	0.283129575
ebi-a-GCST90000514	ukb-b-19191	Mouth/teeth dental problems: Toothache || id:ukb-b-19191	Gastroesophageal reflux disease || id:ebi-a-GCST90000514	Inverse variance weighted	77	0.004038735	0.001763066	0.021978186
ebi-a-GCST90000514	ukb-b-19191	Mouth/teeth dental problems: Toothache || id:ukb-b-19191	Gastroesophageal reflux disease || id:ebi-a-GCST90000514	Simple mode	77	0.001047195	0.006625769	0.874837492
ebi-a-GCST90000514	ukb-b-19191	Mouth/teeth dental problems: Toothache || id:ukb-b-19191	Gastroesophageal reflux disease || id:ebi-a-GCST90000514	Weighted mode	77	0.001257552	0.006146903	0.838444763
ebi-a-GCST90000514	ukb-b-6458	Mouth/teeth dental problems: Mouth ulcers || id:ukb-b-6458	Gastroesophageal reflux disease || id:ebi-a-GCST90000514	MR Egger	77	0.04177879	0.019611096	0.036420579
ebi-a-GCST90000514	ukb-b-6458	Mouth/teeth dental problems: Mouth ulcers || id:ukb-b-6458	Gastroesophageal reflux disease || id:ebi-a-GCST90000514	Weighted median	77	0.009940645	0.003561053	0.005246591
ebi-a-GCST90000514	ukb-b-6458	Mouth/teeth dental problems: Mouth ulcers || id:ukb-b-6458	Gastroesophageal reflux disease || id:ebi-a-GCST90000514	Inverse variance weighted	77	0.009406138	0.003534807	0.007790791
ebi-a-GCST90000514	ukb-b-6458	Mouth/teeth dental problems: Mouth ulcers || id:ukb-b-6458	Gastroesophageal reflux disease || id:ebi-a-GCST90000514	Simple mode	77	0.008845566	0.008580587	0.305866062
ebi-a-GCST90000514	ukb-b-6458	Mouth/teeth dental problems: Mouth ulcers || id:ukb-b-6458	Gastroesophageal reflux disease || id:ebi-a-GCST90000514	Weighted mode	77	0.011547019	0.00807649	0.156899001

calculated by the different analyses were different, all analyses showed a positive relationship between GERD and oral lesions (Figure 2).

Stability analysis by leave-one-out method showed that no single SNP significantly altered the overall effect of GERD on several oral lesions (Figure 3), indicating the stability of our analysis. Also, the funnel plots and forest plots showed that there was no significant heterogeneity of the selected instrumental variable SNPs (Supplementary Figures S1, S2). We then performed a heterogeneity analysis and found a significant heterogeneity in the causal relationship between GERD and loosen tooth (MR Egger p = 0.000375318, IVW p = 0.000484792), bleeding gums (MR Egger p = 0.000140049, IVW p = 0.000163869), mouth ulcers (MR Egger p = 5.68E-08, IVW p = 1.62E-08). The heterogeneity between toothache and gum pain was not significant (Supplementary Table S2). After removing several detected outlier SNPs using MR-PRESSO analysis, heterogeneity analysis showed that all heterogeneity in the causal relationship was not significant between GERD and oral common diseases (Supplementary Tables S3, S4). We then performed the Mendelian randomization analysis and the results still suggested a causal relationship between GERD and oral lesions (Supplementary Table S3). Horizontal pleiotropy analysis showed that, except for gingival bleeding, there was no horizontal pleiotropy between several oral lesions and the occurrence of GERD (p > 0.05) (Supplementary Table S5).

Discussion

In this study, we used a two-sample MR approach to analyze the causal relationship between GERD and oral lesions. We conclude that GERD is positively associated with an increased incidence of oral lesions in the European population. Our findings were valid and stable in IVW analysis before and after exclusion of outliers SNPs, and were also stable in sensitivity analysis.

Clinically, oral lesions are frequently observed in patients with GERD, where gastric contents (pH 1–1.5) consisting of acids, pepsin, bile salts, and trypsin may reflux to the esophagus and reach the oral cavity, leading to high levels of dental erosion and sometimes caries, and may also cause damage to oral soft tissues that are not adapted to their harmful potential (Tjon et al., 2021; Ribolsi et al., 2022). Various studies have demonstrated an increased prevalence of tooth erosion and caries in individuals with GERD compared to controls. At present, there are the following reports and speculations about the causes of different oral lesions caused by GERD.

Dental erosion refers to the reduction of dental mineralization due to chemical or ionization processes caused by non-bacterial factors (Donovan et al., 2021), and is not associated with bacterial infection. Hydroxyapatite crystals in tooth enamel can disintegrate in an acid environment with pH lower than 5.5, while the pH of refluxed gastric contents is usually lower than 2.0, which is conducive to the occurrence of tooth erosion (Shellis et al., 2014). Following tooth erosion, incomplete tooth surfaces are more susceptible to friction and wear, resulting in occlusal wear and loss. In addition, GERD patients often have abnormal esophageal motility, which is closely related to delayed acid clearance. Usually under physiological conditions, gastric reflux is caused by swallowing to induce peristaltic return to the stomach or by stimulating the esophageal mucosa to induce secondary peristaltic clearance. In GERD patients, however, this process is often impeded, and therefore acid clearance is delayed. A study of esophageal motility in patients with tooth erosion found a mean of 8% in patients with tooth erosion and 0% in healthy controls, suggesting that poor esophageal motility may be a risk factor for tooth erosion (Bartlett et al., 2000). Similarly, acidity from gastroesophageal reflux can also lead to oral soft tissue lesions (Watanabe et al., 2017). In GERD patients, palatal mucosal epithelial atrophy and increased fibroblasts were observed. However, these changes which are only detected by morphometry (Silva et al., 2001). In another study, soft/hard palate and uvula erythema and a burning sensation in the mouth were more common in GERD patients (Di Fede et al., 2008). GERD has been reported to cause esophageal mucosal damage and esophagitis (Mari et al., 2022). But so far, there have been very limited reports on whether GERD can lead to oral ulcers. In an experimental model of rat chronic acid reflux esophagitis, in addition to tooth erosion, the researchers also observed inflammatory cell infiltration in the mucosa of the back of the tongue, proving that acid reflux can also lead to an inflammatory response in the oral mucosa (Shimazu et al., 2018). Our study is the first to identify a causal relationship between GERD and oral ulcers through genetic evidence.

The effect on the secretion and properties of saliva is also one of the important causes of oral lesions caused by GERD. Under physiological conditions, the removal of acidic substances in esophageal reflux includes peristaltic clearance and salivary chemical clearance. Saliva not only buffers acid, but also stimulates esophageal motility after being swallowed, causing further acid removal. Therefore, saliva is considered to be an important protective mechanism of the esophagus and oral mucosa against acid reflux, and both the quality and quantity of saliva secretion directly affect the occurrence of dental erosion. In addition to its role in buffering the acidic environment, saliva also plays a major role in the maintenance of oral health and the repair of hard and soft oral tissues, including antibacterial effects, promotion of remineralization and wound healing. A

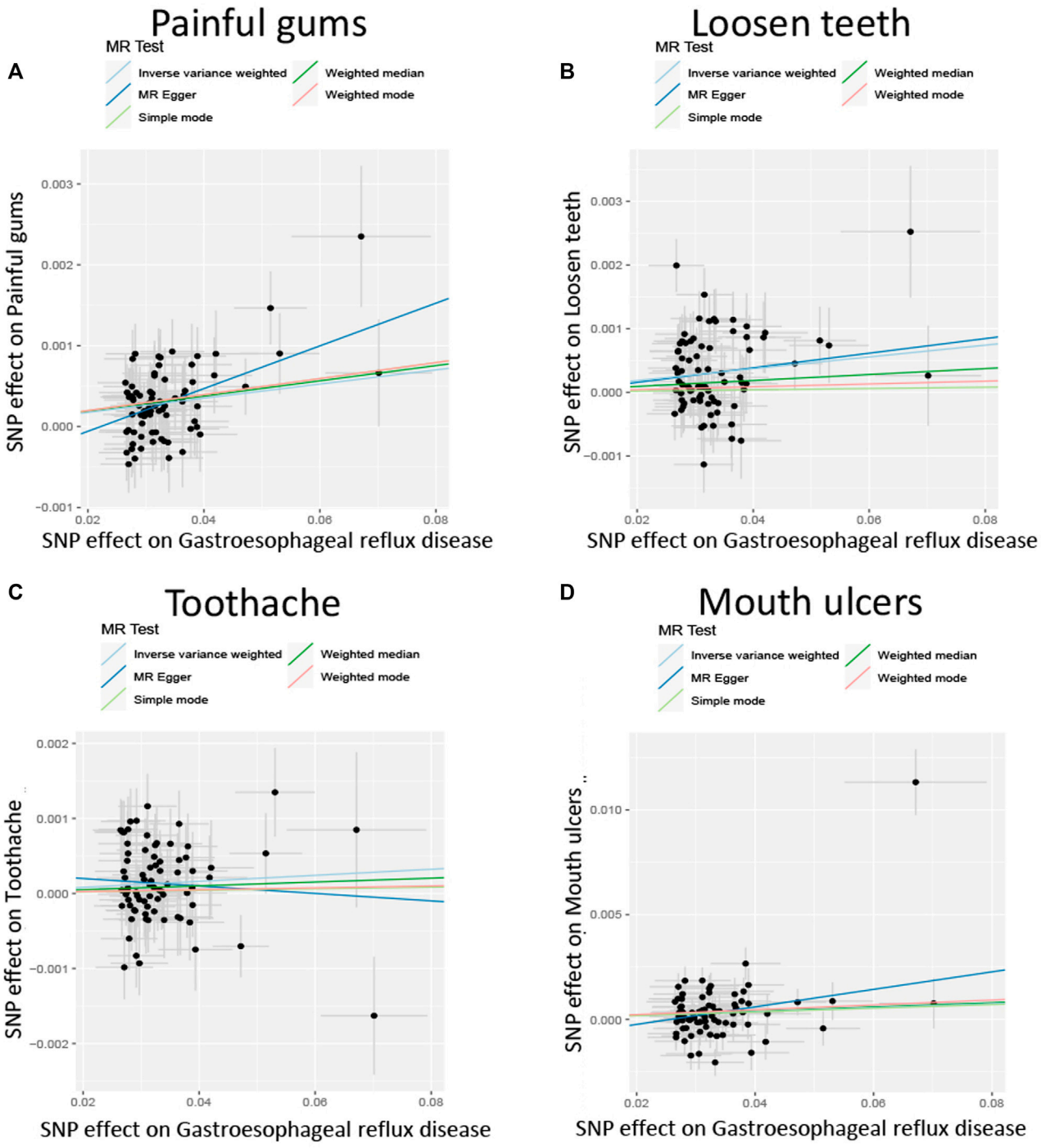

FIGURE 2
Scatterplot of the effect size for each SNP on GERD and the risk of **(A)** Painful gums, **(B)** Loosen teeth, **(C)** Toothache, **(D)** Mouth ulcers.

reduction in saliva flow can speed up the process of tooth erosion. Likewise, a reduction in saliva, along with changes in its quality, is thought to be the main cause of periodontitis in GERD patients. In the study of Song et al. (2014), GERD was considered as an independent risk factor for periodontitis.

In addition, considering that proton pump inhibitors are currently recommended as the preferred treatment for

FIGURE 3
Leave-one-out analysis for the impact of individual SNPs on the association between GERD and the risk of oral lesions. **(A)** Painful gums, **(B)** Loosen teeth, **(C)** Toothache, **(D)** Mouth ulcers.

GERD, the use of proton pump inhibitors (PPI) is thought to affect the secretion and properties of saliva. In GERD patients taking PPIs, their salivary flow rate was significantly lower than controls, and their acid buffering capacity decreased (Tanabe et al., 2021). Therefore, drug use accompanying GERD may also be a causative factor for oral lesions.

Despite the validity and robustness of our MR results, the current study has some limitations. First, since the GWAS data for oral lesions and GERD used in this study were derived from European populations, our findings may not be scalable to other populations. Second, since large-scale oral lesion GWAS are rarely published, we selected only the phenotypes of the major oral lesions disclosed in the UKBB. However, most of these oral lesion phenotypes are local manifestations of common oral diseases (caries, periodontitis) rather than directly representing the occurrence of these diseases. The causal relationship between these diseases and GERD remains to be further confirmed. Finally, the occurrence of all these oral lesions is determined by a combination of genetic as well as environmental factors, and our results only partially explain the causal effect of GERD on oral lesions.

In conclusion, our study demonstrated a causal relationship between GRED and several common oral lesions, including toothache, loose teeth, bleeding gums, painful gums, and oral ulcers, through mendelian randomization analysis. When the MR analysis was repeated after removing outlier SNPs, our results were still robust. The present findings suggest that interventions should be taken to prevent the occurrence of oral lesions in patients with confirmed GERD. Considering that a large number of undiagnosed GERD patients showed oral lesions as the first symptom, dentists should consider GERD in the etiological analysis of these common oral lesions, especially tooth erosion.

Data availability statement

The original contributions presented in the study are included in the article/Supplementary Material, further inquiries can be directed to the corresponding author.

Author contributions

LS and XT designed the project; LS performed the analysis and wrote the manuscript.

Acknowledgments

The authors acknowledge the financial support received from the Innovation Team Building at Institutions of Higher Education in Chongqing in 2016.

Conflict of interest

The authors declare that the research was conducted in the absence of any commercial or financial relationships that could be construed as a potential conflict of interest.

Publisher's note

All claims expressed in this article are solely those of the authors and do not necessarily represent those of their affiliated organizations, or those of the publisher, the editors and the reviewers. Any product that may be evaluated in this article, or claim that may be made by its manufacturer, is not guaranteed or endorsed by the publisher.

Supplementary material

The Supplementary Material for this article can be found online at: https://www.frontiersin.org/articles/10.3389/fgene.2022.1046989/full#supplementary-material

SUPPLEMENTARY TABLE S1
The instrumental variation SNPs selected for MR analysis.

SUPPLEMENTARY TABLE S2
The heterogeneity results of MR analysis from the Cochran's Q test.

SUPPLEMENTARY TABLE S3
The instrumental variation SNPs selected for MR analysis after removal of outlier SNPs.

SUPPLEMENTARY TABLE S4
The heterogeneity results of MR analysis from the Cochran's Q test after removal of outlier SNPs.

SUPPLEMENTARY TABLE S5
The pleiotropy analysis results of MR analysis.

References

Bartlett, D. W., Evans, D. F., Anggiansah, A., Smith, B. G. N., et al. (2000). The role of the esophagus in dental erosion. *Oral Surg. Oral Med. Oral Pathol. Oral Radiol. Endod* 89 (3), 312–315. doi:10.1016/s1079-2104(00)70094-1

Bowden, J., Davey Smith, G., and Burgess, S. (2015). Mendelian randomization with invalid instruments: Effect estimation and bias detection through egger regression. *Int. J. Epidemiol.* 44 (2), 512–525. doi:10.1093/ije/dyv080

Chen, J. H., Wang, H. Y., Lin, H. H., Wang, C. C., and Wang, L. Y. (2014). Prevalence and determinants of gastroesophageal reflux symptoms in adolescents. *J. Gastroenterol. Hepatol.* 29 (2), 269–275. doi:10.1111/jgh.12330

Di Fede, O., Di Liberto, C., Occhipinti, G., Vigneri, S., Lo Russo, L., Fedele, S., et al. (2008). Oral manifestations in patients with gastro-oesophageal reflux disease: A single-center case-control study. *J. Oral Pathol. Med.* 37 (6), 336–340. doi:10.1111/j.1600-0714.2008.00646.x

Donovan, T., Nguyen-Ngoc, C., Abd Alraheam, I., and Irusa, K. (2021). Contemporary diagnosis and management of dental erosion. *J. Esthet. Restor. Dent.* 33 (1), 78–87. doi:10.1111/jerd.12706

El-Serag, H. B., Sweet, S., Winchester, C. C., and Dent, J. (2014). Update on the epidemiology of gastro-oesophageal reflux disease: A systematic review. *Gut* 63 (6), 871–880. doi:10.1136/gutjnl-2012-304269

Ersin, N. K., Onçağ, O., Tümgör, G., Aydogdu, S., and Hilmioglu, S. (2006). Oral and dental manifestations of gastroesophageal reflux disease in children: A preliminary study. *Pediatr. Dent.* 28 (3), 279–284.

Hauk, L. (2018). Laparoscopic Roux-en-Y gastric bypass. *Aorn J.* 107 (3), P12–P14. doi:10.1002/aorn.12107

Hemani, G., Tilling, K., and Davey Smith, G. (2017). Orienting the causal relationship between imprecisely measured traits using GWAS summary data. *PLoS Genet.* 13 (11), e1007081. doi:10.1371/journal.pgen.1007081

Jajam, M., Bozzolo, P., and Niklander, S. (2017). Oral manifestations of gastrointestinal disorders. *J. Clin. Exp. Dent.* 9 (10), e1242–e1248. doi:10.4317/jced.54008

Jung, H. K., Tae, C. H., Song, K. H., Kang, S. J., Park, J. K., Gong, E. J., et al. (2020). 2020 seoul consensus on the diagnosis and management of gastroesophageal reflux disease. *J. Neurogastroenterol. Motil.* 27 (4), 453–481. doi:10.5056/jnm21077

Lawlor, D. A., Harbord, R. M., Sterne, J. A., Timpson, N., and Davey Smith, G. (2008). Mendelian randomization: Using genes as instruments for making causal inferences in epidemiology. *Stat. Med.* 27 (8), 1133–1163. doi:10.1002/sim.3034

Linnett, V., Seow, W. K., Connor, F., and ShepheRd, R. (2002). Oral health of children with gastro-esophageal reflux disease: A controlled study. *Aust. Dent. J.* 47 (2), 156–162. doi:10.1111/j.1834-7819.2002.tb00321.x

Mari, A., Na'amnih, W., Gahshan, A., Ahmad, H. S., Khoury, T., and Muhsen, K. (2022). Comparison in adherence to treatment between patients with mild-moderate and severe reflux esophagitis: A prospective study. *J. Clin. Med.* 11 (11), 3196. doi:10.3390/jcm11113196

Neeland, I. J., and Kozlitina, J. (2017). Mendelian randomization: Using natural genetic variation to assess the causal role of modifiable risk factors in observational studies. *Circulation* 135 (8), 755–758. doi:10.1161/CIRCULATIONAHA.117.026857

Ong, J. S., An, J., Han, X., Law, M. H., Nandakumar, P., 23andMe Research team, et al. (2022). Multitrait genetic association analysis identifies 50 new risk loci for gastro-oesophageal reflux, seven new loci for Barrett's oesophagus and provides insights into clinical heterogeneity in reflux diagnosis. *Gut* 71 (6), 1053–1061. doi:10.1136/gutjnl-2020-323906

Picos, A. M., Poenar, S., Opris, A., Chira, A., Bud, M., Berar, A., et al. (2013). Prevalence of dental erosions in GERD: A pilot study. *Clujul Med.* 86 (4), 344–346.

Ribolsi, M., Frazzoni, M., De Bortoli, N., Tolone, S., Arsie, E., Mariani, L., et al. (2022). Reflux characteristics triggering post-reflux swallow-induced peristaltic wave (PSPW) in patients with GERD symptoms. *Neurogastroenterol. Motil.* 34 (2), e14183. doi:10.1111/nmo.14183

Shellis, R. P., Featherstone, J. D., and Lussi, A. (2014). Understanding the chemistry of dental erosion. *Monogr. Oral Sci.* 25, 163–179. doi:10.1159/000359943

Shimazu, R., Yamamoto, M., Minesaki, A., and Kuratomi, Y. (2018). Dental and oropharyngeal lesions in rats with chronic acid reflux esophagitis. *Auris Nasus Larynx* 45 (3), 522–526. doi:10.1016/j.anl.2017.08.011

Silva, M. A., Damante, J. H., Stipp, A. C., Tolentino, M. M., Carlotto, P. R., and Fleury, R. N. (2001). Gastroesophageal reflux disease: New oral findings. *Oral Surg. Oral Med. Oral Pathol. Oral Radiol. Endod.* 91 (3), 301–310. doi:10.1067/moe.2001.111139

Song, J. Y., Kim, H. H., Cho, E. J., and Kim, T. Y. (2014). The relationship between gastroesophageal reflux disease and chronic periodontitis. *Gut Liver* 8 (1), 35–40. doi:10.5009/gnl.2014.8.1.35

Steele, J. C. (2016). The practical evaluation and management of patients with symptoms of a sore burning mouth. *Clin. Dermatol.* 34 (4), 449–457. doi:10.1016/j.clindermatol.2016.02.017

Tanabe, T., Koeda, M., Kitasako, Y., Momma, E., Hoshikawa, Y., Hoshino, S., et al. (2021). Stimulated saliva secretion is reduced in proton pump inhibitor-resistant severe reflux esophagitis patients. *Esophagus.* 18 (3), 676–683. doi:10.1007/s10388-021-00825-1

Tjon, J., Cooper, M., Pe, M., Boodhan, S., Mahant, S., Avitzur, Y., et al. (2021). Measuring gastric pH in tube-fed children with neurologic impairments and gastroesophageal disease. *J. Pediatr. Gastroenterol. Nutr.* 72 (6), 842–847. doi:10.1097/MPG.0000000000003087

Verbanck, M., Chen, C. Y., Neale, B., et al. (2018). Detection of widespread horizontal pleiotropy in causal relationships inferred from Mendelian randomization between complex traits and diseases. *Nat. Genet.* 50 (5), 693–698. doi:10.1038/s41588-018-0099-7

Watanabe, M., Nakatani, E., Yoshikawa, H., Kanno, T., Nariai, Y., Yoshino, A., et al. (2017). Oral soft tissue disorders are associated with gastroesophageal reflux disease: Retrospective study. *BMC Gastroenterol.* 17 (1), 92. doi:10.1186/s12876-017-0650-5

frontiers | Frontiers in Genetics

TYPE Original Research
PUBLISHED 08 February 2023
DOI 10.3389/fgene.2023.1082911

OPEN ACCESS

EDITED BY
Weimin Lin,
Sichuan University, China

REVIEWED BY
Xiao-Jing Zhu,
Hangzhou Normal University, China
Zhonglin Jia,
Sichuan University, China
Pranidhi Baddam,
University of Alberta, Canada

*CORRESPONDENCE
Qian Bian,
qianbian@shsmu.edu.cn
Xudong Wang,
xudongwang70@hotmail.com

†These authors have contributed equally to this work and share first authorship

SPECIALTY SECTION
This article was submitted to Genetics of Common and Rare Diseases, a section of the journal Frontiers in Genetics

RECEIVED 28 October 2022
ACCEPTED 24 January 2023
PUBLISHED 08 February 2023

CITATION
Luo S, Liu Z, Bian Q and Wang X (2023), Ectomesenchymal *Six1* controls mandibular skeleton formation. *Front. Genet.* 14:1082911. doi: 10.3389/fgene.2023.1082911

Ectomesenchymal *Six1* controls mandibular skeleton formation

Songyuan Luo[1,2†], Zhixu Liu[1,2†], Qian Bian[1,3*] and Xudong Wang[1,2*]

[1]Department of Oral and Craniomaxillofacial Surgery, Shanghai Ninth People's Hospital, Shanghai Jiao Tong University School of Medicine, Shanghai, China, [2]National Center for Stomatology, National Clinical Research Center for Oral Diseases, Shanghai Key Laboratory of Stomatology, Shanghai, China, [3]Shanghai Institute of Precision Medicine, Shanghai, China

Craniofacial development requires intricate cooperation between multiple transcription factors and signaling pathways. Six1 is a critical transcription factor regulating craniofacial development. However, the exact function of Six1 during craniofacial development remains elusive. In this study, we investigated the role of Six1 in mandible development using a *Six1* knockout mouse model (*Six1*$^{-/-}$) and a cranial neural crest-specific, *Six1* conditional knockout mouse model (*Six1*$^{f/f}$*; Wnt1-Cre*). The *Six1*$^{-/-}$ mice exhibited multiple craniofacial deformities, including severe microsomia, high-arched palate, and uvula deformity. Notably, the *Six1*$^{f/f}$*; Wnt1-Cre* mice recapitulate the microsomia phenotype of *Six1*$^{-/-}$ mice, thus demonstrating that the expression of *Six1* in ectomesenchyme is critical for mandible development. We further showed that the knockout of *Six1* led to abnormal expression of osteogenic genes within the mandible. Moreover, the knockdown of *Six1* in C3H10 T1/2 cells reduced their osteogenic capacity *in vitro*. Using RNA-seq, we showed that both the loss of Six1 in the E18.5 mandible and Six1 knockdown in C3H10 T1/2 led to the dysregulation of genes involved in embryonic skeletal development. In particular, we showed that Six1 binds to the promoter of *Bmp4*, *Fat4*, *Fgf18,* and *Fgfr2*, and promotes their transcription. Collectively, our results suggest that Six1 plays a critical role in regulating mandibular skeleton formation during mouse embryogenesis.

KEYWORDS

Six1, craniofacial development, mandibular skeletal development, cranial neural crest cells, osteogenic differentiation

Introduction

The craniofacial development of vertebrates is precisely regulated by various genes and signaling pathways, including BMP, FGF, and WNT (Yin et al., 2015; Graf et al., 2016). Most craniofacial tissues are derived from cranial neural crest cells (CNCCs), which arise from the dorsal central nervous system and migrate into the developing craniofacial region (Liao et al., 2022). Within maxillary and mandibular prominences, CNCCs differentiate into ectomesenchymal cells, and the ectomesenchymal cells subsequently differentiate into various cell and tissue types, including the frontonasal skeleton, bone and cartilage of the jaw and middle ear (Liao et al., 2022). In contrast to other mesoderm-derived bones of the skeleton, the mandibular skeleton is generated during mandibular development *via* an intramembranous process in which ectodermal mesenchymal cells aggregate and then differentiate into bone (Parada and Chai, 2015; Liao et al., 2022).

The intricate regulation of craniofacial development and differentiation requires a number of transcription factors, such as the MSX family, DLX family, and the SIX family transcription factors, among others (Alappat et al., 2003; Takechi et al., 2013). The SIX family is a group of evolutionarily conserved transcription factors, which are expressed in multiple organs of

humans, mice, *drosophila*, and other organisms, and play an essential role in the development of the craniofacial skeleton, kidney, ear, nose, brain, muscle, and gonads (Serikaku and O'Tousa, 1994). The mammalian SIX family consists of six members (SIX1-6). SIX family genetic mutations lead to various deformities, including craniofacial deformities, hearing disorders, visual disturbance, renal hypoplasia, and muscular dysplasia. (Kumar, 2009).

Six1 has been demonstrated to be a crucial member of the SIX family transcription factors in the embryonic development (Wu et al., 2014; Liu et al., 2019). *Six1* knockout mice exhibited craniofacial deformity, hypoplastic kidneys (Xu et al., 2003), and severely dysplastic lungs (El-Hashash et al., 2011). Previous studies have shown that *Six1* exerts versatile transcription regulatory effects by interacting with different molecular partners. SIX1 can form a complex with EYA1 and activate transcription (Li et al., 2003). Moreover, SIX1 can also form a transcription complex with members of the DACH family and repress the expression of downstream genes (Li et al., 2003). Six1 regulates *Fgf10* and *Bmp4* expression in the otic vesicle and interacts with *Runx1* to regulate the cell fate of the Müllerian duct epithelium (Zheng et al., 2003; Terakawa et al., 2020).

It has been suggested that Six1 participates in the development of the craniofacial skeleton (Tavares et al., 2017). *Six1* is widely expressed in craniofacial tissues of different origins, such as ectoderm, mesoderm, and endoderm (Liu et al., 2019). *SIX1* mutation causes human branchio-oto-renal syndrome (BOR), characterized by hearing loss, auricular deformities, residual branchial arches, and renal abnormalities (Kumar et al., 2000; Ruf et al., 2004; Feng et al., 2021). However, the mechanisms by which SIX1 regulates craniofacial development, and skeletogenesis remain unclear.

In this study, we generated a *Six1* knockout mouse model and conditional deletion of *Six1* in cranial neural crest cells to investigate the role of Six1 in ectomesenchymal cells during murine embryonic mandibular development. We found that the mandibles of both $Six1^{-/-}$ and $Six1^{f/f}$; *Wnt1-Cre* were significantly shortened, indicating that ectomesenchymal *Six1* participates in mandibular skeletal development. Combining RNA-seq and immunofluorescence staining, we demonstrated that mandibular osteogenesis is impaired in E18.5 and E16.5 $Six1^{-/-}$ mice. In particular, mRNA expression levels of several key osteogenesis-related genes, such as *Osteopontin* (*Opn*), *Osteocalcin* (*Ocn*) and *Osterix* (*Osx*), were found to be downregulated. *In vitro*, the knockdown of *Six1* in the mouse embryonic mesenchymal stem cell line C3H10 T1/2 resulted in decreased osteogenic differentiation capacity and dysregulation of ossification-related genes. By performing CUT&Tag, we further demonstrated that Six1 directly binds to the promoters of *Bmp4*, *Fgfr2*, *Fgf18,* and *Fat4*, all of which are critical genes involved in skeletal formation and regulates their expression (Hung et al., 2016; Crespo-Enriquez et al., 2019; Motch Perrine et al., 2019; Xu et al., 2021). Taken together, our data suggest that Six1 plays a critical role in the regulation of ossification during embryonic mandibular skeletal development and elucidates the potential Six1-dependent gene regulation networks involved in mandibular development.

Materials and methods

Animals

The *Six1* knockout homozygous ($Six1^{-/-}$) and *Six1* conditional knockout ($Six1^{f/f}$) mouse models were generated using the CRISPR/Cas9 system on a C57BL/6J mouse background by GemPharmatech Co., Ltd (Nanjing, China). The mouse strain creation strategy involved the knockout of exon1-2 of the *Six1*-201 (ENSMUST00000050029.7) transcript region. *Wnt1-Cre* mice were obtained from the Jackson Laboratory (Bar Harbor, ME, United States). $Six1^{f/f}$ mice were crossed with $Six1^{f/+}$; *Wnt1-cre* mice to generate $Six1^{f/f}$; *Wnt1-Cre* embryos. (Supplementary Figure 1; Supplementary Table S1).

Embryos were obtained for subsequent experiments at E18.5, E16.5, and E14.5 days. The day of the appearance of a vaginal plug was defined as E0.5, and the embryos were obtained at 12:30 on each day in question. All mice were maintained and used in experiments according to the guidelines approved by the Institutional Animal Care and Use Committee (IACUC) of the Shanghai Ninth People's Hospital affiliated to Shanghai Jiao Tong University School of Medicine.

Skeletal preparation

Skin and soft tissue were carefully removed from E18.5 embryos and the embryos were treated in 95% ethanol overnight, followed by staining with Alcian blue for 48 h at 37°C. Embryos were washed twice with 95% ethanol for 2 h each, treated with 1% KOH for 1 h, and stained with Alizarin red for 2 h. The embryonic bone tissue was soaked in a gradient mixture of 1% KOH in glycerol (75%, 50%, 25%) and photographed.

Histology and immunofluorescence, and TUNEL assay

The heads of the embryos were surgically isolated and fixed overnight with 4% PFA at 4°C, followed by gradient dehydration using an ethanol solution, embedded using paraffin. Hematoxylin–Eosin (HE) and Alcian blue staining were performed on 7 μm-thick paraffin sections. Immunofluorescence staining was performed with anti-Osteopontin Polyclonal antibody (22952-1-AP, Proteintech, Rosemont, IL, United States; 1:50), anti-Osterix antibody (ab209484, Abcam, Cambridge, United Kingdom; 1:200), or anti-Ki67 antibody (ab16667, Abcam; 1:100) followed by goat secondary antibody to rabbit IgG(A-11008, Thermo Fisher Scientific, Waltham, MA, United States; 1:500) following a previously described protocol (Ha et al., 2022). TUNEL staining was performed using *In Situ* Cell Death Detection Kit (11684795910, Roche, Mannheim, Germany) according to the manufacturer's instructions. Nuclei were counterstained with 4′,6-diamidino-2-phenylindole (DAPI). Images were captured using an Olympus IX83 inverted microscope (Olympus, Tokyo, Japan).

Cell culture, osteogenic differentiation, alkaline phosphatase (ALP) staining and cell proliferation assay

C3H10 T1/2 cells were purchased from the Cell Bank of the Chinese Academy of Sciences, Shanghai. The cells were maintained at 37°C with 5% CO_2, and were cultured in MEM-α containing 10% FBS (10099141C, Gibco™, Thermo Fisher Scientific), 1% penicillin/streptomycin, 1% Non-Essential Amino Acids, and 1% GlutaMAX™ Supplement, and the culture medium was replaced every 2 days. Osteogenic induction medium (MUXMT-90021, Cyagen Biosciences Inc., Guangzhou, China) was used in the process of cell osteogenic differentiation (Ma et al., 2021).

C3H10 T1/2 cells were seeded into 6-well plates at 50,000 cells per well and incubated at 37°C, 5% CO_2 for 24 h. Then the regular cell culture medium was replaced with osteogenic induction medium. The osteogenic induction medium was changed every 48 h. ALP staining and RNA extraction were performed 7 days after osteogenic induction. The cells were fixed for 30 min with 4% paraformaldehyde, and ALP staining was performed using the BCIP/NBT Alkaline Phosphatase color development kit following the manufacturer's instructions (C3206, Beyotime Biotechnology, Beijing, China). Cell proliferation was analyzed using the Cell Counting Kit-8 according to the manufacturer's instructions (C0037, Beyotime Biotechnology). Cells were seeded in a 96-well plate at a density of 1,000 cells per well and incubated at 37°C, 5% with complete MEM-α. At 24, 48, 72, 96, and 120 h, the medium was removed and added CCK-8 solution was added to the medium and incubated for 1 h. Then, the reaction solution was read with a multimode reader (BioTek, Winooski, VT, United States) to obtain the absorbance at 450 nm.

RNA extraction and quantitative RT-PCR

The RNA was extracted using a total RNA extraction kit (LS1040, Promega, Madison, WI, United States). Following the manufacturer's instructions, 1 μg of total RNA was reverse transcribed into cDNA using Hifair first Strand cDNA Synthesis SuperMix (11141ES10, Yeasen Biotech, Shanghai, China) for RT-qPCR analysis. Quantitative PCR was performed on a Lightcycler 96 (Roche, Basel, Switzerland) with Hieff qPCR SYBR Green Master Mix (No Rox) (11201ES03; Yeasen Biotech). The relative expression was calculated for each gene by the $2^{-\Delta\Delta CT}$ method, normalized against GAPDH expression, and presented as fold changes relative to the control. The sequences of all the primers used in this study are shown in Supplementary Table S2.

Construction of knockdown short hairpin RNA vectors and cell infection

Short hairpin RNA (shRNA) targeting *Six1* (NM_009189.3) was designed with the following sequence: GCTCATGTCCAGCTCAGA AGA. The shRNA was transfected into the pLV-shRNA-EGFP(2A) Puro vector. *Six1*-shRNA lentiviruses were packaged and amplified by co-transfecting recombinant vector together with pSPAX2 and pMD2G into 293T cells with lipo8000 and culturing for 48 h. Then the cell culture supernatants were collected and concentrated using a Universal Virus Concentration Kit (C2901M, Beyotime Institute of Biotechnology, Jiangsu, China). The virus concentrate was added to C3H10 T1/2 cells at an MOI of 50 with polybrene(12 μg/mL) and cultured for 6 h. Subsequently, the cell medium was changed and cells were cultured for a further 72 h. To obtain stably transfected cells, C3H10 T1/2 cells were cultured in MEM-α supplemented with puromycin dihydrochloride (10 μg/mL, Beyotime Institute of Biotechnology) for 7 days.

RNA sequencing

An RNA sequencing library was prepared using a NEBNext Ultra™ RNA Library Prep Kit for Illumina and was sequenced on an Illumina novaseq6000. Differentially-expressed genes (DEGs) were determined with log2 expression fold change(log2FC) > 1 and a *p*-value (padj) < 0.05. Gene Ontology (GO) enrichment analysis of DEGs was performed using the clusterProfiler package in R.

Cleavage under targets and tagmentation (CUT&Tag) library preparation

Cleavage under targets and tagmentation (CUT&Tag) libraries were prepared using an *In-Situ* ChIP Library Prep Kit (TD901, Vazyme Biotech, Nanjing, China). Adherent cultured cells were digested with 0.25% trypsin, and 50,000 C3H10 T1/2 cells per sample were used in two biological replicates. After centrifugation at 600 *g* for 5 min at room temperature, the cells were washed twice with Wash Buffer. Cells were bound to conA beads and incubated with anti-Six1 antibody (#12891, CST, Danvers, MA, United States; 1:50) overnight at 4°C. The primary antibody was removed, and then a secondary antibody (Goat Anti-Rabbit IgG, Vazyme) was diluted (1: 100) in DIG Wash buffer and incubated with cells at room temperature in a shaker for 1 h. Next, cells were incubated with pA-Tn5 transposon complex (0.04 μM) at room temperature for 1 h. DNA was extracted and then purified using Hieff NGS® DNA Selection Beads (12601ES03, Yeasen Biotech). The libraries were sequenced on the Novaseq-150PE platform and 150-bp pair-end were generated. The sequencing depth was 10G base pair raw data.

Statistical analysis

GraphPad Prism v.9.0 for Windows (GraphPad Software, LaJolla, CA, United States) was used for statistical analysis. All numerical data are presented as means ± SD. Independent two-tailed Student's *t*-tests were used for comparisons between two groups, and differences were considered statistically significant at a *p*-value < 0.05.

Results

The *Six1* knockout mice exhibited craniofacial deformity

To explore the role of Six1 in craniofacial development, we generated *Six1* knockout mice using the CRISPR/Cas9-based approach. To ensure the efficiency of Six1 knockout in $Six1^{-/-}$ mice, we examined the RNA-seq data at E18.5 and verified the *Six1* expression level by RT-qPCR (Supplementary Figure S5). By comparing gross images and skeletal staining of $Six1^{+/+}$ (n = 4) and $Six1^{+/-}$ (n = 4) embryos at E18.5, we found that the heterozygous embryos had no craniofacial deformities and no differences in mandibular length, and that heterozygous mice survived and reproduced normally (Figures 1A–D). Hence, we used $Six1^{+/-}$ to mate with each other to obtain $Six1^{-/-}$ pups, and the $Six1^{-/-}$ birth probability conformed to the Mendelian ratio (14/55). All the $Six1^{-/-}$ mice that died at birth exhibited a wide range of craniofacial deformities, including microsomia, high arched palate, and a small tongue. Morphologic observation and examination of skeletal preparations at E18.5 revealed that the mandible length of $Six1^{-/-}$ mice (n = 3) was significantly shorter than wild-type or heterozygous littermates. Analyses of HE staining of E16.5 embryos revealed that $Six1^{-/-}$ (n = 3) mice exhibited a high palate and small tongue with

10.3389/fgene.2023.1082911

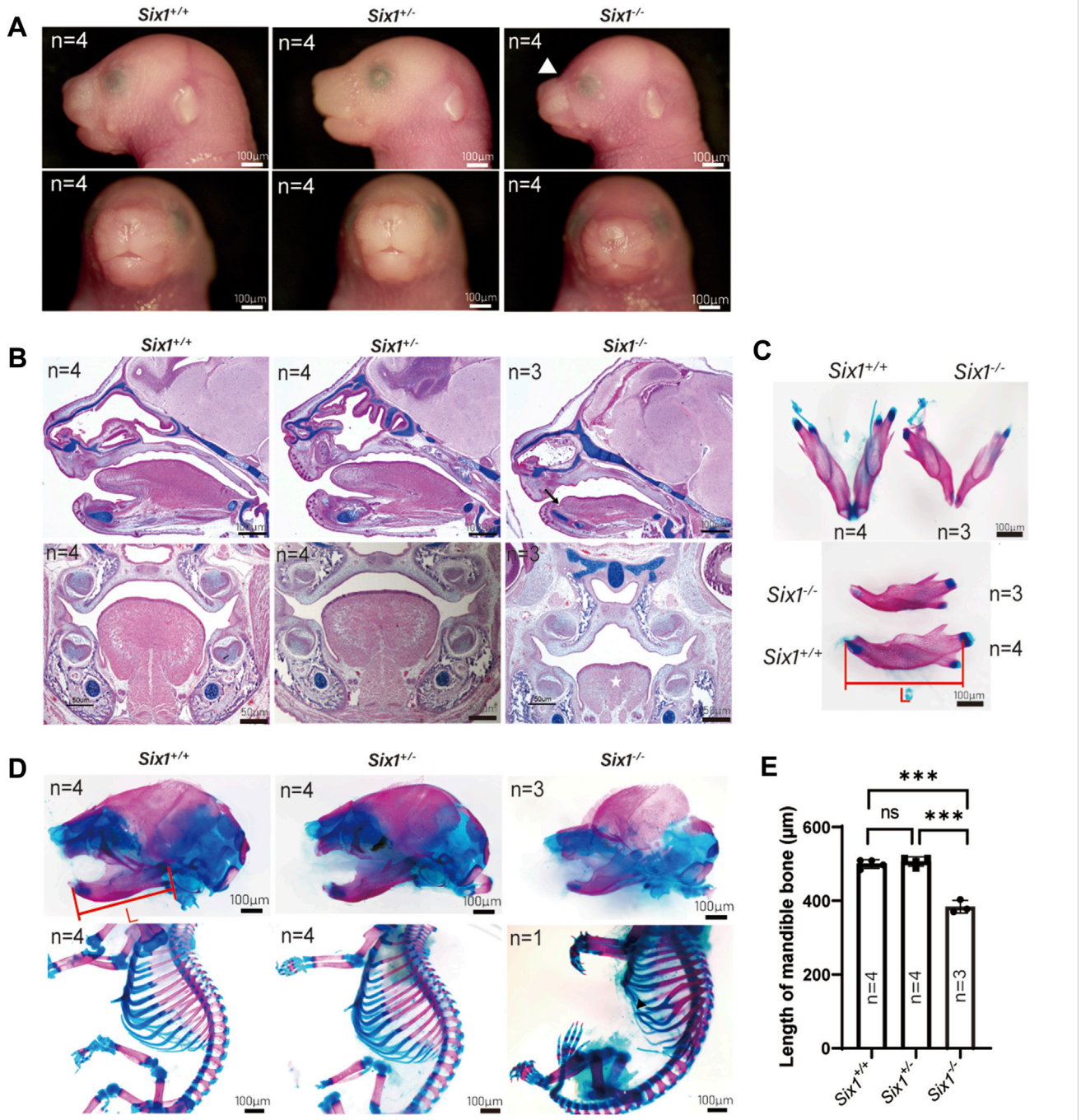

FIGURE 1
The *Six1* deletion mice resulted in craniofacial deformity. **(A)** Lateral view (top) and frontal (bottom) gross morphology of E18.5 heads of the *Six1*$^{-/-}$, *Six1* ± and *Six1*$^{+/+}$ embryos. *Six1*$^{-/-}$ embryos exhibit short mandible and classical abnormal curve between nose and forehead (white arrowhead). **(B)** Hematoxylin and eosin (HE) and Alcian blue staining of sagittal sections (top) and frontal (bottom) sections of *Six1*$^{-/-}$, *Six1*$^{+/-}$ and *Six1*$^{+/+}$ embryo at E16.5. *Six1*$^{-/-}$ embryos display a short mandible, ankyloglossia (black arrow), and uvula deformity (white star). **(C)** Skeletal staining of E18.5 mandible of the *Six1*$^{-/-}$ and *Six1*$^{+/+}$ embryo. *Six1*$^{-/-}$ mice exhibit a shortened mandible. L: length of mandible. **(D)** Skeletal alizarin red and Alcian blue staining of E18.5 heads (top) and body (bottom) of the *Six1*$^{-/-}$, *Six1*$^{+/-}$ and *Six1*$^{+/+}$ embryo. The black arrowhead points to bifurcated ribs. **(E)** Quantification of the mandibular length from *Six1*$^{-/-}$, *Six1*$^{+/-}$ and *Six1*$^{+/+}$ embryos at E18.5.

ankyloglossia (Figure 1B). The volume of tongue muscle of *Six1*$^{-/-}$ mice was significantly reduced. We also found that mice (1/3) exhibited bifurcated ribs, characterized by abnormal fusion between the upper and lower rib cartilage (Figure 1D). The mandibular length of *Six1*$^{-/-}$ (n = 3) embryos at E18.5 was significantly shorter than that of *Six1*$^{+/+}$(n = 4) ($p < 0.0001$) (Figures 1C, E). *Six1* knockout mice exhibited a stable phenotype of a short jaw with 100% penetrance (14/14). The craniofacial phenotype of Six1 knockout mice was similar to that reported in the literature (Liu et al., 2019), and the skeletal deformities were also as reported in the literature (Li et al., 2003).

10.3389/fgene.2023.1082911

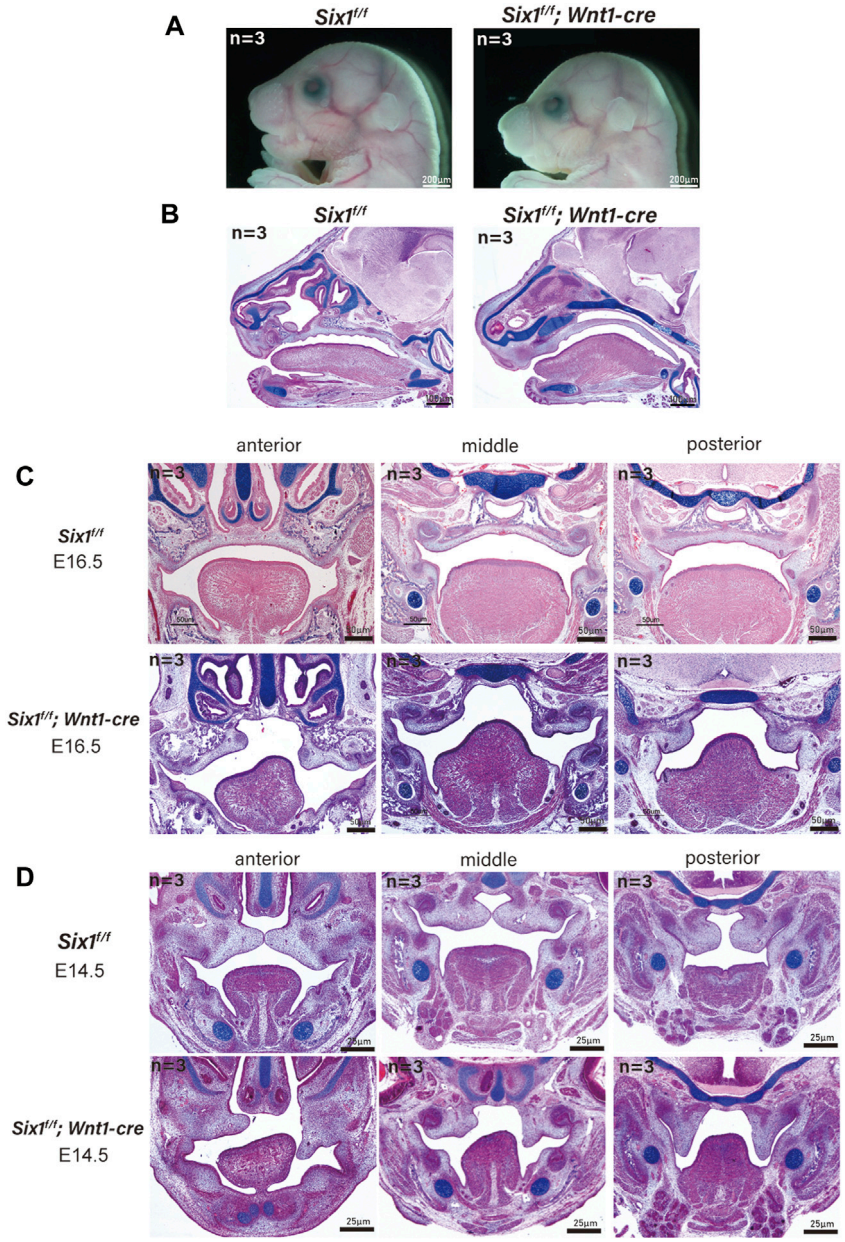

FIGURE 2
The conditional knockout of *Six1* in cranial neural crest cells (CNCCs) results in microsomia. **(A)** Gross morphology of E18.5 heads of the *Six1*$^{f/f}$*; Wnt1-Cre* and *Six1*$^{f/f}$ embryos. **(B)** HE and Alcian blue staining of sagittal sections showing the morphology of mandible of the *Six1*$^{f/f}$*; Wnt1-Cre* and *Six1*$^{f/f}$ embryos at E18.5. *Six1*$^{f/f}$*; Wnt1-Cre* embryo shows a short mandible. **(C, D)** HE and Alcian blue staining of frontal sections of the *Six1*$^{f/f}$*; Wnt1-Cre* and *Six1*$^{f/f}$ embryos at E16.5 **(C)** and E14.5 **(D)**. *Six1*$^{f/f}$*; Wnt1-Cre* embryo shows cleft palate at E16.5 and E14.5.

These results demonstrate that *Six1* knockout mice were successfully constructed, and this model is suitable for studying the causes of the short mandible.

Conditional knockout of *Six1* in cranial neural crest cells caused microsomia and cleft palate

The mandible is derived from neural crest cell-derived tissues (Parada and Chai, 2015). To explicitly assess whether the craniofacial defects were caused by the loss of *Six1* function in CNCC-derived ectomesenchyme, we generated *Six1*$^{f/f}$ mice and crossed them with *Wnt1-Cre* mice to conditionally knockout *Six1* in CNCCs (*Six1*$^{f/f}$*; Wnt1-Cre*). *Wnt1-Cre* pups were born in accordance with the Mendelian ratio. However, the majority of *Six1*$^{f/f}$*; Wnt1-Cre* pups died at birth. By morphological analysis and examination of skeletal preparations at E18.5, we found that all *Six1*$^{f/f}$*; Wnt1-Cre* (n = 3) pups exhibited microsomia compared with control littermates, and the phenotype was similar to that of *Six1* knockout mice (Figure 2A).

Interestingly, a new phenotype, cleft palate (70%, 7/10) with ankyloglossia, was found in *Six1*$^{f/f}$*; Wnt1-Cre* mice without atrophy

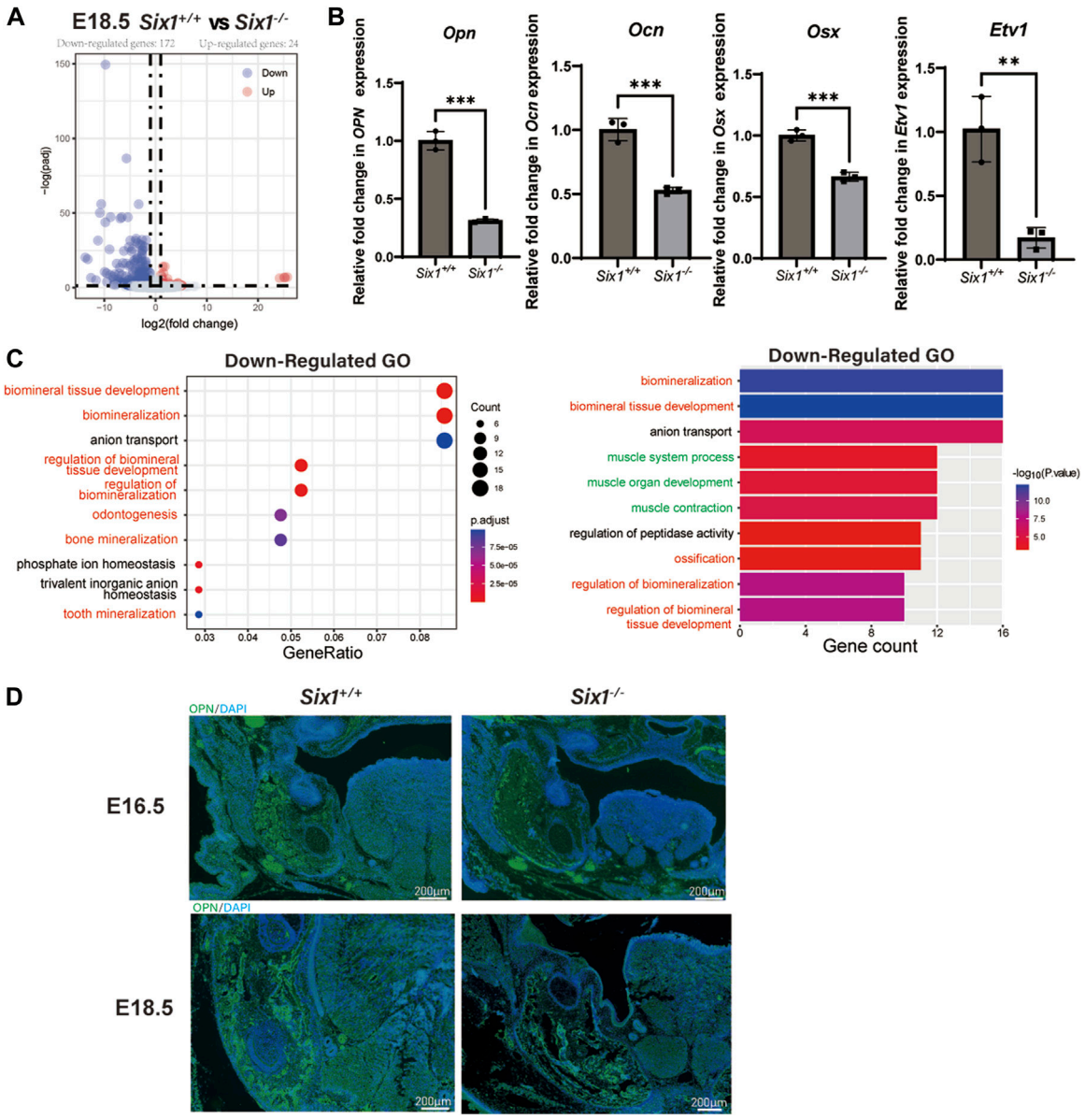

FIGURE 3
RNA-seq of the mandibular tissue from E18.5 *Six1*$^{-/-}$ and *Six1*$^{+/+}$ embryos. **(A)** Volcano plots show differentially expressed genes between *Six1*$^{-/-}$ and *Six1*$^{+/+}$ mandibular samples. **(B)** RT-qPCR analysis of *Opn*, *Ocn*, *Osx* and *Etv1* in *Six1*$^{-/-}$ and *Six1*$^{+/+}$ mandibular tissues at E18.5. **(C)** GO enrichment analysis of genes significantly downregulated in *Six1*$^{-/-}$ mandible. **(D)** Immunofluorescence staining of OPN in mandible of *Six1*$^{-/-}$ and *Six1*$^{+/+}$ embryos at E16.5 and E18.5.

of tongue muscle. We further studied the *Six1*$^{f/f}$; *Wnt1-Cre* mice at E16.5 (n = 3) and E14.5 (n = 3), and found that the tongue muscle occupied the development space of the palate at E14.5, which prevented palatal lifting and led to the development of cleft palate (Figures 2C, D). Tongue connective tissue is derived from CNCCs, whereas the skeletal muscles originate from the myoblasts (Noden and Francis-West, 2006). The reduction in oral volume was due to the lack of mandibular development, while the unaffected tongue muscle volume resulted in an increased tongue muscle height. Therefore, the cleft palate phenotype of conditional knockout *Six1* mice might be a secondary cleft palate. These data indicate that Six1 plays a crucial role in the growth and differentiation of CNCC-derived mesenchyme during craniofacial development.

Six1 knockout resulted in decreased mandibular bone formation and altered gene expression in mice

We reasoned that *Six1* deletion might disrupt the complex gene expression pattern during craniofacial development. To reveal the key genes regulated by the transcription factor Six1 during mandibular development, we surgically isolated mandibular skeletal tissues and surrounding soft tissues from E18.5 *Six1*$^{-/-}$ or littermate control wild-type *Six1*$^{+/+}$ mice and performed bulk RNA-seq on two independent biological replicates for each genotype. Analysis of the RNA-seq data revealed that the *Six1* transcripts were completely absent in *Six1*$^{-/-}$. Comparing the results of *Six1*$^{-/-}$ and *Six1*$^{+/+}$ mice revealed that

196 genes exhibited significant expression changes (log2FC > 1, padj < 0.05). Among these, 172 genes were downregulated, and 24 genes were upregulated (Figure 3A; Supplementary Table S1). Correlation analysis of RNA-seq showed that *Six1*$^{-/-}$ and *Six1*$^{+/+}$ were significantly different (Supplementary Figure S2). The uniquely mapped reads were all greater than 85%, indicating high-quality sequencing data (Supplementary Table S3). Notably, *Six1*$^{-/-}$ showed significantly downregulated expression of osteogenic and mineralization genes at E18.5, including *Opn*, *Ocn,* and *Osx* (Figure 3B). GO enrichment analysis of downregulated DEGs showed that multiple development-related biological processes were impacted, and the DEGs were significantly enriched in "ossification", "biomineralization", and "biomineral tissue development" (Figure 3C; Supplementary Table S2). Using immunofluorescence staining, we further verified that the level of Opn in the *Six1*$^{-/-}$ mandible was significantly lower than that in heterozygous littermates at E16.5 and E18.5 (Figure 3D). We also found a moderate downregulation in the mandibular region of *Six1*$^{-/-}$ mice by Osx immunofluorescence staining, which was consistent with the RT-qPCR results (Supplementary Figure S3). *Six1*$^{-/-}$ knockout mice had no significant effect on the proliferation and apoptosis of the mandible at E16.5 (Supplementary Figure S4). Collectively, these data suggest that the knockout of Six1 impaired mandibular bone formation by regulating the expression of critical genes involved in osteogenesis.

Interestingly, we also found that genes related to muscle development were significantly downregulated (Figure 3C). Observing the downregulated GO term "muscle organ development" revealed that their enriched genes include *Etv1*(Tenney et al., 2019), *Tcap* (Markert et al., 2010), *Lbx1*(Wang et al., 2022), *Actn3* (Nicot et al., 2021), and *Fos* (Almada et al., 2021), which could explain the uvula deformity observed in *Six1*$^{-/-}$ mice. RT-qPCR showed that *Etv1* expression was significantly reduced in the mandibular tissues of *Six1*$^{-/-}$ mice (Figure 3B). These results suggest that the craniofacial defects observed in *Six1*$^{-/-}$ mice result from profound dysregulation of genes related to skeletal and muscle development.

Six1 knockdown decreased the osteogenic differentiation capacity of C3H10 T1/2 cells

To further explore the role of *Six1* during mandibular osteogenesis, we performed osteogenic induction assay on the mouse embryonic mesenchymal stem cell line (C3H10 T1/2) to investigate the potential mechanisms *in vitro*. By performing RT-qPCR, we showed that the expression of *Six1* could be readily detected in C3H10 T1/2 cells (Figure 4A). We then performed *Six1* knockdown by infecting C3H10 T1/2 cells with lentivirus expressing an shRNA specifically targeting *Six1*, and verified that the *Six1* mRNA was markedly depleted in *Six1* knockdown cells ($p < 0.0001$). RT-qPCR analysis showed that several critical osteogenic genes, including *Osx*, *Runx2*, *Alp*, and *Dlk1,* were downregulated in *Six1* knockdown cells (Figure 4B). We further compared the osteogenic differentiation capacity of control and *Six1* knockdown C3H10 T1/2 cells after osteogenic induction for 7 days by quantifying alkaline phosphatase (ALP) staining as well as measuring the mRNA levels of *Alp*, *Osx*, *Opn*, and *Ocn* by RT-qPCR (Figure 4C). *Six1* knockdown C3H10 T1/2 cells exhibited lower ALP activity and downregulation of *Osx*, *Opn*, and *Ocn* expression. The proliferation activity of *Six1* knockdown C3H10 T1/2 cells was inhibited (Supplementary Figure S4). These results indicate that *Six1* knockdown leads to the decline of osteogenic marker genes expression and reduced osteogenic differentiation in osteogenesis.

Six1 promotes osteogenic function by regulating multiple osteogenesis-related genes

To investigate the underlying mechanism by which Six1 regulates osteogenic differentiation of C3H10 T1/2 cells, we analyzed the transcriptional effect of *Six1* knockdown on C3H10 T1/2 cells by performing RNA sequencing on three biological replicates of control and *Six1* knockdown cells. The knockdown and control groups showed a more significant correlation with each other, indicating good quality and repeatability of the RNA sequencing dataset (Figure 5B, Supplementary Figure S2). Analysis of the DEGs (log2FC > 1, padj<0.05) revealed that 662 genes were downregulated and 660 genes were upregulated in *Six1* knockdown cells compared with that in control cells (Figure 5A; Supplementary Table S3). GO analysis of the downregulated DEGs showed that the knockdown of *Six1* suppressed osteogenic differentiation through the regulation of biological processes associated with "ossification" and "muscle tissue development" (Figure 5C; Supplementary Table S4). We further validated the mRNA expression of several osteogenic differentiation related genes in *Six1* knockdown C3H10 T1/2 cells. Consistent with the RNA-Seq results, the mRNA expression of *Bmp4*, *Fat4*, *Fgf18*, *Fgfr2*, and *Runx1* significantly decreased (Figure 5D).

SIX1 directly binds to the promoters of *Bmp4, Fgfr2, Fgf18*, and *Fat4* and regulates their expression

To further explore the mechanism by which Six1 regulates osteogenesis, we examined the genome-wide occupancy of Six1 in C3H10 T1/2 cells by performing CUT&Tag. The IDR consistency test was performed on the two sets of CUT&Tag data, and a total of 19,728 peaks were obtained (Figure 6A; Supplementary Table S5). Among the Six1 peaks, 40.26% were located in the promoter region (≤ 1 kb from the TSS), while 24.87% were located in the distal intergenic region (Figure 6B). These CUT&Tag peaks were annotated to the 10,788 closest genes. In addition, CUT&Tag assay showed that Six1 directly regulated the promoters of *Bmp4*, *Fgfr2*, *Fgf18*, and *Fat4*, all of which have been reported to play important roles in osteogenesis and were downregulated in *Six1* knockdown C3H10 T1/2 cells (Figure 6C). Importantly, nearly 3/4 (2,157/3,027) of the DEGs from RNA-seq were associated with the Six1 peaks (Figure 6D). GO enrichment analysis of these 2,157 Six1-bound DEGs again showed that the ossification function was significantly enriched (Figure 6E). Six1 was also showed to bind to the promoter of *Etv1*, a gene involved in muscle development (Tenney et al., 2019). Taken together, our data strongly suggest that Six1 regulates the expression of a group of genes involved in bone and muscle development by binding to their promoters or cis-regulatory regions, thereby influencing craniofacial development and morphogenesis.

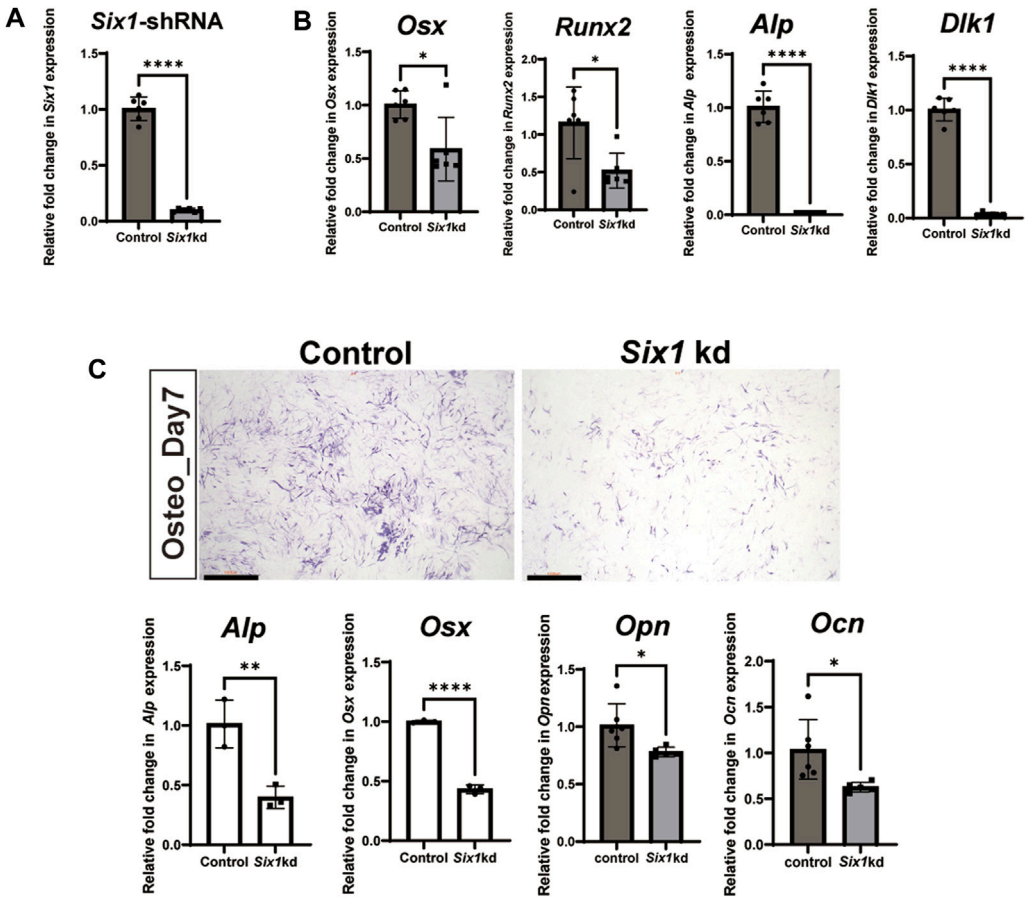

FIGURE 4
The effect of *Six1* on the osteogenic differentiation of C3H10 T1/2 cells. **(A)** RT-qPCR analysis of C3H10 T1/2 cells transfected with negative control (Control) or *Six1* knockdown cells (*Six1*kd) (n = 6). **(B)** RT-qPCR analysis of *Osx*, *Runx2*, *Alp*, and *Dlk1* in control and *Six1* knockdown cells (*Six1*kd). **(C)** Alkaline phosphatase (ALP) staining of negative control C3H10 T1/2 cells (control) and *Six1*kd cells after osteogenic induction for 7 days. RT-qPCR analysis of *Alp*, *Osx*, *Opn*, and *Ocn* after osteogenic induction for 7 days of control and *Six1*kd cells. Scale bar in C, 1000 μm.

Discussion

Six1 plays an important role in embryonic development and is one of the pathogenic genes of human Branchio-oto-renal syndrome (BOR) (Shah et al., 2020). Children with BOR show hearing loss, renal abnormalities, and microsomia(Kochhar et al., 2007). Six1 is widely expressed in the mesenchymal and sensory epithelium of the craniofacial region (Liu et al., 2019; Li et al., 2020). Studies have revealed that Six1 regulates auditory sensory epithelial differentiation, and participates in ear development (Li et al., 2020). For craniofacial development, *Six1*-null mice exhibit abnormal craniofacial skeletal development, including microsomia and the formation of a novel bone in the zygomatic arch (Tavares et al., 2017; Liu et al., 2019). However, the mechanisms of *Six1* during mandibular development remain unclear.

Tavares et al. found that $Six1^{-/-}$ mice upregulated *Edn1* signaling in the first and second branchial epithelium, while Six1 was expressed in the adjacent mesenchymal region, suggesting that Six1 may participate in craniofacial development through epithelial-mesenchymal interaction (Tavares et al., 2017). We demonstrated that the conditional knockout of *Six1* in mesenchyme largely phenocopied the underdevelopment of the mandible observed in $Six1^{-/-}$ mice, thus demonstrating that Six1 regulates development of the mandible in the ectodermal mesenchyme. Interestingly, $Six1^{f/f}$; *Wnt1-Cre* mice showed normal tongue muscle but the cleft palate, a more severe craniofacial deformity. Tongue muscle originates from mesodermal myoblasts, and CNCC-derived mesenchyme in tongue development acts as a scaffold for the organization of migrating myoblasts into the myogenic core (Parada and Chai, 2015). Hence, *Wnt1-cre* does not knockout *Six1* in the tongue muscle, but specifically knockout *Six1* in the mandible. $Six1^{f/f}$; *Wnt1-Cre* mice exhibited no tongue abnormalities, but showed a lack of Six1 expression in the mandible, resulting in reduced oral volume. We surmise that when the palate begins to fuse at E14.5, the insufficient oral volume in $Six1^{f/f}$; *Wnt1-Cre* mice may cause the tongue to occupy the palatal space, thereby affecting the palatal lift and eventually leading to secondary cleft palate.

We found that the expression of osteogenesis-related genes, such as *Opn*, *Ocn* and *Osx*, was significantly downregulated in the mandible of $Six1^{-/-}$ mice at E18.5, suggesting that Six1 may regulate multiple osteogenesis-related genes. It was previously reported that $Six1^{-/-}$ mice showed increased *Osx* expression in the maxillary and hinge region, and zygomatic process hyperplasia which developed into a thicker rod-shaped bone (Tavares et al., 2017). However, in our study, $Six1^{-/-}$

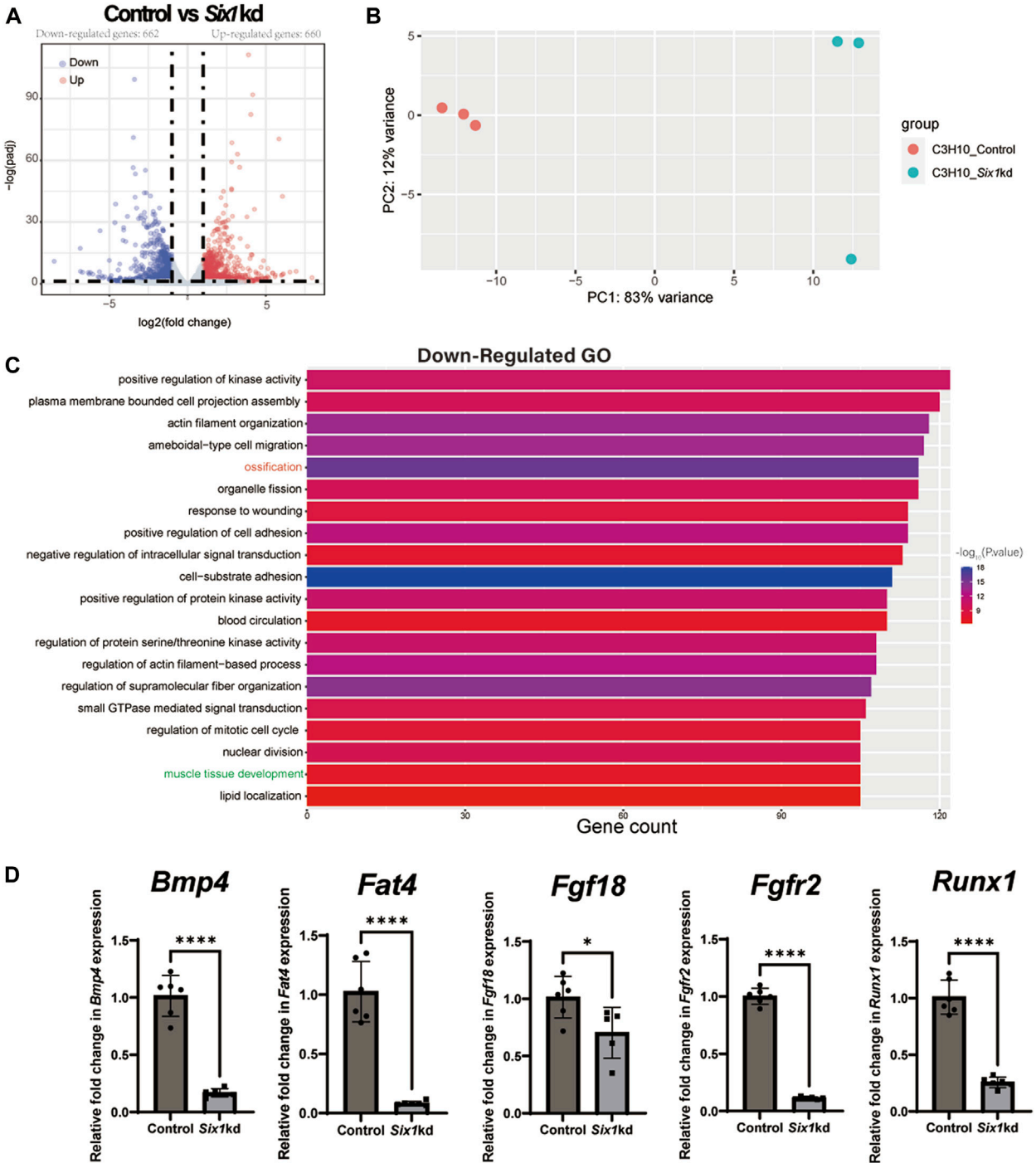

FIGURE 5
RNA-seq of C3H10 T1/2 cells transfected with negative control (Control) or *Six1*-shRNAs (*Six1*kd) lentivirus (n = 3). **(A)** Volcano plots for all the genes of the control and *Six1*kd groups. Dots on both sides indicate up and downregulated differentially expressed genes (DEGs; p-adj < 0.05). **(B)** PCA plot showing the correlation between RNA-seq replicates. **(C)** The terms associated with biological processes (p-adj < 0.05) involving the downregulated genes in the *Six1*kd group. **(D)** RT-qPCR analysis of *Bmp4*, *Fat4*, *Fgf18*, *Fgfr2*, and *Runx1* in control and *Six1*kd cells.

mice showed reduced *Osx* expression in the mandible and defects in mandibular osteogenesis. Six1 does not affect the proliferation and apoptosis of mandibular development at the late stages of embryonic development. We propose that Six1 regulates different signaling pathways in the maxilla and mandible, thus producing different biological effects. More studies are needed further to explore the mechanism of Six1 during craniofacial skeletal development.

Our analyses of C3H10 T1/2 cells and mandibular tissue RNA-seq indicate that Six1 regulates the expression of multiple osteogenesis-related genes. The spatiotemporal expression of Bmp4 highly

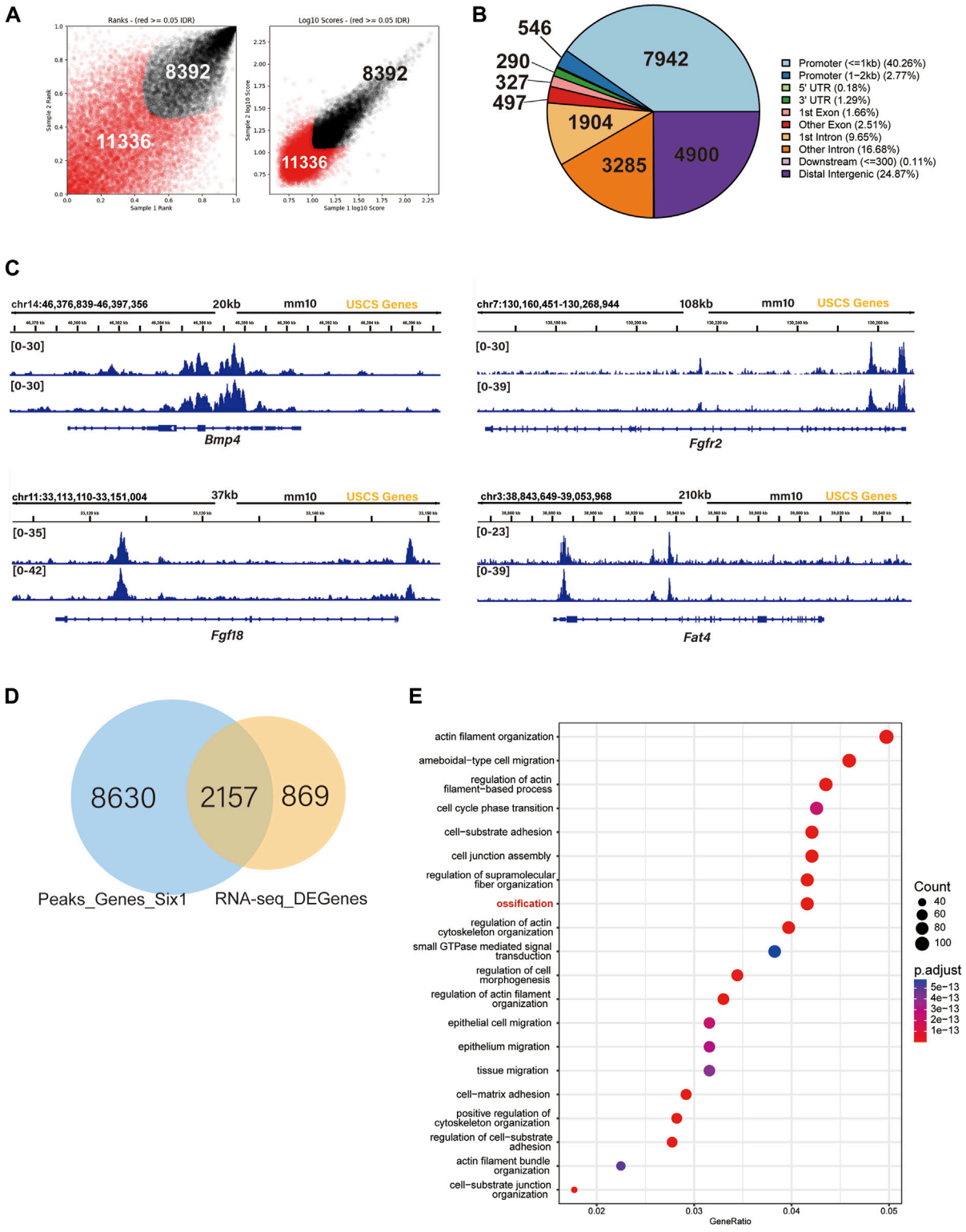

FIGURE 6
SIX1 directly regulates the promoter of osteogenic differentiation-related genes. **(A)** IDR tests the peaks of two biological replication. **(B)** Genomic distribution of *Six1*-enriched regions. **(C)** Six1 directly binds the promoter of *Bmp4*, *Fgfr2*, *Fgf18*, and *Fat4*. **(D)** A Venn diagram indicating overlap of Six1-binding genes and RNA-seq DEGs. **(E)** GO enrichment analysis of shared genes between Six1-binding genes and RNA-seq DEGs.

coincides with that of Six1, and it directly regulates the expression of *Msx1* and other genes in the BMP family, and plays an important role in the process of mandibular osteogenesis(Xu et al., 2021). *Bmp4*$^{f/f}$; *Wnt1-Cre* mutant pups exhibited short mandible (Xu et al., 2021). Similar phenotypes were observed in *Fgf18*$^{-/-}$ embryos (Hung et al., 2016). In addition, mice with deletion of *Fgf18* in neural crest cells also

exhibited a shortened mandible, suggesting that *Six1* and *Fgf18* in neural crest mesenchymal cells may be jointly involved in mandibular osteogenesis (Yue et al., 2021). Low expression of *Fgfr2* is also closely related to cells' decreased osteogenic ability (Jiang et al., 2019). The *Dchs1-Fat4* signaling pathway is involved in the process of osteoblast differentiation in the mouse mandible and skull and plays a positive role in early *Runx2* progenitors (Mao et al., 2016; Crespo-Enriquez et al., 2019). Our data suggest that Six1 regulating mandible development at least in part through regulating downstream genes *Fgfr2*, *Fgf18*, *Bmp4*, and *Fat4*. Future *in vivo* studies will shed more light on how Six1 coordinates the spatiotemporal expression of these genes to achieve proper craniofacial skeletal formation.

CUT&Tag assay showed that nearly half of the Six1 binding sites were located near the promoter of the downstream gene. Our results demonstrated that the changes in gene expression induced by Six1 knockdown were largely due to the direct regulation of Six1 on its downstream genes. For example, Six1 directly binds to the promoters of *Fgfr2*, *Fgf18*, *Bmp4*, and *Fat4* and regulates their transcription. Interestingly, our results also showed that a significant fraction of Six1 peaks are located in the intergenic regions, which likely correspond to cis-regulatory elements such as enhancers. Increasing evidence suggests that the enhancers play critical roles in orchestrating the precise gene expression patterns during craniofacial development (Attanasio et al., 2013). Future investigation on these Six1-bound enhancers may open new avenues for studying the functions of Six1 in craniofacial development and abnormality.

Conclusion

In conclusion, our findings suggest that the transcription factor Six1 is critical for mandible development. Our *Six1* knockout and conditional knockout mouse models provide valuable animal models for future studies of skeletal development during craniofacial development. By integrating RNA-Seq and CUT&Tag, we identified potential target genes of Six1 that are involved in osteogenic differentiation. Future studies building on these findings will further elucidate the mechanisms by which Six1 regulates mandibular osteogenesis during embryonic development.

Data availability statement

The data presented in the study are deposited in the National Center for Biotechnology Information (NCBI) Gene Expression Omnibus (GEO), accession number GSE216761.

Ethics statement

The animal study was reviewed and approved by Institutional Animal Care and Use Committee approval (IACUC) of the Shanghai Ninth People's Hospital affiliated to Shanghai Jiao Tong University School of Medicine.

Author contributions

SL and ZL conceived, designed, and performed the experiments, QB and XW designed the experiment and edited the manuscript. All authors agreed to be accountable for the content of this work.

Funding

This work was supported by the National Natural Science Foundation of China (No. 82071096, No. 82001027, No. 31970585, and No. 32170544), the Rare Disease Registration Platform of Shanghai Ninth People's Hospital, Shanghai Jiao Tong University School of Medicine (JYHJB05), Innovative Research Team of High-Level Local Universities in Shanghai (SHSMU-ZLCX20211700); Opening Research fund from Shanghai Key Laboratory of Stomatology, Shanghai Ninth People's Hospital, College of Stomatology, Shanghai Jiao Tong University School of Medicine (No.2022SKLS-KFKT007), Shanghai Clinical Research Center for Oral Diseases (19MC1910600), Shanghai Municipal Key Clinical Specialty (shslczdzk01601), Shanghai's Top Priority Research Center (2022ZZ01017), and CAMS Innovation Fund for Medical Sciences (CIFMS) (2019-I2M-5-037).

Conflict of interest

The authors declare that the research was conducted in the absence of any commercial or financial relationships that could be construed as a potential conflict of interest.

Publisher's note

Supplementary material

The Supplementary Material for this article can be found online at: https://www.frontiersin.org/articles/10.3389/fgene.2023.1082911/full#supplementary-material

References

Alappat, S., Zhang, Z. Y., and Chen, Y. P. (2003). Msx homeobox gene family and craniofacial development. *Cell Res.* 13 (6), 429–442. doi:10.1038/sj.cr.7290185

Almada, A. E., Horwitz, N., Price, F. D., Gonzalez, A. E., Ko, M., Bolukbasi, O. V., et al. (2021). FOS licenses early events in stem cell activation driving skeletal muscle regeneration. *Cell Rep.* 34 (4), 108656. doi:10.1016/j.celrep.2020.108656

Attanasio, C., Nord, A. S., Zhu, Y., Blow, M. J., Li, Z., Liberton, D. K., et al. (2013). Fine tuning of craniofacial morphology by distant-acting enhancers. *Science* 342 (6157), 1241006. doi:10.1126/science.1241006

Crespo-Enriquez, I., Hodgson, T., Zakaria, S., Cadoni, E., Shah, M., Allen, S., et al. (2019). Dchs1-Fat4 regulation of osteogenic differentiation in mouse. *Development* 146 (14), dev176776. doi:10.1242/dev.176776

El-Hashash, A. H., Al Alam, D., Turcatel, G., Rogers, O., Li, X., Bellusci, S., et al. (2011). Six1 transcription factor is critical for coordination of epithelial, mesenchymal and vascular morphogenesis in the mammalian lung. *Dev. Biol.* 353 (2), 242–258. doi:10.1016/j.ydbio.2011.02.031

Feng, H., Xu, H., Chen, B., Sun, S., Zhai, R., Zeng, B., et al. (2021). Genetic and phenotypic variability in Chinese patients with branchio-oto-renal or branchio-oto syndrome. *Front. Genet.* 12, 765433. doi:10.3389/fgene.2021.765433

Graf, D., Malik, Z., Hayano, S., and Mishina, Y. (2016). Common mechanisms in development and disease: BMP signaling in craniofacial development. *Cytokine Growth Factor Rev.* 27, 129–139. doi:10.1016/j.cytogfr.2015.11.004

Ha, N., Sun, J., Bian, Q., Wu, D., and Wang, X. (2022). Hdac4 regulates the proliferation of neural crest-derived osteoblasts during murine craniofacial development. *Front. Physiol.* 13, 819619. doi:10.3389/fphys.2022.819619

Hung, I. H., Schoenwolf, G. C., Lewandoski, M., and Ornitz, D. M. (2016). A combined series of Fgf9 and Fgf18 mutant alleles identifies unique and redundant roles in skeletal development. *Dev. Biol.* 411 (1), 72–84. doi:10.1016/j.ydbio.2016.01.008

Jiang, Q., Mei, L., Zou, Y., Ding, Q., Cannon, R. D., Chen, H., et al. (2019). Genetic polymorphisms in FGFR2 underlie skeletal malocclusion. *J. Dent. Res.* 98 (12), 1340–1347. doi:10.1177/0022034519872951

Kochhar, A., Fischer, S. M., Kimberling, W. J., and Smith, R. J. (2007). Branchio-oto-renal syndrome. *Am. J. Med. Genet. A* 143a (14), 1671–1678. doi:10.1002/ajmg.a.31561

Kumar, S., Deffenbacher, K., Marres, H. A., Cremers, C. W., and Kimberling, W. J. (2000). Genomewide search and genetic localization of a second gene associated with autosomal dominant branchio-oto-renal syndrome: clinical and genetic implications. *Am. J. Hum. Genet.* 66 (5), 1715–1720. doi:10.1086/302890

Kumar, J. P. (2009). The sine oculis homeobox (SIX) family of transcription factors as regulators of development and disease. *Cell Mol. Life Sci.* 66 (4), 565–583. doi:10.1007/s00018-008-8335-4

Li, X., Oghi, K. A., Zhang, J., Krones, A., Bush, K. T., Glass, C. K., et al. (2003). Eya protein phosphatase activity regulates Six1-Dach-Eya transcriptional effects in mammalian organogenesis. *Nature* 426 (6964), 247–254. doi:10.1038/nature02083

Li, J., Zhang, T., Ramakrishnan, A., Fritzsch, B., Xu, J., Wong, E. Y. M., et al. (2020). Dynamic changes in cis-regulatory occupancy by Six1 and its cooperative interactions with distinct cofactors drive lineage-specific gene expression programs during progressive differentiation of the auditory sensory epithelium. *Nucleic Acids Res.* 48 (6), 2880–2896. doi:10.1093/nar/gkaa012

Liao, J., Huang, Y., Wang, Q., Chen, S., Zhang, C., Wang, D., et al. (2022). Gene regulatory network from cranial neural crest cells to osteoblast differentiation and calvarial bone development. *Cell Mol. Life Sci.* 79 (3), 158. doi:10.1007/s00018-022-04208-2

Liu, Z., Li, C., Xu, J., Lan, Y., Liu, H., Li, X., et al. (2019). Crucial and overlapping roles of Six1 and Six2 in craniofacial development. *J. Dent. Res.* 98 (5), 572–579. doi:10.1177/0022034519835204

Ma, L., Wang, X., Zhou, Y., Ji, X., Cheng, S., Bian, D., et al. (2021). Biomimetic Ti-6Al-4V alloy/gelatin methacrylate hybrid scaffold with enhanced osteogenic and angiogenic capabilities for large bone defect restoration. *Bioact. Mater* 6 (10), 3437–3448. doi:10.1016/j.bioactmat.2021.03.010

Mao, Y., Kuta, A., Crespo-Enriquez, I., Whiting, D., Martin, T., Mulvaney, J., et al. (2016). Dchs1-Fat4 regulation of polarized cell behaviours during skeletal morphogenesis. *Nat. Commun.* 7, 11469. doi:10.1038/ncomms11469

Markert, C. D., Meaney, M. P., Voelker, K. A., Grange, R. W., Dalley, H. W., Cann, J. K., et al. (2010). Functional muscle analysis of the Tcap knockout mouse. *Hum. Mol. Genet.* 19 (11), 2268–2283. doi:10.1093/hmg/ddq105

Motch Perrine, S. M., Wu, M., Stephens, N. B., Kriti, D., van Bakel, H., Jabs, E. W., et al. (2019). Mandibular dysmorphology due to abnormal embryonic osteogenesis in FGFR2-related craniosynostosis mice. *Dis. Model Mech.* 12 (5), dmm038513. doi:10.1242/dmm.038513

Nicot, R., Raoul, G., Vieira, A. R., Ferri, J., and Sciote, J. J. (2021). ACTN3 genotype influences masseter muscle characteristics and self-reported bruxism. *Oral Dis.* 29, 232–244. doi:10.1111/odi.14075

Noden, D. M., and Francis-West, P. (2006). The differentiation and morphogenesis of craniofacial muscles. *Dev. Dyn.* 235 (5), 1194–1218. doi:10.1002/dvdy.20697

Parada, C., and Chai, Y. (2015). Mandible and tongue development. *Curr. Top. Dev. Biol.* 115, 31–58. doi:10.1016/bs.ctdb.2015.07.023

Ruf, R. G., Xu, P. X., Silvius, D., Otto, E. A., Beekmann, F., Muerb, U. T., et al. (2004). SIX1 mutations cause branchio-oto-renal syndrome by disruption of EYA1-SIX1-DNA complexes. *Proc. Natl. Acad. Sci. U. S. A.* 101 (21), 8090–8095. doi:10.1073/pnas.0308475101

Serikaku, M. A., and O'Tousa, J. E. (1994). Sine oculis is a homeobox gene required for Drosophila visual system development. *Genetics* 138 (4), 1137–1150. doi:10.1093/genetics/138.4.1137

Shah, A. M., Krohn, P., Baxi, A. B., Tavares, A. L. P., Sullivan, C. H., Chillakuru, Y. R., et al. (2020). Six1 proteins with human branchio-oto-renal mutations differentially affect cranial gene expression and otic development. *Dis. Model Mech.* 13 (3), dmm043489. doi:10.1242/dmm.043489

Takechi, M., Adachi, N., Hirai, T., Kuratani, S., and Kuraku, S. (2013). The Dlx genes as clues to vertebrate genomics and craniofacial evolution. *Semin. Cell Dev. Biol.* 24 (2), 110–118. doi:10.1016/j.semcdb.2012.12.010

Tavares, A. L. P., Cox, T. C., Maxson, R. M., Ford, H. L., and Clouthier, D. E. (2017). Negative regulation of endothelin signaling by SIX1 is required for proper maxillary development. *Development* 144 (11), 2021–2031. doi:10.1242/dev.145144

Tenney, A. P., Livet, J., Belton, T., Prochazkova, M., Pearson, E. M., Whitman, M. C., et al. (2019). Etv1 controls the establishment of non-overlapping motor innervation of neighboring facial muscles during development. *Cell Rep.* 29 (2), 437–452. doi:10.1016/j.celrep.2019.08.078

Terakawa, J., Serna, V. A., Nair, D. M., Sato, S., Kawakami, K., Radovick, S., et al. (2020). SIX1 cooperates with RUNX1 and SMAD4 in cell fate commitment of Müllerian duct epithelium. *Cell Death Differ.* 27 (12), 3307–3320. doi:10.1038/s41418-020-0579-z

Wang, Y., Li, M., Chan, C. O., Yang, G., Lam, J. C., Law, B. C., et al. (2022). Biological effect of dysregulated LBX1 on adolescent idiopathic scoliosis through modulating muscle carbohydrate metabolism. *Spine J.* 22 (9), 1551–1565. doi:10.1016/j.spinee.2022.04.005

Wu, W., Huang, R., Wu, Q., Li, P., Chen, J., Li, B., et al. (2014). The role of Six1 in the Genesis of muscle cell and skeletal muscle development. *Int. J. Biol. Sci.* 10 (9), 983–989. doi:10.7150/ijbs.9442

Xu, P. X., Zheng, W., Huang, L., Maire, P., Laclef, C., and Silvius, D. (2003). Six1 is required for the early organogenesis of mammalian kidney. *Development* 130 (14), 3085–3094. doi:10.1242/dev.00536

Xu, J., Chen, M., Yan, Y., Zhao, Q., Shao, M., and Huang, Z. (2021). The effects of altered BMP4 signaling in first branchial-arch-derived murine embryonic orofacial tissues. *Int. J. Oral Sci.* 13 (1), 40. doi:10.1038/s41368-021-00142-4

Yin, X., Li, J., Salmon, B., Huang, L., Lim, W. H., Liu, B., et al. (2015). Wnt signaling and its contribution to craniofacial tissue homeostasis. *J. Dent. Res.* 94 (11), 1487–1494. doi:10.1177/0022034515599772

Yue, M., Lan, Y., Liu, H., Wu, Z., Imamura, T., and Jiang, R. (2021). Tissue-specific analysis of Fgf18 gene function in palate development. *Dev. Dyn.* 250 (4), 562–573. doi:10.1002/dvdy.259

Zheng, W., Huang, L., Wei, Z. B., Silvius, D., Tang, B., and Xu, P. X. (2003). The role of Six1 in mammalian auditory system development. *Development* 130 (17), 3989–4000. doi:10.1242/dev.00628

frontiers | Frontiers in Genetics

TYPE Original Research
PUBLISHED 20 February 2023
DOI 10.3389/fgene.2023.1085263

OPEN ACCESS

EDITED BY
Long Guo,
RIKEN Center for Integrative Medical Sciences, Japan

REVIEWED BY
Kai Chen,
University of Western Australia, Australia
Yong Liu,
Fuyang Normal University, China
David D. Eisenstat,
Royal Children's Hospital, Australia

*CORRESPONDENCE
Qian Bian,
qianbian@shsmu.edu.cn
Xudong Wang,
xudongwang70@hotmail.com

†These authors have contributed equally to this work and share first authorship

SPECIALTY SECTION
This article was submitted to Genetics of Common and Rare Diseases, a section of the journal Frontiers in Genetics

RECEIVED 31 October 2022
ACCEPTED 09 February 2023
PUBLISHED 20 February 2023

CITATION
Sun J, Zhang J, Bian Q and Wang X (2023), Effects of Dlx2 overexpression on the genes associated with the maxillary process in the early mouse embryo. *Front. Genet.* 14:1085263. doi: 10.3389/fgene.2023.1085263

Effects of Dlx2 overexpression on the genes associated with the maxillary process in the early mouse embryo

Jian Sun[1†], Jianfei Zhang[1†], Qian Bian[1,2*] and Xudong Wang[1*]

[1]Shanghai Key Laboratory of Stomatology, National Center for Stomatology, National Clinical Research Center for Oral Diseases, Department of Oral and Cranio-Maxillofacial Surgery, College of Stomatology, Shanghai Research Institute of Stomatology, Shanghai Ninth People's Hospital, Shanghai Jiao Tong University School of Medicine, Shanghai Jiao Tong University, Shanghai, China, [2]Shanghai Institute of Precision Medicine, Shanghai, China

The transcription factor Dlx2 plays an important role in craniomaxillofacial development. Overexpression or null mutations of Dlx2 can lead to craniomaxillofacial malformation in mice. However, the transcriptional regulatory effects of Dlx2 during craniomaxillofacial development remain to be elucidated. Using a mouse model that stably overexpresses Dlx2 in neural crest cells, we comprehensively characterized the effects of Dlx2 overexpression on the early development of maxillary processes in mice by conducting bulk RNA-Seq, scRNA-Seq and CUT&Tag analyses. Bulk RNA-Seq results showed that the overexpression of Dlx2 resulted in substantial transcriptome changes in E10.5 maxillary prominences, with genes involved in RNA metabolism and neuronal development most significantly affected. The scRNA-Seq analysis suggests that overexpression of Dlx2 did not change the differentiation trajectory of mesenchymal cells during this development process. Rather, it restricted cell proliferation and caused precocious differentiation, which may contribute to the defects in craniomaxillofacial development. Moreover, the CUT&Tag analysis using DLX2 antibody revealed enrichment of MNT and Runx2 motifs at the putative DLX2 binding sites, suggesting they may play critical roles in mediating the transcriptional regulatory effects of Dlx2. Together, these results provide important insights for understanding the transcriptional regulatory network of *Dlx2* during craniofacial development.

KEYWORDS

Dlx2, bulk RNA-seq, maxillary process, craniofacial development, scRNA-Seq

Introduction

Dlx2 (Distal-less homeobox 2) is a member of the Dlx family transcription factors that play critical roles in forebrain and craniofacial development. In mice, *Dlx2* is located on chromosome 2 at 42.65 cM (Tan and Testa, 2021). During embryonic development, *Dlx2* is expressed in the epithelial cells of the maxillary and mandibular processes, as well as the cranial neural crest cells (CNCC)-derived mesenchyme, indicative of its significant regulatory functions during the development of craniomaxillofacial tissues.

Dlx2 has been shown to regulate several critical signaling pathways involved in development and differentiation. *Dlx2* is a transcription activator for Wnt1 and can activate the Wnt/β-Catenin signaling pathway (Zeng et al., 2020). It can also promote

the expression of TARBP2 and thus further activates the JNK/AKT signaling pathway (Fang et al., 2020). The Dlx2/GLS1/Gln metabolic axis is an important regulator of the TGF-β/Wnt-induced snail-dependent epithelial-mesenchymal transition (Lee et al., 2016).

The regulation of skeletogenesis by *Dlx2* has been extensively demonstrated *in vitro*. An experiment in human bone marrow mesenchymal stem cells confirmed that overexpression of *Dlx2* can upregulate the expression of osterix, BSP, and MSX2 and elevate cellular alkaline phosphatase activity in the early stage of osteogenesis induction. It can also upregulate OCN expression at a later stage, thereby accelerating the mineralization of BMSC (Qu et al., 2014; Zeng et al., 2020). Studies in MC3T3-E1 cells have also reached the same conclusion, that *Dlx2* overexpression can upregulate osteogenic related genes, such as *Alp* and *Msx2* (Sun et al., 2015). *Dlx2* overexpression can also stimulate both OCN and ALP promoter activity, thereby enhancing osteogenic differentiation (Zhang et al., 2019). MMP13 is a major collagenase that degrades aggrecan and type II collagen in the late stage of chondrogenesis. Its promoter contains two *Dlx2*-response elements. *Dlx2* can inhibit the expression of MMP13 and reduce cartilage degradation by directly combining with these two elements (Zhang et al., 2018).

In addition to regulating osteogenesis and chondrogenesis, *Dlx2* also plays a critical regulatory role in neural development. Mice lacking DLX1 and DLX2 have a time-dependent block in striatal differentiation (Anderson et al., 1997b), showed no detectable cell migration from the subcortical telencephalon to the neocortex and also had few GABA-expressing cells in the neocortex (Anderson et al., 1997a). The transient overexpression of the transcription factors *Ascl1* and *Dlx2* in neural progenitor cells is sufficient to induce neuronal morphology, GABAergic gene expression and synaptic electrophysiological maturity (Barretto et al., 2020).

Recent advances in the development of transgenic mouse models have provided critical insights for understanding craniofacial development and malformations (Chai and Maxson, 2006). Previous studies have shown that *Dlx2* deletion and overexpression mutants exhibit craniofacial malformations. It has also been revealed that a null mutation of *Dlx2* may cause odontogenic cells to reprogram into chondrocytes and express *Sox9* (Thomas et al., 1997). In E13.5 mouse dental germ, overexpression of *Dlx2* can also increase the expression of *Sox9* (Dai et al., 2017). Hence, it is speculated that *Sox9* may be a downstream effector of *Dlx2*. In addition, in mouse E13.5 dental germ that exhibits overexpression of *Dlx2*, the expression levels of TGFβR1, TGFβR2, Smad4, and *Msx2* are upregulated. In the epithelium, *Msx2* is also upregulated and the expression of *Runx2*, an osteogenic and odontogenic marker, is downregulated in dental germ and alveolar bone (Dai et al., 2017). This indicates that the overexpression of *Dlx2* may interfere with the development of tooth and bone through its interaction with these genes. However, the complex gene regulatory network, downstream of *Dlx2*, has not yet been fully described.

In our earlier work, we constructed a mouse model that can overexpress *Dlx2* in cells derived from neural crest cells (Sun et al., 2022). Such a mouse model enables us to determine the transcriptional effects of *Dlx2* overexpression on the mouse maxilla. In the present study, by comparing the transcriptomes of the maxillary process in E10.5 *Dlx2*-overexpressing mice and wild-type mice, we showed that the effect of *Dlx2* overexpression on the development of the maxillary process began at the earliest stage of maxillary process development and the transcriptional effect changed over time. Single-cell RNA sequencing (scRNA-Seq) of the early maxillary process showed that *Dlx2* inhibited cell proliferation and promoted cell differentiation without changing the trajectory of differentiation. Moreover, cleavage under targets and tagmentation (CUT&Tag) analysis revealed the putative target genes that *Dlx2* may interact with. These comprehensive analyses provide important insights for understanding the regulatory roles of *Dlx2* during craniofacial development and pave the road for further functional dissection of the downstream regulatory network of *Dlx2*.

Materials and methods

Animals

We obtained $wnt1^{cre}$ mice from the Jackson laboratory. The $Rosa26^{CAG\text{-}LSL\text{-}Dlx2\text{-}3xFlag}$ mouse was constructed by the Shanghai Model Organisms Center, Inc. (Shanghai, China). To generate $wnt1^{cre}$; $Rosa26^{Dlx2/-}$ mice, which could specifically overexpress *Dlx2* in neural crest cells, we mated $wnt1^{cre}$ mice with $Rosa26^{CAG\text{-}LSL\text{-}Dlx2\text{-}3xFlag}$ mice. Wildtype C57BL/6J mice were purchased from Shanghai Jihui Laboratory Animal Care Co. Ltd. (Shanghai, China). All mice were maintained under SPF conditions at the Animal Center of the Ninth People's Hospital affiliated with Shanghai Jiao Tong University School of Medicine. The day of the appearance of a vaginal plug was defined as E0.5 in all timed pregnancies. Embryos at the E10.5 and E12.5 stages (12:00 h of the day when the vaginal plug was detected was counted as E0.5) and P0 pups were collected for subsequent experiments. All animal experiments were approved by the Animal Care and Usage Committee of the Ninth People's Hospital affiliated to Shanghai Jiao Tong University School of medicine.

Micro-computed tomographic (micro-CT) imaging and 3D reconstruction

Micro-CT was performed using a SkyScan 1176 (Bruker, Germany). Micro-CT images were acquired from P0 mice, with an x-ray source voltage of 45 kV and current of 550 μA. The data were collected at a resolution of 18 μm. Volume rendering in 3D was achieved using Mimics Medical 21.0 (Materialize). We evaluated micro-CT scans from three replicates per genotype. All landmarks were determined based on *Mouse Development* (Eds. J Rossant and P.L.Tam, 2002) and www.getahead.la.psu.edu.

All bones used in this study were manually segmented. Micro-CT scanning data were uploaded to Mimics as DICOM files. The background noise from these segmentations and bones outside the scope of this study were manually removed using Mimics' editor tools. The remaining craniofacial bones were isolated and labeled using pre-scale thresholds that allowed only bones to be labeled. Reconstruction data were then rendered using Mimics' 3D calculation tools and analysis tools were used for the measurements of isolated bones. The mean measurements of the maxillary bones were compared between the P0 wildtype and *Dlx2* overexpression groups.

Statistical analysis

GraphPad Prism v.8 for Windows (GraphPad Software, La Jolla, CA, United States) was used for the statistical analysis. For all graphs, error bars represent standard deviations. Independent two-tailed Student's *t*-tests were applied for comparisons between two groups. Differences were considered to be statistically significant at p-values < 0.05.

Isolation of mouse maxillary processes

In E10.5 and E12.5, pregnant C57BL/6 females were euthanized using isoflurane and cervical dislocation. The embryos were removed from the uterus into cold PBS and transferred into a 6 cm Petri dish, using a disposable glass straw. For sequences library construction, complete maxillary processes were carefully dissected out from embryos using micro tweezers under a stereomicroscope.

Bulk RNA-seq and data analysis

Total RNA was extracted using Trizol from freshly dissected E10.5 maxillary process tissues. Three independent RNA samples were prepared for each genotype (WT and *wnt1*^{cre}*; Rosa26*$^{Dlx2/-}$). We used 2 μg total RNA as input material for the library preparations for each sample. Sequencing libraries were generated using the NEBNext® UltraTM RNA Library Prep Kit for Illumina® (#E7530L, NEB, United States) following the manufacturer's recommendations. The libraries were sequenced on an Illumina HiSeq X ten platform and 150 bp paired-end reads were generated. Sequenced reads were mapped to the mm 10 genome using STAR aligner version 2.7.3a. Comparisons between the RNA-seq datasets were performed using the DESeq2 package in *R*. Enrichment analyses and visualization of functional profiles of differentially expressed genes (DEGs) were performed using the clusterProfiler package in *R*.

ScRNA-seq and UMAP analysis

Fresh maxillary process tissues were conserved in the GEXSCOPE® Tissue Preservation Solution (Singleron) until library preparation. The scRNA-Seq libraries were constructed in accordance with the Singleron GEXSCOPE™ protocol from the GEXSCOPE™ Single-Cell RNA Library Kit (Singleron Biotechnologies). Pools were sequenced on the Illumina HiSeq X to generate 150 bp paired-end reads. Unsupervised clustering of cell populations was performed using the tSNE and UMAP analysis from the Seurat R package.

CUT&Tag analysis

After obtaining fresh cells from the maxillary processes of E12.5 wildtype mice, the CUT&Tag libraries were prepared using the Hyperactive *In-Situ* ChIP Library Prep Kit for Illumina (Vazyme Biotech, TD901) as previously described (Zuo et al., 2021). Approximately 50,000 cells were used per sample. The Anti-DLX2 antibody (Abcam, ab272902) was used as the primary antibody and goat anti-rabbit IgG (Vazyme, Ab206-10-AA) was used as the secondary antibody. All CUT&Tag libraries were sequenced on the Illumina Nova Seq 6000 platform at PE150 mode. Low-quality reads and adapters were trimmed by Trim Galore (v0.6.5). The clean reads were mapped to the mm 10 genome using bowtie2 (v2.4.2).

Results

Micro-CT reveals abnormal bone formation in *Wnt1*^{cre}*; Rosa26*$^{Dlx2/-}$ mouse

The *wnt1*^{cre}; *Rosa26*$^{Dlx2/-}$ mice, with *Dlx2* overexpressed in neural crest-derived cells exhibit craniofacial deformities such as cleft palate (Sun et al., 2022). To quantify the effect of *Dlx2* overexpression on craniofacial bone formation, we performed Micro-CT scanning on the head of P0 wild-type and *wnt1*^{cre}*; Rosa26*$^{Dlx2/-}$ mice. Micro-CT analysis provides comprehensive information on anatomical landmarks and the size of each craniofacial bone (Ho et al., 2015). The premaxilla and nasal bone, maxilla, palatine bone, frontal bone, parietal bone, interparietal bone, occipital bone and mandible were isolated for analysis (Figure 1A). Obvious ectopic bone formation and absorption were found in the premaxilla and nasal bone, frontal bone and parietal bone of the *wnt1*^{cre}*; Rosa26*$^{Dlx2/-}$ mice. The cranial anteroposterior diameter of the *wnt1*^{cre}*; Rosa26*$^{Dlx2/-}$ mice was significantly smaller than that of wild-type mice. We isolated the maxilla from wild-type and *wnt1*^{cre}*; Rosa26*$^{Dlx2/-}$ mice and defined the anatomical landmarks (Figure 1B). We next quantitatively compared the sizes of the maxilla using the landmarks (Figures 1C–G). The full width and half-width of the maxilla of the *wnt1*^{cre}*; Rosa26*$^{Dlx2/-}$ mice were significantly decreased (Figures 1D, E) but there was no significant difference in the length and height (Figures 1C–F). The distance between the left and right halves of the maxilla in *wnt1*^{cre}*; Rosa26*$^{Dlx2/-}$ mice was significantly increased (Figure 1G), which was consistent with the cleft palate phenotype. In summary, the quantitative comparison of Micro-CT scans revealed that *Dlx2* overexpression had a teratogenic effect on the mouse maxilla.

Dlx2 overexpression causes substantial gene expression changes in the E10.5 maxillary process

In previous research, it was found that the overexpression of *Dlx2* had an impact on gene expression in E12.5 maxillary processes. However, the temporal and spatial expression analysis of *Dlx2* showed that the overexpression was already evident in the earliest stage (E10.5) of maxillary process formation (Sun et al., 2022). In order to further understand how the overexpression of *Dlx2* affects the development of maxillary processes, bulk RNA-Seq was performed on the

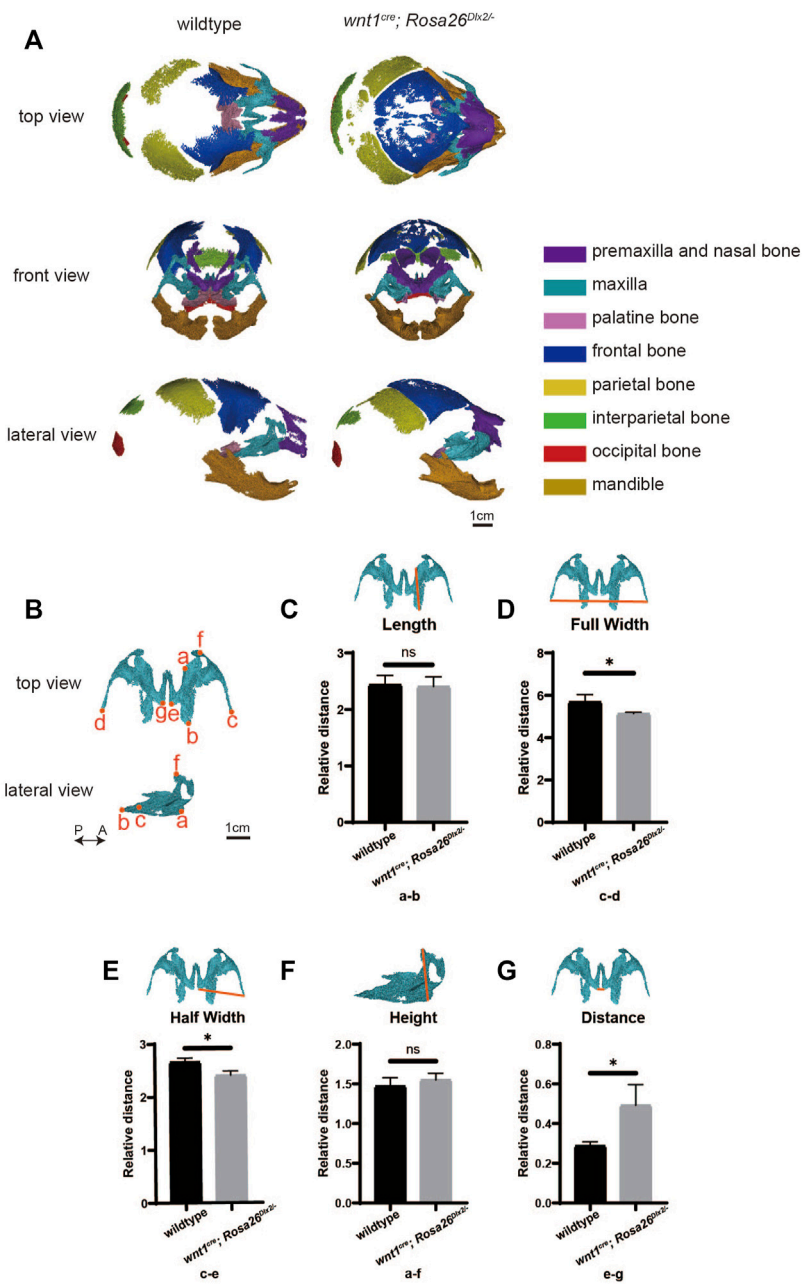

FIGURE 1
The conditional overexpression of *Dlx2* in cranial neural crest cells results in underdeveloped maxilla. **(A)** Top, front and lateral views of micro-computed tomographic rendering of a skull of a P0 wildtype and *wnt1*^{cre}; *Rosa26*$^{Dlx2/-}$ mouse. **(B)** Isolated maxilla from wildtype and *wnt1*^{cre}; *Rosa26*$^{Dlx2/-}$ mice. P←→A: Posterior to Anterior. Definitions of landmarks: a. Medial point of the premaxillary-maxillary suture; b. Posterior point of the maxilla; c. Right tip of the zygomatic process of maxilla; d. Left tip of the zygomatic process of maxilla; e. Right posterior-medial point of the palatine process of the maxilla; f. Anterior point of the maxilla; g. Left posterior-medial point of the palatine process of the maxilla. **(C–G)** Quantification of the size (length **(C)**, full width **(D)**, half width **(E)**, height **(F)**, and distance **(G)**) of the maxilla in wildtype and *wnt1*^{cre}; *Rosa26*$^{Dlx2/-}$ mice. *<0.05; ns. not significant. Definitions of landmarks: a. medial point of the premaxillary-maxillary suture; b. posterior point of the maxilla; cd. tip of the zygomatic process of maxilla; e.g., posterior-medial point of the palatine process of the maxilla; f. anterior point of the maxilla.

maxillary processes of E10.5 wild-type and *wnt1*^{cre}; *Rosa26*$^{Dlx2/-}$ mice. The individual replicates exhibited a high degree of correlation among the same genotype but a lower correlation was observed between replicates of different genotypes (Figure 2A), suggesting the overexpression of *Dlx2* already induced transcriptome changes at this stage.

Comparisons between the *wnt1*^{cre}; *Rosa26*$^{Dlx2/-}$ and wild-type mice revealed that 6,230 genes exhibited significant expression changes. Of these genes, 2,192 genes were significantly upregulated and 1,762 genes were significantly downregulated (Figure 2B). The Gene Ontology (GO) enrichment analysis of DEGs that were significantly upregulated revealed that they are

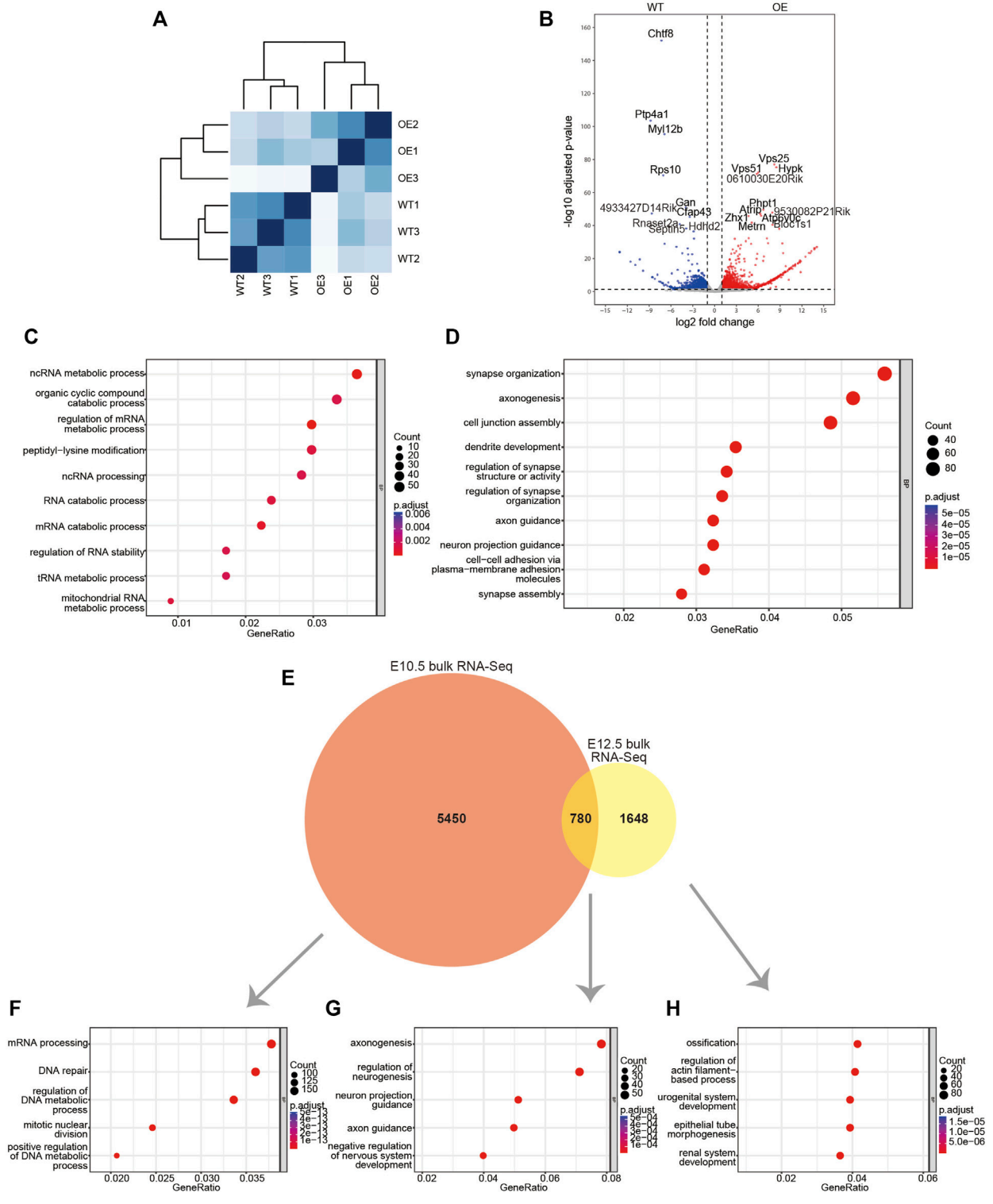

FIGURE 2
Bulk RNA-Seq data for the maxillary processes from E10.5 wildtype and *wnt1*^{cre}; *Rosa26*$^{Dlx2/-}$ embryos. **(A)** Sample distances matrix showing the correlation between RNA-seq replicates. **(B)** Volcano plots to show differentially expressed genes between wildtype and *wnt1*^{cre}; *Rosa26*$^{Dlx2/-}$ samples. **(C,D)** GO enrichment analysis of genes significantly upregulated or downregulated in *wnt1*^{cre}; *Rosa26*$^{Dlx2/-}$. **(E)** Venn diagram to show the overlap between DEGs obtained from bulk RNA-Seq analysis of E10.5 and E12.5 mice. **(F–H)** GO enrichment analysis of genes expressed in E10.5 mice only **(F)**, E10.5-E12.5 overlap **(G)**, E12.5 only **(H)**. WT, wildtype; OE, *wnt1*^{cre}; *Rosa26*$^{Dlx2/-}$.

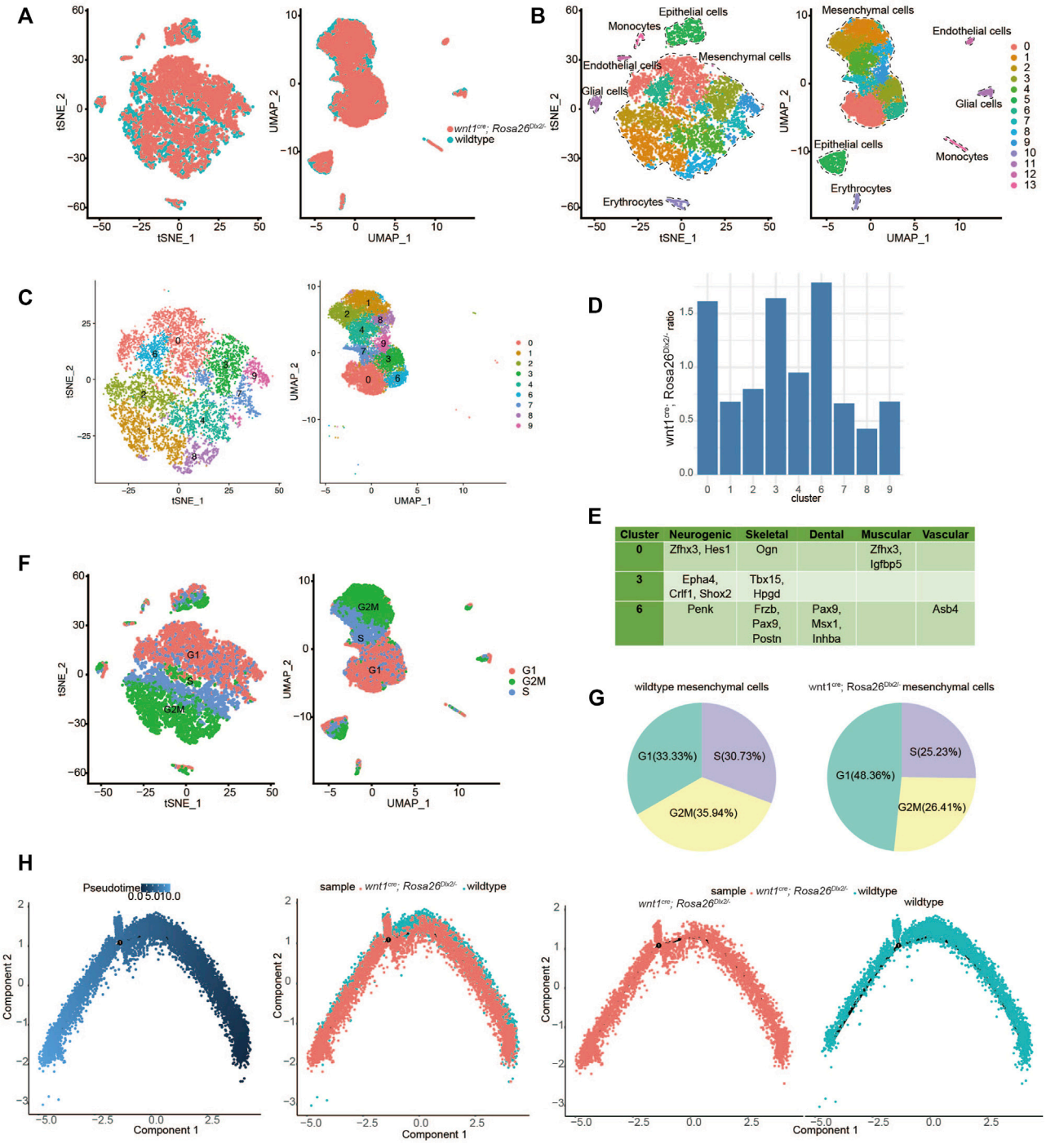

FIGURE 3
ScRNA-Seq analysis suggested that *Dlx2* overexpression inhibits proliferation and promotes cell differentiation of maxillary process cells. **(A)** Combined scRNA-Seq data of E12.5 wildtype and *wnt1*^{cre}; *Rosa26*$^{Dlx2/-}$ mice. The coincidence degree was high. **(B)** TSNE and UMAP showing all cell clustering of combined data. **(C)** TSNE and UMAP showing mesenchymal cell clustering of combined data. **(D)** The cell proportions of *wnt1*^{cre}; *Rosa26*$^{Dlx2/-}$ mice samples to wildtype cells in each mesenchymal cell cluster corresponds to Figure 3C. It was higher in clusters 0, 3, 6, and lower in clusters 1, 8. **(E)** Some differentially expressed markers in clusters 0, 3, 6, which include multiple developmental systems. **(F)** Schematic diagram of cell cycle of mesenchymal cells after data was combined. **(G)** Pie chart of cell cycle proportion of wildtype (left) and *wnt1*^{cre}; *Rosa26*$^{Dlx2/-}$ (right) mesenchymal cells in the combined data. **(H)** Pseudotime differentiation trajectories of combined data from E12.5 wildtype and *wnt1*^{cre}; *Rosa26*$^{Dlx2/-}$ mice.

involved in critical biological processes and molecular pathways, such as organic cyclic compound catabolic process, peptidyl-lysine modification, ncRNA processing and RNA catabolic process. The upregulated genes were also involved in a variety of RNA metabolic processes, which included ncRNA metabolic process, regulation of mRNA metabolic process, tRNA metabolic

process and mitochondrial RNA metabolic process (Figure 2C). Notably, the downregulated DEGs are enriched for functional terms related to neuronal development, such as synapse organization, axonogenesis, dendrite development and axon guidance (Figure 2D), which reflects the neural crest-origin of the maxillary processes.

We found the DEGs of E10.5 are significantly different from the previously reported bulk RNA-Seq DEGs of the mouse maxillary process in E12.5 wildtype and *wnt1*^{cre}; *Rosa26*$^{Dlx2/-}$ mice (Sun et al., 2022). Between the 6230 E10.5 DEGs and the 2428 E12.5 DEGs, only 780 genes are common (Figure 2E). Among the 5,450 genes that were unique to E10.5, the most enriched GO terms are related to cell proliferation and transcription, such as mRNA processing, DNA repair, regulation of DNA metadata process and mitotic nuclear division (Figure 2F). The 780 DEGs that were shared by E10.5 and E12.5 are enriched for GO terms involved in neuronal development, such as axonogenesis, regulation of neurogenesis, neuron project guidance and axon guidance (Figure 2G). Notably, the 1648 DEGs that were unique to E12.5 mice are enriched for ossification related genes (Figure 2H). Thus, the overexpression of *Dlx2* can lead to different transcriptional responses and physiological outcomes at different stages of craniofacial development.

Dlx2 overexpression inhibits proliferation and promotes cell differentiation in maxillary process cells

Our bulk RNA-Seq analyses reveal pronounced transcriptional regulatory effects of *Dlx2* during early maxillary development. However, the inability to distinguish among different cell subpopulations within maxillary processes precludes further dissection of transcriptome changes associated with the differentiation of mesenchyme. Overcoming these limitations requires transcriptome profiling at single-cell resolution.

In the maxillary process at E10.5, the differentiation of most tissue types has not occurred and the mesenchymal cell population is relatively homogeneous. In order to more clearly reveal whether overexpression of *Dlx2* affects the differentiation trajectory of cells, we isolated the maxillary process tissues of E12.5 wild-type and *wnt1*^{cre}; *Rosa26*$^{Dlx2/-}$ mice for single-cell RNA sequencing. The two scRNA-Seq datasets were combined and further analyzed. After dimensional reduction, the main cell populations from the two different samples largely overlapped with each other, indicating the batch effect was minimal (Figure 3A). The combined data were further clustered into 14 cell populations, with the largest cell populations corresponding to mesenchymal cells (Figure 3B). The nine mesenchymal clusters (clusters 0, 1, 2, 3, 4, 6, 7, 8, and 9) were selected for further analysis (Figure 3C).

In order to identify the cell populations most affected by *Dlx2* overexpression, we quantified the relative proportions of *wnt1*^{cre}; *Rosa26*$^{Dlx2/-}$ mice samples to wild-type cells in each of the 9 mesenchymal cell clusters. In each cell cluster, the number of cells from *wnt1*^{cre}; *Rosa26*$^{Dlx2/-}$ mice samples was divided by the number of cells from the wild-type samples. We found that the *wnt1*^{cre}; *Rosa26*$^{Dlx2/-}$ cells were relatively enriched in clusters 0, 3, and 6, while depleted in the other clusters, particularly for clusters 1 and 8 (Figure 3D). To further understand the identities of clusters 0, 3, and 6, we examined their marker genes. For each of these clusters, several marker genes related to different tissue types can be found (Figure 3E), suggesting these cells may represent various precursor cells that have not fully committed to a specific cell type.

Notably, we also found that there are a large number of marker genes related to the cell cycle in each cell population (Supplementary Figure S1). We assessed the cell cycle stages for each mesenchymal cell and found that clusters 0, 3, and 6 mainly consisted of cells in the G1 phase, while clusters 1 and 8 consisted of cells in the G2M phase (Figure 3F). When comparing the cell cycle composition of mesenchymal cells from the two genotypes, we found that the proportion of cells in the G1 phase markedly increased, while the proportion of cells in G2M and S phase decreased in the *wnt1*^{cre}; *Rosa26*$^{Dlx2/-}$ mice cells (Figure 3G). These results suggest the overexpression of *Dlx2* led to a slowdown of cell cycle progression and inhibition of cell proliferation.

To further understand how the overexpression of *Dlx2* affects the differentiation trajectory of maxillary mesenchymal cells, we performed pseudotime developmental trajectory analysis on the combined scRNA-Seq dataset. While the cells from wild-type and *Dlx2*-overexpressing mice exhibit similar trajectories without obvious divergence, the cells from the *wnt1*^{cre}; *Rosa26*$^{Dlx2/-}$ mice were located at more downstream positions on the pseudotime trajectory compared to the wild-type cells (Figure 3H). This difference was further confirmed by quantifying the pseudotime scores for the cells from the two genotypes (Supplementary Figure S2). These analyses thus suggest the overexpression of *Dlx2* caused the mesenchymal cells within the maxillary process to enter a more differentiated state.

Taken together, our scRNA-Seq result suggests that overexpression of *Dlx2* had two related effects: inhibition of cell proliferation and promotion of differentiation. In *Dlx2*-overexpressing mice, the maxillary process cells may have precociously entered a more downstream differentiation state before they had sufficient proliferation, thereby impairing the development of the maxillary bone and ultimately causing the phenotypes of narrowing width, widening distance and cleft palate.

CUT&Tag identifies candidate targets of DLX2

To uncover the regulatory mechanism of *Dlx2* in early maxillary process development, CUT&Tag analysis was performed. CUT&Tag is a novel and highly sensitive method used to identify transcription factor occupancy sites (Kaya-Okur et al., 2019; Kaya-Okur et al., 2020). We used this method to identify candidate direct targets of DLX2. We performed DLX2 CUT&Tag on two replicates of wild-type mice maxillary processes and identified 14,738 and 6899 peaks in each replicate. Intersection

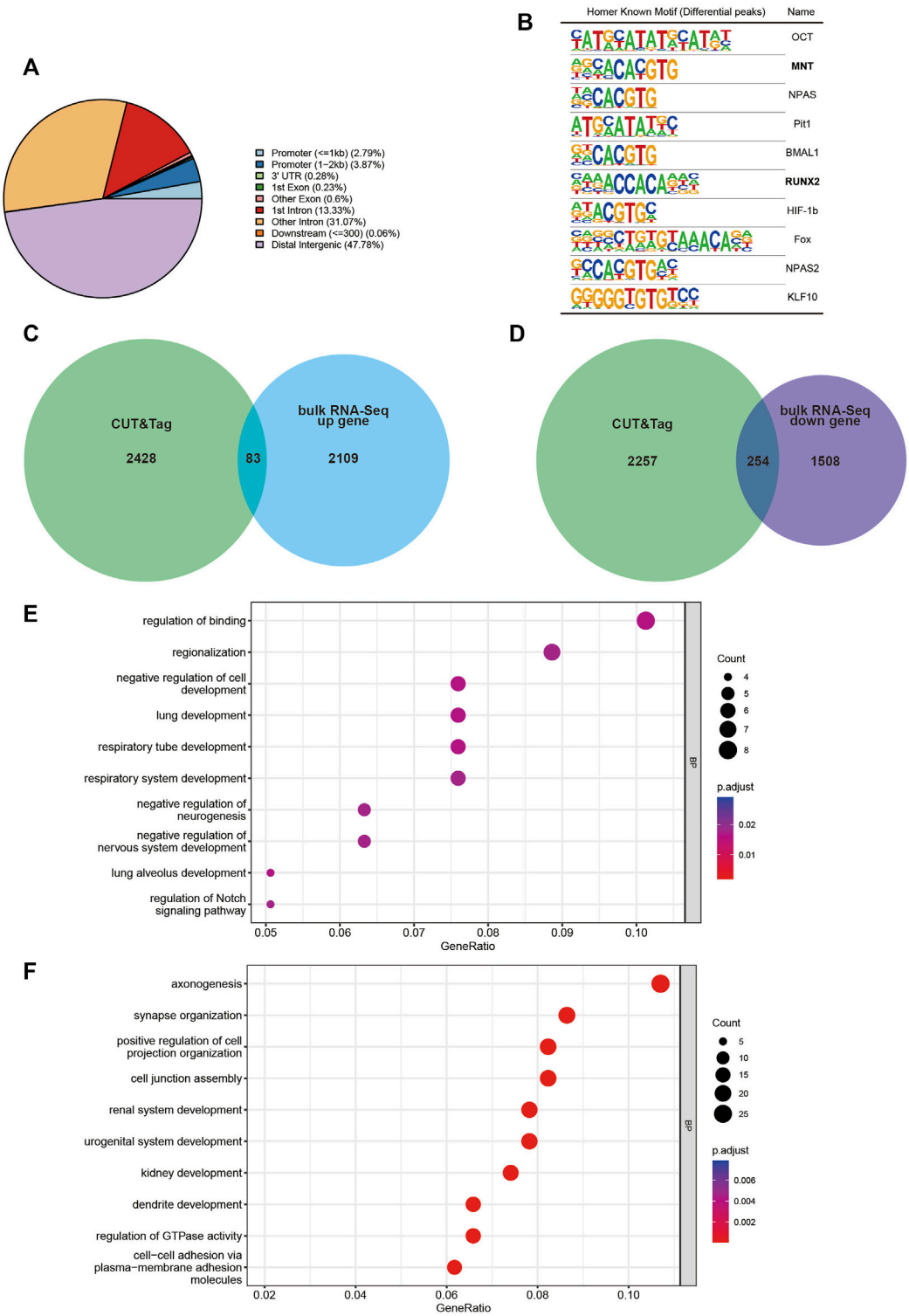

FIGURE 4
CUT&Tag analysis display of *Dlx2* downstream regulatory gene locus information. **(A)** Location of DLX2-occupancy peaks relative to the nearest annotated gene identified by CUT&Tag analysis. **(B)** Ten most enriched sequence motifs at DLX2-occupancy sites as determined using HOMER. The matched Motifs contained Mnt and Runx2. **(C,D)** Venn diagram to show the overlap between annotated genes identified by CUT&Tag analysis and E10.5 upregulated **(C)** or downregulated **(D)** DEGs. **(E, F)** GO enrichment analysis of the overlapping genes between annotated genes identified by CUT&Tag analysis and E10.5 upregulated **(E)** or downregulated **(F)** DEGs.

was used to obtain 3518 peaks that were common to both replicates. Through annotation of these peaks, we found that less than 7% were located in the promoter area (within 2 kb from the TSS) (Figure 4A). The largest proportion of DLX2 occupancy sites was located between genes, which indicated that DLX2 may bind to potential enhancer regions to regulate the expression of protein-coding genes (Figure 4A).

The ten most enriched known motifs identified by HOMER software are listed in Figure 4B. Among these enriched motifs, Runx2 was of particular interest because substantial *in vivo* and *in vitro* studies have shown that this gene is strongly associated with osteogenesis (Tosa et al., 2019; Deiana et al., 2020). This suggested that Dlx2 may function in collaboration with Runx2 to reshape the transcriptome when Dlx2 is overexpressed. Mnt is likely to be a transcriptional repressor and an antagonist of Myc-dependent transcriptional activation and cell growth (Hurlin et al., 1997), which may explain in part the inhibition of cell proliferation found by scRNA-Seq.

The CUT&Tag peak annotation identified 2,511 genes that are associated with DLX2 peaks. By cross-referencing these genes with bulk RNA-Seq upregulated DEGs, 83 upregulated *Dlx2* target genes were obtained (Figure 4C). These genes were enriched for genes involved in the regulation of binding, regionalization, negative regulation of cell development and regulation of Notch signaling pathway (Figure 4E). Interestingly, the Notch signaling pathway has been shown to play an important role in palatal development (Casey et al., 2006). The 254 downregulated *Dlx2* target genes were enriched for genes involved in axonogenesis and synapse organization (Figures 4D, F), consistent with the earlier analysis results. Among these downregulated genes, key osteogenic genes such as *Zeb2* (Wang et al., 2022) and *Rora* (Tao C et al., 2022) were significantly expressed in mesenchymal cell clusters 0 and 3 of scRNA-seq respectively, and these two clusters of cells constituted the majority of the mesenchymal cell group of $wnt1^{cre}$; $Rosa26^{Dlx2/-}$. Overexpression of Dlx2 affects the osteogenesis of most mesenchymal cells. These putative *Dlx2* target genes may be the most direct effectors in the downstream regulatory network of *Dlx2*.

Discussion

The conditional overexpression mouse model makes it possible to obtain stable *Dlx2* overexpression in mouse craniofacial tissues across different developmental stages. In previous work, we have performed a preliminarily exploration of the phenotypic characteristics of this mouse and described the gene expression changes of *Dlx2* overexpression in the maxillary process of E12.5 mice. The maxillary process is formed at the E9.5 stage. As *Dlx2* was overexpressed at the beginning of the maxillary process formation, we chose the earlier E10.5 maxillary process to describe the changes in gene expression. The DEGs at E10.5 share some similarities with those at E12.5, but there were also notable differences. Both sets of DEGs contain genes involved in the development of the nervous system, such as axonogenesis and regulation of neurogenesis. However, the DEGs specific to E10.5 are enriched for genes involved in RNA metabolism. In contrast, the DEGs specific to E12.5 are more enriched for genes involved in ossification. Such stage-dependent transcription effects may be attributed to several reasons. First, this may reflect the differences between the endogenous maxillary transcriptome at E10.5 *versus* E12.5, as early neurogenesis starts at E10.5 (Yun et al., 2002), which is slightly earlier than bone development. Second, maxillary cells at E10.5 and E12.5 may exhibit different chromatin accessibility landscapes. As a result, overexpression of *Dlx2* may affect different target genes in different stages. Third, maxillary cells at E10.5 and E12.5 may express different sets of transcriptional co-activators/co-repressors that function collaboratively with *Dlx2*, leading to different transcriptional outcomes.

By performing scRNA-Seq and comparing the pseudotime development trajectories of wildtype and $wnt1^{cre}$; $Rosa26^{Dlx2/-}$ cells, we found that overexpression of *Dlx2* had little effect on the differentiation trajectory of cells and did not cause alterations in cell fates, or loss of specific cell types. Thus, although the overexpression of *Dlx2* resulted in abnormal gene expression in early maxillary processes, this did not significantly change the direction of cell development. Rather, the main effects of *Dlx2* overexpression are decreased cell proliferation and premature differentiation. The precocious differentiation was sufficient to disrupt the normal developmental timing of tissues, which resulted in defects of maxillary development and a series of other phenotypes, highlighting the intricacies of the gene regulation of craniofacial development.

As a transcription factor, there are many downstream target genes of *Dlx2* in this regulatory process. Our CUT&Tag results suggest *Dlx2* may regulate some genes in collaboration with Mnt and Runx2. However, more experimental evidence is needed to further confirm their co-occupancy at Dlx2 binding sites and collaboration in transcriptional regulation. In addition to the previously recognized Wnt signaling pathway, we found that Notch signaling pathway was also regulated by *Dlx2*. The Notch signaling pathway has a central role in cell fate specification and differentiation (Yun et al., 2002). Early activation of this pathway is a common feature of most potent inducers of neural differentiation (Teratani-Ota et al., 2016) and there was a direct link between the level of Notch activation, pro-osteogenic gene expression and corresponding osteogenic induction (Kostina et al., 2021).

Although this study is an in-depth analysis of the regulatory role and mechanism of *Dlx2* in the early stage of maxillary process development, the roles of approximately 300 direct regulatory gene sites in the downstream complex regulatory network are still unclear. A large number of *in vivo* or *in vitro* experiments are still needed to verify the targets. Still, our study provides important information and resources that will facilitate the functional dissection of the *Dlx2* regulatory network down the road.

Data availability statement

The data presented in the study have been deposited in the National Center for Biotechnology Information (NCBI) Gene Expression Omnibus (GEO) under the accession codes GSE217214. The bulk RNA-Seq data for E12.5 mouse maxillary process have been deposited in GEO under the accession code

GSE185279. The scRNA-Seq data for E12.5 wildtype mice maxillary process have been deposited in GEO under the number GSE161143.

Ethics statement

The animal study was reviewed and approved by Animal Care and Usage Committee of the Ninth People's Hospital affiliated to Shanghai Jiao Tong University School of medicine.

Author contributions

XW and QB designed this experiment and coordinated the experiment. JS carried out all the experimental operations and analyzed them together with JZ.

Funding

This work was supported by the National Natural Science Foundation of China (82071096 to XW, 31801056 and 31970585 to QB), Rare Disease Registration Platform of Shanghai Nineth People's Hospital, Shanghai Jiao Tong University School of Medicine (JYHJB05), Fundamental research program funding of Ninth People's Hospital affiliated to Shanghai Jiao Tong University School of Medicine (JYZZ179 to JS).

Conflict of interest

The authors declare that the research was conducted in the absence of any commercial or financial relationships that could be construed as a potential conflict of interest.

Publisher's note

Supplementary material

The Supplementary Material for this article can be found online at: https://www.frontiersin.org/articles/10.3389/fgene.2023.1085263/full#supplementary-material

SUPPLEMENTARY FIGURE S1
The top 10 differentially expressed genes of each cell cluster in Figure 3B.

SUPPLEMENTARY FIGURE S2
The quantification of the pseudotime difference between wildtype and *wnt1*^{cre}; *Rosa26*$^{Dlx2/-}$ cells.

References

Anderson, S. A., Eisenstat, D. D., Shi, L., and Rubenstein, J. L. (1997a). Interneuron migration from basal forebrain to neocortex: Dependence on Dlx genes. *Science* 278, 474–476. doi:10.1126/science.278.5337.474

Anderson, S. A., Qiu, M., Bulfone, A., Eisenstat, D. D., Meneses, J., Pedersen, R., et al. (1997b). Mutations of the homeobox genes Dlx-1 and Dlx-2 disrupt the striatal subventricular zone and differentiation of late born striatal neurons. *Neuron* 19 (1), 27–37. doi:10.1016/s0896-6273(00)80345-1

Barretto, N., Zhang, H., Powell, S. K., Fernando, M. B., Zhang, S., Flaherty, E. K., et al. (2020). ASCL1-and DLX2-induced GABAergic neurons from hiPSC-derived NPCs. *J. Neurosci. Methods* 334, 108548. doi:10.1016/j.jneumeth.2019.108548

Casey, L. M., Lan, Y., Cho, E. S., Maltby, K. M., Gridley, T., and Jiang, R. (2006). Jag2-Notch1 signaling regulates oral epithelial differentiation and palate development. *Dev. Dyn.* 235 (7), 1830–1844. doi:10.1002/dvdy.20821

Chai, Y., and Maxson, R. E., Jr. (2006). Recent advances in craniofacial morphogenesis. *Dev. Dyn.* 235 (9), 2353–2375. doi:10.1002/dvdy.20833

Dai, J., Si, J., Ouyang, N., Zhang, J., Wu, D., Wang, X., et al. (2017). Dental and periodontal phenotypes of Dlx2 overexpression in mice. *Mol. Med. Rep.* 15 (5), 2443–2450. doi:10.3892/mmr.2017.6315

Deiana, M., Dalle Carbonare, L., Serena, M., Cheri, S., Mutascio, S., Gandini, A., et al. (2020). A potential role of RUNX2- RUNT domain in modulating the expression of genes involved in bone metastases: An *in vitro* study with melanoma cells. *Cells* 9 (3), 751. doi:10.3390/cells9030751

Fang, T., Zhao, Z., Yuan, F., He, M., Sun, J., Guo, M., et al. (2020). Actinidia Chinensis Planch Root extract attenuates proliferation and metastasis of hepatocellular carcinoma by inhibiting the DLX2/TARBP2/JNK/AKT pathway. *J. Ethnopharmacol.* 251, 112529. doi:10.1016/j.jep.2019.112529

Ho, T. V., Iwata, J., Ho, H. A., Grimes, W. C., Park, S., Sanchez-Lara, P. A., et al. (2015). Integration of comprehensive 3D microCT and signaling analysis reveals differential regulatory mechanisms of craniofacial bone development. *Dev. Biol.* 400 (2), 180–190. doi:10.1016/j.ydbio.2015.02.010

Hurlin, P. J., Queva, C., and Eisenman, R. N. (1997). Mnt: A novel max-interacting protein and Myc antagonist. *Curr. Top. Microbiol. Immunol.* 224, 115–121. doi:10.1007/978-3-642-60801-8_11

Kaya-Okur, H. S., Janssens, D. H., Henikoff, J. G., Ahmad, K., and Henikoff, S. (2020). Efficient low-cost chromatin profiling with CUT&Tag. *Nat. Protoc.* 15 (10), 3264–3283. doi:10.1038/s41596-020-0373-x

Kaya-Okur, H. S., Wu, S. J., Codomo, C. A., Pledger, E. S., Bryson, T. D., Henikoff, J. G., et al. (2019). CUT&Tag for efficient epigenomic profiling of small samples and single cells. *Nat. Commun.* 10 (1), 1930. doi:10.1038/s41467-019-09982-5

Kostina, A., Lobov, A., Semenova, D., Kiselev, A., Klausen, P., and Malashicheva, A. (2021). Context-specific osteogenic potential of mesenchymal stem cells. *Biomedicines* 9 (6), 673. doi:10.3390/biomedicines9060673

Lee, S. Y., Jeon, H. M., Ju, M. K., Jeong, E. K., Kim, C. H., Park, H. G., et al. (2016). Dlx-2 and glutaminase upregulate epithelial-mesenchymal transition and glycolytic switch. *Oncotarget* 7 (7), 7925–7939. doi:10.18632/oncotarget.6879

Qu, B., Liu, O., Fang, X., Zhang, H., Wang, Y., Quan, H., et al. (2014). Distal-less homeobox 2 promotes the osteogenic differentiation potential of stem cells from apical papilla. *Cell Tissue Res.* 357 (1), 133–143. doi:10.1007/s00441-014-1833-9

Sun, H., Liu, Z., Li, B., Dai, J., and Wang, X. (2015). Effects of DLX2 overexpression on the osteogenic differentiation of MC3T3-E1 cells. *Exp. Ther. Med.* 9 (6), 2173–2179. doi:10.3892/etm.2015.2378

Sun, J., Ha, N., Liu, Z., Bian, Q., and Wang, X. (2022). A neural crest-specific overexpression mouse model reveals the transcriptional regulatory effects of Dlx2 during maxillary process development. *Front. Physiol.* 13, 855959. doi:10.3389/fphys.2022.855959

Tan, Y., and Testa, J. R. (2021). DLX genes: Roles in development and cancer. *Cancers (Basel)* 13 (12), 3005. doi:10.3390/cancers13123005

Tao C, L. J., Li, Z., Lai, P., Zhang, S., Qu, J., Tang, Y., et al. (2022). DNMT1 is a negative regulator of osteogenesis. *Biol. Open* 11 (3), bio058534. doi:10.1242/bio.058534

Teratani-Ota, Y., Yamamizu, K., Piao, Y., Sharova, L., Amano, M., Yu, H., et al. (2016). Induction of specific neuron types by overexpression of single transcription factors. *Vitro Cell Dev. Biol. Anim.* 52 (9), 961–973. doi:10.1007/s11626-016-0056-7

Thomas, B. L., Tucker, A. S., Qui, M., Ferguson, C. A., Hardcastle, Z., Rubenstein, J. L., et al. (1997). Role of Dlx-1 and Dlx-2 genes in patterning of the murine dentition. *Development* 124 (23), 4811–4818. doi:10.1242/dev.124.23.4811

Tosa, I., Yamada, D., Yasumatsu, M., Hinoi, E., Ono, M., Oohashi, T., et al. (2019). Postnatal Runx2 deletion leads to low bone mass and adipocyte accumulation in mice

bone tissues. *Biochem. Biophys. Res. Commun.* 516 (4), 1229–1233. doi:10.1016/j.bbrc.2019.07.014

Wang, Q., Lin, H., Ran, J., Jiang, Z., Ren, Q., He, W., et al. (2022). miR-200a-3p represses osteogenesis of human periodontal ligament stem cells by targeting ZEB2 and activating the NF-κB pathway. *Acta Odontol. Scand.* 80 (2), 140–149. doi:10.1080/00016357.2021.1964593

Yun, K., Fischman, S., Johnson, J., Hrabe de Angelis, M., Weinmaster, G., and Rubenstein, J. L. (2002). Modulation of the notch signaling by Mash1 and Dlx1/2 regulates sequential specification and differentiation of progenitor cell types in the subcortical telencephalon. *Development* 129 (21), 5029–5040. doi:10.1242/dev.129.21.5029

Zeng, X., Wang, Y., Dong, Q., Ma, M. X., and Liu, X. D. (2020). DLX2 activates Wnt1 transcription and mediates Wnt/β-catenin signal to promote osteogenic differentiation of hBMSCs. *Gene* 744, 144564. doi:10.1016/j.gene.2020.144564

Zhang, J., Zhang, W., Dai, J., Wang, X., and Shen, S. G. (2019). Overexpression of Dlx2 enhances osteogenic differentiation of BMSCs and MC3T3-E1 cells via direct upregulation of Osteocalcin and Alp. *Int. J. Oral Sci.* 11 (2), 12. doi:10.1038/s41368-019-0046-1

Zhang, J., Zhang, W., Shi, J., Dai, J., and Shen, S. G. (2018). Dlx2 overexpression enhanced accumulation of type II collagen and aggrecan by inhibiting MMP13 expression in mice chondrocytes. *Biochem. Biophys. Res. Commun.* 503 (2), 528–535. doi:10.1016/j.bbrc.2018.05.066

Zuo, W., Chen, G., Gao, Z., Li, S., Chen, Y., Huang, C., et al. (2021). Stage-resolved Hi-C analyses reveal meiotic chromosome organizational features influencing homolog alignment. *Nat. Commun.* 12 (1), 5827. doi:10.1038/s41467-021-26033-0

frontiers | Frontiers in Pediatrics

TYPE Review
PUBLISHED 27 June 2023
DOI 10.3389/fped.2023.1117493

OPEN ACCESS

EDITED BY
Long Guo,
RIKEN Center for Integrative Medical Sciences, Japan

REVIEWED BY
Nathalia Carolina Fernandes Fagundes, University of Alberta, Canada
Nuntigar Sonsuwan, Chiang Mai University, Thailand

*CORRESPONDENCE
Petra Borilova Linhartova
petra.linhartova@recetox.muni.cz

RECEIVED 06 December 2022
ACCEPTED 06 June 2023
PUBLISHED 27 June 2023

CITATION
Marincak Vrankova Z, Krivanek J, Danek Z, Zelinka J, Brysova A, Izakovicova Holla L, Hartsfield Jr JK and Borilova Linhartova P (2023) Candidate genes for obstructive sleep apnea in non-syndromic children with craniofacial dysmorphisms – a narrative review. Front. Pediatr. 11:1117493. doi: 10.3389/fped.2023.1117493

Candidate genes for obstructive sleep apnea in non-syndromic children with craniofacial dysmorphisms – a narrative review

Zuzana Marincak Vrankova[1,2,3], Jan Krivanek[4], Zdenek Danek[2,3], Jiri Zelinka[2], Alena Brysova[1], Lydie Izakovicova Holla[1], James K. Hartsfield Jr[5] and Petra Borilova Linhartova[1,2,3]*

[1]Clinic of Stomatology, Institution Shared with St. Anne's University Hospital, Faculty of Medicine, Masaryk University, Brno, Czech Republic, [2]Clinic of Maxillofacial Surgery, Institution Shared with the University Hospital Brno, Faculty of Medicine, Masaryk University, Brno, Czech Republic, [3]RECETOX, Faculty of Science, Masaryk University, Kotlarska 2, Brno, Czech Republic, [4]Department of Histology and Embryology, Faculty of Medicine, Masaryk University, Brno, Czech Republic, [5]E. Preston Hicks Professor of Orthodontics and Oral Health Research, University of Kentucky Center for the Biologic Basis of Oral/Systemic Diseases, Hereditary Genetics/Genomics Core, Lexington, KE, United States

Pediatric obstructive sleep apnea (POSA) is a complex disease with multifactorial etiopathogenesis. The presence of craniofacial dysmorphisms influencing the patency of the upper airway is considered a risk factor for POSA development. The craniofacial features associated with sleep-related breathing disorders (SRBD) – craniosynostosis, retrognathia and micrognathia, midface and maxillary hypoplasia – have high heritability and, in a less severe form, could be also found in non-syndromic children suffering from POSA. As genetic factors play a role in both POSA and craniofacial dysmorphisms, we hypothesize that some genes associated with specific craniofacial features that are involved in the development of the orofacial area may be also considered candidate genes for POSA. The genetic background of POSA in children is less explored than in adults; so far, only one genome-wide association study for POSA has been conducted; however, children with craniofacial disorders were excluded from that study. In this narrative review, we discuss syndromes that are commonly associated with severe craniofacial dysmorphisms and a high prevalence of sleep-related breathing disorders (SRBD), including POSA. We also summarized information about their genetic background and based on this, proposed 30 candidate genes for POSA affecting craniofacial development that may play a role in children with syndromes, and identified seven of these genes that were previously associated with craniofacial features risky for POSA development in non-syndromic children. The evidence-based approach supports the proposition that variants of these candidate genes could lead to POSA phenotype even in these children, and, thus, should be considered in future research in the general pediatric population.

KEYWORDS

pediatric obstructive sleep apnea, syndrome, craniofacial dysmorphism, candidate gene, skeletal anomaly

1. Introduction

Both pediatric (POSA) and adult obstructive sleep apnea (OSA) count among sleep-related breathing disorders (SRBD). POSA is considered a multifactorial disease triggered by the combination of genetic predispositions and several risk factors, including obesity, neuromuscular factors, adenotonsillar hypertrophy, and specific craniofacial features (1, 2). In adults, the genetic background leading to the OSA phenotype has been studied more intensively than in children.

So far, several studies on candidate genes, phenome-wide association studies of OSA genomic variation, and genome/phenome-wide association studies (GWAS/PheWAS) on adult patients with OSA have been published (3–5), while only a single GWAS focusing on children has been reported (6). That study included 1,486 subjects, 1 week to 18 years old, 46.3% of whom were European-Americans and 53.7% African-Americans. The study identified genomic loci associated with POSA at 1p36.22, 15q26.1, 18p11.32 (rs114124196), 1q43 (rs12754698), 2p25 (rs72775219). 8q21.11 (rs6472959), 11q24.3 (rs4370952), and 15q21.1 (rs149936782); children with craniofacial disorders were excluded from that study (6).

Moreover, single nucleotide polymorphisms (SNPs) in genes encoding apolipoprotein E, fatty-acid binding protein 4, nicotinamide adenine dinucleotide phosphate (NADPH) oxidase, and the macrophage migration inhibitory factor were associated with increased or decreased odds of POSA development in children (7–9). These genes are considered to be candidate genes for POSA development (i.e., they are likely to be related to this disease because of their genomic location or known function). All four mentioned genes are associated with lipid metabolism and/or immune system function. It is, therefore, possible that the susceptibility of carriers of these SNPs to POSA is associated with their role in the development of obesity.

However, genetic background is involved, to some extent, in all of the most commonly reported POSA risk factors – besides obesity, body fat distribution, ventilation control mechanisms, upper airway neural control, and soft tissue morphology, genetic background plays a role also in craniofacial dysmorphisms (10–13). In this narrative review, we closely focus on specific genes involved in the development of the orofacial area and of certain craniofacial features, which makes them possible candidate genes for POSA. Thus, we aimed to (i) describe craniofacial anomalies associated with POSA development, (ii) select syndromes characterized by severe craniofacial dysmorphisms associated with OSA and/or high prevalence of pediatric SRBD, (iii) summarize information about the genetic background of these syndromes, and (iv) suggest candidate genes for POSA in non-syndromic patients with craniofacial dysmorphisms.

2. Craniofacial characteristics associated with POSA development

As the upper airway dimensions and morphology of the craniofacial area are closely related, it is no surprise that some abnormalities in its soft and bony structures may contribute to the narrowing and easier collapse of the airway, resulting in OSA, both in children and adults (14–16). Patients suffering from severe skeletal craniofacial malformations could be at a three times higher risk of POSA development than the general pediatric population (17). The importance of craniofacial morphology in OSA development was confirmed also by Kim et al., who reported the presence of craniofacial dysmorphisms, such as the narrow nasomaxillary complex or underdeveloped mandible, in 93.3% of children diagnosed with sleep-disordered breathing (18).

Multiple studies described craniofacial characteristics that are more often present in children suffering from SRBD than in children without these conditions (19–24). These include the size of the maxillo-mandibular complex, their (absolute and mutual) position, and growth pattern, as well as dental occlusion and facial appearance. The craniofacial dysmorphisms associated with the increased risk of POSA development are summarized in **Figure 1**. Extended facial profile and retrognathia have also been suggested to be more common in children with OSA; however, a recent systematic review by Fagundes et al. did not confirm this association (25).

2.1. Skeletal anomalies in the orofacial area risky for POSA development

Premature bone fusion, craniosynostosis, is one of the key features playing role in the narrowing and easier collapse of the airways. It is often diagnosed together with midface hypoplasia, i.e., a combination of the underdevelopment of the maxilla, cheekbones, and eye sockets (although both these features may occur also independently). Even though these features are well-recognized factors in POSA development, the etiology is usually multifactorial and many children suffer from multilevel airway obstruction (24). Underdevelopment of the upper jaw, i.e., maxillary hypoplasia or, in the case of more pronounced narrowing, maxillary constriction, which are often associated also with narrow and/or high arched palate and lateral crossbite, are other characteristics often present in children suffering from POSA (19, 23, 24, 26). Severe reduction of the naso- and oro-pharyngeal airway space may be present in children with craniosynostosis, in patients with clefts originating from prenatal incomplete tissue fusion (20, 21, 27), or in those with anomalies of the mandible, especially if the mandible is undersized, (i.e., micrognathia; (19, 23, 24, 26). However, the underdevelopment of the maxillo-mandibular complex is not the only factor decreasing the airway patency. According to cephalometric studies, sagittal and vertical maxillo-mandibular complex discrepancies, such as mandibular retrognathia, often diagnosed as skeletal class II malocclusion, and increased overjet or open bite, which may appear due to increased mandibular plane angle, are overrepresented in children diagnosed with POSA (22, 26, 28, 29). This hyperdivergent skeletal pattern may lead to the development of the long-face syndrome, which is another facial appearance typical of patients with SRBD (28, 30, 31). Negative

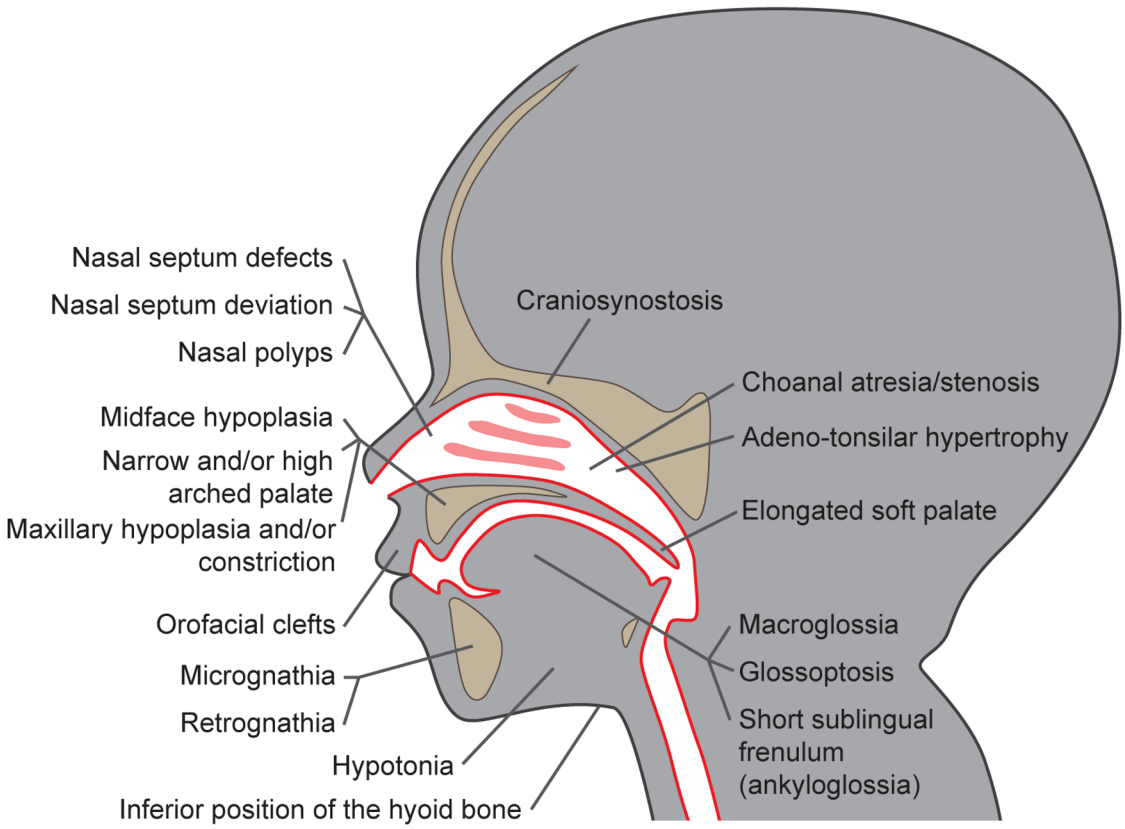

FIGURE 1
Craniofacial dysmorphisms as risk factors for pediatric obstructive sleep apnea development.

anterior overjet and skeletal class III malocclusion are not as often associated with POSA; still, the association is possible, especially if they are caused by severe maxillary deficiency (32). The lower position of the hyoid bone is another skeletal risk factor that can be diagnosed in a cephalogram. As some lingual muscles insert on that bone, their pull in a downward direction can also cause the narrowing of the airway space and, in effect, apnea (14, 33–35).

2.2. Soft tissue anomalies in the orofacial area risky for POSA development

The morphology of soft tissues plays an important role, too. Adeno-tonsillar hypertrophy is a well-described etiological factor of POSA. The deviation or deformity of the nasal septum, hypertrophy of nasal turbinates, or nasal polyps may also increase nasal resistance (36–38) and contribute towards mouth breathing, often accompanied by unphysiological head posture, insufficient lip seal or open bite, all of which are characteristics often present in patients with POSA (16). The lack of nasal breathing accompanied by an imbalance in muscle activity, often associated with the hypotony of orofacial muscles, have a huge impact on the development and growth of the maxillo-mandibular complex and may contribute to its abnormal shape and size (16, 39, 40).

The tongue is another factor playing a key role in the narrowing and collapse of the upper airway. The short sublingual frenulum (or ankyloglossia) in its most severe form leads to a low tongue position and disrupted tongue movement and has been already associated with the POSA phenotype (16, 41–43). An insufficient stimulation of the palatal suture, caused by this unphysiological tongue position, may result in the formation of a narrow palate and decreased volume of nasal cavities, which, again, contributes to the preference for mouth breathing and airway narrowing (16, 33). POSA has also a high prevalence in patients with glossoptosis, which is a down- and backward position of the base of the tongue (44). The combination of glossoptosis with micrognathia or retrognathia leads to a high risk of tongue-based airway obstruction (24, 45). In addition, macroglossia and/or an elongated soft palate could reduce airway volume and contribute to airway obstruction (14, 34).

These craniofacial characteristics are associated with several syndromes; however, they could be also found in non-syndromic children (14, 15, 19). Even though they are usually present in less severe forms, they could still contribute to airway obstruction. Craniofacial features associated with POSA could be easily diagnosed and their heritability is estimated to be high. This is especially true for the size of the maxillo-mandibular complex and the timing of its growth (11, 13, 46).

3. Craniofacial syndromes associated with a high prevalence of pediatric SRBD

The prevalence of SRBD, including POSA, may be very high in syndromic children with a severe form of craniofacial dysmorphism. In a population-based case-control study, an OSA diagnosis was associated with the presence of craniofacial anomalies, in particular with orofacial clefting and Down syndrome (46). To better understand the role of genetic factors in both POSA and craniofacial anomalies associated with this diagnosis, we have reviewed the current body of literature and selected syndromes, which: (1) are characterized by severe craniofacial abnormalities associated with POSA, (2) have a high prevalence, or have been already related to the co-incidence of SRBD and POSA in children, and (3) have a known genetic background.

Based on these criteria, 26 syndromes and disorders were selected, namely achondroplasia, Antley-Bixler, Apert, Auriculocondylar, Beare-Stevenson, Cohen, and Collins syndromes, congenital central hypoventilation, craniofacial microsomia (Goldenhar syndrome, oculo-auriculo-vertebral spectrum), craniofrontonasal dysplasia, Crouzon, Down, Ehlers-Danlos, Ellis-van Creveld, Jackson-Weiss, Marfan, and Marshall-Stickler syndromes, mucopolysaccharidosis IV and VI, Muenke, Noonan, abd Pfeiffer syndromes, Pierre Robin sequence, Prader-Willi, Saethre-Chotzen and Treacher-Collins syndromes. From the craniofacial dysmorphisms associated with OSA, craniosynostosis, oral clefts, midface and maxillary hypoplasia, narrow high-arched palate, micrognathia, retrognathia, choanal atresia, macroglossia, and glossoptosis were the features found most frequently in these syndromes (21, 4–70). It is necessary to mention that in syndromes associated with high POSA prevalence, a combination of several of these features is often present. For example, the Pierre Robin sequence associated with high POSA prevalence consists of the following: micrognathia, glossoptosis, narrow and/or high-arched palate, and cleft palate (45).

The information about the genetic background and prevalence of SRBD in these syndromes, including POSA, is summarized in **Supplementary Table S1** in the Supplement. The prevalence of pediatric SRBD in children suffering from the mentioned syndromes ranges between 10%–87.5%, which is much higher than in the common pediatric population (2%–4%) (21, 45, 53, 54, 56, 58, 63, 69–87). High prevalences of SRBD were found particularly in populations of children with Treacher-Collins syndrome, mucopolysaccharidosis IV and VI, Apert, and Prader-Willi syndrome, in which limited midfacial development is a characteristic feature (21, 53, 54, 69, 70, 72). Despite their shared relationship to craniofacial dysmorphisms and high SRBD prevalence, these syndromic phenotypes are associated with different genes. In total, aneuploidy in Down syndrome and variations in 30 genes in the other 25 mentioned syndromes (see **Supplementary Table S1** in the Supplement) are considered causative or risk factors for SRBD development.

4. Possible candidate genes for POSA development in children with craniofacial dysmorphisms

We prepared an overview of possible candidate genes and loci for pediatric SRBD. **Figure 2** depicts genes and loci associated both with POSA in children without craniofacial features, and those associated with syndromes manifested by craniofacial features risky for SRBD in children (6–9).

Although these syndromes do not share the same genetic background, some of the associated genes affect similar processes, such as the skeletal system development (including the cranial area), organ growth, or embryonic organ morphogenesis. **Figure 3** demonstrates both known and predicted interactions and similarities among 30 considered genes; their functions and importance are described below.

4.1. Genes associated with non-/syndromic craniosynostosis

The etiology of craniosynostosis may involve genetic, epigenetic, and/or environmental factors (88). Craniosynostosis is associated with a high prevalence of POSA. It is a common feature in patients with Antley-Bixler, Apert, Beare-Stevenson, Crouzon, Pfeiffer, Muenke, Jackson-Weiss, Craniofrontonasal, and Saethre-Chotzen syndromes (89–92). SRDB was present also in 50% of children suffering from non-syndromic craniosynostosis (NSC) (89).

Deviations in the development of the craniofacial area are also associated with a variability in the fibroblast growth factor receptor (*FGFR*) genes, which are important for cell specialization as well as for bone growth and modeling, especially in the process of ossification and bone fusion (48, 93, 94). Severe mutations in *FGFR* genes are associated with premature cranial bone fusion and craniosynostosis. These mutations were found in several craniofacial syndromes with a high prevalence of SRBD in children, such as achondroplasia, Antley-Bixler, Beare-Stevenson, Jackson-Weiss, Apert, Crouzon, Pfeiffer, and Saethre-Chotzen syndromes (21, 51, 92, 95–99). These *FGFR*-related craniosynostosis syndromes are autosomal-dominantly inherited.

Moreover, variants in *FGFR* genes could also lead to NSC (95, 100, 101). Genes most commonly mutated in familial craniosynostosis include, besides *FGFR2* and *FGFR3*, the twist family bHLH transcription factor 1 (*TWIST1*) and ephrin-B1 (*EFNB1*) (102). More than 100 mutations in the *EFNB1* gene have been found to cause the craniofrontonasal syndrome, which was confirmed in a study with knockout mice models (103). This rare x-linked disorder shows paradoxically greater severity in heterozygous females than in hemizygous males. TWIST1 acts through Eph–ephrin interactions to regulate the development of the boundary that forms the coronal suture (104). The *TWIST1* gene associated with the Saethre-Chotzen syndrome is believed to regulate bone formation through other genes, such as *FGFR* and *RUNX2* (63, 64). Genetic testing of *FGFR1, FGFR2, FGFR3*, and

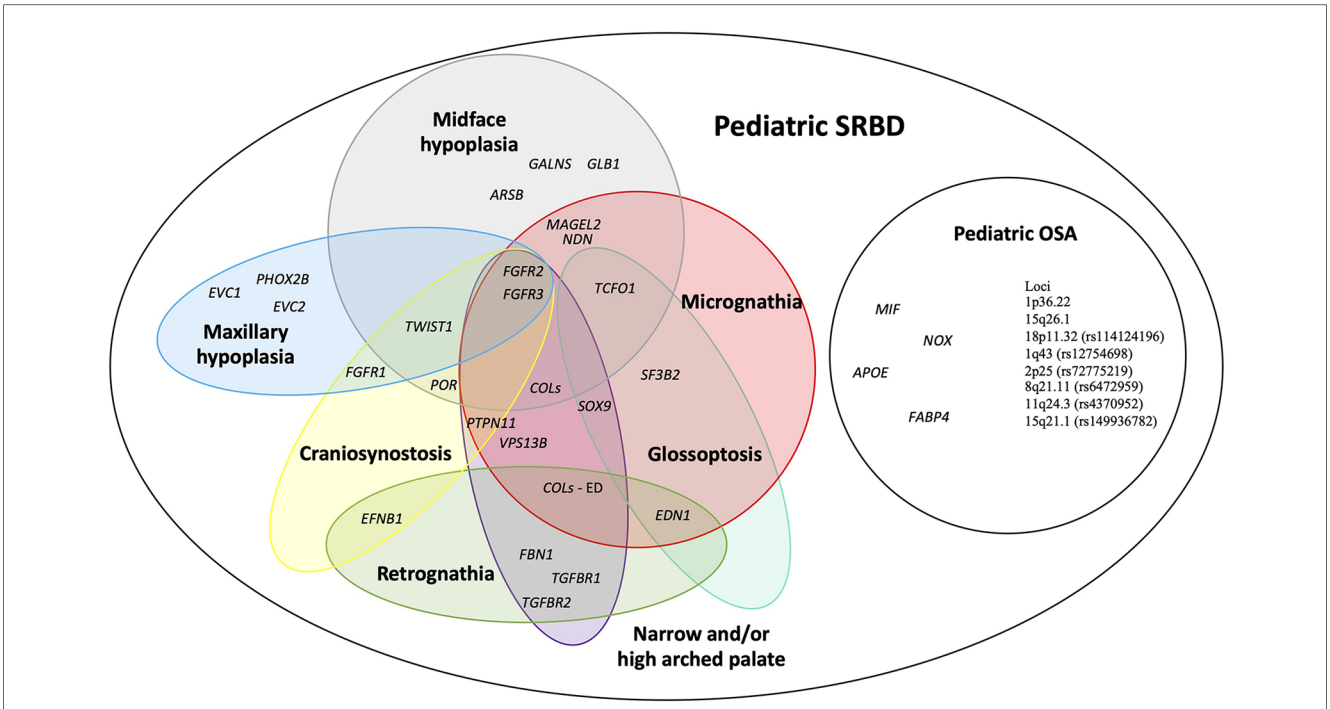

FIGURE 2
An overview of possible candidate genes for pediatric sleep-related breathing disorders (SRBD), especially pediatric obstructive sleep apnea (POSA) in children with craniofacial dysmorphisms. *APOE*, apolipoprotein E; *ARSB*, N-acetylgalactosamine-4 sulfatase; *COLs* (- ED), collagens gene family (genes associated with Ehlers-Danlos syndrome); *EFNB1*, ephrin-B1; *EDN1*, endothelin 1; *EVC1*, EvC ciliary complex subunit 1; *EVC2*, EvC ciliary complex subunit 2; *FABP4*, fatty acid-binding protein 4; *FBN1*, fibrillin 1; *FGFR1*, fibroblast growth factor receptor 1; *FGFR2*, fibroblast growth factor receptor 2; *FGFR3*, fibroblast growth factor receptor 3; *GALNS*, galactosamine-6-sulfatase; *GLB1*, b-D-galactosidase; *MAGEL2*, MAGE-like protein 2; *MIF*, macrophage migration inhibitory factor; *NDN*, necidin; *NOX*, NADPH oxidase 1; *PHOX2B*, paired like homeobox 2B; POR, cytochrome P450 oxidoreductase; *PTPN11*, protein tyrosine phosphatase non-receptor type 11; *SF3B2*, splicing factor 3B subunit 2; *SOX9*, SRY-box 9; *SNORD116*, CD box 116; *TCOF1*, treacle ribosome biogenesis factor 1; *TGFBR1*, transforming growth factor-β receptor 1; *TGFBR2*, transforming growth factor-β receptor 2; *TWIST1*, twist family bHLH transcription factor 1; *VPS13B*, vacuolar protein sorting 13 homolog B.

TWIST1 was even suggested as a first-line test for patients with NSC (101).

Interestingly, not only rare mutations of these genes but also SNPs of these genes are associated with craniofacial dysmorphia. For example, Da Fontoura et al. found an association between SNPs rs11200014 and rs2162540 in *FGFR2* and sagittal maxilla-mandibular discrepancy, so-called skeletal malocclusion (both skeletal class II and III). They also found an association between the SNP rs2189000 in *TWIST1* and a larger body and shorter ramus of the mandible (62). Although *FGFR3* gene variants are associated with Muenke and Crouzon syndromes manifested by craniosynostosis, this feature, surprisingly, was not exhibited in the *FGFR3* $^{A385E/+}$ mice model (105–107). Thus, *FGFR2* seems to be more important for craniosynostosis development than *FGFR3*. On the other hand, a mutation in *FGFR3* causes achondroplasia, which, according to a recent study by Legare et al., has craniosynostosis as a co-occurring feature (108).

A missense mutation in the Protein Tyrosine Phosphatase Non-Receptor Type 11 (***PTPN11***) gene was found in almost 50% of patients diagnosed with Noonan syndrome (109). This gene encodes tyrosine phosphatase Shp-2, an enzyme involved in multiple signal transduction cascades including receptors for growth factors involved in the developmental processes, such as FGFR (110). The Noonan syndrome is manifested by micrognathia, maxillomandibular discrepancy, narrow and/or high-arched palate, and long face syndrome (hyperdivergence) (111, 112). Also, craniosynostosis was described in some patients suffering from this syndrome. Mutations in the *PTPN11*, *KRAS*, or Leucine-Rich Repeat Scaffold Protein (*SHOC2*) gene are causally involved in craniosynostosis (113–115). In patients with the Antley-Bixler syndrome, characterized by craniosynostosis, brachycephaly, midface hypoplasia, and choanal atresia and/or stenosis, variants have been found not only in *FGFR2*, but also in the gene encoding cytochrome p450 oxidoreductase (***POR***) (116–119). This enzyme transfers electrons from NADPH to all microsomal cytochrome P450 enzymes. While individuals with an ABS-like phenotype and normal steroidogenesis are carriers of *FGFR2* mutations, those with genital anomalies and disordered steroidogenesis should be recognized as having a POR deficiency (116).

4.2. Genes associated with non-/syndromic retrognathia and/or micrognathia

The SRY-box 9 transcription factor (***SOX9***) gene plays an important regulatory role during craniofacial development (120). In a rat model with upper airway obstruction, SOX9 level was

10.3389/fped.2023.1117493

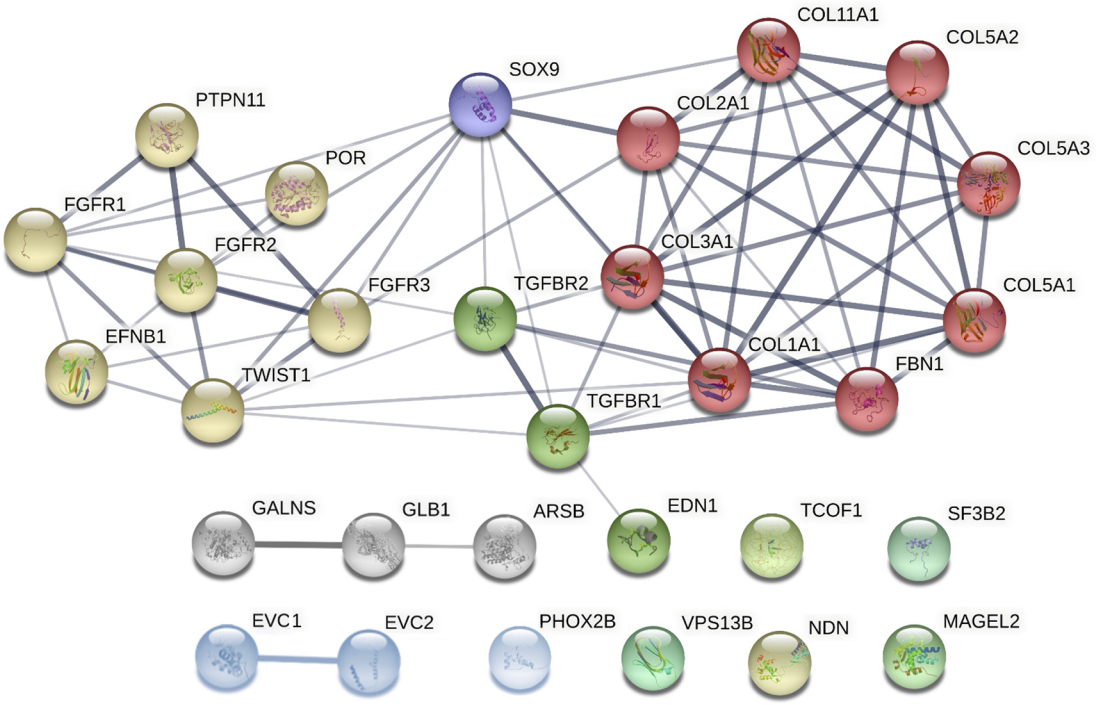

FIGURE 3
Clusters of candidate genes for pediatric obstructive sleep apnea (POSA) development in children with craniofacial dysmorphisms and their interactions (created in string, https://string-db.org/cgi/network?taskId = bF5B2GAcAUOE&sessionId = bSUqeClqj6OL). Proteins encoded by these genes are clustered into 3 main groups using the Markov Clustering Algorithm. yellow dots: genes associated with non-/syndromic craniosynostosis. red, purple, and green dots: other genes associated with non-/syndromic retrognathia and/or micrognathia. grey and blue dots: other genes associated with non-/syndromic midface or maxillary hypoplasia. *ARSB,* N-acetylgalactosamine-4 sulfatase; *COL1A1,* collagen type I alpha 1 chain; *COL2A1,* collagen type II alpha 1 chain; *COL3A1,* collagen type III alpha 1 chain; *COL5A1,* collagen type V alpha 1 chain; *COL5A2,* collagen type V alpha 2 chain; *COL5A3,* collagen type V alpha 3 chain; *COL11A1,* collagen type XI alpha 1 chain; *EFNB1,* ephrin-B1*; EDN1,* endothelin 1; *EVC1,* EvC ciliary complex subunit 1*; EVC2,* EvC ciliary complex subunit 2*; FBN1,* fibrillin 1; *FGFR1,* fibroblast growth factor receptor 1; *FGFR2,* fibroblast growth factor receptor 2; *FGFR3,* fibroblast growth factor receptor 3; *GALNS,* galactosamine-6-sulfatase; *GLB1,* b-D-galactosidase; *MAGEL2,* MAGE-like protein 2; *NDN,* necidin; *PHOX2B,* paired like homeobox 2B; POR, cytochrome P450 oxidoreductase; *PTPN11,* protein tyrosine phosphatase non-receptor type 11; *SF3B2,* splicing factor 3B subunit 2*; SOX9,* SRY-box 9; *SNORD116,* CD box 116; *TCOF1,* treacle ribosome biogenesis factor 1; *TGFBR1,* transforming growth factor-β receptor 1; *TGFBR2,* transforming growth factor-β receptor 2; *TWIST1,* twist family bHLH transcription factor 1; *VPS13B,* vacuolar protein sorting 13 homolog B.

found to be downregulated, which explains the bone architecture abnormalities (121). This gene is also associated with the Pierre Robin sequence (122). Repressed *SOX9* expression leads to changes in the expression of genes essential for normal development of the mandible, causing micrognathia, and, consequently, glossoptosis, airway obstruction, and often, cleft palate (123). The expression of *SOX9* is influenced, among others, by *FGFR3.* Therefore, dysregulation of SOX9 levels, a major regulator of chondrogenesis, is an important underlying mechanism in skeletal diseases caused by mutations in *FGFR3* (124–126). Interestingly, the SNP rs12941170 of *SOX9* was associated with non-syndromic orofacial clefting. However, its role in these non-syndromic clefts remains unclear (124).

Similarly to *SOX9*, variants in endothelin 1 (***EDN1***), the Splicing factor 3B subunit (***SF3B2***), and Treacle ribosome biogenesis factor 1 (***TCOF1***) were associated with syndromes manifesting in children by both micrognathia and glossoptosis. ***EDN1*** encodes a vasoactive peptide belonging to the family of endothelins and is associated with the auriculocondylar syndrome (127), a rare syndrome that usually affects facial features. It is characterized by micrognathia, microstomia, and anomalies in the temporomandibular joint and the condyle (127). Also, studies using mice models with the *EDN1* gene knocked out or deficient have shown several craniofacial dysmorphisms, mandibular dysfunction, and severe retrognathism (62, 127). ***SF3B2*** may be, according to a study by Timberlake et al., an important factor in the development of craniofacial microsomia, which was also confirmed by a recent review covering this congenital facial anomaly (128, 129). ***TCOF1*** presents an important factor for the undisrupted formation and development of the craniofacial area, cartilage, and skeleton (55, 130, 131). Mutations in these genes were found in patients with Treacher-Collins syndrome (130, 131).

Ehlers-Danlos syndrome, manifesting through retrognathia, micrognathia, and maxillary constriction, has been previously proposed as a genetic model for pediatric OSA (60, 61, 132). Variants in genes encoding and/or influencing the expression of collagens (***COL*** gene family) and others (see **Supplementary Table S1** in the Supplement) were associated with this rare connective tissue disorder (60, 133). The minor allele of SNP

rs2249492 in the Collagen type I alpha 1 chain (***COL1A1***) has been previously associated with the increased risk of a sagittal maxilla-mandibular discrepancy (skeletal class III malocclusion) in non-syndromic children (62). The results of the study by Topârcean et al. showed a tendency towards a class II skeletal malocclusion pattern determined by mandibular retrognathism rather than maxillary prognathism among the individuals possessing the mutant allele of this SNP (134).

Other genes for collagens, ***COL2A1*** and ***COL11A1,*** are associated with Marshall-Stickler syndrome (86). Collagens II and XI are present throughout the Meckel's cartilage, which provides mechanical support for the developing mandible. The characteristic craniofacial features of Marshall-Stickler syndrome are midface hypoplasia, micrognathia, cleft palate, and Pierre Robin anomaly (50). Variants in *COL2A1* and *COL11A1* were also associated with the Robin sequence in nonsyndromic patients (135).

Besides collagens, fibrillin and elastin are also present in the architectural scaffolds that impart specific mechanical properties to tissues and organs. The ***FBN1*** gene is essential for the production of fibrillin, and its mutation could cause Marfan syndrome (57, 136).

Fibrillin is crucial for bone and muscle rigidity; hence, its disruption can increase the laxity of airway connective tissues and predispose them to easier collapsibility (56). At the same time, patients often have their maxillo-mandibular complex in a retrognathic position, with a narrow maxilla and palate, and a "long face" appearance (56–58, 137).

Besides *FBN1*, mutations in the transforming growth factor-β receptor 1 (*TGFBR1)* and transforming growth factor-β receptor 2 (*TGFBR2)* may also be found in Marfan syndrome (138). TGFBR2 protein forms a complex with TGFBR1, and both are involved in a signaling pathway responsible for the proliferation, differentiation, and apoptosis of cells throughout the body (139). They are extremely important for bone growth and extracellular matrix formation; moreover, they play a role in the fusion of craniofacial sutures (140). The development of micrognathia and retrognathism was observed in mice with an impaired *TGFB2* gene, giving evidence to its importance in craniofacial morphology (141).

The gene for vacuolar protein sorting-associated protein 13B (*VPS13B)*, also called the *COH1* gene, encodes a protein forming a part of the Golgi apparatus membrane. Its disruption may be involved through various cellular mechanisms, in several clinical features of Cohen syndrome (142, 143), including micrognathia, constricted hard palate, insufficient lip seal, and truncal obesity. All of these issues increase the risk of the collapse of the upper airway and the development of POSA (65, 66, 142, 143).

Mutations in necidin (*NDN*) and the melanoma antigen family member L2 (*MAGEL2*), both localized on chromosome 15, were found in the Prader-Willi syndrome, a complex genetic disorder characterized by several features, such as midface hypoplasia and micrognathia (144). The phenotype of this syndrome includes hypoplastic midface area, hypotonia, and a changed viscosity in secretions. All these factors facilitate the collapse of upper airways and apnea (52, 53, 144). Some polymorphisms in *NDN* were determined in extremely obese German children and adolescents as well as in neonates examined by polysomnography. However, there was a lack of association with juvenile-onset human obesity or sleep and respiratory parameters (145, 146).

4.3. Genes associated with non-/syndromic midface or maxillary hypoplasia

Midface or maxillary hypoplasia are typical features of several syndromes, including mucopolysaccharidosis, Ellis-van Creveld, or congenital central hypoventilation syndrome, the genetic backgrounds of which are described below.

Mucopolysaccharidosis (MPS) is a metabolic disorder characterized by the deficiency or total absence of enzymes responsible for the degradation of glycosaminoglycans. It can be classified into 7 types based on the specific malfunctioning enzyme and clinical manifestations (147). The Morquio syndrome (MPS IV) can be caused by a mutation either in the N-acetylgalactosamine-6-sulfatase (***GALNS***) gene (MPS type IVA), or in the gene for galactosidase beta 1 (***GLB1***; MPS type IVB). Among other clinical manifestations, the Morquio syndrome includes also craniofacial dysmorphisms such as mid-facial hypoplasia, condylar deformities, open bite, macroglossia, or abnormal teeth (148, 149).

The mutated gene for arylsulfatase B (***ARSB***) leads to the reduced function of the enzyme, causing a lysosomal storage disorder – MPS type VI, also known as Maroteaux-Lamy syndrome (117). This syndrome is associated with orofacial manifestations such as macroglossia, malocclusions, or disrupted dental eruption (150).

In syndromic children, the ***TWIST*** gene and the genes of the ***FGFR* family**, described in detail above, were associated with maxillary hypoplasia. In addition, the EvC ciliary complex subunit 1 (***EVC1***) and subunit 2 (***EVC2***) genes were found to be causative for the formation of the Ellis-van Creveld syndrome manifested also by maxillary hypoplasia and mandibular prognathism (151, 152). They encode proteins, the functions of which are not completely understood yet, but appear to be important in the physiological growth and development of bones and teeth (153).

The paired-like homeobox 2B (PHOX2B) transcription factor plays a crucial role in the autonomic nervous system development. Mutations in the ***PHOX2B*** gene are known to cause the congenital central hypoventilation syndrome with a specific craniofacial phenotype – maxillary hypoplasia, box-shaped face, and brachycephaly (68). However, a "silent" mutation in this gene was found in children with class III skeletal malocclusion and a history of sleep apnea (63, 154, 155).

5. Discussion

As POSA may cause serious health problems in young, growing patients, it would be highly beneficial to diagnose the increased risk

of its development as soon as possible. While much of the POSA etiopathogenesis remains underexplored, craniofacial dysmorphisms leading to the narrowing of the airways undoubtedly play an important role (15, 17). Their severe forms can be found in craniofacial syndromes, which are also associated with a much higher prevalence of SRBD and POSA compared to the general pediatric population (21, 45, 53, 54, 56, 58, 63, 69–87). However, similar craniofacial features may be present also in healthy, non-syndromic patients. These skeletal variations could be mild when compared to syndromic phenotypes, but they could still lead to the collapse of the upper airways and POSA development. This is supported by Kim et al. who reported that the majority of non-syndromic, non-obese children diagnosed with POSA have craniofacial anomalies that are possible risk factors for POSA (18).

Several studies have already explored genes associated with OSA etiopathogenesis in adults, including the genes associated with the craniofacial area and characteristic features (4, 156). The heritability of craniofacial traits varies but is generally estimated to be high and very similar in healthy subjects and in patients suffering from OSA (11, 13, 46, 157). This is supported by several studies reporting an increased incidence of the above-mentioned OSA risk features among relatives (157–160). The first phenome-wide association study of genomic variation in adult OSA was recently published by Veatch et al. (5). None of the three SNPs in the leptin receptor (*LEPR*), the matrix metallopeptidase 9 (*MMP9*), and the Gamma-aminobutyric acid type B receptor subunit 1 (*GABBR1*), the association of which with OSA diagnosis was validated in their study, was associated with other non-OSA clinical traits once they controlled for multiple testing (5).

Cade at al. performed a GWAS investigating genetic associations of OSA in Hispanic/Latino Americans from three cohorts. They identified two loci (rs11691765 in the G protein-coupled receptor 83 gene, *GPR83*; and rs35424364 in the pseudogene *CCDC162P*) associated with the AHI and the respiratory event duration, respectively (3). Another GWAS study, focusing on European Caucasians, reported five genes to be associated with facial characteristics, namely the paired-box gene 3 (*PAX3*), the PR-set domain 16 (*PRDM16*), the transcription factor *TP63*, small integral membrane protein 23 (*C5orf50*), and the Collagen type XVII alpha 1 chain (*COL17A1A*), the variants of which contribute to the facial morphology in young adults (4). Some variants of these genes and their possible association with craniofacial abnormalities were also explored in another GWAS study focusing on young adults of European-ancestry from the Avon Longitudinal Study of Parents and Children (161) as well as in mice models (162, 163).

Unfortunately, most publications focus on the genetic background of OSA in adult patients, not the pediatric population. To this date, only one GWAS has been performed in relation to POSA, including European American and African American children without craniofacial disorders (6). The study identified several genomic loci (see the Introduction). However, only one genetic marker, located at 18p11.32, was shared by groups of both ancestries. Their study, therefore, emphasizes the importance of study populations with diverse ethnic backgrounds to identify unique and shared genetic markers that contribute to the heterogeneity of POSA (6).

It follows that specific genes involved in the development of the orofacial area and associated with craniofacial OSA features should be also considered as candidate genes for POSA. Here, we provide an overview of genes that are known to be involved in the development of craniofacial syndromes in children with high SRBD prevalence, including POSA, see **Supplementary Table S1** in the Supplement. All these genes are, to some extent, involved in the formation of tissues of the orofacial area. The candidate genes for POSA can be classified into three major groups based on their involvement in the development of specific craniofacial features. These groups would consist of genes associated with non-/syndromic (i) craniosynostosis, (ii) retrognathia and/or micrognathia, and (iii) midface or maxillary hypoplasia. While certain mutations cause various rare syndromes, other variants in these same genes were suggested to be associated with non-syndromic skeletal variations in the orofacial area (62, 63, 101, 154, 164). So far, variants in ***FGFR1***, ***FGFR2***, ***FGFR3***, ***TWIST***, ***SOX9***, ***COL1A1***, and ***PHOX2B*** are known to play a role in syndrome development as well as in the development of skeletal malocclusions (sagittal maxillo-mandibular complex discrepancies in non-syndromic patients). These genes, therefore, can be considered promising candidate genes for testing of genetic susceptibility to POSA development in various populations.

Although the inheritance pattern of POSA as well as OSA is unclear, most cases with these diseases do not adhere to classical models of inheritance, suggesting that multiple genes could be involved in their development. We believe that besides the GWAS approach, strategies based on candidate genes are also necessary for further research of both these multifactorial diseases. Considering the results of the mentioned genetic association studies (3–9) it appears that there is not much overlap between candidate variants/genes for the POSA and OSA development. In addition, these studies also revealed a high interpopulation variability that should be taken into account in the further research of these disorders. The low match in candidate genes for OSA between children and adults is to be expected since those diseases differ in their etiopathogenesis, clinical presentation as well as polysomnographic characteristics; there are also major differences in therapy approaches and possible consequences if left untreated (165).

Recently, Yoon et al. proposed a clinical guideline for application of multidisciplinary care in children with SRBD, emphasizing the importance of dentofacial interventions that target variable growth patterns (166). In the last years, craniofacial modification by orthodontic techniques is increasingly incorporated into the multidisciplinary management of SRBD in children and adolescents. In view of the multifactorial etiology of POSA, a better understanding of the risk factors contributing to its development may be useful not only for predicting the risk of POSA development but, even more importantly, for selecting the best therapeutic approach. Research of genetic predispositons to OSA in children as well as in adults may improve our understanding of the underlying biological mechanisms of susceptibility to these diseases.

6. Conclusion

Genetic background plays an important role in both POSA and craniofacial dysmorphisms. Therefore, genes associated with specific craniofacial features more common in patients suffering from POSA may be also considered candidate genes for this disease. We have reviewed a large body of literature and focused on the genes known to be involved in the development of cranio-facial syndromes with a high POSA prevalence. Based on the review, we chose 30 candidate genes for pediatric SRBD. Variants in seven of them (***FGFR1***, ***FGFR2***, ***FGFR3***, ***TWIST***, ***SOX9***, ***COL1A1***, and ***PHOX2B***) are known to play a role not only in syndrome development but also in skeletal malocclusions that are typical of pediatric orthodontic patients. Considering this, these seven genes appear to have the highest potential for targeted analysis of POSA risk in non-syndromic children.

Author contributions

ZMV: as an orthodontist specialized in sleep medicine, performed the literature search, co-wrote this review, and prepared the **Figure 1**. JK: critically reviewed the article from the perspective of a specialist in the morphology of the orofacial area and prepared the **Figure 1**. ZD and JZ: critically reviewed the article from the perspective of maxillofacial surgeons. AB and LIH: critically reviewed the article from the perspective of an orthodontist and pediatric dentist, respectively. JH: critically reviewed the article from the perspective of a specialist in craniofacial genetics and orthodontic treatment. PBL: as a specialist in molecular genetics and complex diseases, performed the literature search, co-wrote this review, and prepared **Figures 2**, **3**. All authors contributed to the article and approved the submitted version.

Funding

This research was supported by the Ministry of Health of the Czech Republic (grant no. NV17-30439A). All rights reserved. This work was supported by a project provided by the Faculty of Medicine Masaryk University Brno MUNI/A/1445/2021 and by a project provided by the University Hospital Brno, Ministry of Health of the Czech Republic – RVO (FNBr, 65269705). The study was created as part of an internal grant supported by the St. Anne's University Hospital Brno. This publication has received funding from the European Union's Horizon 2020 Research and Innovation Programme under grant agreement No. 857560. This publication reflects only the authoŕs view and the European Commission is not responsible for any use that may be made of the information it contains. Authors also thank the Research Infrastructure RECETOX RI (grant no LM2023069) and the project CETOCOEN EXCELLENCE (grant no CZ.02.1.01/0.0/0.0/17_043/0009632) financed by the Ministry of Education, Youth and Sports for supportive background. The article was supported by a grant from the Czech Orthodontic Society.

Conflict of interest

The authors declare that the research was conducted in the absence of any commercial or financial relationships that could be construed as a potential conflict of interest.

Publisher's note

Supplementary material

The Supplementary Material for this article can be found online at: https://www.frontiersin.org/articles/10.3389/fped.2023.1117493/full#supplementary-material

References

1. Xu Z, Wu Y, Tai J, Feng G, Ge W, Zheng L, et al. Risk factors of obstructive sleep apnea syndrome in children. *J Otolaryngol Head Neck Surg*. (2020) 49:11. doi: 10.1186/s40463-020-0404-1

2. Xiao L, Su S, Liang J, Jiang Y, Shu Y, Ding L. Analysis of the risk factors associated with obstructive sleep apnea syndrome in Chinese children. *Front Pediatr*. (2022) 10:1032. doi: 0.3389/fped.2022.900216

3. Cade BE, Chen H, Stilp AM, Gleason KJ, Sofer T, Ancoli-Israel S, et al. Genetic associations with obstructive sleep apnea traits in hispanic/latino Americans. *Am J Respir Crit Care Med*. (2016) 194:886–97. doi: 10.1164/rccm.201512-2431OC

4. Liu F, van der Lijn F, Schurmann C, Zhu G, Chakravarty MM, Hysi PG, et al. A genome-wide association study identifies five loci influencing facial morphology in Europeans. *PLoS Genet*. (2012) 8:e1002932. doi: 10.1371/journal.pgen.1002932

5. Veatch OJ, Bauer CR, Keenan BT, Josyula NS, Mazzotti DR, Bagai K, et al. Characterization of genetic and phenotypic heterogeneity of obstructive sleep apnea using electronic health records. *BMC Med Genomics*. (2020) 13:1–14. doi: 10.1186/s12920-020-00755-4

6. Quinlan CM, Chang X, March M, Mentch FD, Qu H-Q, Liu Y, et al. Identification of novel loci in obstructive sleep apnea in European American and African American children. *Sleep*. (2022). doi: 10.1093/sleep/zsac182

7. Gozal D, Khalyfa A, Capdevila OS, Kheirandish-Gozal L, Khalyfa AA, Kim J. Cognitive function in prepubertal children with obstructive sleep apnea: a modifying role for nadph oxidase P22 subunit gene polymorphisms? *Anttioxid Redox Signal*. (2012) 16:171–7. doi: 10.1089/ars.2011.4189

8. Bhushan B, Khalyfa A, Spruyt K, Kheirandish-Gozal L, Capdevila OS, Bhattacharjee R, et al. Fatty-acid binding protein 4 gene polymorphisms and

plasma levels in children with obstructive sleep apnea. *Sleep Med*. (2011) 12:666–71. doi: 10.1016/j.sleep.2010.12.014

9. Khalyfa A, Kheirandish-Gozal L, Capdevila OS, Bhattacharjee R, Gozal D. Macrophage migration inhibitory factor gene polymorphisms and plasma levels in children with obstructive sleep apnea. *Pediatric Pulmonol*. (2012) 47:1001–11. doi: 10.1002/ppul.22560

10. Taheri S, Mignot E. The genetics of sleep disorders. *Lancet Neurol*. (2002) 1:242–50. doi: 10.1016/s1474-4422(02)00103-5

11. Casale M, Pappacena M, Rinaldi V, Bressi F, Baptista P, Salvinelli F. Obstructive sleep apnea syndrome: from phenotype to genetic basis. *Curr Genomics*. (2009) 10:119–26. doi: 10.2174/138920209787846998

12. Gaultier C, Guilleminault C. Genetics, control of breathing, and sleep-disordered breathing: a review. *Sleep Med*. (2001) 2:281. doi: 10.1016/s1389-9457(01)00098-3

13. Redline S, Tishler PV. The genetics of sleep apnea. *Sleep Med Rev*. (2000) 4:583–602. doi: 10.1053/smrv.2000.0120

14. Johal A, Patel SI, Battagel JM. The relationship between craniofacial anatomy and obstructive sleep apnoea: a case-controlled study. *J Sleep Res*. (2007) 16:319–26. doi: 10.1111/j.1365-2869.2007.00599.x

15. Capistrano A, Cordeiro A, Capelozza Filho L, Almeida VC, Martinez S, Almeida-Pedrin R. Facial morphology and obstructive sleep apnea. *Dental Press J Orthod*. (2015) 20:60–7. doi: 10.1590/2177-6709.20.6.060-067.oar

16. Guilleminault C, Huang YS. From oral facial dysfunction to dysmorphism and the onset of pediatric OSA. *Sleep Med Rev*. (2018) 40:203–14. doi: 10.1016/j.smrv.2017.06.008

17. Canepa I, Elshebiny T, Valiathan M. OSA prevalence in a general pediatric craniofacial population. *J Dent Sleep Med*. (2019) 6. doi: 10.15331/jdsm.7084

18. Kim JH, Guilleminault C. The nasomaxillary complex, the mandible, and sleep-disordered breathing. *Sleep Breath*. (2011) 15:185–93. doi: 10.1007/s11325-011-0504-2

19. Hansen C, Markström A, Sonnesen L. Specific dento-craniofacial characteristics in non-syndromic children can predispose to sleep-disordered breathing. *Acta Paediatr*. (2022) 111:473–7. doi: 10.1111/apa.16202

20. Moore MH. Upper airway obstruction in the syndromal craniosynostoses. *Br J Plast Surg*. (1993) 46:355–62. doi: 10.1016/0007-1226(93)90039-e

21. Inverso G, Brustowicz K, Katz E, Padwa B. The prevalence of obstructive sleep apnea in symptomatic patients with syndromic craniosynostosis. *Int J Orral Maxillofac Surg*. (2016) 45:167–9. doi: 10.1016/j.ijom.2015.10.003

22. Lee Y-H, Huang Y-S, Chen I-C, Lin P-Y, Chuang L-C. Craniofacial, dental arch morphology, and characteristics in preschool children with mild obstructive sleep apnea. *J Dent Sci*. (2020) 15:193–9. doi: 10.1016/j.jds.2019.09.005

23. Katyal V, Pamula Y, Daynes CN, Martin J, Dreyer CW, Kennedy D, et al. Craniofacial and upper airway morphology in pediatric sleep-disordered breathing and changes in quality of life with rapid maxillary expansion. *Am J Orthod Dentofacial Orthop*. (2013) 144:860–71. doi: 10.1016/j.ajodo.2013.08.015

24. Tan H-L, Kheirandish-Gozal L, Abel F, Gozal D. Craniofacial syndromes and sleep-related breathing disorders. *Sleep Med Rev*. (2016) 27:74–88. doi: 10.1016/j.smrv.2015.05.010

25. Fagundes NCF, Gianoni-Capenakas S, Heo G, Flores-Mir C. Craniofacial features in children with obstructive sleep apnea: a systematic review and meta-analysis. *J Clin Sleep Med*. (2022) 18(7):1865–75. doi: 10.5664/jcsm.9904

26. Aroucha Lyra MC, Aguiar D, Paiva M, Arnaud M, Filho AA, Rosenblatt A, et al. Prevalence of sleep-disordered breathing and associations with malocclusion in children. *JJ Clin Sleep Med*. (2020) 16:1007–12. doi: 10.5664/jcsm.8370

27. Marino A, Malagnino I, Ranieri R, Villa MP, Malagola C. Craniofacial morphology in preschool children with obstructive sleep apnoea syndrome. *Eur J Paediatr Dent*. (2009) 10:181–4.

28. Caprioglio A, Zucconi M, Calori G, Troiani V. Habitual snoring, OSA and craniofacial modification. Orthodontic clinical and diagnostic aspects in a case control study. *Minerva Stomatol*. (1999) 48:125–37.

29. Kawashima S, Niikuni N, Chia-hung L, Takahasi Y, Kohno M, Nakajima I, et al. Cephalometric comparisons of craniofacial and upper airway structures in young children with obstructive sleep apnea syndrome. *Ear Nose Throat J*. (2000) 79:499–506. doi: 10.1177/014556130007900708

30. Zucconi M, Caprioglio A, Calori G, Ferini-Strambi L, Oldani A, Castronovo C, et al. Craniofacial modifications in children with habitual snoring and obstructive sleep apnoea: a case-control study. *Eur Respir J*. (1999) 13:411–7. doi: 10.1183/09031936.99.13241199

31. Pacheco MC, Fiorott BS, Finck NS, Araújo MT. Craniofacial changes and symptoms of sleep-disordered breathing in healthy children. *Dental Press J Orthod*. (2015) 20:80–7. doi: 10.1590/2176-9451.20.3.080-087.oar

32. Coban G, Buyuk SK. Sleep disordered breathing and oral health-related quality of life in children with different skeletal malocclusions. *Cranio*. (2022) 40:1–8. doi: 10.1080/08869634.2022.2080960

33. Huang YS, Guilleminault C. Pediatric obstructive sleep apnea and the critical role of oral-facial growth: evidences. *Front Neurol*. (2012) 3:184. doi: 10.3389/fneur.2012.00184

34. Lee RW, Sutherland K, Cistulli PA. Craniofacial morphology in obstructive sleep apnea: a review. *Clin Pulm Med*. (2010) 17:189–95. doi: 10.1097/CPM.0b013e3181e4bea7

35. Pirilä-Parkkinen K, Löppönen H, Nieminen P, Tolonen U, Pirttiniemi P. Cephalometric evaluation of children with nocturnal sleep-disordered breathing. *Eur J Orthod*. (2010) 32:662–71. doi: 10.1093/ejo/cjp162

36. Marcus CL. Pathophysiology of childhood obstructive sleep apnea: current concepts. *Respir Physiol*. (2000) 119:143–54. doi: 10.1093/ejo/cjp162

37. Edwards BA, Eckert DJ, Jordan AS. Obstructive sleep apnoea pathogenesis from mild to severe: is it all the same? *Respirology*. (2017) 22:33–42. doi: 10.1111/resp.12913

38. Yeom SW, Kim MG, Lee EJ, Chung SK, Kim DH, Noh SJ, et al. Association between septal deviation and OSA diagnoses: a nationwide 9-year follow-up cohort study. *J Clin Sleep Med*. (2021) 17:2099–106. doi: 10.5664/jcsm.9352

39. Pirilä-Parkkinen K, Pirttiniemi P, Nieminen P, Tolonen U, Pelttari U, Löppönen H. Dental arch morphology in children with sleep-disordered breathing. *Eur J Orthod*. (2009) 31:160–7. doi: 10.1093/ejo/cjn061

40. Guilleminault C, Akhtar F. Pediatric sleep-disordered breathing: new evidence on its development. *Sleep Med Rev*. (2015) 24:46–56. doi: 10.1016/j.smrv.2014.11.008

41. Guilleminault C, Huseni S, Lo L. A frequent phenotype for paediatric sleep apnoea: short lingual frenulum. *ERJ Open Res*. (2016) 2:00043-2016. doi: 10.1183/23120541.00043-2016

42. Villa MP, Evangelisti M, Barreto M, Cecili M, Kaditis A. Short lingual frenulum as a risk factor for sleep-disordered breathing in school-age children. *Sleep Med*. (2020) 66:119–22. doi: 10.1016/j.sleep.2019.09.019

43. Huang Y, Quo S, Berkowski J, Guilleminault C. Short lingual frenulum and obstructive sleep apnea in children. *Int J Pediatr Res*. (2015) 1:273. doi: 10.23937/2469-5769/1510003

44. Schweiger C, Manica D, Kuhl G. Glossoptosis. *Semin Pediatr Surg*. (2016) 25 (3):123–7. doi: 10.1053/j.sempedsurg.2016.02.002

45. Cielo CM, Marcus CL. Obstructive sleep apnoea in children with craniofacial syndromes. *Paediatr Respir Rev*. (2015) 16:189–96. doi: 10.1016/j.prrv.2014.11.003

46. Lam DJ, Jensen CC, Mueller BA, Starr JR, Cunningham ML, Weaver EM. Pediatric sleep apnea and craniofacial anomalies: a population-based case–control study. *Laryngoscope*. (2010) 120:2098–105. doi: 10.1002/lary.21093

47. Onodera K, Niikuni N, Chigono T, Nakajima I, Sakata H, Motizuki H. Sleep disordered breathing in children with achondroplasia. Part 2. relationship with craniofacial and airway morphology. *Int J Pediatr Otorhinolaryngol*. (2006) 70:453–61. doi: 10.1016/j.ijporl.2005.07.016

48. Vajo Z, Francomano CA, Wilkin DJ. The molecular and genetic basis of fibroblast growth factor receptor 3 disorders: the achondroplasia family of skeletal dysplasias, muenke craniosynostosis, and crouzon syndrome with acanthosis Nigricans. *Endocr Rev*. (2000) 21:23–39. doi: 10.1210/edrv.21.1.0387

49. Zaffanello M, Antoniazzi F, Tenero L, Nosetti L, Piazza M, Piacentini G. Sleep-disordered breathing in paediatric setting: existing and upcoming of the genetic disorders. *Ann Transl Med*. (2018) 6:343. doi: 10.21037/atm.2018.07.13

50. Carinci F, Pezzetti F, Locci P, Becchetti E, Carls F, Avantaggiato A, et al. Apert and crouzon syndromes: clinical findings, genes and extracellular matrix. *J Craniofac Surg*. (2005) 16:361–8. doi: 10.1097/01.scs.0000157078.53871.11

51. Lajeunie E, Heuertz S, El Ghouzzi V, Martinovic J, Renier D, Le Merrer M, et al. Mutation screening in patients with syndromic craniosynostoses indicates that a limited number of recurrent Fgfr2 mutations accounts for severe forms of pfeiffer syndrome. *Eur J Hum Genet*. (2006) 14:289–98. doi: 10.1038/sj.ejhg.5201558

52. Lin HY, Lin SP, Lin CC, Tsai LP, Chen MR, Chuang CK, et al. Polysomnographic characteristics in patients with prader–willi syndrome. *Pediatr Pulmonol*. (2007) 42:881–7. doi: 10.1002/ppul.20673

53. Sedky K, Bennett DS, Pumariega A. Prader willi syndrome and obstructive sleep apnea: co-occurrence in the pediatric population. *J Clin Sleep Med*. (2014) 10:403–9. doi: 10.5664/jcsm.3616

54. Akre H, Øverland B, Åsten P, Skogedal N, Heimdal K. Obstructive sleep apnea in treacher collins syndrome. *Eur Arch Otorhinolaryngol*. (2012) 269:331–7. doi: 10.1007/s00405-011-1649-0

55. Ma X, Forte AJ, Persing JA, Alonso N, Berlin NL, Steinbacher DM. Reduced three-dimensional airway volume is a function of skeletal dysmorphology in treacher collins syndrome. *Plast Reconstr Surg*. (2015) 135:382e–92e. doi: 10.1097/PRS.0000000000000993

56. Cistulli PA, Sullivan CE. Sleep apnea in marfan's syndrome: increased upper airway collapsibility during sleep. *Chest*. (1995) 108:631–5. doi: 10.1378/chest.108.3.631

57. De Coster P, Pauw GD, Martens L, De Paepe A. Craniofacial structure in marfan syndrome: a cephalometric study. *Am J Med Genet A*. (2004) 131:240–8. doi: 10.1002/ajmg.a.30393

58. Sedky K, Gaisl T, Bennett DS. Prevalence of obstructive sleep apnea in joint hypermobility syndrome: a systematic review and meta-analysis. *J Clin Sleep Med*. (2019) 15:293–9. doi: 10.5664/jcsm.7636

59. Robin P. Glossoptosis due to atresia and hypotrophy of the mandible. *Am J Dis Child*. (1934) 48:541–7.

60. Guilleminault C, Primeau M, Chiu HY, Yuen KM, Leger D, Metlaine A. Sleep-disordered breathing in Ehlers-Danlos syndrome: a genetic model of OSA. *Chest*. (2013) 144:1503–11. doi: 10.1378/chest.13-0174

61. Malfait F, Wenstrup RJ, De Paepe A. Clinical and genetic aspects of Ehlers-Danlos syndrome, classic type. *Genet Med*. (2010) 12:597–605. doi: 10.1097/GIM.0b013e3181eed412

62. da Fontoura CS, Miller SF, Wehby GL, Amendt BA, Holton NE, Southard TE, et al. Candidate gene analyses of skeletal variation in malocclusion. *J Dent Res*. (2015) 94:913–20. doi: 10.1177/0022034515581643

63. Hartsfield JK Jr, Morford LA, Jacob GJ, Kluemper GT. Genetic factors affecting facial morphology associated with sleep apnea.

64. Zhang Y, Blackwell EL, McKnight MT, Knutsen GR, Vu WT, Ruest LB. Specific inactivation of twist1 in the mandibular arch neural crest cells affects the development of the ramus and reveals interactions with Hand2. *Dev Dyn*. (2012) 241:924–40. doi: 10.1002/dvdy.23776

65. Cohen MM Jr. A new syndrome with hypotonia, obesity, mental deficiency, and facial, oral, ocular, and limb anomalies. *J Pediatr*. (1973) 83:280–4. doi: 10.1016/s0022-3476(73)80493-7

66. Chandler K, Kidd A, Al-Gazali L, Kolehmainen J, Lehesjoki A-E, Black GC, et al. Diagnostic criteria, clinical characteristics, and natural history of cohen syndrome. *J Med Genet*. (2003) 40:233–41. doi: 10.1136/jmg.40.4.233

67. Kurihara Y, Kurihara H, Suzuki H, Kodama T, Maemura K, Nagai R, et al. Elevated blood pressure and craniofaclal abnormalities in mice deficient in endothelin-1. *Nature*. (1994) 368:703–10. doi: 10.1038/368703a0

68. Todd ES, Weinberg SM, Berry-Kravis EM, Silvestri JM, Kenny AS, Rand CM, et al. Facial phenotype in children and young adults with Phox2b-determined congenital central hypoventilation syndrome: quantitative pattern of dysmorphology. *Pediatr Res*. (2006) 59:39–45. doi: 10.1203/01.pdr.0000191814.73340.1d

69. Berger KI, Fagondes SC, Giugliani R, Hardy KA, Lee KS, McArdle C, et al. Respiratory and sleep disorders in mucopolysaccharidosis. *J Inherit Metab Dis*. (2013) 36:201–10. doi: 10.1007/s10545-012-9555-1

70. Pal AR, Brown N, Jones SA, Bigger BW, Bruce IA. Obstructive sleep apnea in mps: a systematic review of pretreatment and posttreatment prevalence and severity. *J Inborn Errors Metab Screen*. (2019) 3:1–10. doi: 10.1177/2326409815616392

71. Afsharpaiman S, Saburi A, Waters KA. Respiratory difficulties and breathing disorders in achondroplasia. *Paediatr Respir Rev*. (2013) 14:250–5. doi: 10.1016/j.prrv.2013.02.009

72. Plomp RG, Bredero-Boelhouwer HH, Joosten KF, Wolvius EB, Hoeve HL, Poublon RM, et al. Obstructive sleep apnoea in treacher collins syndrome: prevalence, severity and cause. *Int J Oral Maxillofac Surg*. (2012) 41:696–701. doi: 10.1016/j.ijom.2012.01.018

73. Dahlqvist Å, Rask E, Rosenqvist C-J, Sahlin C, Franklin KA. Sleep apnea and down's syndrome. *Acta Otolaryngol*. (2003) 123:1094–7. doi: 10.1080/00016480310015362

74. Ng DK, Chan C-H. Obesity is an important risk factor for sleep disordered breathing in children with down syndrome. *Sleep*. (2004) 27:1023–4; author reply 5.

75. Churchill SS, Kieckhefer GM, Landis CA, Ward TM. Sleep measurement and monitoring in children with down syndrome: a review of the literature, 1960–2010. *Sleep Med Rev*. (2012) 16:477–88. doi: 10.1016/j.smrv.2011.10.003

76. Khayat A, Bin-Hassan S, Al-Saleh S. Polysomnographic findings in infants with pierre robin sequence. *Ann Thor Med*. (2017) 12:25–9. doi: 10.4103/1817-1737.197770

77. Domany KA, Hantragool S, Smith DF, Xu Y, Hossain M, Simakajornboon N. Sleep disorders and their management in children with Ehlers-Danlos syndrome referred to sleep clinics. *J Clin Sleep Med*. (2018) 14:623–9. doi: 10.5664/jcsm.7058

78. Stöberl AS, Gaisl T, Giunta C, Sievi NA, Singer F, Möller A, et al. Obstructive sleep apnoea in children and adolescents with Ehlers-Danlos syndrome. *Respiration*. (2019) 97:284–91. doi: 10.1159/000494328

79. Perkins JA, Sie KC, Milczuk H, Richardson MA. Airway management in children with craniofacial anomalies. *Cleft Palate- Craniofac J*. (1997) 34:135–40. doi: 10.1597/1545-1569_1997_034_0135_amicwc_2.3.co_2

80. Storm AL, Johnson JM, Lammer E, Green GE, Cunniff C. Auriculo-condylar syndrome is associated with highly Variable ear and mandibular defects in multiple kindreds. *Am J Med Genet A*. (2005) 138:141–5. doi: 10.1002/ajmg.a.30883

81. Wang A, Kun S, Diep B, Davidson Ward SL, Keens TG, Perez IA. Obstructive sleep apnea in patients with congenital central hypoventilation syndrome ventilated by diaphragm pacing without tracheostomy. *J Clin Sleep Med*. (2018) 14:261–4. doi: 10.5664/jcsm.6948

82. Abraham C, Virbalas J, DelRosso LM. Severe obstructive sleep apnea in a child with goldenhar syndrome and nasal obstruction. *J Clin Sleep Med*. (2017) 13:825–7. doi: 10.5664/jcsm.6626

83. Baugh A, Wooten W, Chapman B, Drake A, Vaughn B. Sleep characteristics in goldenhar syndrome. *Int J Pediatf Otorhinolaryngol*. (2015) 79:356–8. doi: 10.1016/j.ijporl.2014.12.024

84. Chan J, Edman JC, Koltai PJ. Obstructive sleep apnea in children. *Am Fam Physician*. (2004) 69:1147–54.

85. Kourelis K, Gouma P, Naxakis S, Kalogeropoulou C, Goumas P. Oculoauriculovertebral Complex with an atypical cause of obstructive sleep apnea. *Int J Pediatr Otorhinolaryngol*. (2009) 73:481–5. doi: 10.1016/j.ijporl.2008.11.004

86. Snead MP, Yates JR. Clinical and molecular genetics of stickler syndrome. *J Med Genet*. (1999) 36:353–9. doi: 10.1136/jmg.36.5.353

87. Miloro M. Mandibular distraction osteogenesis for pediatric airway management. *J Oral Maxillofac Surg*. (2010) 68:1512–23. doi: 10.1016/j.joms.2009.09.099

88. Kutkowska-Kaźmierczak A, Gos M, Obersztyn E. Craniosynostosis as a clinical and diagnostic problem: molecular pathology and genetic counseling. *J Appl Genet*. (2018) 59:133–47. doi: 10.1007/s13353-017-0423-4

89. Alsaadi MM, Iqbal SM, Elgamal EA, Salih MA, Gozal D. Sleep-disordered breathing in children with craniosynostosis. *Sleep Breath*. (2013) 17:389–93. doi: 10.1007/s11325-012-0706-2

90. Driessen C, Joosten KF, Bannink N, Bredero-Boelhouwer HH, Hoeve HL, Wolvius EB, et al. How does obstructive sleep apnoea evolve in syndromic craniosynostosis? A prospective cohort study. *Arch Dis Child*. (2013) 98:538–43. doi: 10.1136/archdischild-2012-302745

91. Wenger T, Miller D, Evans K. Fgfr craniosynostosis syndromes overview. In: Adam MP, Everman DB, Mirzaa GM, Pagon RA, Wallace SE, Bean LJH, editors. *Genereviews®*. Seattle, WA: University of Washington (1993).

92. Huang N, Pandey AV, Agrawal V, Reardon W, Lapunzina PD, Mowat D, et al. Diversity and function of mutations in P450 oxidoreductase in patients with Antley-Bixler syndrome and disordered steroidogenesis. *Am J Hum Genet*. (2005) 76:729–49. doi: 10.1086/429417

93. L'Hôte CG, Knowles MA. Cell responses to Fgfr3 signalling: growth, differentiation and apoptosis. *Exp Cell Res*. (2005) 304:417–31. doi: 10.1016/j.yexcr.2004.11.012

94. Horton WA, Lunstrum GP. Fibroblast growth factor receptor 3 mutations in achondroplasia and related forms of dwarfism. *Rev Endocr Metab Disord*. (2002) 3:381–5. doi: 10.1023/a:1020914026829

95. Azoury SC, Reddy S, Shukla V, Deng CX. Fibroblast growth factor receptor 2 (Fgfr2) mutation related syndromic craniosynostosis. *Int J Biol Sci*. (2017) 13:1479–88. doi: 10.7150/ijbs.22373

96. Crouzon O. Dysostose cranio-faciale hereditair. *Bull Mem Soc Med Hop Paris*. (1912) 33:545–55.

97. Tartaglia M, Di Rocco C, Lajeunie E, Valeri S, Velardi F, Battaglia PA. Jackson-Weiss syndrome: identification of two novel Fgfr2 missense mutations shared with crouzon and pfeiffer craniosynostotic disorders. *Hum Genet*. (1997) 101:47–50. doi: 10.1007/s004390050584

98. Slavotinek A, Crawford H, Golabi M, Tao C, Perry H, Oberoi S, et al. Novel Fgfr2 deletion in patient with beare-stevenson-like syndrome. *Am J Med Genet A*. (2009) 149:1814. doi: 10.1002/ajmg.a.32947

99. Bochukova EG, Roscioli T, Hedges DJ, Taylor IB, Johnson D, David DJ, et al. Rare mutations of Fgfr2 causing apert syndrome: identification of the first partial gene deletion, and an alu element insertion from a new subfamily. *Hum Mutat*. (2009) 30:204–11. doi: 10.1002/humu.20825

100. Boyadjiev SA, Consortium IC. Genetic analysis of non-syndromic craniosynostosis. *Orthod Craniofac Res*. (2007) 10:129–37. doi: 10.1111/j.1601-6343.2007.00393.x

101. Lattanzi W, Barba M, Di Pietro L, Boyadjiev SA. Genetic advances in craniosynostosis. *Am J Med Genet A*. (2017) 173:1406–29. doi: 10.1002/ajmg.a.38159

102. Johnson D, Wilkie AO. Craniosynostosis. *Eur J Hum Genet*. (2011) 19:369–76. doi: 10.1038/ejhg.2010.235

103. Bereza S, Yong R, Gronthos S, Arthur A, Ranjitkar S, Anderson PJ. Craniomaxillofacial morphology in a murine model of Ephrinb1 conditional deletion in osteoprogenitor cells. *Arch I Oral Biol*. (2022) 137:105389. doi: 10.1016/j.archoralbio.2022.105389

104. Morriss-Kay GM, Wilkie AO. Growth of the normal skull vault and its alteration in craniosynostosis: insights from human genetics and experimental studies. *J Anat*. (2005) 207:637–53. doi: 10.1111/j.1469-7580.2005.00475.x.

105. Cornille M, Moriceau S, Khonsari RH, Heuzé Y, Loisay L, Boitez V, et al. Fgfr3 overactivation in the brain is responsible for memory impairments in crouzon syndrome mouse model. *J Exp Med*. (2022) 219. doi: 10.1084/jem.20201879

106. Bellus GA, McIntosh I, Smith EA, Aylsworth AS, Kaitila I, Horton WA, et al. A recurrent mutation in the tyrosine kinase domain of fibroblast growth factor receptor 3 causes hypochondroplasia. *Nat Genet*. (1995) 10:357–9. doi: 10.1038/ng0795-357

107. Khominsky A, Yong R, Ranjitkar S, Townsend G, Anderson PJ. Extensive phenotyping of the orofacial and dental complex in crouzon syndrome. *Arch Oral Biol*. (2018) 86:123–30. doi: 10.1016/j.archoralbio.2017.10.022

108. Legare JM, Pauli RM, Hecht JT, Bober MB, Smid CJ, Modaff P, et al. Clarity: co-occurrences in achondroplasia—craniosynostosis, seizures, and decreased risk of diabetes mellitus. *Am J Med Genet A*. (2021) 185:1168–74. doi: 10.1002/ajmg.a.62096

109. van der Burgt I. Noonan syndrome. *Orphanet J Rare Dis*. (2007) 2:4. doi: 10.1186/1750-1172-2-4

110. Neel BG, Gu H, Pao L. The 'Shp'ing news: Sh2 domain-containing tyrosine phosphatases in cell signaling. *Trends Bochem Sci*. (2003) 28:284–93. doi: 10.1016/S0968-0004(03)00091-4

111. Allanson JE. Noonan syndrome. *J Med Genet*. (1987) 24:9. doi: 10.1136/jmg.24.1.9

112. Cardiel Ríos SA. Correction of a severe class ii malocclusion in a patient with noonan syndrome. *Am J Orthod Dentofacial Orthop*. (2016) 150:511–20. doi: 10.1016/j.ajodo.2015.09.032

113. Ueda K, Yaoita M, Niihori T, Aoki Y, Okamoto N. Craniosynostosis in patients with rasopathies: accumulating clinical evidence for expanding the phenotype. *Am J Med Genet A*. (2017) 173:2346–52. doi: 10.1002/ajmg.a.38337

114. Takenouchi T, Sakamoto Y, Miwa T, Torii C, Kosaki R, Kishi K, et al. Severe craniosynostosis with noonan syndrome phenotype associated with Shoc2 mutation: clinical evidence of crosslink between Fgfr and Ras signaling pathways. *Am J Med Genet A*. (2014) 164a:2869–72. doi: 10.1002/ajmg.a.36705

115. Addissie YA, Kotecha U, Hart RA, Martinez AF, Kruszka P, Muenke M. Craniosynostosis and noonan syndrome with kras mutations: expanding the phenotype with a case report and review of the literature. *Am J Med Genet A*. (2015) 167a:2657–63. doi: 10.1002/ajmg.a.37259

116. Li H, Zhao A, Xie M, Chen L, Wu H, Shen Y, et al. Antley-Bixler syndrome arising from compound heterozygotes in the P450 oxidoreductase gene: a case report. *Transl Pediatr*. (2021) 10:3309–18. doi: 10.21037/tp-21-499

117. Garrido E, Cormand B, Hopwood JJ, Chabás A, Grinberg D, Vilageliu L. Maroteaux-Lamy syndrome: functional characterization of pathogenic mutations and polymorphisms in the arylsulfatase B gene. *Mol Genet Metab*. (2008) 94:305–12. doi: 10.1016/j.ymgme.2008.02.012

118. Kwon YS, Jo JK, Lim YH, Yon JH, Kim KM. Anesthetic management of a neonate with Antley-Bixler syndrome: a case report. *Anesth Pain Med*. (2011) 6:89–92.

119. Antley R. Trapezoidocephaly, midfacial hypoplasia and cartilage abnormalities with multiple synostoses and skeletal fractures. *Birth Defects Orig Artic Ser*. (1975) 11:397–401.

120. Benko S, Fantes JA, Amiel J, Kleinjan D-J, Thomas S, Ramsay J, et al. Highly conserved non-coding elements on either side of Sox9 associated with pierre robin sequence. *Nat Genet*. (2009) 41:359–64. doi: 10.1016/j.prrv.2014.11.003

121. Tarasiuk A, Levi A, Assadi MH, Troib A, Segev Y. Orexin plays a role in growth impediment induced by obstructive sleep breathing in rats. *Sleep*. (2016) 39:887–97. doi: 10.5665/sleep.5648

122. Gordon CT, Attanasio C, Bhatia S, Benko S, Ansari M, Tan TY, et al. Identification of novel craniofacial regulatory domains located far upstream of sox 9 and disrupted in pierre robin sequence. *Hum Mutat*. (2014) 35:1011–20. doi: 10.1002/humu.22606

123. Dash S, Bhatt S, Falcon K, Sandell L, Trainor P. Med23 regulates Sox9 expression during craniofacial development. *J Dent Res*. (2021) 100:406–14. doi: 10.1177/0022034520969109

124. Jia Z-L, He S, Jiang S-Y, Zhang B-H, Duan S-J, Shi J-Y, et al. Rs12941170 at Sox9 gene associated with orofacial clefts in Chinese. *Arch Oral Biol*. (2017) 76:14–9. doi: 10.1016/j.archoralbio.2016.12.010

125. Shung C-Y, Ota S, Zhou Z-Q, Keene DR, Hurlin PJ. Disruption of a Sox9–*B*-catenin circuit by mutant Fgfr3 in thanatophoric dysplasia type ii. *Hum Mol Genet*. (2012) 21:4628–44. doi: 10.1093/hmg/dds305

126. Zhou Z-Q, Ota S, Deng C, Akiyama H, Hurlin PJ. Mutant activated Fgfr3 impairs endochondral bone growth by preventing Sox9 downregulation in differentiating chondrocytes. *Hum Mol Genet*. (2015) 24:1764–73. doi: 10.1093/hmg/ddu594

127. Gordon CT, Petit F, Kroisel PM, Jakobsen L, Zechi-Ceide RM, Oufadem M, et al. Mutations in endothelin 1 cause recessive auriculocondylar syndrome and dominant isolated question-mark ears. *Am J Hum Genet*. (2013) 93:1118–25. doi: 10.1016/j.ajhg.2013.10.023

128. Timberlake AT, Griffin C, Heike CL, Hing AV, Cunningham ML, Chitayat D, et al. Haploinsufficiency of Sf3b2 causes craniofacial microsomia. *Nat Commun*. (2021) 12:1–11. doi: 10.1038/s41467-021-24852-9

129. Tingaud-Sequeira A, Trimouille A, Sagardoy T, Lacombe D, Rooryck C. Oculo-auriculo-vertebral spectrum: new genes and literature review on a complex disease. *J Med Genet*. (2022) 59:417–27. doi: 10.1136/jmedgenet-2021-108219

130. Sakai D, Trainor PA. Treacher collins syndrome: unmasking the role of Tcof1/treacle. *Int J Biochem Cell Biol*. (2009) 41:1229–32. doi: 10.1016/j.biocel.2008.10.026

131. Chen Y, Guo L, Li C-L, Shan J, Xu H-S, Li J-Y, et al. Mutation screening of Chinese treacher collins syndrome patients identified novel Tcof1 mutations. *Mol Genet Genomics*. (2018) 293:569–77. doi: 10.1007/s00438-017-1384-3

132. Van Camp N, Aerden T, Politis C. Problems in the orofacial region associated with Ehlers-Danlos and marfan syndromes: a case series. *Br J Oral Maxillofac Surg*. (2020) 58:208–13. doi: 10.1016/j.bjoms.2019.11.018

133. Van Damme T, Colman M, Syx D, Malfait F. The Ehlers-Danlos syndromes against the backdrop of inborn errors of metabolism. *Genes*. (2022) 13:265. doi: 10.3390/genes13020265

134. Topârcean AM, Acatrinei A, Rusu I, Mircea C, Feştilă D, Lucaciu OP, et al. Preliminary data regarding the influence of the collal Rs2249492 polymorphism on the risk of malocclusion in the Romanian population. *Studia Universitatis Babes-Bolyai, Biologia*. (2021) 66.

135. Melkoniemi M, Koillinen H, Männikkö M, Warman ML, Pihlajamaa T, Kääriäinen H, et al. Collagen Xi sequence variations in nonsyndromic cleft palate, robin sequence and micrognathia. *Eur J Hum Genet*. (2003) 11:265–70. doi: 10.1038/sj.ejhg.5200950

136. Loeys B, De Backer J, Van Acker P, Wettinck K, Pals G, Nuytinck L, et al. Comprehensive molecular screening of the Fbn1 gene favors locus homogeneity of classical marfan syndrome. *Hum Mutat*. (2004) 24:140–6. doi: 10.1002/humu.20070

137. Docimo R, Maturo P, D'Auria F, Grego S, Costacurta M, Perugia C, et al. Association between oro-facial defects and systemic alterations in children affected by marfan syndrome. *J Clin Diagn Res*. (2013) 7:700–3. doi: 10.7860/JCDR/2013/5656.2885

138. Du Q, Zhang D, Zhuang Y, Xia Q, Wen T, Jia H. The molecular genetics of marfan syndrome. *Int J Med Sci*. (2021) 18:2752–66. doi: 10.7150/ijms.60685

139. Heldin CH, Landström M, Moustakas A. Mechanism of Tgf-beta signaling to growth arrest, apoptosis, and epithelial-mesenchymal transition. *Curr Opin Cell Biol*. (2009) 21:166–76. doi: 10.1016/j.ceb.2009.01.021

140. Frazier BC, Mooney MP, Losken HW, Barbano T, Moursi A, Siegel MI, et al. Comparison of craniofacial phenotype in craniosynostotic rabbits treated with anti–Tgf-*B*2 at suturectomy site. *Cleft Palate Craniofac J*. (2008) 45:571–82. doi: 10.1597/07-095.1

141. Sanford LP, Ormsby I, Gittenberger-de Groot AC, Sariola H, Friedman R, Boivin GP, et al. Tgfbeta2 knockout mice have multiple developmental defects that are non-overlapping with other Tgfbeta knockout phenotypes. *Development*. (1997) 124:2659–70. doi: 10.1242/dev.124.13.2659

142. Limoge F, Faivre L, Gautier T, Petit JM, Gautier E, Masson D, et al. Insulin response dysregulation explains abnormal fat storage and increased risk of diabetes Mellitus type 2 in cohen syndrome. *Hum Mol Genet*. (2015) 24:6603–13. doi: 10.1093/hmg/ddv366

143. Duplomb L, Duvet S, Picot D, Jego G, El Chehadeh-Djebbar S, Marle N, et al. Cohen syndrome is associated with major glycosylation defects. *Hum Mol Genet*. (2014) 23:2391–9. doi: 10.1093/hmg/ddt630

144. Irizarry KA, Miller M, Freemark M, Haqq AM. Prader willi syndrome: genetics, metabolomics, hormonal function, and new approaches to therapy. *Adv Pediatr*. (2016) 63:47. doi: 10.1016/j.yapd.2016.04.005

145. Oeffner F, Korn T, Roth H, Ziegler A, Hinney A, Goldschmidt H, et al. Systematic screening for mutations in the human necdin gene (Ndn): identification of two naturally occurring polymorphisms and association analysis in body weight regulation. *Int J Obes Relat Metab Disord*. (2001) 25:767–9. doi: 10.1038/sj.ijo.0801626

146. Wong SB, Zhao LL, Chuang SH, Tsai WH, Yu CH, Tsai LP. Is prone sleeping dangerous for neonates? Polysomnographic characteristics and Ndn gene analysis. *Ci Ji Yi Xue Za Zhi*. (2019) 31:113–7. doi: 10.4103/tcmj.tcmj_29_18

147. Gómez-González A, Rosales-Berber MÁ, Ávila-Rojas D, Pozos-Guillén A, Garrocho-Rangel A. Pediatric dental management of an uncommon case of mucopolysaccharidosis type iv a (morquio a syndrome): a case report of a three-year follow-up. *Case Rep Dent*. (2020) 2020. doi: 10.1155/2020/2565486

148. de Almeida-Barros RQ, de Medeiros PFV, de Almeida Azevedo MQ, de Oliveira Lira Ortega A, Yamamoto ATA, Dornelas SKL, et al. Evaluation of oral manifestations of patients with mucopolysaccharidosis iv and vi: clinical and imaging study. *Clin Oral Investig*. (2018) 22:201–8. doi: 10.1007/s00784-017-2100-8

149. Yadav P. Morquio syndrome from a Dentist's aspect.

150. Guimarães M, Farias S, Costa A, Amorim R. Maroteaux-Lamy syndrome: orofacial features after treatment by bone marrow transplant. *Oral Health Prev Dent*. (2010) 8:139–42.

151. Galdzicka M, Patnala S, Hirshman M, Cai J-F, Nitowsky H, Egeland J, et al. A new gene, Evc2, is mutated in Ellis–Van creveld syndrome. *Mol Genet Metab*. (2002) 77:291–5. doi: 10.1016/s1096-7192(02)00178-6

152. Ruiz-Perez VL, Ide SE, Strom TM, Lorenz B, Wilson D, Woods K, et al. Mutations in a new gene in Ellis-Van creveld syndrome and weyers acrodental dysostosis. *Nat Genet*. (2000) 24:283–6. doi: 10.1038/73508

153. Valencia M, Lapunzina P, Lim D, Zannolli R, Bartholdi D, Wollnik B, et al. Widening the mutation spectrum of Evc and Evc2: ectopic expression of weyer variants in Nih 3t3 fibroblasts disrupts hedgehog signaling. *Hum Mutat*. (2009) 30:1667–75. doi: 10.1002/humu.21117

154. Lavezzi AM, Casale V, Oneda R, Gioventù S, Matturri L, Farronato G. Obstructive sleep apnea syndrome (osas) in children with class iii malocclusion: involvement of the Phox2b gene. *Sleep Breath*. (2013) 17:1275–80. doi: 10.1007/s11325-013-0833-4

155. Mainieri G, Montini A, Nicotera A, Di Rosa G, Provini F, Loddo G. The genetics of sleep disorders in children: a narrative review. *Brain Sci*. (2021) 11:1259. doi: 10.3390/brainsci11101259

156. Larkin EK, Patel SR, Goodloe RJ, Li Y, Zhu X, Gray-McGuire C, et al. A candidate gene study of obstructive sleep apnea in European Americans and

African Americans. *Am J Respir Crit Care Med*. (2010) 182:947–53. doi: 10.1164/rccm.201002-0192OC

157. Chi L, Comyn F-L, Keenan BT, Cater J, Maislin G, Pack AI, et al. Heritability of craniofacial structures in normal subjects and patients with sleep apnea. *Sleep*. (2014) 37:1689–98. doi: 10.5665/sleep.4082

158. Tiro A, Dzemidzic V, Salaga-Nefic S, Redzic I, Nakas E. Heritability of craniofacial characteristics in twins-cephalometric study. *Med Arch*. (2019) 73:205. doi: 10.5455/medarh.2019.73.205-208

159. Šešelj M, Duren DL, Sherwood RJ. Heritability of the human craniofacial Complex. *Anat Rec*. (2015) 298:1535–47. doi: 10.1002/ar.23186

160. Mathur R, Douglas NJ. Family studies in patients with the sleep apnea-hypopnea syndrome. *Ann Intern Med*. (1995) 122:174–8. doi: 10.7326/0003-4819-122-3-199502010-00003

161. Paternoster L, Zhurov AI, Toma AM, Kemp JP, St Pourcain B, Timpson NJ, et al. Genome-wide association study of three-dimensional facial morphology identifies a variant in Pax3 associated with nasion position. *Am J Hum Genet*. (2012) 90:478–85. doi: 10.1016/j.ajhg.2011.12.021

162. Bjork BC, Turbe-Doan A, Prysak M, Herron BJ, Beier DR. Prdm16 is required for normal palatogenesis in mice. *Hum Mol Genet*. (2010) 19:774–89. doi: 10.1093/hmg/ddp543

163. Warner DR, Horn KH, Mudd L, Webb CL, Greene RM, Pisano MM. Prdm16/Mel1: a novel smad binding protein expressed in murine embryonic orofacial tissue. *Biochim Biophys Acta*. (2007) 1773:814–20. doi: 10.1016/j.bbamcr.2007.03.016

164. Robinson PN, Arteaga-Solis E, Baldock C, Collod-Béroud G, Booms P, De Paepe A, et al. The molecular genetics of marfan syndrome and related disorders. *J Med Genet*. (2006) 43:769–87. doi: 10.1136/jmg.2005.039669

165. Katz ES, Marcus CL. Obstructive sleep apnea: children versus adults. In: Pack AI, editor. *Sleep apnea*. Boca Raton: CRC Press (2016). p. 382–410.

166. Yoon A, Gozal D, Kushida C, Pelayo R, Liu S, Faldu J, et al. A roadmap of craniofacial growth modification for children with sleep disordered breathing: a multidisciplinary proposal. *Sleep*. (2023) 46:zsad095.

frontiers | Frontiers in Genetics

TYPE Case Report
PUBLISHED 18 October 2023
DOI 10.3389/fgene.2023.1150613

OPEN ACCESS

EDITED BY
Weimin Lin,
Sichuan University, China

REVIEWED BY
Dominique Bremond-Gignac,
Hôpital Necker-Enfants Malades, France
Hala El-Bassyouni,
National Research Centre, Egypt

*CORRESPONDENCE
Yi Wang,
wangyieye@126.com

RECEIVED 24 January 2023
ACCEPTED 15 September 2023
PUBLISHED 18 October 2023

CITATION
Zhou J, Wang Y, Zhang Y, You D and Wang Y (2023), Case report: ADULT syndrome: a rare case of congenital lacrimal duct abnormality.
Front. Genet. 14:1150613.
doi: 10.3389/fgene.2023.1150613

Case report: ADULT syndrome: a rare case of congenital lacrimal duct abnormality

Jichao Zhou[1], Yuchen Wang[1], Yinghong Zhang[2], Debo You[1] and Yi Wang[1]*

[1]Department of Ophthalmology, Peking University Third Hospital, Beijing Key Laboratory of Restoration of Damaged Ocular Nerve, Peking University Third Hospital, Beijing, China, [2]Department of Otolaryngology, Peking University Third Hospital, Beijing Key Laboratory of Restoration of Damaged Ocular Nerve, Peking University Third Hospital, Beijing, China

Acro-dermato-ungual-lacrimal-tooth (ADULT) syndrome is a rare autosomal dominant inherited disease caused due to mutations in the *TP63* gene. More commonly, mutations in the *TP63* gene result in ectodermal dysplasia and/or orofacial cleft. ADULT syndrome is a type of ectoderm-related tissue dysplasia. This case report describes a patient with chronic tearing, congenital atresia, and obstruction of the lacrimal ducts, which are the main clinical manifestations of ADULT syndrome. This patient also presented with some clinical manifestations that were different from those of ADULT syndrome, namely, mild eyelid fusion and abnormal development of the fifth finger (a stiff fifth finger with camptodactyly that was shortened in length). The gene mutation in this patient was also at a site different from those usually reported in the literature. In this patient, c.518G > T resulted in p. G173V (accession number: NM_003722; exon4). We performed successful dacryocystorhinostomy and artificial lacrimal duct implantation. As shown above, we discussed the clinical characteristics and genetics of the disease in detail. In sharing this case, we aim to contribute to the current understanding of the genes and clinical manifestations of ADULT syndrome and to assist clinicians in the clinical diagnosis of *TP63* mutation-related diseases.

KEYWORDS

TP63 gene, ADULT syndrome, congenital nasolacrimal duct obstruction, ectodermal dysplasia, dacryocystorhinostomy

Introduction

The presence of epiphora early in life is recognized as congenital nasolacrimal duct obstruction, with an incidence ranging from 5% to 20% (Petris and Liu, 2017). When considered as a single disease, obstruction is most often caused by a membrane at the end of the nasolacrimal duct called the valve of Hasner; this manifestation accounts for 73% of this disease, and 96% of the obstructions caused by the valve of Hasner resolve spontaneously (CASSADY, 1952). However, when congenital nasolacrimal duct obstruction or atresia is associated with dysplasia of other systemic organs, ectodermal dysplasia is often suspected. Acro-dermato-ungual-lacrimal-tooth (ADULT) syndrome is a common congenital disease associated with dysplasia of the lacrimal duct. It is a rare autosomal dominant genetic disease, first described in 1993, and is a type of ectodermal dysplasia. Other forms of ectodermal dysplasia include (Rinne et al., 2007) ankyloblepharon-ectodermal dysplasia-clefting syndrome (AEC), limb mammary syndrome (LMS), Rapp–Hodgkin syndrome (RHS), split-hand/split-foot malformation (SHFM), and ectrodactyly ectodermal dysplasia-cleft

lip/palate syndrome (EEC). These ectodermal dysplasia types, including ADULT syndrome, are associated with mutations in the *TP63* gene (Avitan-Hersh et al., 2010; Prontera et al., 2011), which has a critical role in embryonic development, especially in the development of the limbs, ectodermal tissues, such as hair, skin, teeth, nails, and mammary glands. ADULT syndrome is characterized by sparse hair on the scalp and the axilla, lacrimal duct stenosis or atresia, onychodysplasia, hypodontia or the early loss of permanent teeth, athelia or hypoplastic nipples, and breast hypoplasia (Chan et al., 2004; Slavotinek et al., 2005). Some of the features of ADULT syndrome overlap with those of the other five types (mentioned above) of ectodermal dysplasia. The literature

TABLE 1 Clinical features noted in the affected family members.

		TP63 mutation syndromes		
		Proband	Mother	Brother
Sex		Female	Female	Male
Age		16	50	5
Ectodermal	Teeth	√	√	√
	Skin	√	√	√
	Hair	√	√	√
	Nails	√	√	√
	Lacrimal ducts	√	√	√
	Breasts	√	√	√
	Sweat glands	-	-	-
Fused eyelids		√	-	-
Ectrodactyly		-	-	-
Ccenter lip and palate		-	-	-
Others		-	-	-

√ The clinical manifestations were observed, - The clinical manifestations were not observed.

FIGURE 1
The eyes of the patient **(A)** The clinical appearance of the eyes. **(B)** The enlargement around the lower lacrimal tubules. **(C)** Absence of the upper puncta and closure of lower puncta.

FIGURE 2
Orofacial and mammary glands' features of the patient **(A)** Facial phenotype of the proband with sparse eyebrows with tattooing, absent eyelashes, small ears, and a hooked nose. **(B)** Sparse brown hair, especially in the front of her scalp. **(C)** A hollow facial appearance. **(D)** Dental abnormalities including hypodontia or oligodontia and conically shaped teeth. **(E, F)** Absent mammary glands with bilateral hypoplastic nipples.

suggests that frequently mutated amino acids including R298Q, R298G, R243W, R227Q, P127L, R337Q, V114M and N6H, may be involved in ADULT syndrome (Slavotinek et al., 2005; Berk et al., 2012). In this report, we describe a patient with ADULT syndrome associated with a rare mutation of the *TP63* gene and atypical clinical features including mild symblepharon and a shortened, stiff fifth finger with camptodactyly.

Case report

A 16-year-old Chinese female was referred to our hospital because of epiphora. The patient had experienced continuous and excessive production of tears without any stimuli since childhood, and there has been no significant change over the past 10 years. Over the last 4 years, she experienced sustained swelling, mild tenderness, and a detectable local mass on the right inner canthus that progressively enlarged. The ocular skin became dark and dull, and excessive tearing persisted. The patient's personal and menstrual history were normal. Both the patient and her parents did not have any significant medical history, including history of carcinomas. Moreover, the patient's mother and brother also presented with similar features including abnormal hair, nails, teeth, skin, and lacrimal ducts (Table 1). On clinical examination, the patient demonstrated the following features. The puncta were stenotic and bilaterally covered with a membrane. As a result, probing of the nasolacrimal duct was not possible on either side. Thus, aplasia of both lacrimal ducts with chronic tear production and the expansion of the obstructed lacrimal ducts leading to local enlargement around the lower lacrimal tubules were assumed. Furthermore, mild fused lower eyelids were evident.

On physical examination, the following features were observed. (1) Skin: sweaty, pale, and without freckles; (2) Hair: brown and sparse, especially in the front of her scalp; (3) Oral cavity: conical teeth and hypodontia or oligodontia; (4) Nose and ears: small ears and a hooked nose; (5) Mammary glands: absent and bilateral hypoplastic nipples; (6) Hands: brachydactyly, which was most prominent in her fifth fingers, and bilateral fifth finger clinodactyly and camptodactyly; (7) Nails: discolored and irregularly shaped, with short and dystrophic nail plates and horizontal grooves along the length of the nails (Figures 1–3).

After obtaining written informed consent from the patient and her parents, peripheral blood samples were collected. Whole-exome sequencing was performed to screen for candidate mutations. Called mutations were validated using Sanger sequencing. We identified a heterozygous G>T transition at cDNA position 518 of *TP63* (accession number: NM_003722; exon4; OMIM number 103285) (Figure 4). This mutation is predicted to result in amino acid substitution p. G173V, and

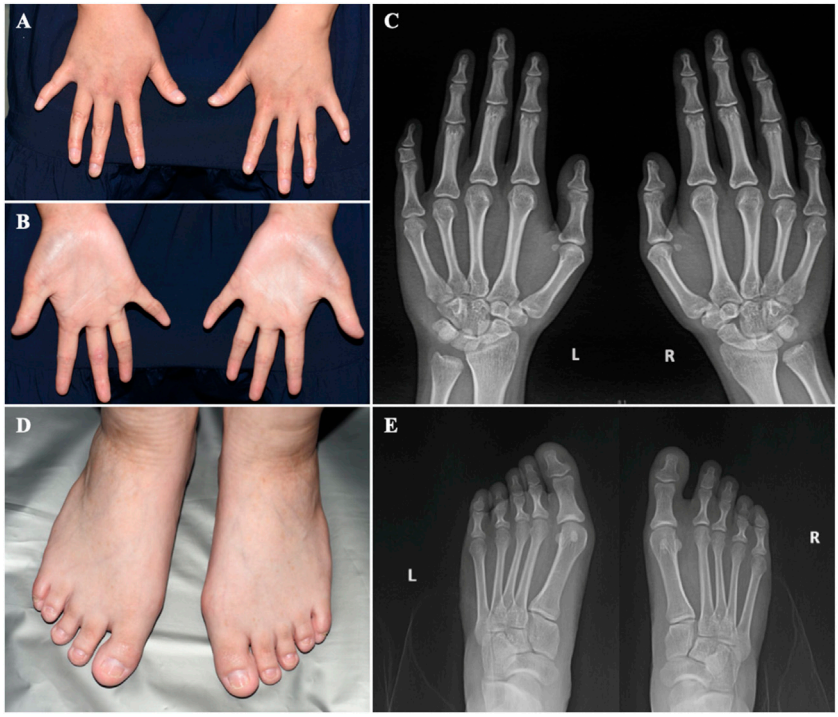

FIGURE 3
The hands and feet of the patient **(A)** Bilateral clinodactyly of the fifth finger. **(B)** Palmar hyperlinearity. **(C)** Radiograph of the hands showing clinodactyly of the fifth fingers. **(D)** Dystrophic nail plates and horizontal grooves along the length of the nails. **(E)** Radiograph of the feet.

its functional effect, analyzed by two prediction tools (SIFT and PolyPhen), was predicted to be deleterious, thus supporting its pathogenicity. In the literature, mutation at cDNA position 518 has been previously reported (Chan et al., 2004) in a patient with ADULT syndrome, with cleft lip and palate. However, the transverse changes of the amino acids in that case were different from those in our patient. To the best of our knowledge, this is the first reported clinical variation of ADULT syndrome with a rare mutation, distinguished by the clinical manifestation of symblepharon and camptodactyly. After confirming the diagnosis, the patient's chronic epiphora was addressed via binocular dacryocystorhinostomy under general anesthesia, during which artificial tear ducts were placed to drain the tears, and the enlarged lacrimal duct was removed. The surgery was successful, and the patient showed no lacrimal abnormalities on follow-up (Figure 5).

Discussion

The *TP63* gene is highly expressed in the nuclei of the basal cells of the skin, cervix, tongue, mucosa, esophagus, mammary glands, prostate, and urothelium (Rinne et al., 2007). A crucial transcriptional regulator factor, *p63* is often expressed in the epithelial and mesenchymal tissues (Otsuki et al., 2020). It is expressed very early during embryogenesis and epidermal development and plays an essential role in the induction of the ectoderm and the orofacial, limb, and epidermal stratification processes. Moreover, the expression of P-cadherin, which is regulated by *p63*, acts as a critical regulator of hair development. Previous studies have confirmed that the normal expression of *p63* can inhibit the terminal differentiation of keratinocytes, which contributes to maintaining the proliferative potential of the basal cell layer and promoting its formation and integrity (Avitan-Hersh et al., 2010). In view of this, *in vitro* experiments performed in 1999 confirmed that *TP63* gene knockout mice developed ectodermal developmental defects, such as limb defects and the loss of the prostate, mammary glands, epidermis, and other related tissues (Wang et al., 2009). These features were representative of defective ectodermal stem cells and were consistent with the physiological functions of the *TP63* gene (Rinne et al., 2007). Since then, syndromes associated with *TP63* mutations have been recognized in multiple reports, including the AEC, LMS, ADULT, RHS, SHFM, and EEC. The specific clinical manifestations of these six diseases are summarized in Table 2 (Duijf et al., 2002; Rinne et al., 2006a; Rinne et al., 2006b; Rinne et al., 2007; Otsuki et al., 2016).

Our patient presented with clinical features of ectodermal dysplasia, with sparse hair, dystrophic nails, small teeth, oligodontia (11 teeth left), lacrimal duct stenosis, and hypoplastic nipples. These clinical features are observed in different syndromes. For EEC, orofacial cleft and ectrodactyly are typical manifestations. In contrast, cleft lip and palate are typically not detected in ADULT syndrome. Hence, this feature can be used to distinguish EEC from ADULT syndrome. On the contrary, it is difficult to distinguish between LMS and ADULT syndrome. LMS also manifests as a form of ectodermal dysplasia with oligodontia, lacrimal atresia, and nail dystrophy, in addition to abnormal development of the mammary glands and hypoplastic nipples. These findings may render a definitive diagnosis challenging. However, most patients with ADULT syndrome present with ectrosyndactylia and hair and skin abnormalities that have not been reported in LMS, and thus, these features may assist with

10.3389/fgene.2023.1150613

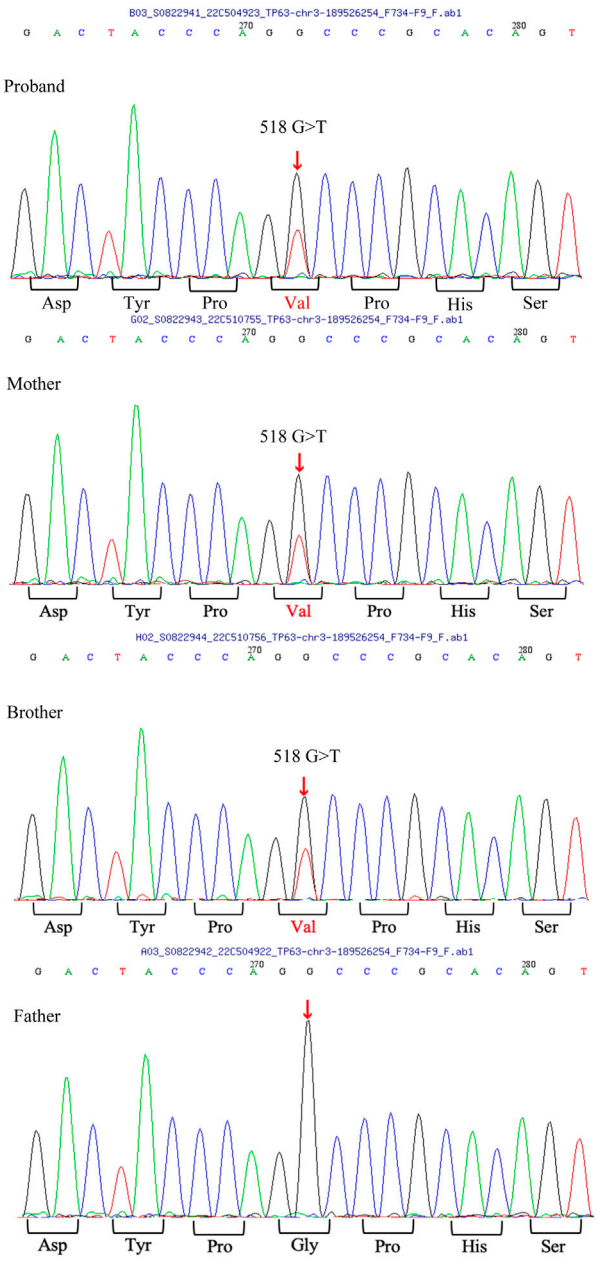

FIGURE 4
TP63 mutation analysis A heterozygous G>T transition at cDNA position 518 of the *TP63* gene is found in the patient, as well as in her mother and brother.

diagnosis. Moreover, our patient had mild symblepharon that can also be observed in AEC, as well as ectodermal-related manifestations, which led us to suspect that the patient may have AEC. However, according to a literature review (Slavotinek et al., 2005; Kawasaki de Araujo et al., 2017), cleft lip and palate are characteristic of most patients with AEC, and more than half of all patients with AEC have hearing impairment and urinary system diseases, which were not consistent with the presentation of our patient. Furthermore, AEC is not typically associated with abnormal limb development. Hence, our patient, with her shortened fifth fingers, was suspected to have ADULT syndrome. Clinically, the six diseases mentioned above share some common manifestations. However, they have different gene inheritance patterns and also some relatively unique features (Rinne et al., 2006a; Rinne et al., 2006b; Rinne et al., 2007).

The literature suggests that the most common site of mutation of the *TP63* gene is the DNA binding region, due to a missense point mutation, resulting in the substitution of arginine 298 by glycine or glutamine. *In vitro* experiments (Chan et al., 2004) confirmed that R298 is not adjacent to the DNA binding domain. Therefore, the mutation of amino acid 298 does not lead to any adverse effects, but results in high transactivation activities of ΔN-p63γ, which may be 25% higher than those of wild-type *p63* (Duijf et al., 2002). Missense point mutations in exon 3 can result in the substitution of p. N6H (asparagine to histidine), ultimately resulting in ADULT syndrome. N6H is in the upstream region of the DNA domain of *p63* and is only contained in the *p63* subtype of the transactivation domain of this protein, which does not affect the activity of the *p63* DNA binding domain (DBD) (Slavotinek et al., 2005). However, the above mutations are significantly different from those in EEC. For example, R298G and R298Q increase the activity of *p63*, while N6H, which is outside the functional domain of *p63*, does not affect the expression of *p63*. However, missense mutations in EEC are likely to result in the loss of DNA binding and impaired transactivation activities (Amiel et al., 2001). As a result, an essential difference is detectable at the genetic level, and this can be used to exclude ADULT syndrome.

In our patient, the mutation site was *p63*, p. G173V, which was consistent with a previously reported mutation. Monti et al. (2013) detected the transactivation abnormality and interfering ability of this mutant protein in yeast and mammalian cells and quantified the protein functional changes after mutation. Monti et al. detected wild-type and *p63* p. G173V protein changes by inducing galactosyl-dependent protein expression in yeast through the inducible GAL1, 10 promoter and revealed that the mutation resulted in a 20% reduction in transactivation activities at relatively high galactose concentrations (0.128%). In mammalian cells, the mutation p. G173V retains partial transactivation activity. For example, p. G173V mutants show a high residual transactivation potential on the P21, MDM2, PUMA, and BAX targets, which are regulated by *p63*, and are involved in the regulation of the cell cycle, protein stability, apoptosis, and epithelial cells.

PERP and COL18A1 are well-known *p63*-regulated genes involved in skin and epithelial development. As for the interfering ability, the p. G173V mutant clearly interferes only with PERP and COL18A1 targets to lower the transactivation ability compared to wild-types. Considering the corresponding structure and function, the region corresponding to amino acid 173 protrudes on the surface of the protein, so that the protein's functional structure does not change. The reason for these functional changes may be that amino acid 173 is close to the N-terminus of the DBD, which is involved in the recruitment and assembly of tetramer proteins that affects the machinery of transcription proteins. Meanwhile, amino acid 173 is located in the proline-rich region of the C-terminus, which is important for the structural integrity and apoptosis-inducing function of the transcription protein. Thus, the mutation induces changes in the transactivation and interference ability of the protein.

Different amino acid mutations result in different transactivation abnormalities and interfering abilities, as well as different clinical phenotypes. However, it can be seen from the above discussion that the clinical manifestations of the six *TP63*-related syndromes overlapped greatly. One amino acid mutation site can cause more than one syndrome. For example, as reported by Avitan-Hersh et al. (2010),

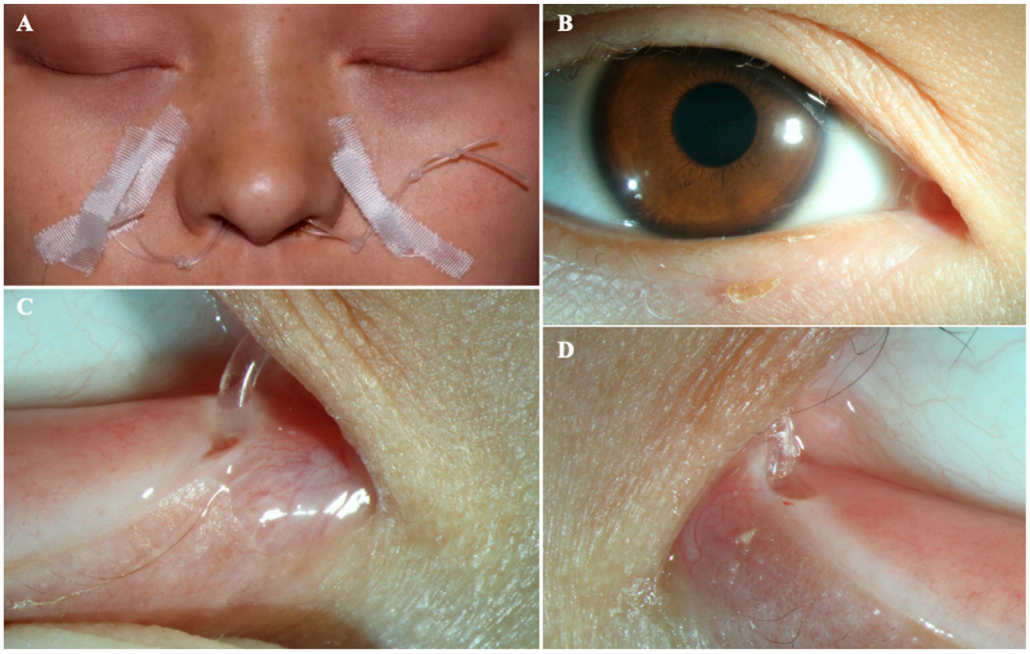

FIGURE 5
The patient after surgery **(A–B)** The ocular appearance after surgery. **(C)** The artificial nasolacrimal duct. **(D)** The close-up appearance of the opened punctum.

TABLE 2 Clinical features in six overlapping syndromes.

			TP63 mutation syndromes					
		Our case	AEC	LMS	ADULT	RHS	SHFM	EEC
Ectodermal	*Teeth*	√	+++	++	+++	+	-	+++
	Skin	√	+++	-	+++	+	-	+++
	Hair	√	+++	-	+++	+	-	+++
	Nails	√	+++	+++	+++	+	-	+++
	Lacrimal ducts	√	+++	+++	+++	+	-	+++
	Breasts	√	+++	+++	+	-	-	+
	Sweat glands	-	+++	++	-	+++	-	+
Fused eyelids		√	+++	-	-	-	-	-
Ectrodactyly		-	-	+++	-	++	+++	+++
Ccenter lip and palate		-	++	++	-	+++	-	+++
Others		-	Hearing impairment++	-	-	-	-	Hearing impairment+
			Genito-urinary++					Urinary+

√ The clinical manifestations were observed. - The clinical manifestations were not observed.
$^{+++}$Frequently observed in >50% of patients, ++ observed in 30%–50% of patients, + occasionally observed in 30% of patients, and rarely or never observed.
AEC, ankyloblepharon-ectodermal dysplasia-ccentering syndrome; LMS, limb mammary syndrome; ADULT, Acro-dermato-ungual-lacrimal-tooth syndrome; RHS, Rapp–Hodgkin syndrome; SHFM, split-hand/split-foot malformation; EEC, ectrodactyly ectodermal dysplasia-ccenter lip/palate syndrome.

the mutated amino acid p. R243W was previously reported to be associated with EEC and LMS. Brunner and Van Bokhoven (2002) also reported a patient with the ADULT syndrome phenotype, but her mutated amino acid (R227Q) was previously related to EEC and LMS. As such, in addition to the overlapping clinical phenotypes, the mutations affecting the amino acids in the *TP63* gene also have a certain crossover potential. In other words, even subtle phenotypic differences can represent diversities at the molecular level. For example, the ADULT syndrome mutations can occur in exons 3, 4, 6, or 8, while LMS mutations can occur in exons 4, 13, and 14 (Rinne

et al., 2007), and EEC mutations can occur in exon 5–8, 13, or 14 (Rinne et al., 2007; Whittington et al., 2016). For this reason, (Monti et al., 2013), proposed that clinical conditions should be integrated with the functional parameters of *p63* mutated proteins, such as the transactivation ability of target genes involved in specific developmental pathways and the interaction and interference ability of mutant isomers, for better genetic diagnosis and differentiation of the overlapping clinical phenotypes (Serra et al., 2011).

At present, there is no treatment for conditions caused by *TP63* mutations. However, we can focus on ensuring an accurate diagnosis by differentiating the different types of diseases with *TP63* mutations and further improve the accuracy of genetic counseling through gene analysis. In the future, we hope we can assist patients in making reproductive plans and offer therapeutic means to cure the genetic disease from the embryonic stage through the classification of gene variants, such as gain-functional mutations or loss-functional mutations (van Zelst-Stams and van Steensel, 2009; Monti et al., 2013).

Conclusion

In summary, we reported a case of ADULT syndrome caused by a rare amino acid mutation with a rare clinical phenotype, including eyelid fusion and abnormal development of the fifth finger. These findings add to our current understanding of ADULT syndrome and other *TP63*-related diseases.

All relevant information was explained to the patient and his mother, and written informed consent was obtained from the patient and his mother for publication of this case report and accompanying images.

Data availability statement

The original contributions presented in the study are included in the article/Supplementary Material, further inquiries can be directed to the corresponding author.

Ethics statement

Written informed consent was obtained from the individual(s), and minor(s) legal guardian/next of kin, for the publication of any potentially identifiable images or data included in this article. Written informed consent was obtained from the participant/patient(s) for the publication of this case report.

Author contributions

All authors contributed to the study conception and design. Material preparation, data collection and analysis were performed by JZ and YW. The first draft of the manuscript was written by JZ and YW, and all authors commented on previous versions of the manuscript. All authors contributed to the article and approved the submitted version.

Acknowledgments

We thank YiW and his team at the Clinical Genetics Center for the DNA analysis. We also thankYinghong Zhang, the otolaryngologist, for her very useful comments, and the otolaryngology department at Peking University Third Hospital for investigating the patients' hearing and doing the operation with us. We appreciate the kindness of the mother and daughter for allowing us to use their medical and dental information for publication and for the advancement of science. This article is solely dedicated to them.

Conflict of interest

The authors declare that the research was conducted in the absence of any commercial or financial relationships that could be construed as a potential conflict of interest.

Publisher's note

Supplementary material

The Supplementary Material for this article can be found online at: https://www.frontiersin.org/articles/10.3389/fgene.2023.1150613/full#supplementary-material

References

Amiel, B. G., Francannet, C., Raclin, V., Munnich, A., Lyonnet, S., and Frebourg, T. (2001). TP63 gene mutation in ADULT syndrome. *Eur. J. Hum. Genet.* 9 (8), 624–625. doi:10.1038/sj.ejhg.5200676

Avitan-Hersh, E., Indelman, M., Bergman, R., and Sprecher, E. (2010). ADULT syndrome caused by a mutation previously associated with EEC syndrome. *Pediatr. Dermatol* 27 (6), 643–645. doi:10.1111/j.1525-1470.2010.01131.x

Berk, D. R., Shinawi, M., and Whelan, A. J. (2012). ADULT syndrome due to an R243W mutation in TP63. *Int. J. Dermatol* 51 (6), 693–696. doi:10.1111/j.1365-4632.2011.05375.x

Brunner, H. B., and Van Bokhoven, H. (2002). The p63 gene in EEC and other syndromes. *J. Med. Genet.* 39 (6), 377–381. doi:10.1136/jmg.39.6.377

Cassady, J. V. (1952). Developmental anatomy of nasolacrimal duct. *AMA Arch. Ophthalmol.* 47 (2), 141–158. doi:10.1001/archopht.1952.01700030146003

Chan, H. J., Mellerio, J. E., and McGrath, J. A. (2004). ADULT ectodermal dysplasia syndrome resulting from the missense mutation R298Q in the p63 gene. *Clin. Exp. Dermatol* 29 (6), 669–672. doi:10.1111/j.1365-2230.2004.01643.x

Duijf, P. H., Propping, P., Friedl, W., Krieger, E., McKeon, F., Dötsch, V., et al. (2002). Gain-of-function mutation in ADULT syndrome reveals the presence of a second transactivation domain in p63. *Hum. Mol. Genet.* 11 (7), 799–804. doi:10.1093/hmg/11.7.799

Kawasaki de Araujo, T., Lustosa-Mendes, E., Dos Santos, A. P., Coelho Molck, M., Mazzariol Volpe-Aquino, R., and Gil-da-Silva-Lopes, V. L. (2017). ADULT phenotype

and rs16864880 in the TP63 gene: two new cases and review of the literature. *Mol. Syndromol.* 8 (4), 201–205. doi:10.1159/000470025

Monti, P., Russo, D., Bocciardi, R., Foggetti, G., Menichini, P., Divizia, M. T., et al. (2013). EEC- and ADULT-associated TP63 mutations exhibit functional heterogeneity toward P63 responsive sequences. *Hum. Mutat.* 34 (6), 894–904. doi:10.1002/humu.22304

Otsuki, Y., Ueda, K., Nuri, T., Satoh, C., Maekawa, R., and Yoshiura, K. I. (2020). EEC-LM-ADULT syndrome caused by R319H mutation in TP63 with ectrodactyly, syndactyly, and teeth anomaly: A case report. *Med. Baltim.* 99 (44), e22816. doi:10.1097/MD.0000000000022816

Otsuki, Y., Ueda, K., Satoh, C., Maekawa, R., Yoshiura, K. I., and Iseki, S. (2016). Intermediate phenotype between ADULT syndrome and EEC syndrome caused by R243Q mutation in TP63. *Plast. Reconstr. Surg. Glob. Open* 4 (12), e1185. doi:10.1097/GOX.0000000000001185

Petris, C., and Liu, D. (2017). Probing for congenital nasolacrimal duct obstruction. *Cochrane Database Syst. Rev.* 7, CD011109. doi:10.1002/14651858.CD011109.pub2

Prontera, P., Garelli, E., Isidori, I., Mencarelli, A., Carando, A., Silengo, M. C., et al. (2011). Cleft palate and ADULT phenotype in a patient with a novel TP63 mutation suggests lumping of EEC/LM/ADULT syndromes into a unique entity: ELA syndrome. *Am. J. Med. Genet. A* 155A (11), 2746–2749. doi:10.1002/ajmg.a.34270

Rinne, T., Brunner, H. G., and van Bokhoven, H. (2007). p63-associated disorders. *Cell Cycle* 6 (3), 262–268. doi:10.4161/cc.6.3.3796

Rinne, T., Hamel, B., van Bokhoven, H., and Brunner, H. G. (2006a). Pattern of p63 mutations and their phenotypes--update. *Am. J. Med. Genet. A* 140 (13), 1396–1406. doi:10.1002/ajmg.a.31271

Rinne, T., Spadoni, E., Kjaer, K. W., Danesino, C., Larizza, D., Kock, M., et al. (2006b). Delineation of the ADULT syndrome phenotype due to arginine 298 mutations of the p63 gene. *Eur. J. Hum. Genet.* 14 (8), 904–910. doi:10.1038/sj.ejhg.5201640

Serra, V., Castori, M., Paradisi, M., Bui, L., Melino, G., and Terrinoni, A. (2011). Functional characterization of a novel TP63 mutation in a family with overlapping features of Rapp-Hodgkin/AEC/ADULT syndromes. *Am. J. Med. Genet. A* 155A (12), 3104–3109. doi:10.1002/ajmg.a.34335

Slavotinek, A. M., Tanaka, J., Winder, A., Vargervik, K., Haggstrom, A., and Bamshad, M. (2005). Acro-dermato-ungual-lacrimal-tooth (ADULT) syndrome: report of a child with phenotypic overlap with ulnar-mammary syndrome and a new mutation in TP63. *Am. J. Med. Genet. A* 138A (2), 146–149. doi:10.1002/ajmg.a.30900

van Zelst-Stams, W. A., and van Steensel, M. A. (2009). A novel TP63 mutation in family with ADULT syndrome presenting with eczema and hypothelia. *Am. J. Med. Genet. A* 149A (7), 1558–1560. doi:10.1002/ajmg.a.32881

Wang, X., Tao, A. L., Yang, W. L., and Zhang, H. J. (2009). Mutation analysis of p63 gene in the first Chinese family with ADULT syndrome. *Chin. Med. J. Engl.* 122 (16), 1867–1871. doi:10.3760/cma.j.issn.0366-6999.2009.16.006

Whittington, A., Stein, S., and Kenner-Bell, B. (2016). Acro-dermato-ungual-lacrimal-tooth syndrome: an uncommon member of the ectodermal dysplasias. *Pediatr. Dermatol* 33 (5), e322–e326. doi:10.1111/pde.12938

Frontiers in Genetics

Highlights genetic and genomic inquiry relating to all domains of life

The most cited genetics and heredity journal, which advances our understanding of genes from humans to plants and other model organisms. It highlights developments in the function and variability of the genome, and the use of genomic tools.

Discover the latest Research Topics

See more →

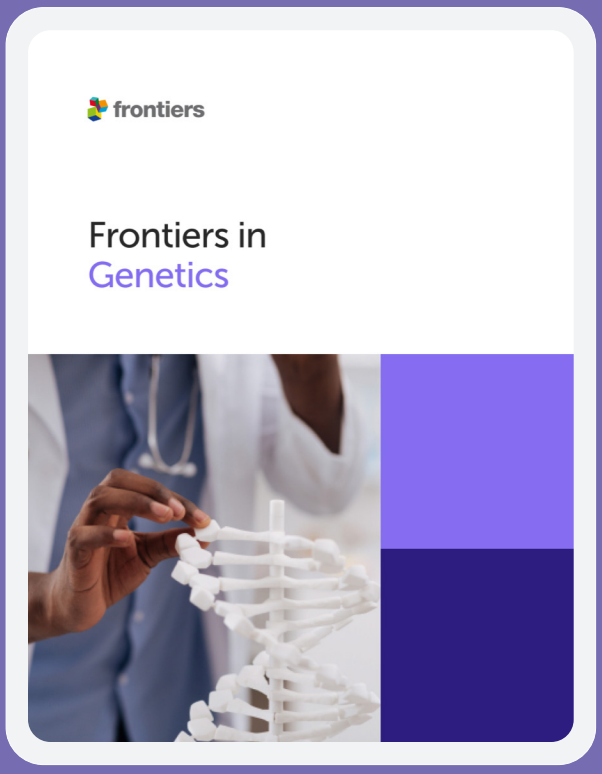

Frontiers

Avenue du Tribunal-Fédéral 34
1005 Lausanne, Switzerland
frontiersin.org

Contact us

+41 (0)21 510 17 00
frontiersin.org/about/contact